



**STRUCTURAL SYSTEMS  
RESEARCH PROJECT**

Report No.  
**SSRP-10/02**

**Development of Seismic Design Guidelines  
for Segmental Construction**

*by*

**Marc Veletzos**

**José I. Restrepo**

Final Report

March 18, 2013

Department of Structural Engineering  
University of California, San Diego  
La Jolla, California 92093-0085

University of California, San Diego  
Department of Structural Engineering  
Structural Systems Research Project

Report No. SSRP-10/02

## **DEVELOPMENT OF SEISMIC DESIGN GUIDELINES FOR SEGMENTAL CONSTRUCTION**

By

**Marc J. Veletzos**

*Assistant Professor, Merrimack College  
North Andover, MA*

**José I. Restrepo**

*Professor of Structural Engineering*

Final Report Submitted to Caltrans

Department of Structural Engineering  
University of California, San Diego  
La Jolla, California 92093-0085

March 18, 2013

## Technical Report Documentation Page

1. Report No.	2. Government Accession No.	3. Recipient's Catalog No.	
4. Title and Subtitle Development of Seismic Design Guidelines for Segmental Construction		5. Report Date March 18, 2013	
		6. Performing Organization Code	
7. Author(s) Marc J. Veletzos and José I. Restrepo		8. Performing Organization Report No. SSRP – 10/02	
9. Performing Organization Name and Address  Department of Structural Engineering School of Engineering University of California, San Diego La Jolla, California 92093-0085		10. Work Unit No. (TRAIS)	
		11. Contracts or Grant No. 59A0622	
12. Sponsoring Agency Name and Address  California Department of Transportation Engineering Service Center 1801 30 <sup>th</sup> St., West Building MS #9-2/5 Sacramento, California 95816		13. Type of Report and Period Covered Final Report	
		14. Sponsoring Agency Code	
15. Supplementary Notes Prepared in cooperation with the State of California Department of Transportation.			
16. Abstract <p>Segmental construction of precast concrete bridges can accelerate construction and minimize the cost in highly congested urban environments or environmentally sensitive regions. In addition, they have proven cost effective for difficult to access ravines, and wide river crossings where medium to long repetitive spans are needed. Despite their proven benefits, the use of precast concrete segmental bridges in seismic regions of the United States is limited. A main obstacle to their use is concern regarding the seismic response of segment joints. This research project identified and addressed three major gaps in knowledge that have inhibited the used of segmental construction in seismic zones. These knowledge gaps include: 1) a lack of understanding of appropriate vertical earthquake load combinations for segmental bridges; 2) a lack of understanding of appropriate methods to address vertical earthquake demands for 'Ordinary' and 'Important' bridges; and 3) the absence of a suitable model to estimate the flexural bond length of multi-strand tendons. This report presents the results of numerous studies and analyses to address the first two knowledge gaps. Furthermore, the results and conclusions of three full-scale experiments on precast concrete blocks are presented to address the third knowledge gap. The experiments indicate that a gap opening of at least 1.6 in, can be attained between precast segments at the level of the tendon before rupture of the tendons takes place. Deliverables for this research project include: a preliminary set of standard sections for precast segmental bridges for spans of 300 to 500 feet; a peer reviewed seismic design framework; peer reviewed seismic design guidelines for segmental construction; and sample calculations that illustrate the use of the proposed seismic design guidelines. These documents are included in this final report.</p>			
17. Key Words Vertical seismic, precast, segmental, tendon debond		18. Distribution Statement Unlimited	
19. Security Classification (of this report) Unclassified	20. Security Classification (of this page) Unclassified	21. No. of Pages 214	22. Price

## **Disclaimer**

The contents of this report reflect the views of the authors who are responsible for the facts and the accuracy of the data presented herein. The contents do not necessarily reflect the official views or policies of the State of California or the Federal Highway Administration. This report does not constitute a standard, specification or regulation.

This research project was suspended in the middle of the construction of the test units by the State of California through Executive Order S-09-08, which halted all research work funded by the state. Some of the instrumentation was lost as a result of weathering during this hiatus. The authors have made their best effort at interpreting the results obtained from the experiment but uncertainty remains in some of the results.

## **Acknowledgments**

This research project was made possible by funding from the California Department of Transportation under contract No. 59A0622. The input of Charly Sikorsky and others at Caltrans was greatly appreciated.

The authors would like to acknowledge Daniel Tassin and Ben Soule of International Bridge Technologies, Sami Megally of PBS&J, John Corven of Corven Engineering, Joe Tagnoli, Dan Fitzwilliam, Sajid Abbas and David Goodyear of T.Y. Lin International for their valuable contributions to this document.

The authors would also like to acknowledge Dywidag Systems International (DSI) for donating post-tensioning materials and CMC Fontana Steel for donating the reinforcing bars for the experiments. .

The large scale experiments could not have been completed without the dedication and hard work of Matthew Tobolski, Wonjae Song, Andy Gunthardt, Chris Latham, Fernando Pacheco and the staff of the Powell Laboratory at UCSD.

## **Abstract**

Segmental construction of precast concrete bridges can accelerate construction and minimize the cost in highly congested urban environments or environmentally sensitive regions. In addition, they have proven cost effective for difficult to access ravines, and wide river crossings where medium to long repetitive spans are needed. Despite their proven benefits, the use of precast concrete segmental bridges in seismic regions of the United States is limited. A main obstacle to their use is concern regarding the seismic response of segment joints. This research project identified and addressed three major gaps in knowledge that have inhibited the used of segmental construction in seismic zones. These knowledge gaps include: 1) a lack of understanding of appropriate vertical earthquake load combinations for segmental bridges; 2) a lack of understanding of appropriate methods to address vertical earthquake demands for ‘Ordinary’ and ‘Important’ bridges; and 3) the absence of a suitable model to estimate the flexural bond length of multi-strand tendons. This report presents the results of numerous studies and analyses to address the first two knowledge gaps. Furthermore, the results and conclusions of three full-scale experiments on precast concrete blocks are presented to address the third knowledge gap. The experiments indicate that a gap opening of at least 1.6 in, can be attained between precast segments at the level of the tendon before rupture of the tendons takes place. Deliverables for this research project include: a preliminary set of standard sections for precast segmental bridges for spans of 300 to 500 feet; a peer reviewed seismic design framework; peer reviewed seismic design guidelines for segmental construction; and sample calculations that illustrate the use of the proposed seismic design guidelines. These documents are included in this final report.

# Table of Contents

<b>Disclaimer .....</b>	<b>ii</b>
<b>Acknowledgments .....</b>	<b>iii</b>
<b>Abstract.....</b>	<b>iv</b>
<b>Table of Contents .....</b>	<b>v</b>
<b>List of Figures.....</b>	<b>viii</b>
<b>List of Tables .....</b>	<b>xi</b>
<b>Notation.....</b>	<b>xii</b>
<b>Chapter 1:        <b>Introduction .....</b></b>	<b>1</b>
1.1..Knowledge Gaps.....	2
1.2..Report Organization.....	3
<b>Chapter 2:        <b>Experimentation of Precast Concrete Blocks .....</b></b>	<b>5</b>
2.1..Objectives .....	5
2.2..Development.....	5
2.2.1 Specimen Design .....	6
2.2.2 Specimen Construction.....	8
2.2.3 Instrumentation .....	9
2.2.4 Loading Protocol .....	10
2.2.5 Material Properties.....	10
2.3..Experimental Results .....	12
2.3.1 Visual Performance .....	12
2.3.2 Axial Force-Axial Displacement Response.....	14
2.3.3 Tendon Strain Readings.....	17
2.3.4 Tendon Stress/Strain - Total Segment Displacement Relationship .....	19
2.3.5 Tendon Stress/ Strain - Crack Width Relationship.....	20
2.4..Equivalent Unbonded Length .....	20
<b>Chapter 3:        <b>Standard Sections .....</b></b>	<b>23</b>
3.1..Objective.....	23
3.2..Introduction.....	23

3.3..Discussion.....	23
<b>Chapter 4: General Seismic Design Framework.....</b>	<b>25</b>
4.1..Objectives .....	25
4.2..Proposed Seismic Design Framework for Segmental Bridges .....	25
4.2.1 Performance Based Seismic Design Framework.....	25
4.2.2 Capacity Design.....	26
4.2.3 Longitudinal Push-Over Analysis.....	26
4.2.4 Vertical/Horizontal Earthquake Load Combinations .....	26
4.2.5 Vertical Earthquake Load Combinations.....	27
4.2.6 Horizontal Earthquake Load Combinations .....	27
4.2.7 Vertical Earthquake Demands .....	27
4.2.8 FEE Design Level of ‘Ordinary’ Bridges.....	28
4.2.9 SEE Design Level of ‘Ordinary’ Bridges.....	28
4.2.10 FEE Design Level of ‘Important’ Bridges.....	28
4.2.11 SEE Design Level of ‘Important’ Bridges.....	29
4.3..Superstructure Segment Joint Capacity .....	29
4.3.1 Segment Joint Capacity .....	30
4.3.2 ‘Ordinary’ Bridges.....	30
4.3.3 ‘Important’ Bridges .....	30
4.3.4 Definition of Capacity Levels.....	30
4.3.5 Flexural Bond Length and Unbonded Length of Tendons ....	33
4.4..Vertical Earthquake Demand Modeling Approaches .....	36
4.4.1 Modal Analysis.....	36
4.4.2 Time History Analysis.....	36
4.4.3 Superstructure Collapse Mechanisms.....	37
4.5..Earthquake Hazards, Design Spectra and Ground Motions .....	39
4.5.1 Earthquake Hazard Levels.....	39
4.5.2 Time History Ground Motions .....	40
4.5.3 Vertical Design Spectrum.....	41
<b>Chapter 5: Study of Earthquake Demand Methods .....</b>	<b>44</b>
5.1..Objectives .....	44
5.2..Finite Element Models.....	44
5.2.1 Linear Elastic Model.....	44
5.2.2 Nonlinear Elastic Model.....	45
5.2.3 Nonlinear Inelastic Model .....	45
5.2.4 Moment Rotation Curves.....	46
5.2.5 Calibration of Nonlinear Models.....	48
5.3..Model Validations .....	49

5.3.1	Modal Properties.....	49
5.3.2	Elastic Superstructure Time History Comparison .....	51
5.4..	Design Spectra and Ground Motions.....	52
5.5..	Limit States .....	56
5.6..	Results.....	57
5.6.1	Elastic Time History vs. Elastic Modal Analysis .....	57
5.6.2	Collapse Mechanism Check .....	60
5.6.3	Nonlinear Elastic Model vs. Nonlinear Inelastic Model .....	61
5.7..	Recommendations.....	63
5.7.1	‘Ordinary’ Bridges.....	63
5.7.2	‘Important’ Bridges .....	64
<b>Chapter 6:</b>	<b>Load Combination Investigation.....</b>	<b>65</b>
6.1..	Objectives .....	65
6.2..	Introduction.....	65
6.3..	Thermal Gradient.....	65
6.4..	Creep and Shrinkage.....	70
6.4.1	Shrinkage .....	70
6.4.2	Creep.....	71
6.5..	Discussion.....	72
6.5.1	Thermal Gradient.....	73
6.5.2	Creep and Shrinkage.....	73
6.6..	Recommendations.....	73
<b>Chapter 7:</b>	<b>Peer Reviewed Design Recommendations.....</b>	<b>75</b>
7.1..	Objectives .....	75
7.2..	Detailed Design Procedure for ‘Ordinary’ Bridges .....	76
7.3..	Detailed Design Procedure for “Important” Bridges.....	83
7.4..	Design Flowcharts .....	90
<b>Chapter 8:</b>	<b>Conclusions.....</b>	<b>92</b>
<b>References.....</b>		<b>94</b>
<b>Appendix A – Drawings of Experimental Program .....</b>		<b>96</b>
<b>Appendix B – Standard Sections .....</b>		<b>118</b>
<b>Appendix C - Verification of Proposed Design Approach .....</b>		<b>136</b>

## List of Figures

Figure 1 Overview of test setup .....	7
Figure 2 View of a test unit before testing.....	8
Figure 3 Loading protocol .....	10
Figure 4 Strand measured and analytical stress-strain relationship around the yield point .....	11
Figure 5 Cracking in the midspan region of unit 2706-1 .....	12
Figure 6- Close up failure at midspan of unit 2706-1 .....	13
Figure 7- Slices of Specimen 2706-1 after testing.....	14
Figure 8 Recorded axial force –axial displacement responses .....	15
Figure 9 Axial force vs. 6 inch gage length displacement responses of the 2706 test units .....	17
Figure 10 Tendon strains at different locations and at different stages during the tests...	18
Figure 11 Total Segment Displacements .....	19
Figure 12 Segment Joint Crack Width.....	20
Figure 13 Tendon Equivalent Unbonded Length.....	21
Figure 14 Normalized Equivalent Unbonded Length.....	21
Figure 15 Proposed Superstructure Modeling Approach for SEE Design Level of ‘Important’ Bridges.....	29
Figure 16 Sample Moment-Curvature Diagram for ‘Ordinary’ Bridges .....	31
Figure 17 Sample Moment-Rotation Diagram for ‘Important’ Bridges.....	32
Figure 18 Flexural Bond Length in Post-Tensioned Beams.....	34
Figure 19 Unbonded Length of Tendons across Segment Joints in Finite Element Models .....	34
Figure 20 Bond Surface Area for PT Tendons .....	36
Figure 21 End Span Collapse Mechanism .....	38
Figure 22 Interior Span Collapse Mechanism .....	38
Figure 23 Example of Uniform Hazard Spectrum for Various Return Periods.....	40
Figure 24 Deaggregation of a UHS at a Period of 1.0 seconds .....	41
Figure 25 Sample Vertical Design Spectrum.....	42
Figure 26 V/H ratio for Various Parameters (Bozorgnia and Campbell, 2004) .....	42
Figure 27 Schematic of the Linear Elastic Model .....	44

Figure 28 Detail of the Segment Joints Adjacent to the Piers in the Nonlinear Elastic Model .....	45
Figure 29 Schematic of the Nonlinear Inelastic Model .....	46
Figure 30 Details of the Segment Joints Adjacent to the Piers and Near Midspan .....	46
Figure 31 Moment-Rotation Curves for NEM with Moment Offset - Segment Joint D1/U1 .....	47
Figure 32 Moment-Rotation Curves for NEM with Moment Offset - Segment Joint at Midspan.....	47
Figure 33. Offset in Moment-Rotation Curves required for SAP2000.....	48
Figure 34. Schematic of Segment Joint Forces Required to Calibrate the NIM and NEM. NIM shown, NEM similar. ....	49
Figure 35 Period Comparison .....	50
Figure 36 Longitudinal Modal Mass Participation Comparison.....	51
Figure 37 Vertical Modal Mass Participation Comparison .....	51
Figure 38 Dead Load Bending Moment Comparison – LEM vs. Elastic version of NIM .....	52
Figure 39 Elastic Time History Comparison – LEM vs. Elastic NEM vs. Elastic NIM .	52
Figure 40. Vertical Design Earthquake Spectrum .....	53
Figure 41. Horizontal Design Earthquake Spectrum .....	53
Figure 42 2500 Year Hazard Spectrum .....	56
Figure 43. Definition of Effective Moment and Effective Rotation Capacities .....	57
Figure 44. Median Bending Moment Envelopes for the Time History Analyses from the LEM. ....	58
Figure 45. Median Bending Moment Envelopes for the Modal Analyses from the LEM	58
Figure 46. Ratio of Median Bending Moment Envelopes for the 2500 Year Hazard .....	59
Figure 47 2% Rayleigh Damping used for Time History Analyses .....	60
Figure 48 Kawashima and Aizawa (1986) Response Spectra Damping Scale Factors ...	60
Figure 49 Sample Collapse Mechanism Calculations – 2500 Year Hazard – End Span.	61
Figure 50 Sample Collapse Mechanism Calculations – 2500 Year Hazard – Interior Spans .....	61
Figure 51. Segment Joint Rotation Envelopes for the NEM .....	62
Figure 52. Segment Joint Rotation Envelopes for the NIM.....	62
Figure 53: Maximum Positive Temperature Differences on the San Antonio “Y” Project (Roberts-Wollman et al., 2002) .....	66
Figure 54: Maximum Negative Temperature Differences on the San Antonio “Y” Project (Roberts-Wollman et al., 2002) .....	66
Figure 55: Comparison of Solar Radiation and the Maximum Positive Temperature Difference x 1.8 on the San Antonio “Y” Project (Roberts-Wollman et al., 2002)..	67

Figure 56: 1995, Thermocouple Readings on the North Halawa Valley Viaduct (Shushkewich, 1998).....	68
Figure 57: July 1995, Thermocouple Readings on the North Halawa Valley Viaduct (Shushkewich, 1998).....	68
Figure 58: July 1, 1995, Thermocouple Readings on the North Halawa Valley Viaduct (Shushkewich, 1998).....	69
Figure 59: Thermocouple Locations on the North Halawa Valley Viaduct (Shushkewich, 1998) .....	69
Figure 60: July 1, 1995, Temperature Differences between Thermocouple 14E and 22E on the North Halawa Valley Viaduct.....	70
Figure 61: Shrinkage vs Time.....	71
Figure 62: Creep vs Time .....	72
Figure 63 Sample Vertical Design Spectra.....	76
Figure 64 V/H ratio for Various Parameters (from Bozorgnia and Campbell, 2004) .....	77
Figure 65 Sample Moment-Curvature Diagram for ‘Ordinary’ Bridges .....	78
Figure 66 End Span Collapse Mechanism .....	79
Figure 67 Interior Span Collapse Mechanism .....	80
Figure 68 Sample Vertical Design Spectra.....	83
Figure 69 V/H ratio for Various Parameters (from Bozorgnia and Campbell, 2004) .....	84
Figure 70 Deaggregation of a 2500 Year Return Design Sspectra at a Period of 0.5 sec. ....	85
Figure 71 Deaggregation of a 2500 Year Return Design Sspectra at a Period of 4.0 sec. ....	85
Figure 72 Sample Moment-Rotation Diagram for SEE of ‘Important’ Bridges .....	87
Figure 73 Recommended Superstructure Modeling Approach for SEE Design Level of ‘Important’ Bridges.....	88
Figure 74. Offset in Moment-Rotation Curves Required for Modeling of Segment Joints .....	89
Figure 75 Design Flowchart for ‘Ordinary’ Bridges .....	90
Figure 76 Design Flowchart for ‘Important’ bridges.....	91

## List of Tables

Table 1	Test unit description.....	5
Table 2	Mild reinforcement properties .....	11
Table 3	Day of test cementitious material properties .....	12
Table 4	Existing Segmental Bridges used to Develop the Standard Sections .....	24
Table 5	Performance Objectives and Hazard Levels .....	25
Table 6	Modeling Approach for Vertical Earthquake Demands .....	28
Table 7	Consequences of Exceeding Design Paramaters .....	33
Table 8	Period Comparison .....	50
Table 9	Source Ground Motions.....	55
Table 10	Summary of Median Time History to Modal Bending Moment Ratio.....	59
Table 11	Typical Effective Thickness for Precast Segmental Bridges.....	71

## Notation

ABC	Accelerated bridge construction
$A_{bot}$	Total area of the post tension in the bottom flange at a segment joint
$A_{cont}$	Total area of the continuity tendons at a segment joint
$A_{st}$	Mild steel reinforcement area
$A_p$	Prestressing tendon area
$A_{top}$	Total area of the post tension in the top flange at a segment joint
$b_{bf}$	Width of the superstructure bottom flange at a segment joint of interest
$b_{tf}$	Width of the superstructure top flange at a segment joint of interest
Caltrans	California department of transportation
$c_c$	Concrete cover to mild steel reinforcement, measure from the bar end to the segment joint
CQC	Complete quadratic combination
CS	Creep and shrinkage
DC	Limit state identifying the decompression of extreme compression fibers
$d_b$	Diameter of post-tensioning strand
$DL_{CS}$	Dead load demands after the majority of creep and shrinkage has occurred
$DL_{EOC}$	Dead load demands at the end of construction
$D_{vert}$	Vertical earthquake demands for collapse mechanism check
EOC	End of construction
EOS	End of service
$E_p$	Modulus of Elasticity of prestressing steel
$E_s$	Modulus of Elasticity of mild steel
EQ	Earthquake
$EQ_{vert}$	Vertical earthquake demands
$f'_c$	Concrete strength
FEE	Functional evaluation earthquake
$f_{pe}$	Effective stress in post-tensioning strand or tendon
$f_{ps}$	Full design stress in the post-tensioning strand
$f_{pt}$	Stress in the prestressing tendon
$f_r$	Modulus of rupture of concrete
$f_s$	Stress in mild steel reinforcement
$f_y$	Yield strength of mild steel reinforcement

$f_u$	Ultimate stress of the prestressing tendon
LCSA	Longitudinal construction staging analysis
$L_d$	Development length of mild steel reinforcement
$L_{end}$	End span length from the abutment bearing centerline to the first segment joint near the pier
$L_i$	Length from the abutment centerline to the segment joint under consideration
$L_{int}$	Clear interior span length between the first segment joints near the piers
LP	Limit state identifying the limit of proportionality of the post tensioning steel
$L_{sg}$	Length of segment
$L_u$	Equivalent unbonded length
$M_{cr}$	Cracking moment
$M_{CS}$	Moment demand in a segment joint after combining vertical earthquake demands with the dead load moments after considering creep and shrinkage losses
$M_{dc}$	Decompression moment
$M_{EOC}$	Moment demand in a segment joint after combining vertical earthquake demands with the dead load moments at the end of construction
$M_i^+$	Ultimate positive bending capacity of the end span segment joint under consideration
$M_{Midspan}^+$	Ultimate positive bending capacity of the midspan segment joint of interior spans
$M_p$	Idealized plastic moment capacity
$M_{Pier}^-$	Ultimate negative bending capacity of the segment joint adjacent to the pier
$M_{push}$	Moment demands in a segment joint from the longitudinal push over analysis
$M_u$	Ultimate moment capacity
PBSD	Performance based seismic design
$PGA_v$	Vertical peak ground acceleration
PT	Post tensioning
$S_{c_{end}}$	Capacity of the end span collapse mechanism in terms of vertical earthquake accelerations
$S_{c_{int}}$	Capacity of the interior span collapse mechanism in terms of vertical earthquake accelerations
SDC	Seismic design criteria
SEE	Safety evaluation earthquake
$t_{bf}$	Thickness of the superstructure bottom flange at a segment joint
$t_{tf}$	Thickness of the superstructure top flange at a segment joint
$w_{end}$	Uniform distributed load that will develop an end span collapse mechanism

$W_{end}$	Total weight of the end span segments
$w_{int}$	Uniform distributed load that will develop an interior span collapse mechanism
$W_{int}$	Total weight of the interior span segments
$\Delta_j$	Segment axial elongation at the level of a tendon, including tendon bond-slip
$\epsilon_{ps,u}^R$	Reduced ultimate prestressing steel strain
$\epsilon_c$	Concrete strain
$\epsilon_{pe}$	Effective tendon strain
$\epsilon_{pt}$	Strain in the prestressing tendon
$\epsilon_{p1}$	Strain in the prestressing tendon at the segment joint
$\epsilon_{p2}$	Smearred prestressing tendon strain in a segment
$\theta_{CS}$	Rotational demand of a segment joint from the model calibrated to stresses after considerations for creep and shrinkage
$\theta_{el}$	Elastic rotation limit
$\theta_{EOC}$	Rotational demand of a segment joint from the model calibrated to end of construction stresses

## **Chapter 1: INTRODUCTION**

In many areas of the United States and the world, precast segmental bridge construction has proven to be a very effective method of construction for spanning deep valleys, long water crossings, environmentally sensitive areas and also in urban areas where construction can result in traffic disruption. The construction of new freeways in the densely populated and heavily congested areas of urban California requires attention to a significant number of new problems not encountered often before. Environmental issues as well as minimal traffic disruption are two major requirements in many areas of the State. Precast segmental construction is one of the most viable construction alternatives because environmental pollutants such as dust, noise, and debris are much better controlled with segmental construction. In addition, and equally important, existing traffic flow continues virtually unabated with segmental construction. However, the jointed nature of precast segmental construction results in behavioral modes that differ from conventional prestressed concrete construction and that may affect a bridge's response to seismic input. Because of the jointed nature of precast segmental construction, mild steel reinforcement is often detailed only within the segments themselves, creating regions of discontinuity at the joints. Such discontinuities act as crack initiators and confine cracking to within the segment joints which can result in significant local rotations and joint opening during a seismic event (Megally et al, 2009). The main concern with significant joint opening is the potential for plastic deformations that may reduce the load carrying capacity of the section. In addition, residual joint opening after a seismic event may affect readability and maintenance.

The common design framework in California is to prevent joint opening using a capacity design approach in which all load combinations, including those corresponding to the development of plastic hinge overstrength, have to be balanced by the uncracked superstructure. Despite this design approach, recent research (Veletzos and Restrepo, 2009) has shown that the effect of vertical earthquake motion, particularly in the near field, can cause segment joints to open. In addition, the pre-earthquake stress-state of the superstructure can affect the segment joint response.

The principal objective of this research project is to develop design criteria for segmental bridge construction in zones of high seismicity, such as California, that allows nonlinear elastic response in the superstructure only in rare earthquakes and by preventing the opening of joint segments in frequent earthquakes. The design criteria will

use capacity design principles similar to the approach being currently implemented. To this end, three main gaps in knowledge, as listed in the following page, were identified and investigated to ensure completeness in research and to reduce uncertainty.

### ***1.1 Knowledge Gaps***

A major gap in knowledge is a lack of understanding of appropriate upper and lower bounds for pre-earthquake stress-states and appropriate vertical earthquake load combinations for segmental bridges. The stress state of pre-stressed concrete bridges changes on a daily basis due to temperature effects, particularly temperature gradients, and over the bridge service life due to creep, shrinkage and relaxation. It has been shown that the superstructure pre-earthquake stress state can affect the response of segmental bridges (Veletzos and Restrepo, 2009). The extreme pre-earthquake stress-states (i.e. at end of construction plus temperature gradient or after creep and shrinkage plus temperature gradient) typically exhibit the largest superstructure demands. The temperature gradient is caused by solar radiation which heats the top of the bridge superstructure while the shaded webs and bottom soffit remain cool. This effect is increased when the bridge crosses low over water which can further cool the bridge soffit. This temperature gradient is largest during the hottest part of summer days. Thus, combining the full temperature gradient with earthquake is likely over conservative. However, neglecting pre-earthquake stress-states may result in undesirable superstructure damage during a design level earthquake scenario. Thus appropriate design guidelines to address the pre-earthquake stress-state of segmental bridge superstructures need to be developed.

The second major gap in knowledge with precast segmental construction is a lack of understanding of appropriate methods to address vertical earthquake demands. The jointed nature of precast segmental bridges makes them highly susceptible to vertical earthquake loading (Veletzos and Restrepo, 2009), particularly at near field sites, where vertical spectral accelerations can be larger than horizontal spectral accelerations (Bozorgnia and Campbell, 2004). Vertical earthquake demands can be estimated by a number of different methods: vertical static loads; vertical modal analysis; vertical linear time history analysis; and vertical non-linear time history analysis. Currently, vertical earthquake demands are not considered for ‘Ordinary’ bridges with a horizontal PGA less than 0.6g. If the horizontal PGA exceeds 0.6g, a 0.25g vertical acceleration is considered but with out combination with horizontal earthquake loading. Earthquake demands for ‘Important’ bridges are typically determined based on non-linear time history analysis in which the superstructure is modeled with linear elastic elements. Given the jointed nature of precast segmental bridges, design guidelines that address appropriate means to estimate the vertical earthquake demands and vertical/horizontal earthquake load combinations need to be developed.

There is a knowledge gap regarding the fundamental relationship between tendons incremental tensile strain, that is, strain after crack opening, crack width and residual crack width. These relationships are fundamental for the development of a suitable macroscopic model for use in non-linear dynamic time history analysis. Two main limitations have been identified in past research (i) Component and system testing have provided very limited information on the fundamental tendon tensile strain-crack width relationships due to premature failure of strain gages. Failure of strain gages in strands frequently occurs during the strand installation. (ii) Controlled testing to determine the incremental tensile strain-crack width has been carried out on components prestressed with single strands. The group effect of multi-strand tendons is unknown. Moreover, no residual strain – contact stress – residual crack widths have been reported in the literature.

## ***1.2 Report Organization***

To address the gaps in knowledge this research program was organized into six analytical tasks and a series of large scale experiments on precast concrete blocks

This chapter provides background, outlines the principal research objectives and identifies knowledge gaps that this research program addressed.

Chapter 2 describes the experimentation of precast blocks. Accurate information on the multi-strand tendon slip-crack width-residual crack width relationship allowed for the calibration of a refined model which was incorporated into the nonlinear dynamic time history analyses described in Chapters 5, 7 and Appendix C.

Chapter 3 presents a catalog of standard superstructure cross sections balanced cantilever segmental bridges with span lengths from 300 to 500 feet. The standard sections were organized in 50 foot increments and were based on a review of cross sections of existing bridges.

Chapter 4 describes a general seismic design framework for precast segmental bridges. This framework was peer reviewed by Caltrans and industry professionals with segmental bridge design experience to ensure that the framework can be implemented easily. This framework is the basis for the complete design recommendations discussed in Chapter 7.

Chapter 5 describes a study of earthquake demand methods. Analysis of a 300 foot span segmental bridge is conducted through three different methods. The results from these different methods are compared. The most appropriate approach for estimating the vertical seismic demands for ‘Ordinary’ and ‘Important’ segmental bridges is recommended.

Chapter 6 describes the load combinations investigation. Pre-earthquake stress-states, at end of construction and after creep and shrinkage has occurred, were considered

in conjunction with temperature gradients and vertical earthquake demands. The results were incorporated into the complete design recommendations given in Chapter 7

Chapter 7 presents seismic design recommendations for precast segmental bridges. These recommendations were peer reviewed by Caltrans and industry professionals with segmental bridge design and construction experience to check for practicality and ease of use.

Chapter 8 summarizes the main conclusions from the experimental research and the various analytical studies.

The Appendices included drawings of the experimental test units described in Chapter 2, the standard sections described in Chapter 3, and sample calculations illustrating the use of the design recommendations of Chapter 7.

## Chapter 2: EXPERIMENTATION OF PRECAST CONCRETE BLOCKS

This chapter describes the development of the experimental program and key findings related to tendon strain versus joint deformation.

### 2.1 Objectives

The primary objectives of the testing program are as follows:

1. Obtain information on the multi-strand tendon slip-crack width-residual crack width relationship that will allow for the calibration of a tendon unbonded length equation.
2. Determine the hysteretic bond slip relationship between the tendon and the grout to estimate residual gap openings based on peak tendon strains.

### 2.2 Development

As a means to investigate the incremental strain distribution associated with multi-strand tendons and to observe the strain penetration of the tendon from a simulated segment joint into the segments themselves, three match-cast epoxy bonded test units were constructed and tested under pure axial load conditions. The test specimens provided an adequate representation of the construction details and methods in precast segmental bridges, particularly in the midspan regions, where shear is practically absent and where vertical earthquake excitation, and because of the discontinuity of mild steel in the joints between segments, can cause opening of the joints. The three test units were investigated the potential influence of grout type and number of tendons. A summary of the specimen variables is shown in Table 1.

Table 1 Test unit description

<i>Test Unit</i>	<i>No. of 15 mm (0.6 in.) Diameter Strands</i>	<i>PT Stress after losses (ksi)</i>	<i>Concrete Stress (% <math>f'_c</math>)</i>	<i>Grout Type</i>
2706-1	27	160 (= $0.6f_u$ )	30%	ASBI
2706-2	27	160 (= $0.6f_u$ )	30%	Caltrans
1506-1	15	160 (= $0.6f_u$ )	17%	ASBI

### 2.2.1 Specimen Design

Three match cast epoxy bonded test units were built and be tested under pure axial tension using four 500 kip (2,200 kN) capacity servo-controlled hydraulic actuators acting in parallel as shown in Figure 1. The test units were divided into several precast elements to enhance maneuverability and construction in the laboratory and to minimize material costs. Each test unit consisted of two tendon blocks and four actuator load blocks. The tendons had a small bend near the anchorage to promote grouping of the tendon strands that is expected in actual bridges. The tendon blocks had a 19 in. by 19 in. cross-section and the clear span between ears was 204 in. Complete details of the test set-up and the test units, are given in Appendix B. Figure 2 depicts Unit 2706-1 before beginning of testing.

# Experimentation of Precast Concrete Blocks

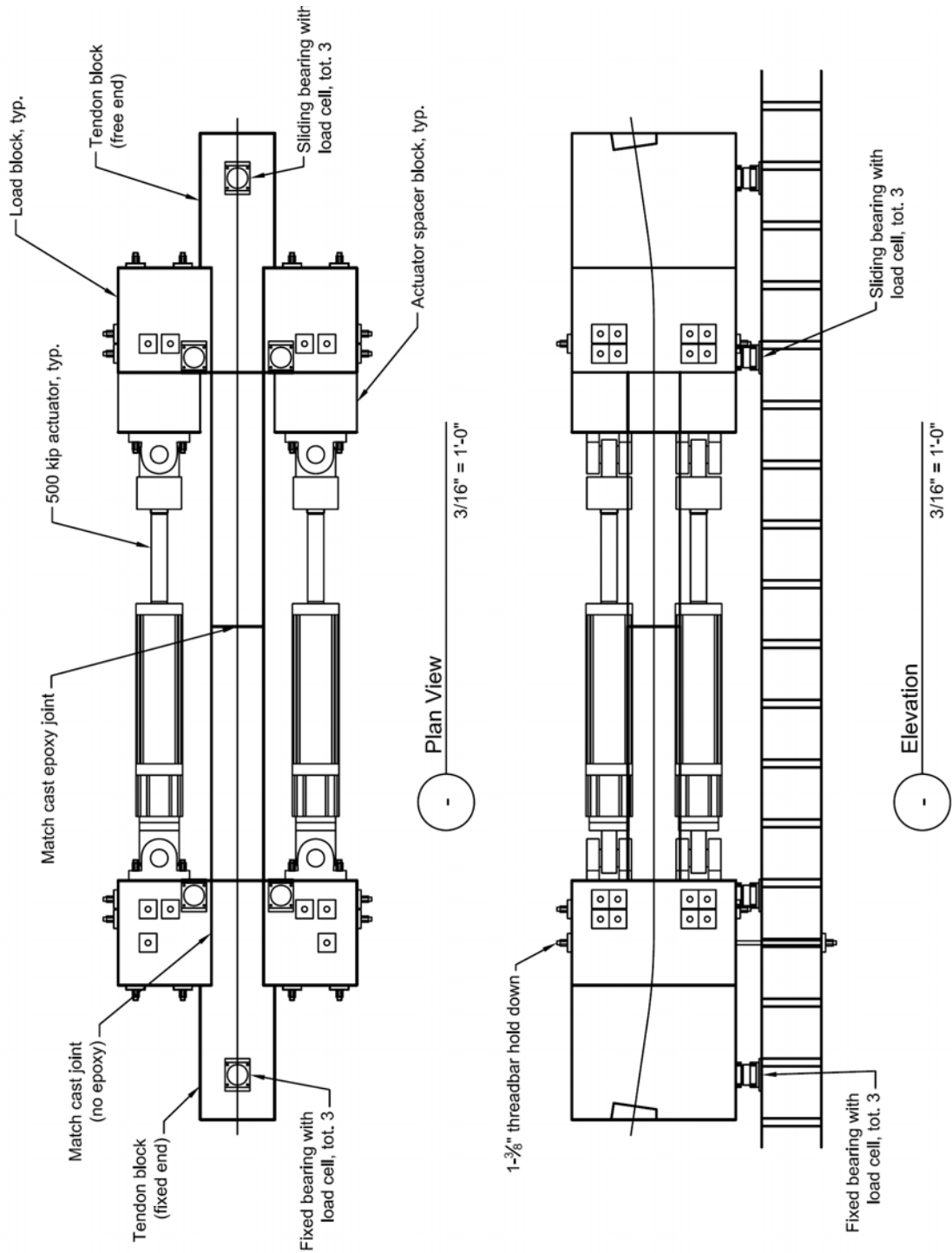


**Figure 1 Overview of test setup**



**Figure 2 View of a test unit before testing**

### 2.2.2 Specimen Construction

The segments were all constructed in the casting bed located at the University of California San Diego Powell Structures labs. As a first step, the loading blocks were fabricated including the placement of alignment keys on the face against which the main tendon segment will be cast. The main tendon bond segments were cast in two pieces to provide the joint at mid length. Both segments were match cast against the respective loading ears to ensure proper alignment during erection. After the first tendon bond segment was cast and allowed to cure, the second segment was match cast against it to ensure proper fit and connection during construction.

Once all segments were allowed to cure with adequate time, they were erected on the main laboratory floor at UCSD. As a first step, one side of the specimen was placed at its final location. The tendon bond segment was placed first followed by the placement and transverse post-tensioning of the loading ears. The loading ears are required during main construction activities to ensure there is sufficient stability of the testing specimen. Subsequently, the tendon was fed into the first half of the test specimen as a attempt to preserve the integrity of the instrumentation on the tendons. Once the first half of the tendon was in place, the other tendon bond segment was carefully flown in using the overhead gantry crane. While the segment was moved into position, the tendon was carefully fed into the duct with associated instrumentation wiring fed through their

respective ports. The block was placed approximately one foot from the face of the previously set segment. The loading ears were then installed and transversely post-tensioned into place. Sliding bearing were placed under this segment and loading ears.

To move the segment into its final positions, post-tensioning rods and jacks were installed through the loading ears. The jacks were employed to physically pull the second half of the segment into place with proper alignment. Prior to initiation of the final setting, epoxy was applied to the face of both joints. Following the placement of the uncured epoxy on each face, the segment was pulled into place.

The post-tensioning tendon was stressed following the final placement and closure of the joint. Post-tensioning was performed by a local contractor using multi-strand jacks on both anchorages. Two jacks were used to minimize the movement of the tendon at the mid-section where instrumentation was placed. To ensure the jacks were pulling a similar amount at each anchorage, linear potentiometers were installed to monitor the stressing head movement at each end. Following the installation of wedges and locking in the post-tensioning, the contractor grouted the ducts using the material specified.

The grout was allowed to cure for a minimum of twenty one days (21). During this curing time, external instrumentation was installed on the unit. The actuators were then installed and all instrumentation hooked up to the data acquisition system to facilitate the recording of all data for testing. During this time, all strain gages were investigated for functionality. It was noted for all specimens that a significant number of strain gages on the post-tensioning tendons and surface gages were damaged.

### 2.2.3 Instrumentation

An array of sensors was installed on each test specimen to obtain information pertinent to the development of an incremental strain relationship. Instrumentation included both internal and external items such as strain gages, linear potentiometers and string potentiometers. Detailed information regarding the placement and type of instrumentation can be found in an attachment to this report with the construction drawings.

Strain gages were placed on two strands of each tendon along the length of the tendon in order to gain information regarding the distribution of strains along the member. Additionally, two small diameter reinforcing bars were placed within each main bond segment with strain gages along the length to investigate the transfer of forces within the segment. Surface mounted strain gages were also placed on each face of the main tendon bond segments.

A series of three linear potentiometers were installed across the joint with gage lengths of 6, 12 and 24 inches on both the top and bottom of the segment. Linear potentiometers were also installed along the height of the loading blocks to determine if

any rigid body deformations occurred at the loading ends. String potentiometers were installed at each corner of the loading blocks for total segment deformation determinations. Additionally, the actuator forces and displacements were recorded.

#### 2.2.4 Loading Protocol

The testing specimens were physically separated using four 500-kip actuators. These actuators were controlled in displacement control and set to hold the displacement at a specified joint opening as determined using the average of the top and bottom 6 inch linear potentiometers. After reaching the specified joint displacement, the actuators were brought back to a zero force state thereby allowing residual displacements to occur. The target joint opening was set to increase with each cycle in accordance with the following target openings: 0.3 mm, 0.5 mm, 0.8 mm, 1.2 mm, 1.8 mm, 3 mm, 5 mm, 8 mm, 12 mm, 18 mm, 30 mm, 45 mm and 60 mm. A figure of the system loading protocol is shown in Figure 3.

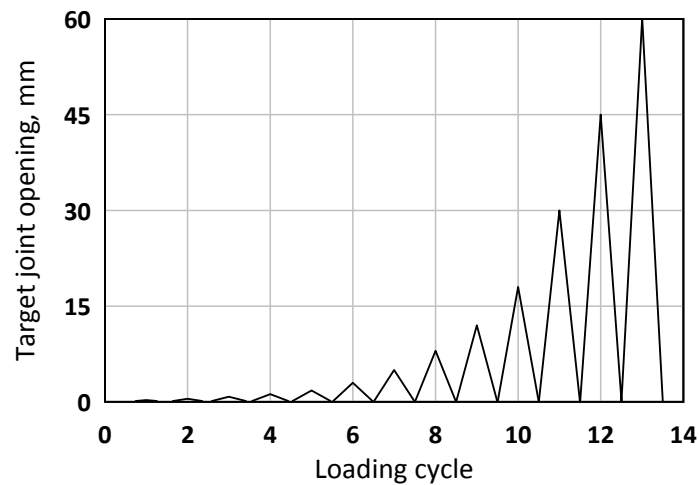


**Figure 3 Loading protocol**

#### 2.2.5 Material Properties

Material properties were determined for concrete and steel items based on testing at the UCSD lab or from manufacturer's mill certifications. A summary of the mild reinforcement properties as provided by the rebar fabricator are shown in Table 2.

**Table 2 Mild reinforcement properties**

<i>Item</i>	<i>Yield Stress (ksi)</i>	<i>Ultimate Strength (ksi)</i>	<i>Fracture Strain</i>
No. 4	69.3	98.0	0.160
No. 5	66.0	94.0	0.150

The 0.6 in. strands had a ultimate tensile strength of 284.4 ksi and a strain at the peak tensile force of 5.2%. Figure 4 plots compares the measured stress-strain relationship measured for the strands and the analytical relationship calibrated using a Ramberg-Osgood equation (Mattock, 1979) given by equation 2-1:

$$f_p = 29,000 \left( 0.0127 + \frac{1 - 0.0127}{(1 + (107.45 \varepsilon_p)^9)^{1/9}} \right) \quad 2-1$$

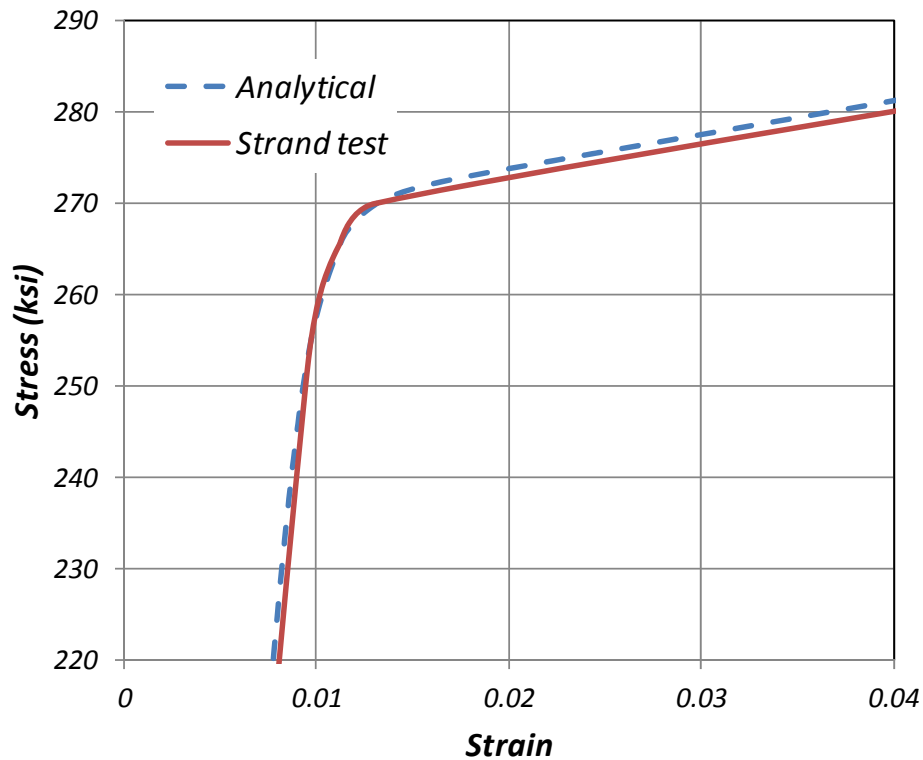


**Figure 4 Strand measured and analytical stress-strain relationship around the yield point**

The concrete properties and grout properties for each specimen are shown in Table 3. Properties for the cementitious materials were determined based on the average of three cylinder breaks under uniaxial compression on the day of the specimen testing. It

is notable that the compressive strength obtained for the ASBI grout in test specimen 2706-1 was much lower than that for the other two test specimens,

**Table 3 Day of test cementitious material properties**

<i>Specimen</i>	<i>Concrete Strength (ksi)</i>	<i>Grout Strength (ksi)</i>
2706-1	9.3	5.3
2706-2	9.5	9.0
1506-1	10.2	8.4

### **2.3 Experimental Results**

#### **2.3.1 Visual Performance**

All the three tests show very similar visual behavior. A large vertical crack developed adjacent to the midspan joint and large deformations occurred in along this crack, as expected. These cracks developed not at the joint itself, which had been epoxy-coated but in its immediate vicinity. Eventually the tendons fractured at this crack. Vertical and bond split cracks were also see along the segments themselves. A close up of the large crack and the smaller segment cracks is shown in Figure 5, while Figure 6 shows a close up of the failure of the tendon in unit 2706-1.

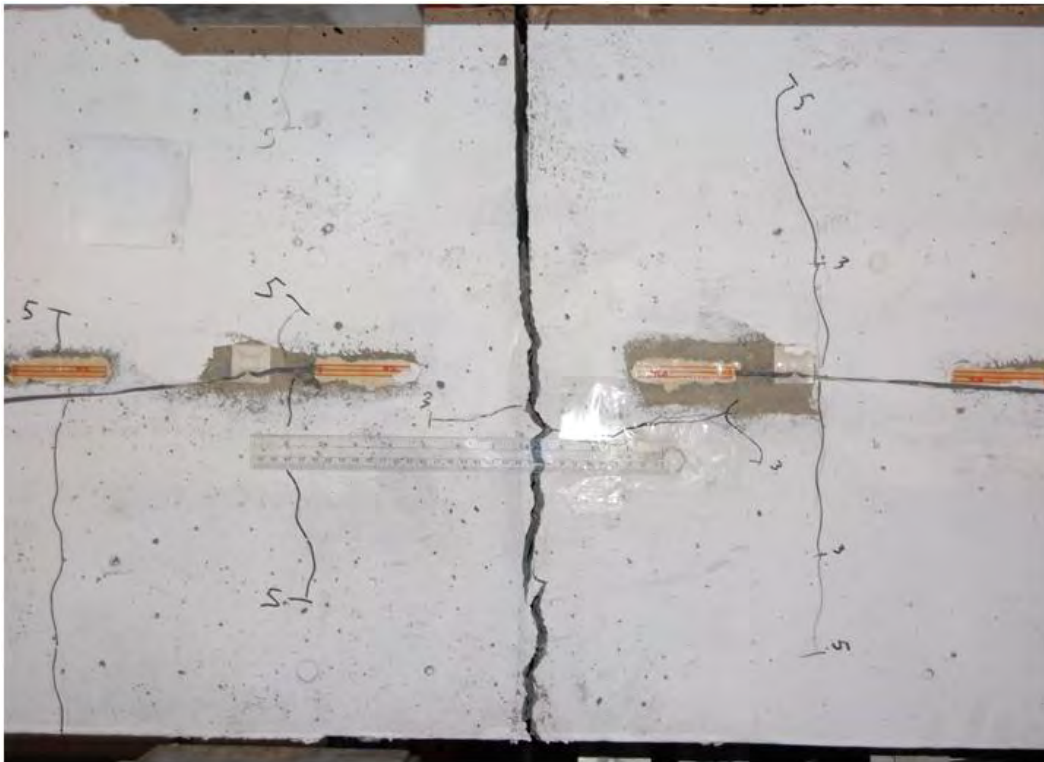


**Figure 5 Cracking in the midspan region of unit 2706-1**



**Figure 6- Close up failure at midspan of unit 2706-1**

To support the strain readings, that became erroneous as the tests progressed, Unit 2706-1 was sliced with a diamond saw to obtain evidence of the slippage of the strands along the length of the segments. Photos of the different sections are shown in Figure 7. The distance listed in each photo is that measured from midspan. Each photo shows the location of the strands and of some of the mild steel reinforcement. It was very surprising to observe that strand-grout slip appeared to have been very limited and only in the segment closest to the midspan joint (see the right hand side of the duct the photo taken at 4 in. (100 mm) from midspan). A number of radial cracks were observed throughout, suggesting that beyond 13.8 in. (350 mm) the duct acted as a single entity, with no slip noted between the individual strands and the surrounding grout.

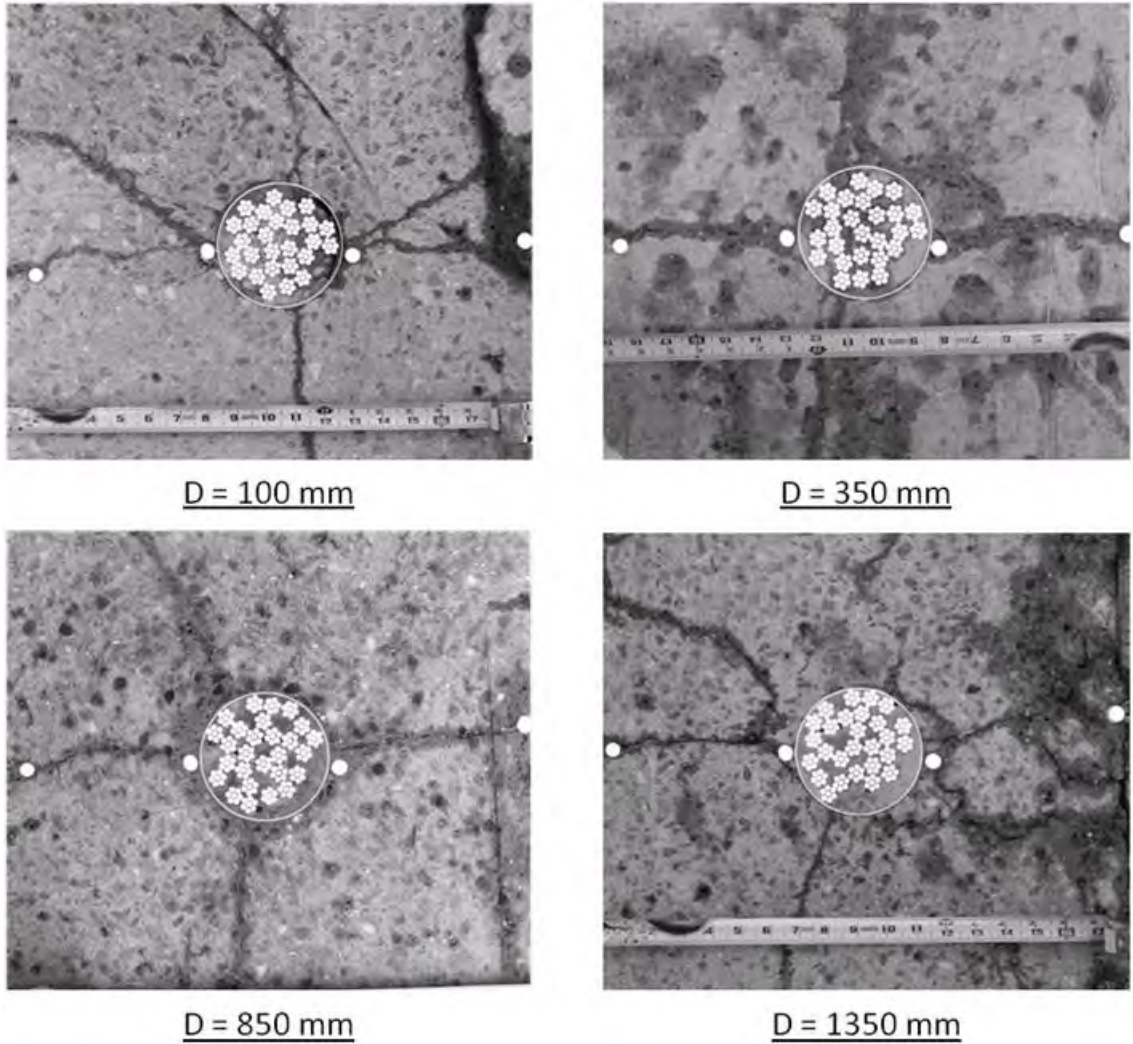


**Figure 7- Slices of Specimen 2706-1 after testing**

### 2.3.2 Axial Force-Axial Displacement Response

The axial displacements in the test units were recorded with string potentiometers along the span of 204 in. (5180 mm) and with linear potentiometers along 6, 12 and 24 in. (152, 305 and 610 mm) centered in the plane of the joint. Figure 8 plots the recorded displacements versus recorded axial force for the three units. The 6 in. and 12 in. displacement transducers in units 2706-2 and 1506-1, respectively, malfunctioned and their data is not presented in Figure 8.

Experimentation of Precast Concrete Blocks

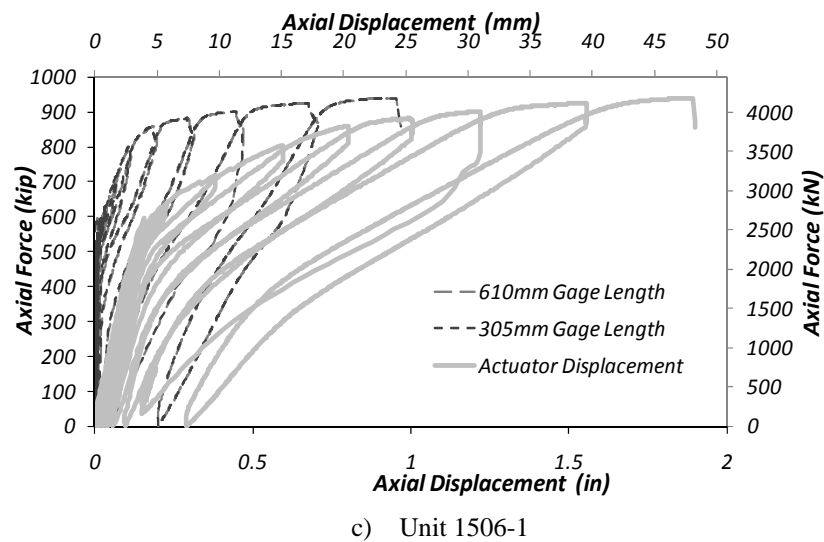
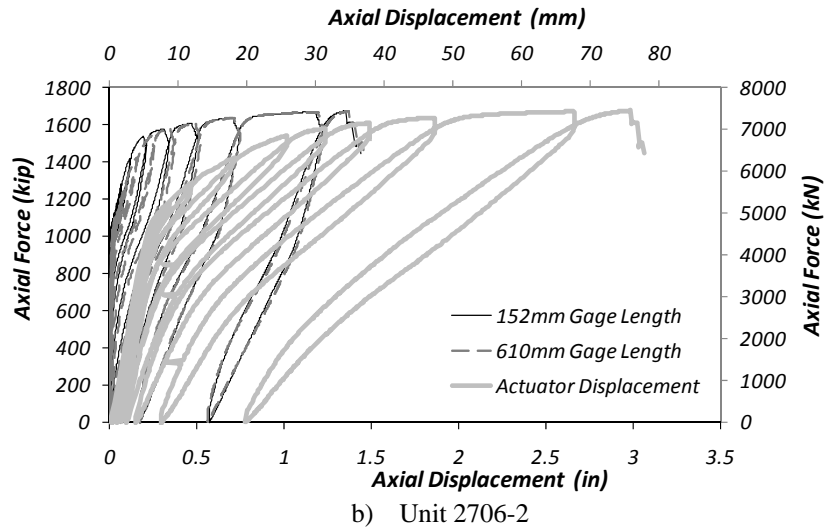
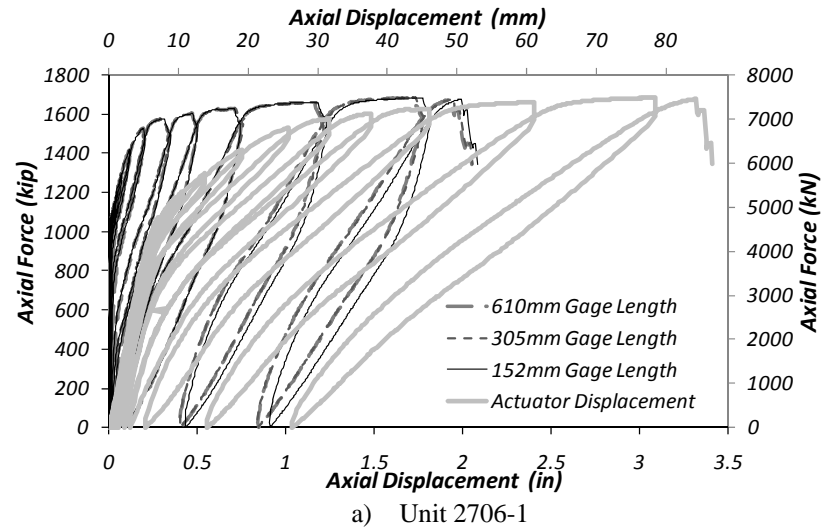


Figure 8 Recorded axial force –axial displacement responses

In general, the three gauge lengths showed similar displacements, suggesting that they all measured the midspan segment joint crack with little influence from strain in the adjacent concrete. One exception to this general observation can be seen in the measurements from test unit 2706-1 (see Figure 8a) for displacements greater than 1 inch, where the 6 inch gage length measured the largest motions, while the 24 inch gage length measured the smallest. This behavior is due to the fact that a splitting crack altered the location of the instruments with 6 and 12 inch gage lengths such that they were no longer taking measurements parallel to the member, thereby increasing their recorded measurements.

Another exception to the general observation mentioned above, is in the measured displacements of the 6 and 24 inch gage length instruments of test unit 2706-2 (see Figure 8b). At displacements below about 0.5 inches, the 24 inch gage length measured noticeably larger displacements than the 6 inch gage length, but as the displacements increase, these measurements converged. This response was likely due to a crack located between the two instruments. At small joint openings, the strain accumulated at this crack and was measured only in the 24 inch gage length instrument. At large joint openings, the debond mechanism is more fully developed, and the strain accumulated in the segment joint, rather than the adjacent crack, and was measured by both instruments.

By far, the largest axial displacements were recorded by the string potentiometers near the actuators, which integrated all the axial strains along the 204 inch test region. The axial displacements at failure recorded by the string potentiometers were 3.31, 2.97 and 1.77 inches for units 2706-1, 2706-2 and 1506, respectively. From this point of view the two 2706 test units showed very similar ultimate displacements, indicating that the tendon's grout has little influence in the ultimate displacement. Unit 1506 failed at a significantly smaller axial displacement than the 2706 test units. This is an indication that mild steel reinforcement constrained this unit further than the 2706 test units and that the tendon size plays a strong role in the debonding characteristics of multi-strand tendons.

It should be noted that the 6 inch gauge length displacement transducers in the 2706 test units measured quite different maximum joint openings at fracture: 1.97 inch for unit 2706-1 and 1.34 inches for unit 2706-2. However the backbone curves are virtually identical to each other (see Figure 9), which suggests that the tendon debond behavior is similar. The difference in maximum joint opening at fracture is likely due to variability in the ultimate strain of the strands. It is interesting to note that, based on the size of the unloading and reloading loops, the 2706-1 test unit dissipated more energy than the 2706-2 test unit. Furthermore, the 2706-1 test unit exhibited a smaller residual displacement for at a given load cycle. This is particularly evident in the 30 mm load cycle (see Figure 8).

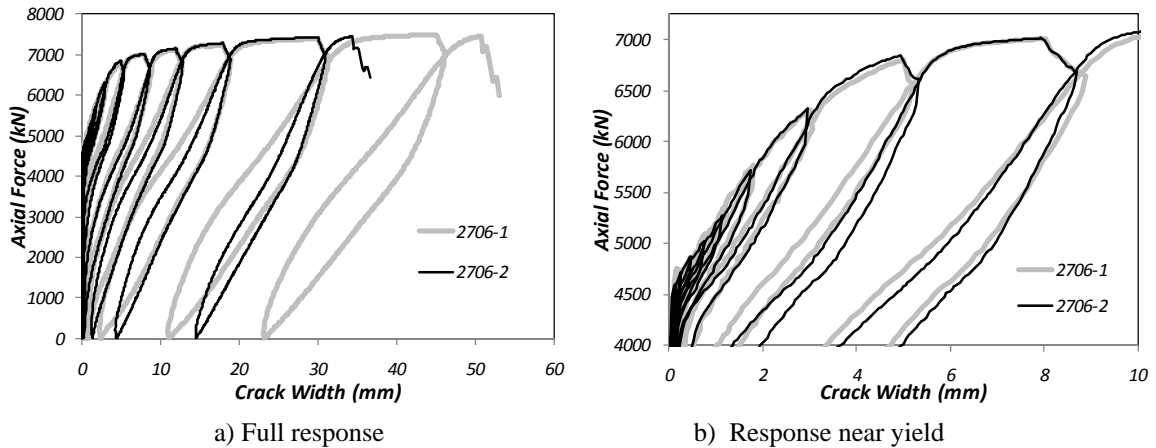


**Figure 9 Axial force vs. 6 inch gage length displacement responses of the 2706 test units**

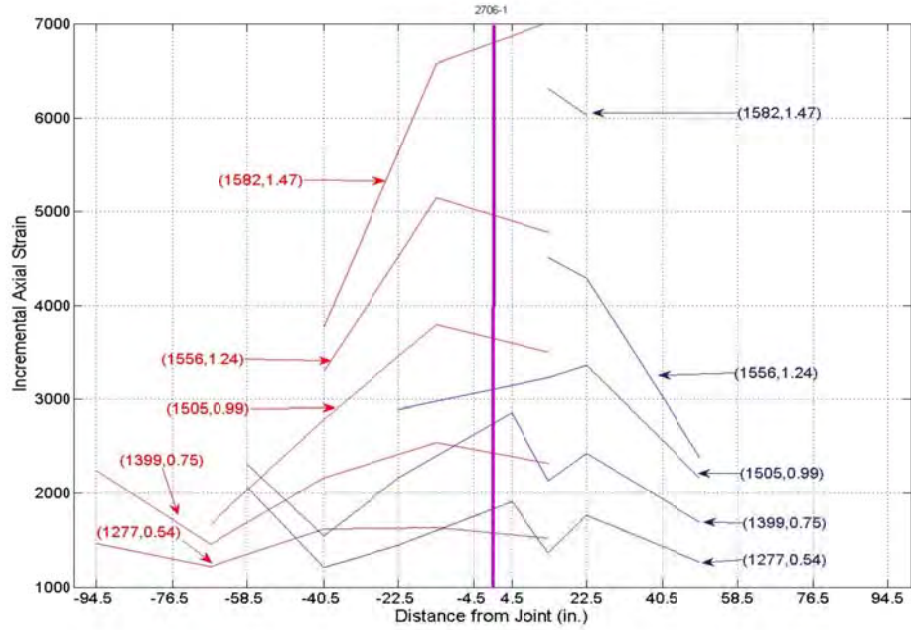
The average incremental axial strains in the post-tensioned blocks outside the 24 inch region near the segment joint were 0.74%, 0.88% and 0.56% in units 2706-1, 2706-2 and 1506, respectively. These strains were calculated based on the ultimate displacement measured over the entire 204 inch test region, minus the axial displacement measured by the 24 inch gauge length linear potentiometers, divided by 180 inches (=204 – 24 inches). Adding these average incremental strains to the prestrain locked into the tendon after setting the anchorages and grouting (approximately 0.6%) indicates that the average tendon strains were 1.36%, 1.50%, and 1.16% for test units 2706-1, 2706-2 and 1506, respectively. Note that all these strains are larger than the yield strain of 1.0%, indicating that the tendons yielded along the full length of the testing region prior to fracture at the segment-to-segment joint.

### 2.3.3 Tendon Strain Readings

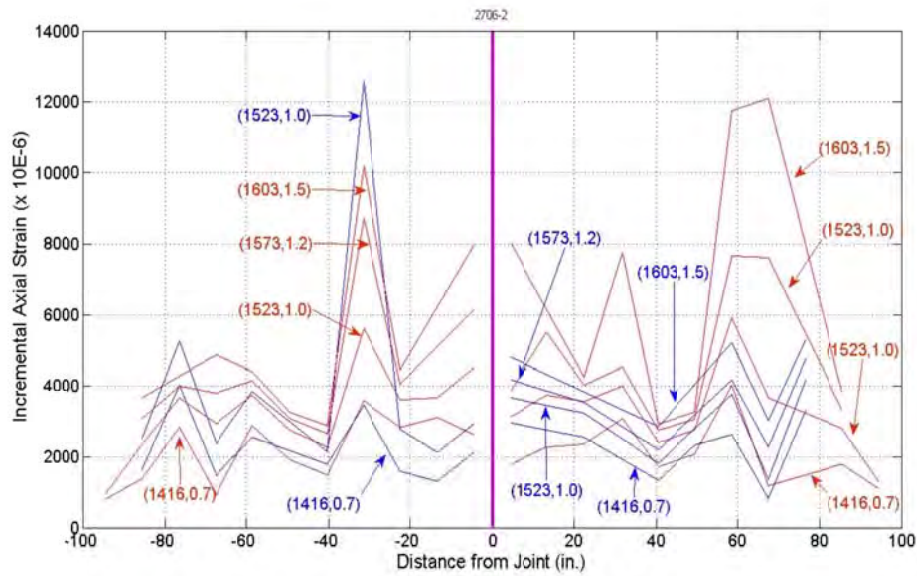
Strain gauge readings were very unreliable in general. In anticipation of damaged strain gages on the tendons, strain gages were placed along reinforcing bars next to the duct and on the concrete surface. Some tendon strain gages worked fine up to intermediate strain levels, but became unreliable at higher applied axial displacements, possibly due to elongation in the lead wires caused by tendon-to concrete slip, particularly in test unit 1506-1. The last set of reliable readings was obtained at about one-half the ultimate displacement. Figure 10 plots the tendon strains of two strands in the tendon of each unit at different locations and at different stages during the tests. For identification purposes readings are labeled with the tendon force as well as with the overall axial displacement obtained over the 204 in. span. These strains are considered “reliable” after being examined comprehensively for strain gage delamination or damage. Tendon strain readings for unit 2706-1 show clearly that there is no uniform strain penetration of the tendon inside the post-tensioned blocks, which is the cause of local bond-slip. Strain readings for Units 2706-2 and 1506-1 show large strain peaks in the

Experimentation of Precast Concrete Blocks

tendon at a significant distance away from the midspan joint, but such strain were no associated with large cracking in these regions, for which it can be presumed there was significant tendon-to-concrete slip there.

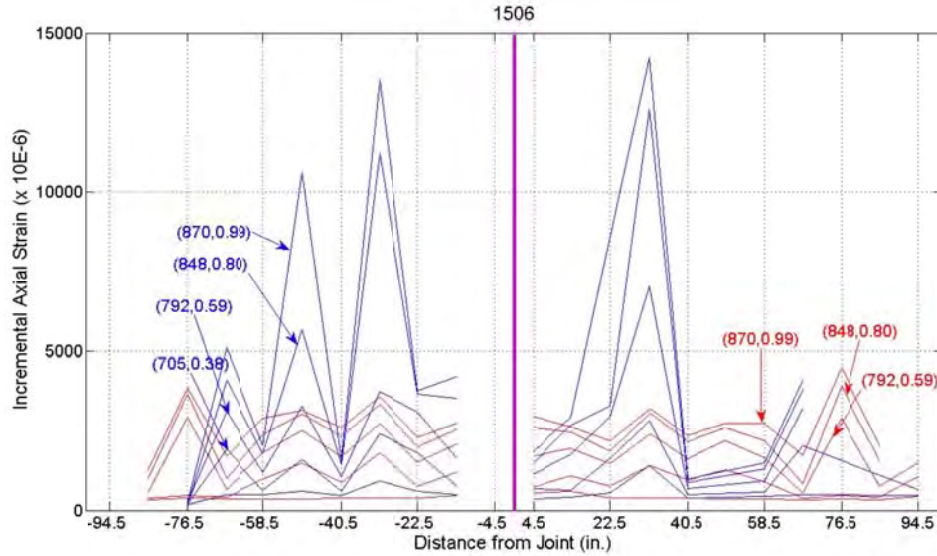


a) Unit 2706-1



b) Unit 2706-2

Figure 10 Tendon strains at different locations and at different stages during the tests



c) Unit 1506-1

Figure 10 Tendon strains at different locations and at different stages during the tests (cont.)

### 2.3.4 Tendon Stress/Strain - Total Segment Displacement Relationship

Figure 11 shows the total segment displacement as a function of tendon stress and strain. The 2706 test units behaved in a similar manner and the 1506 test unit showed smaller displacements for the same stress or strain. This figure indicates that for the same amount of mild steel reinforcement in the member, the size of the tendon plays an important role in estimating the overall segment displacement.

It is important to note that Figure 11b was generated using the stress-strain model of the PT strands described in Equation 1.

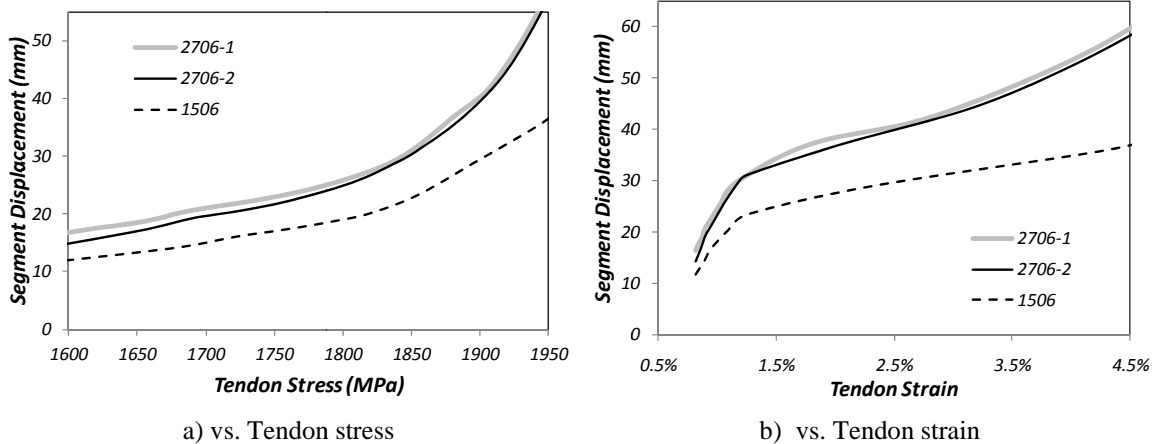


Figure 11 Total Segment Displacements

### 2.3.5 Tendon Stress/ Strain - Crack Width Relationship

Figure 12 shows the segment joint crack width as a function of tendon stress and strain. The 2706 test units behaved in a similar manner and the 1506 unit showed smaller crack widths for the same stress/strain. This figure indicates that, for the same amount of mild steel reinforcement in the member, the size of the tendon plays an important role in estimating the crack width at a segment joint.

The crack widths were defined based on the measurements from the 12 mm gauge length for test units 2706-1 and 1506 and as the average of the 6 and 24 inch gage lengths for test unit 2706-2. Recall, in unit 2706-2, one of the 12 inch gage potentiometers malfunctioned and rendered the data recorded with such gage length unreliable. As it can be seen in Figure 8, the joint opening recorded over different gauge lengths was very similar in all the test units, and only differed slightly in unit 2706-2 at a joint opening below 0.5 inches (13 mm).

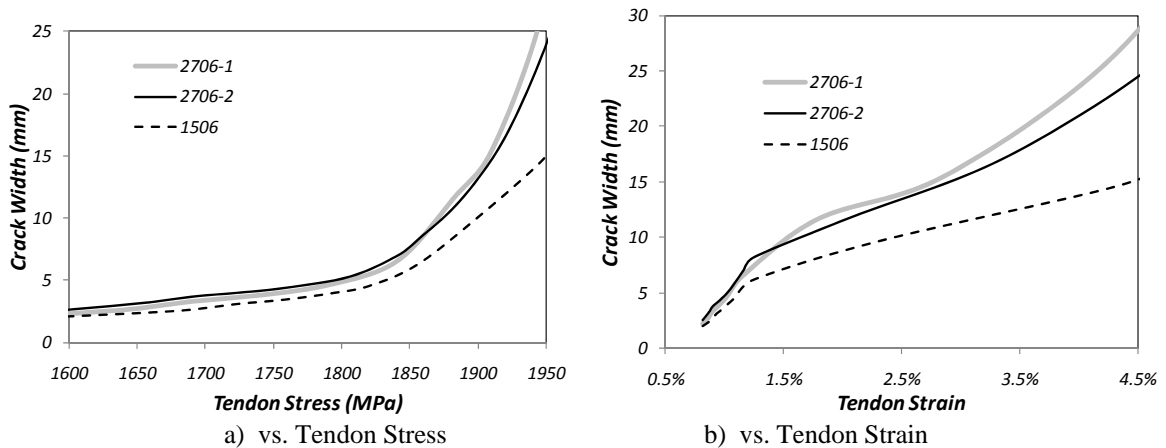


Figure 12 Segment Joint Crack Width

### 2.4 Equivalent Unbonded Length

The tendon equivalent unbonded length was determined for different stages during the testing of each of the test units. The equivalent unbonded length was calculated as one-half of the crack width, as defined above, divided by the tendon incremental strain. Given the fact that tendon incremental strains were not reliably measured, the strain was back-calculated using the modified Ramberg-Osgood relationship (Mattock, 1979) calibrated for the stress-strain relationship of the strands. The tendon stress was calculated as the force measured in the test divided by the tendon area.

Figure 13 plots the equivalent unbonded lengths computed for units 2706-1, 2706-2 and 1506 at various tendon strains. Recall that the locked in strain after stressing and losses was approximately 0.6%, thus an incremental strain of 0.4% represents tendon

yield and an incremental strain of 0.6% represents “full yield” of the tendon. This figure indicates that the equivalent unbonded lengths are essentially constant up to an incremental strain of 0.8%. The equivalent unbonded length for the 2706 test units are approximately 33% larger than that of the 1506 test units.

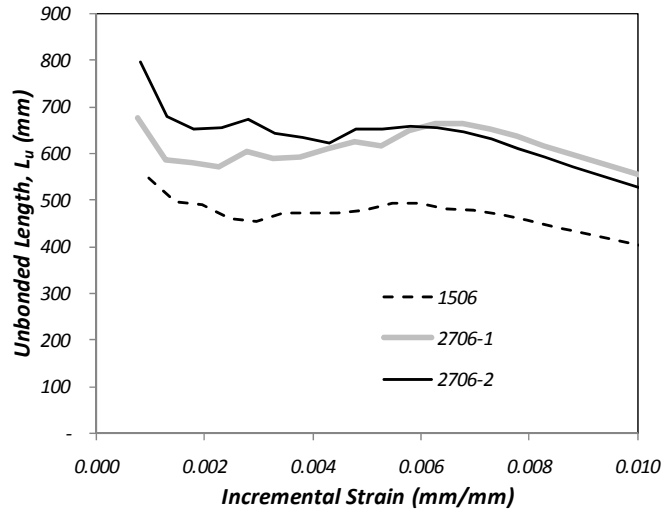


Figure 13 Tendon Equivalent Unbonded Length

Figure 14 shows the tendon equivalent unbonded length normalized by the square root of the tendon cross section area. The average value for all test units between incremental strains of 0.1% and 0.8% is 10.3 and all test units are within 10% of the average. Based on this figure it is clear that, at the onset of the “full yield” limit-state, the equivalent unbonded length can be represented as:

$$L_u = 10.3\sqrt{A_{PT}} \quad 2-2$$

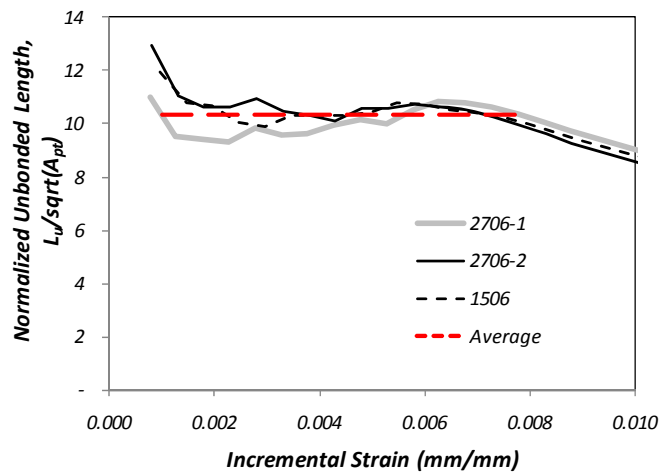


Figure 14 Normalized Equivalent Unbonded Length

Eqn. (1) is valid up to full yielding of the tendon (i.e. tendon strains of 1.2%) grouted in a metal duct and in a segment detailed with a 0.45% longitudinal reinforcement ratio and is appropriate for modeling since full yielding of the tendon is the most critical limit state at segment joints. Segments detailed with a longitudinal reinforcement ratio less than 0.45% will likely have an equivalent unbonded length slightly larger than that estimated by Eqn. (1). Furthermore, the equivalent unbonded length of multi-strand tendons is related to the development length of the mild longitudinal reinforcement in the section (as indicated in Figure 1). Thus any parameter that decreases the development length of reinforcement will also decrease the equivalent unbonded length.

## **Chapter 3: STANDARD SECTIONS**

### ***3.1 Objective***

To develop a catalog of standard cross sections for precast segmental bridge superstructures with span lengths from 300 to 500 feet.

### ***3.2 Introduction***

It was believed that cost savings could be achieved by developing a catalog of standard superstructure cross sections for precast segmental bridges. This will encourage and simplify the use of segmental bridges in seismic regions of the United States by standardizing the equipment necessary for fabrication of the superstructure and allow for reuse of precast forms instead of purchasing/fabricating new ones for each project.

The standard sections were developed in conjunction with the American Segmental Bridge Institute (ASBI) for span lengths from 300 to 500 feet and organized in 50 foot increments. The existing ASBI standard sections were used as a starting point. Data on existing bridges (see Table 4) with span lengths of interest was collected. The first draft of the standard sections was completed and sent to Caltrans and industry partners for review. UCSD received comments on the first draft and was in the process of addressing those comments when Caltrans issued a stop work order on July 31, 2008, due to state budgetary concerns.

### ***3.3 Discussion***

During the meeting with Caltrans on October 1, 2009 in Sacramento, CA, it was decided that no additional work on this task was required. This decision was made based on lack of interest in the industry for a catalog of standard sections. The first draft of these standard sections is included in the appendix as well as the review comments from Caltrans and industry professionals.

Standard Sections

**Table 4 Existing Segmental Bridges used to Develop the Standard Sections**

<b>Bridge</b>	<b>Br. Location</b>	<b>Span (ft)</b>	<b>Midspan Section Depth</b>	<b>Pier Section Depth</b>
San Francisco-Oakland Bay Bridge Skyway	Oakland, CA	525	18'-1"	29'-6"
Smart Rd. Bridge (Wilson Creek Bridge)	Virginia	472	12'-2"	31'-2"
Wando River Bridge	Columbia, South Carolina	400	10'-3"	20'-0"
Tsable River Bridge	Victoria, BC	387	11'-10"	21'-8"
Hobucken Bridge	North Carolina	381	7'-6"	18'-0"
Putnam Bridge	Marietta, Ohio	362	8'-2"	18'-1"
Hathaway Bridge	Orlando, Florida	330	10'-0"	18'-0"
SH 23 over Lake Sakakawea	North Dakota	316	7'-7"	16'-7"
Confederation Br. - E. Approach	Northumberland	305	9'-10"	16'-7"
Escatawpa River Bridge	Jackson Co, Miss.	300	7'-0"	14'-0"
Otay River Bridge	San Diego, CA	297	9'-10"	16'-3"
Interstate H3	Hawaii	280	8'-0"	16'-0"
Baldwin Bridge	Connecticut	275	11'-8"	11'-8"
Roosevelt Bridge	Florida	260	11'-0"	12'-0"
Natchez Trace	Tennessee	246	7'-6"	13'-10"
Sunshine Skyway - Approach	Florida	240	14'-0"	14'-0"

## Chapter 4: GENERAL SEISMIC DESIGN FRAMEWORK

The information presented in this chapter forms the basis for the complete design recommendations shown in Chapter 7 and was reviewed by both Caltrans in industry professionals.

### 4.1 Objectives

The primary objectives were to:

- Address seismic design issues specific to precast segmental construction that are not included in the Caltrans Seismic Design Criteria (Caltrans, 2009).
- Address the effects of vertical earthquake demands on segmental bridges to ensure the desired performance of the bridge is achieved.
- Address the effects of time dependent stress states in the design process to ensure the desired performance of the bridge is achieved.

### 4.2 Proposed Seismic Design Framework for Segmental Bridges

#### 4.2.1 Performance Based Seismic Design Framework

A two-level performance based seismic design (PBSD) approach is prescribed in which different performance limits are required for different earthquake hazard levels as shown in Table 5. The return period varies for these earthquake events depending on the bridge classification and is ultimately left up to the bridge owners. Common FEE design levels range from 100 to 500 years, while SEE design levels often range from 1000 to 2500 years.

Table 5 Performance Objectives and Hazard Levels

Bridge Classification	Functional Evaluation Earthquake (FEE)	Safety Evaluation Earthquake (SEE)
‘Ordinary’	No joint opening	No collapse
‘Important’	No joint opening	Non-linear elastic segment joint response

For the lower level functional evaluation earthquake (FEE), the superstructure shall be designed such that the segment joints remain closed. For the safety evaluation

earthquake (SEE), the design approach varies depending on the classification of the bridge. ‘Ordinary’ bridges shall be designed for a no collapse criteria with a simple collapse mechanism check and ‘Important’ bridge structures shall be designed to remain undamaged. The superstructure of ‘Important’ bridges should be designed to allow joint opening but ensure that the PT tendons remain elastic, i.e.,  $f_{pt} < 0.78f_u = 210$  ksi, and that the unconfined concrete does not crush, i.e.,  $\epsilon_c < 0.003$ , where  $f_{pt}$  is the stress in the prestressing tendon,  $f_u$  is the ultimate stress of the prestressing tendon, and  $\epsilon_c$  is the concrete strain. Different design approaches are used to streamline the design process and minimize design costs where appropriate.

It should be noted that the proposed seismic design framework is not intended for seismic design considerations during construction.

#### 4.2.2 Capacity Design

Capacity design principles are essential to control the seismic performance of the column-superstructure connection and to prevent permanent joint opening and yielding of the PT tendons adjacent to the piers. Capacity design of the superstructure must account for all sources of column overstrength. The overstrength capacity of a column is primarily due to higher than expected material strengths, strain hardening of the reinforcement, and higher than expected axial loads on the column. It is important to note that capacity design principles that aim to protect the superstructure based on column overstrength moments will have no effect near midspan, thus capacity design principles are insufficient on their own.

#### 4.2.3 Longitudinal Push-Over Analysis

In addition to the requirements for capacity protected components (SDC Section 3.4), a longitudinal push-over analysis shall be performed for all bridges regardless of importance classification. The superstructure shall be designed for flexural to remain essentially elastic when the columns reach their flexural overstrength capacity. Column flexural overstrengths shall be determined based on the requirements of the Caltrans Seismic Design Criteria Section 4.3.1.

#### 4.2.4 Vertical/Horizontal Earthquake Load Combinations

The peak vertical and horizontal earthquake demands are not likely to occur simultaneously due to the differences between the periods of the dominant modes and between the characteristics (i.e. frequency content and arrival time) of the vertical and horizontal input motions. Thus, it is reasonable to consider the two effects independently. The horizontal earthquake combinations are addressed adequately in the Caltrans Seismic Design Criteria (Caltrans, 2009) and will not be discussed herein. Vertical earthquake

load combinations shall include considerations for the pre-earthquake stress-state of the superstructure (see Section 4.2.5).

#### 4.2.5 Vertical Earthquake Load Combinations

The superstructure dead load demands at the end of construction and after the majority of creep and shrinkage has occurred, as determined from a full longitudinal construction staging analysis, shall be combined with the vertical earthquake demands (see Section 4.2.7) for all bridge classifications and earthquake demand levels, except for the SEE design level of “Ordinary” bridges (See Section 4.2.9). The vertical earthquake load combinations are as follows.

$$DL_{EOC} \text{ \& } EQ_{Vert} \qquad \qquad \qquad \mathbf{4-1a}$$

$$DL_{CS} \text{ \& } EQ_{Vert} \qquad \qquad \qquad \mathbf{4-1b}$$

where,  $EQ_{Vert}$  are vertical earthquake demands and  $DL_{EOC}$  and  $DL_{CS}$  are dead load demands at the end of construction and after the majority of creep and shrinkage has occurred, respectively.

#### 4.2.6 Horizontal Earthquake Load Combinations

The horizontal (i.e. longitudinal and transverse) earthquake load combinations outlined in Section 2.1.2 of the Caltrans Seismic Design Criteria (SDC), are considered appropriate for segmental bridges. Thus special considerations are not provided herein.

#### 4.2.7 Vertical Earthquake Demands

The vertical earthquake ground motion can significantly increase the demands on segmental superstructures and shall be considered in the design process. The method to estimate the vertical earthquake demands depends on the design level (i.e., FEE or SEE) and the importance classification of the bridge as summarized in Table 6. As discussed in Section 4.4 of this report, 2% damping shall be used for elastic modal analysis as the superstructure is required to remain uncracked, thus minimal energy dissipation will occur. Similarly, 2% damping shall be specified in non-linear time history analysis as the structure will remain uncracked, except at discrete locations where non-linear elastic elements will be defined.

**Table 6 Modeling Approach for Vertical Earthquake Demands**

<b>Bridge Classification</b>	<b>Functional Evaluation Earthquake (FEE)</b>	<b>Safety Evaluation Earthquake (SEE)</b>
<b>‘Ordinary’</b>	Elastic Modal Analysis	Check Collapse Mechanism
<b>‘Important’</b>	Elastic Modal Analysis	Non-Linear Time History Analysis

#### 4.2.8 FEE Design Level of ‘Ordinary’ Bridges

The vertical earthquake demands for the FEE design level of ‘Ordinary’ bridges shall be determined from a vertical modal analysis based on a design spectrum per Section 4.5.3. Sufficient number of modes shall be considered in the modal analysis to capture a minimum of 90% of the superstructure bridge mass in the vertical direction.

These vertical earthquake demands shall be combined with dead load demands and consider the effects of creep, shrinkage and post-tensioning using the load combinations described in Section 4.2.5.

#### 4.2.9 SEE Design Level of ‘Ordinary’ Bridges

Designers shall satisfy the no collapse criteria for ‘Ordinary’ bridges by checking the capacity of all vertical collapse mechanisms relative to the vertical design spectrum. Designers shall determine the capacity of the collapse mechanism for both interior and end spans based on Equation 4-5 (see Section 4.4.3). The capacity,  $S_c$ , must be greater than the vertical peak ground acceleration,  $PGA_v$ , in the vertical design spectrum.  $PGA_v$  is used as the basis of comparison to simplify the approach and because, on average, the spectral accelerations of the dominant vertical modes, which are typically greater than 0.3 seconds, will likely be equal or less than  $PGA_v$ .

Pre-earthquake stress-states do not need to be considered in the capacity of the collapse mechanisms as they will not significantly affect the ultimate capacity of the superstructure.

#### 4.2.10 FEE Design Level of ‘Important’ Bridges

The vertical earthquake demands for the FEE design level of ‘Important’ bridges shall be determined from a vertical modal analysis as outlined in Section 4.2.8, or from a full 3D non-linear dynamic time history analysis as discussed in Section 4.2.11. Time history analysis is considered to be more realistic than modal analysis and is also considered appropriate for the FEE design level.

#### 4.2.11 SEE Design Level of ‘Important’ Bridges

The vertical earthquake demands for the SEE design level of ‘Important’ bridges shall be determined from 3D non-linear dynamic time history analysis, based on horizontal and vertical ground motions per Section 4.5.2. The superstructure shall be modeled with non-linear elastic moment-rotation hinging elements at a minimum of two segment joints adjacent to the piers and three segment joints near midspan (Figure 15). The remainder of the superstructure may be modeled using elastic elements. The moment-rotation characteristics of each joint should be determined from local finite element models as outlined in Section 4.3.3. Extreme pre-earthquake stress-states of the segment joints must be considered based on the load combinations in Section 4.2.5. Thus, forces shall be applied across the non-linear segment joint members to calibrate the model to these extreme pre-earthquake stress-states.

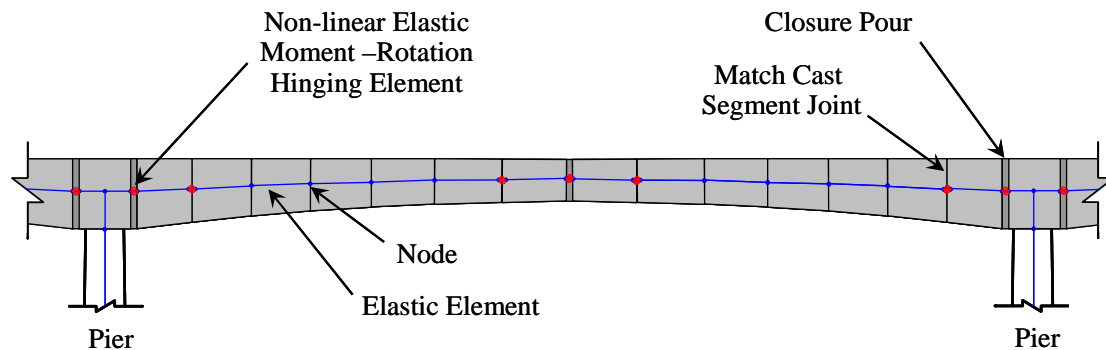


**Figure 15 Proposed Superstructure Modeling Approach for SEE Design Level of ‘Important’ Bridges**

### 4.3 Superstructure Segment Joint Capacity

The capacity of superstructure segment joints can be determined using a number of different methods, such as simple hand calculations, moment-curvature analyses or detailed local non-linear finite element models. These different methods are discussed below.

Simple hand calculations can generate very good moment capacity estimates and should always be used as a check of other methods. Detailed hand calculations can also account for the unbonded length of PT tendons and can be used to approximate the rotation capacity, although the calculations can become cumbersome when multiple tendons, with different jacking loads, are used.

Moment-curvature analyses are advantageous because there are many readily available and easy to use programs with excellent graphical interfaces that can generate

accurate moment capacities. The disadvantage of this tool is that it cannot consider the unbonded length of the PT tendons. Thus, the rotation capacities will be incorrect.

Local non-linear finite element models of the superstructure segment joints are advantageous because they can simulate the unbonded length of the PT tendons and will produce the most accurate joint rotation capacities. The disadvantage is that they require significant effort to develop and should be calibrated with experimental data.

In summary, all methods should generate similar moment capacities at cracking, yield and ultimate. Moment-curvature analyses will not accurately estimate the rotation capacity because they do not account for the unbonded length of the PT tendons. Both local non-linear finite element models and detailed hand calculations are able to estimate segment joint rotation capacities.

#### 4.3.1 Segment Joint Capacity

#### 4.3.2 ‘Ordinary’ Bridges

Moment-curvature analysis shall be used to determine the moment capacity of the segment joints of ‘Ordinary’ bridges at cracking (i.e., joint opening) for the FEE design level, and at ultimate for the SEE design level. Expected concrete and pre-stressing material properties shall be used in these calculations as outlined in Section 3.3.1 of the Caltrans Seismic Design Criteria (Caltrans, 2009). The superstructure concrete should be treated as unconfined. The preload in the tendons shall be based on the expected tendon force at the end of construction and after considering losses due to creep, shrinkage and relaxation.

#### 4.3.3 ‘Important’ Bridges

The moment capacity of segment joints of ‘Important’ bridges shall be determined using detailed local non-linear finite element models based on the expected concrete and prestressing material properties per Section 3.2 of the Caltrans Seismic Design Criteria (SDC). These models must capture the non-linear characteristics of the extreme concrete fibers in both tension and compression. In addition, the model must capture the non-linear characteristics of the PT tendons with accurate estimates of the pretension forces. These models shall be subjected to monotonic rotational push analyses to determine the moment-rotation characteristics of the segment joints. Cyclic push analyses are not required, thus the hysteretic rules used for the concrete and PT members are unimportant. The unbonded length (see Section 4.3.5) of the PT tendons shall be determined based on Equation 2-2.

#### 4.3.4 Definition of Capacity Levels

Figure 16 shows a sample moment-curvature diagram of a superstructure segment joint for an ‘Ordinary’ bridge. The critical design moments are the nominal moment,  $M_n$ ,

and the ultimate moment,  $M_u$ . The nominal moment capacity,  $M_n$ , shall be defined as the moment when the stress in the tendons reaches the limit of proportionality, defined as a stress of 210 ksi. The ultimate moment shall be determined based on a reduced ultimate prestressing steel strain,  $\epsilon_{ps,u}^R$ , of 0.03 or the strain in the extreme compression fibers  $\epsilon_c$  reaches 0.003.

Figure 17 shows a sample moment-rotation diagram of a superstructure segment joint for an ‘Important’ bridge. The critical design parameters are the decompression moment,  $M_{dc}$ , and the elastic rotation limit,  $\theta_{el}$ . The elastic rotation limit shall be determined based on a concrete strain,  $\epsilon_c$ , of 0.003, or a stress in the ASTM A416 prestressing tendon,  $f_{pt}$ , of 210 ksi, whichever generates the smaller rotation.

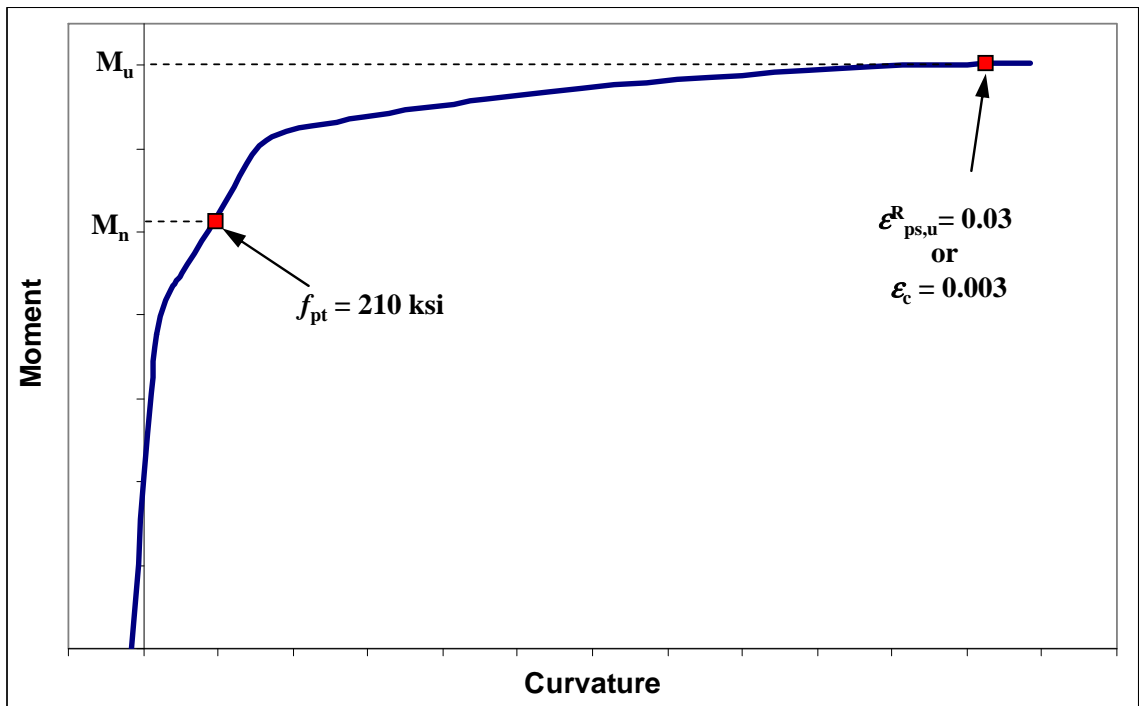


Figure 16 Sample Moment-Curvature Diagram for ‘Ordinary’ Bridges

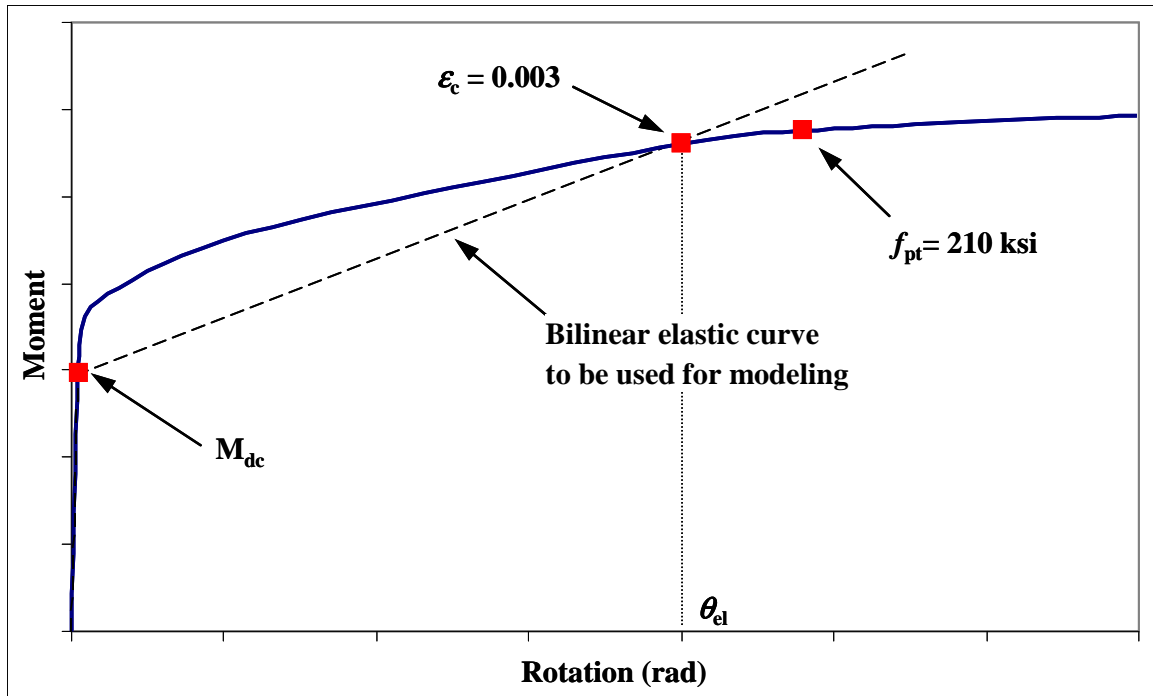


Figure 17 Sample Moment-Rotation Diagram for 'Important' Bridges

Figure 17 also indicates the bi-linear elastic curve to be used for the modeling of segment joints. The curve follows the gross section stiffness until the decompression moment is reached. At this point the curve will deviate towards the lesser of the point where the concrete strain reaches 0.003 or the tendon stress reaches 210 ksi.

The consequences of exceeding the various design parameters discussed above are outlined in Table 7.

**Table 7 Consequences of Exceeding Design Parameters**

<b>Design Parameter</b>	<b>Description</b>	<b>Consequences of Exceedance</b>
$M_{dc}$	Decompression moment zero compression stress in the extreme concrete fibers	No consequences if the section was previously uncracked. If section was previously cracked, the joint will open, creating a small gap that will likely close completely
$M_{cr}$	Cracking Moment $f_c = f_r$	Section cracks. Small gap will open, but will close completely
$\theta_{el}$	Elastic rotation limit $\epsilon_c=0.003$ or $f_{pt} = 210$ ksi	Begin to lose force in tendons, small residual cracks may occur
$M_u$	Ultimate Moment $\epsilon_{pt}=0.03$	Incipient collapse

#### 4.3.5 Flexural Bond Length and Unbonded Length of Tendons

As segment joints in a precast segmental bridge open, the strain in the PT tendons crossing the segment joints must increase to accommodate the deformations. The increased tendon strains penetrate into the segments and will cause debonding of the tendon strands within the grouted duct. This length is somewhat related to the flexural bond length (see Figure 18), except that in precast segmental bridges, the strain penetration can be more influenced by the presence of the mild steel reinforcement present in the segments, particularly at the bridge midspan. Recent research (Veletzos and Restrepo, 2009) has shown that the length of debonding significantly impacts the rotation capacity of precast segmental bridge joints, thus correctly determining this length is critical to accurately estimate the deformation capacity of segmental joints with bonded tendons.

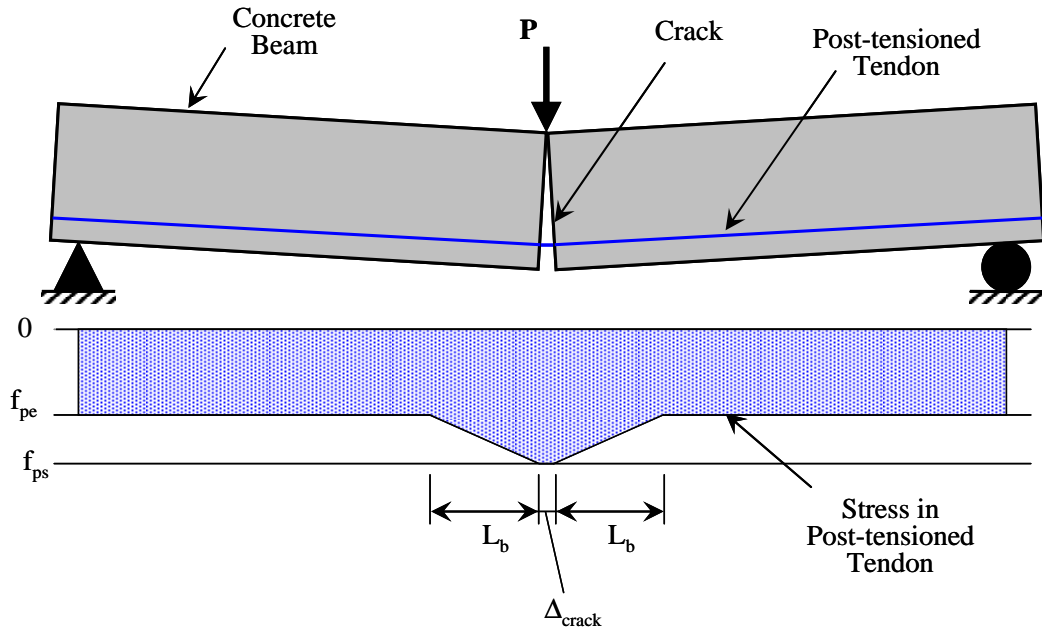


**Figure 18 Flexural Bond Length in Post-Tensioned Beams**

A gradual increase in the tendon stress along the flexural bond length, as shown in Figure 18, is very difficult to achieve in a detailed analytic simulations of segment joints. For simplicity, an equivalent unbonded length,  $L_u$ , is used as shown in Figure 19.

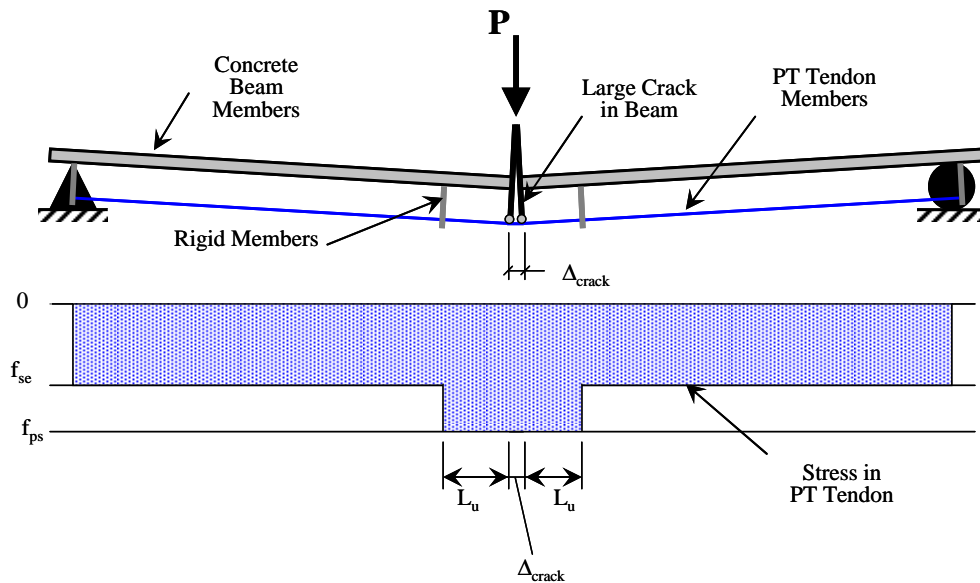


**Figure 19 Unbonded Length of Tendons across Segment Joints in Finite Element Models**

Barnes et al. (1999) gives a comprehensive and critical review of the research work leading to various equations for calculating the flexural bond length. A reasonable

estimate of the flexural bond length is the equation developed by Zia and Mostafa (1977) after extensive study of previous research.

$$L_b = 1.25(f_{ps} - f_{pe})d_b \quad 4-2$$

Where  $f_{ps}$  is the full design strength of post-tensioning strand,  $f_{pe}$  is the effective stress in post-tensioning strand and  $d_b$  is the diameter of the strand. This equation is applicable to seven wire strand and is based on an assumed bond stress of 200 psi.

Equation 4-2 forms the basis for the required development length for strands in various design codes in the United States (ACI, 2005; AASHTO, 2006). The primary difference being that the code equations were developed to estimate the upper bound development length, while Equation 4-2 was developed to approximate the average flexural bond length of the experimental data set.

NCHRP 12-60 (Ramirez and Russell, 2007) proposed a new design equation for the flexural bond length of pre-tensioned strands in high strength concrete.

$$L_b = \frac{225}{\sqrt{f'_c}} d_b \quad 4-3$$

Equation 4-3 is a function of concrete strength,  $f'_c$ , and strand diameter,  $d_b$ , only. Presumably the differential stress indicated in Equation 4-3 is assumed to be constant and is built into the proposed NCHRP 12-60 equations.

While Equation 4-2 and Equation 4-3 can give an estimate of the flexural bond length on either side of a segment joint crack, they were developed for a single seven wire strand and are inappropriate for multi-strand tendons. This is because the strands in a tendon tend to cluster together and act as a group. The effective bond surface of the group is not a simple multiple of the strand bond area, but can be either the surface area of the whole group, as shown in Figure 20, or the surface area between the duct and the surrounding concrete. Thus, multi-strand tendons may show a debond length that is not represented by either Equation 4-2 or Equation 4-3. Furthermore, flexural bond length equations derived from prestressed-only test beams with a relatively short shear span may not adequately represent the boundary conditions encountered in precast segmental bridges. The presence of minimum mild steel reinforcement, that is discontinuous at the segment ends and the very large shear span ratios are the reason for the lack of applicability of these equations. The experimental work described in Chapter 2 of this report provided experimental evidence for the development of an unbounded length equation for tendons.

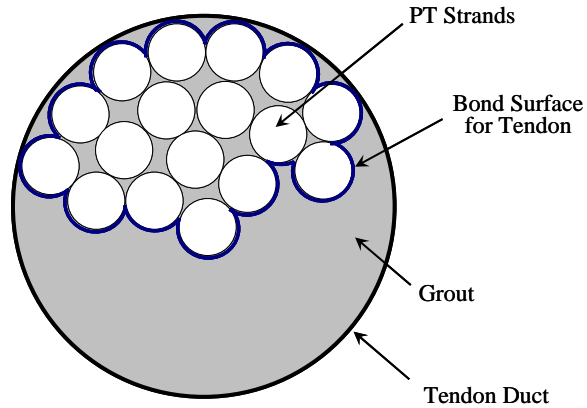


Figure 20 Bond Surface Area for PT Tendons

## 4.4 Vertical Earthquake Demand Modeling Approaches

### 4.4.1 Modal Analysis

Vertical earthquake demands can be approximated based on a vertical modal analysis using the complete quadratic combination (CQC) modal combination method (Clough and Penzien, 1993). Modal analysis is generally considered an acceptable tool for linear elastic structures only and thus is not appropriate if non-linear response in the superstructure is anticipated. The analysis shall be based on a vertical design spectrum with realistic vertical to horizontal (V/H) spectral ratios as discussed in Section 4.5.3. In addition, the vertical design spectrum shall be generated based on a 2% structural damping, not 5% damping that is commonly used. This is because modal analysis is only valid if the superstructure remains elastic and 2% damping is more appropriate for an elastic superstructure response since concrete cracking or other means of energy dissipation are unlikely, given the design objectives of the FEE event (see Section 4.2.7). Furthermore, bridge designers should ensure that 2% damping is specified in the structural analysis program they are using to perform the modal combinations.

### 4.4.2 Time History Analysis

Time history analysis is generally considered the most accurate way to estimate earthquake demands. The envelope value of three sets of spectrum compatible ground motions shall be used to estimate the seismic demands on the bridge. See Section 4.5.2 for a discussion on spectrum compatible ground motions. The damping model used in non-linear time history analysis can dramatically influence the results of the analysis. Thus, the damping model must be selected carefully. The goal of the capacity design principle is to limit inelastic response to specific locations in the bridge, thus structural damping is unlikely to occur outside of the plastic hinge regions of the column or at select superstructure joints that may open during a seismic event. Hysteretic energy

dissipation of these regions should be built into the model using non-linear members with appropriate hysteretic characteristics. For these reasons, 2% initial stiffness Rayleigh damping should be defined at frequencies where (i) the cumulative vertical modal mass exceeds 20% and (ii) the cumulative vertical modal mass exceeds 80%. The damping value at all dominant vertical modes shall be checked to ensure that these modes are neither overdamped nor underdamped. A dominant mode is defined as a mode with at least 20% mass participation. Damping of all dominant modes must be greater than 1% and must not exceed 5%. The specified Rayleigh damping periods shall be adjusted to ensure these damping restrictions are achieved.

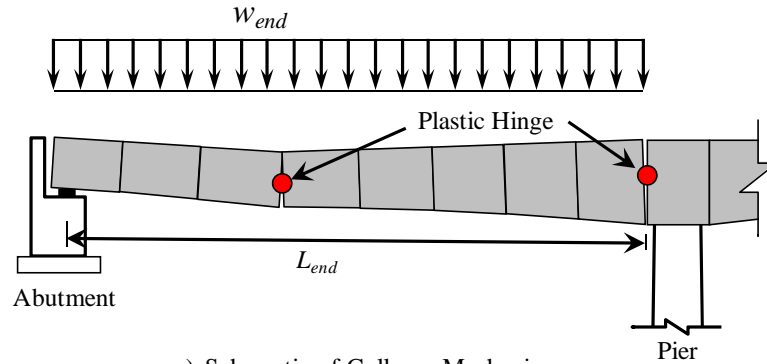
#### 4.4.3 Superstructure Collapse Mechanisms

The default seismic design requirement in California is a no collapse criteria. A check of vertical superstructure collapse mechanisms can be used as a means to satisfy this no collapse criteria. The most likely vertical collapse mechanisms for end and interior spans are shown in Figure 21 and Figure 22, respectively. The uniform distributed load,  $w_{end}$  and  $w_{int}$ , that will develop these collapse mechanisms are shown in Equation 4-4 for both end and interior spans.

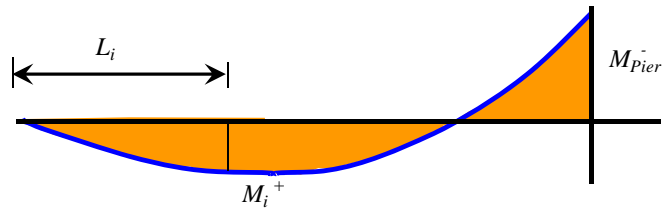
$$\text{End Spans} \quad w_{end} = \frac{8}{4L_{end}L_i - 4L_i^2} \left( \left| M_{Pier}^- \right| \frac{L_i}{L_{end}} + M_i^+ \right) \quad 4-4a$$

$$\text{Interior Spans} \quad w_{int} = \frac{8}{L_{int}^2} \left( \left| M_{Pier}^- \right| + M_{Midspan}^+ \right) \quad 4-4b$$

where  $M_{Pier}^-$  is the ultimate negative bending capacity of the segment joint adjacent to the pier,  $M_{Midspan}^+$  is the ultimate positive bending capacity of the midspan segment joint of interior spans,  $M_i^+$  is the ultimate positive bending capacity of the end span segment joint of interest,  $L_i$  is the length from the abutment centerline to the segment joint of interest,  $L_{end}$  is the clear end span length and  $L_{int}$  is the clear interior span length.

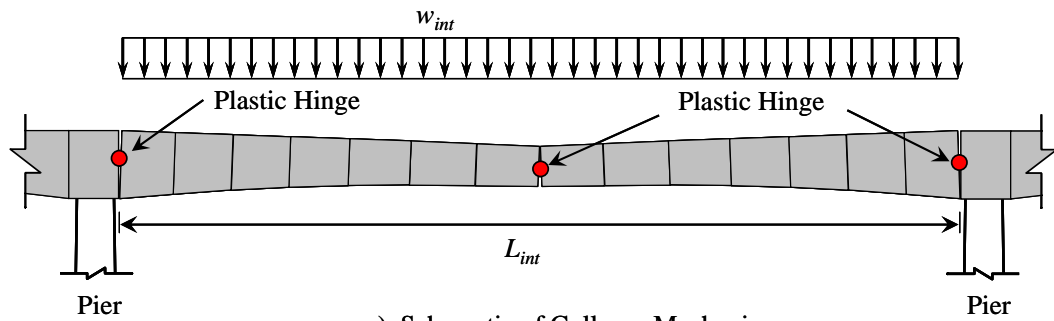


a) Schematic of Collapse Mechanism

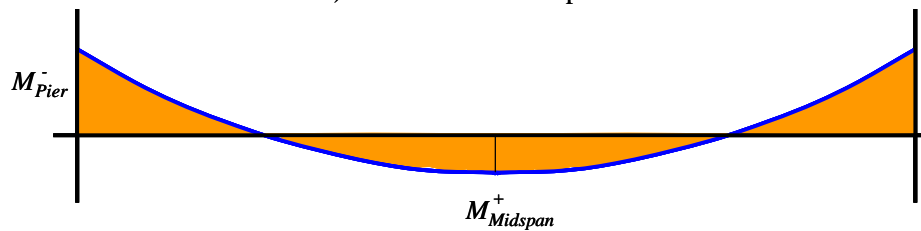


b) Bending Moment Diagram

**Figure 21 End Span Collapse Mechanism**



a) Schematic of Collapse Mechanism



b) Bending Moment Diagram

**Figure 22 Interior Span Collapse Mechanism**

These uniform distributed loads can be divided by the average unit weight of the superstructure for the span of interest to determine the capacity of the collapse mechanism in terms of multiples of the bridge self weight. Subtract unity from this ratio to obtain the capacity,  $S_c$ , of the collapse mechanism in terms of vertical earthquake accelerations as shown in Equation 4-5.

$$\text{Interior Spans} \quad S_{c_{int}} = \frac{W_{int}}{W_{int}/L_{int}} - 1 \quad 4-5a$$

$$\text{End Spans} \quad S_{c_{end}} = \frac{W_{end}}{W_{end}/L_{end}} - 1 \quad 4-5b$$

where,  $W_{int}$  and  $W_{end}$  are the total weights of the interior and end span segments, respectively. This value can be conservatively compared with the peak vertical ground acceleration,  $PGA_v$ , as defined in Section 4.5.3, to determine if the superstructure is likely to collapse during a significant seismic event.

## 4.5 Earthquake Hazards, Design Spectra and Ground Motions

The design of a bridge can be highly dependent on the amount of ground shaking experienced by the bridge. Thus, it is very important that bridge owners understand the consequences, both in terms of construction costs as well as risk of damage or down time, of selecting the design events for the bridge. In addition, the response of segmental bridges can vary depending on the approach used to determine the design spectrum and the ground motions used for time history analysis. This chapter discusses the important issues related to earthquake hazards and provides guidance for the appropriate development of time history ground motions and vertical design spectrum.

### 4.5.1 Earthquake Hazard Levels

It is the responsibility of bridge owners to determine the level of safety they would like in their bridge. Bridge owners should base their decision on the expected life span of the bridge and the consequences of damage to the bridge in terms of life safety and regional economics, with considerations for the future growth of the region.

The level of shaking at a bridge site depends on a number of factors that include: proximity to the fault; magnitude of the seismic event; soil conditions on the site; and the mechanism of the fault (i.e. strike-slip, normal, reverse, etc.). For design purposes, the level of ground shaking is demonstrated using a design spectrum. Design spectra are commonly generated based on a probabilistic seismic hazard analysis (PSHA). PSHA considers all possible ground motion scenarios (i.e. earthquake magnitude, distance to fault) for all the faults in the region as well as the probability of each possible scenario. The typical end result is a uniform hazard spectrum (UHS) which provides the spectral acceleration for various periods. The probability of exceeding the spectral acceleration indicated on a UHS is the same for all periods. In other words, a UHS indicates the spectral acceleration that a single degree of freedom structure will likely experience during a seismic event that occurs over a chosen return period (i.e. every 500, 1000, 2500 years). Figure 23 illustrates possible UHS for various return period events.

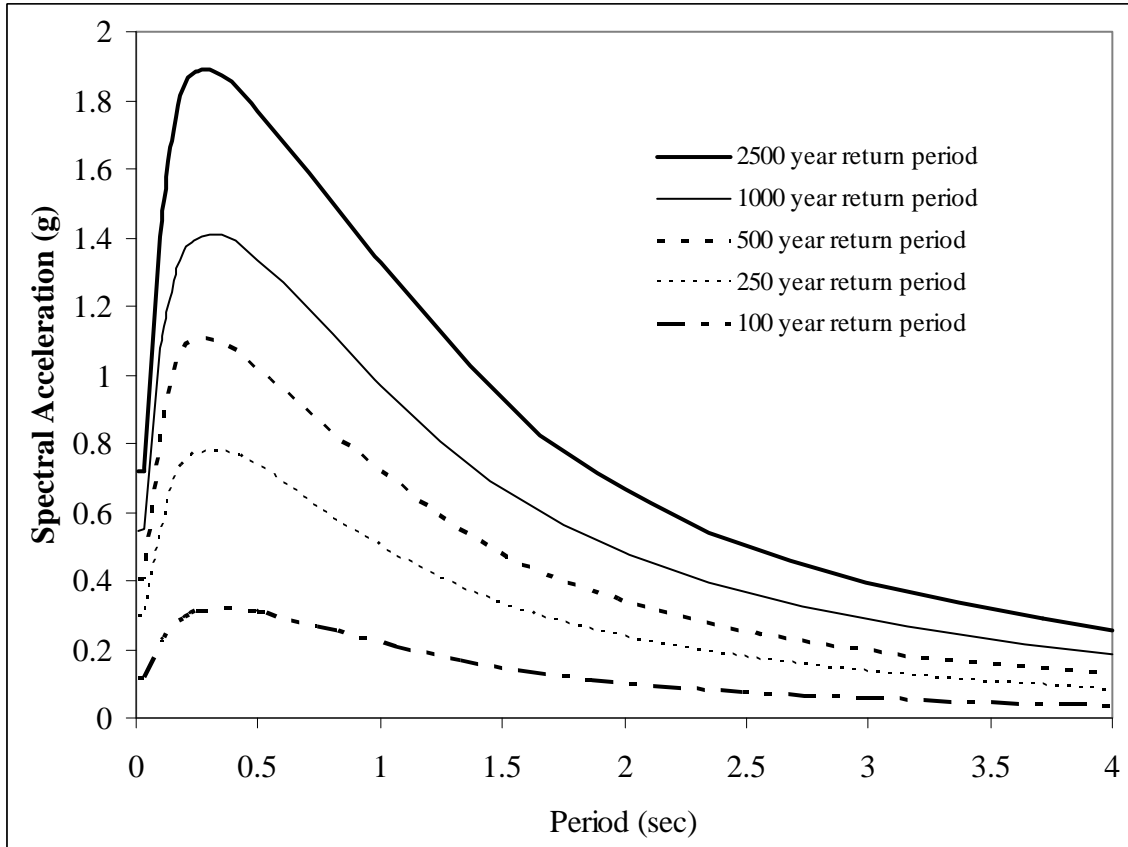


**Figure 23 Example of Uniform Hazard Spectrum for Various Return Periods**

It is important to note that a UHS is typically generated only for horizontal directions, not vertical, and can differ based upon the orientation to the fault for near field (within 10 km) events. For faults in California (i.e. strike-slip faults), the fault normal UHS will likely be larger than fault parallel UHS at periods larger than 1 second.

#### 4.5.2 Time History Ground Motions

It is common to use three sets of spectrum compatible ground motions to estimate the seismic demands on a bridge and to design for the maximum bridge response from these three sets of ground motions. Bridge design engineers should obtain ground motions from geotechnical engineers based on a deaggregation of the UHS. A deaggregation is typically a 3D plot that indicates the earthquake scenario (i.e. magnitude and distance) that contributes most to the UHS at a given period. That is, it indicates the type of earthquake that contributes most to the UHS (i.e. a large magnitude earthquake from a far away fault, or a small magnitude earthquake from a fault that is very close). A sample deaggregation is shown in Figure 24. The characteristics of different earthquake scenarios can be quite different and can affect the response of the bridge. The source ground motions used to create the spectrum compatible ground motions should be from

earthquake scenarios that are similar to the ones indicated in the deaggregation of the UHS. The algorithm that alters the seed ground motions should use wavelets in the time domain (Mukherjee and Gupta, 2002; Abrahamson, 1992) to match the design uniform hazard spectrum.

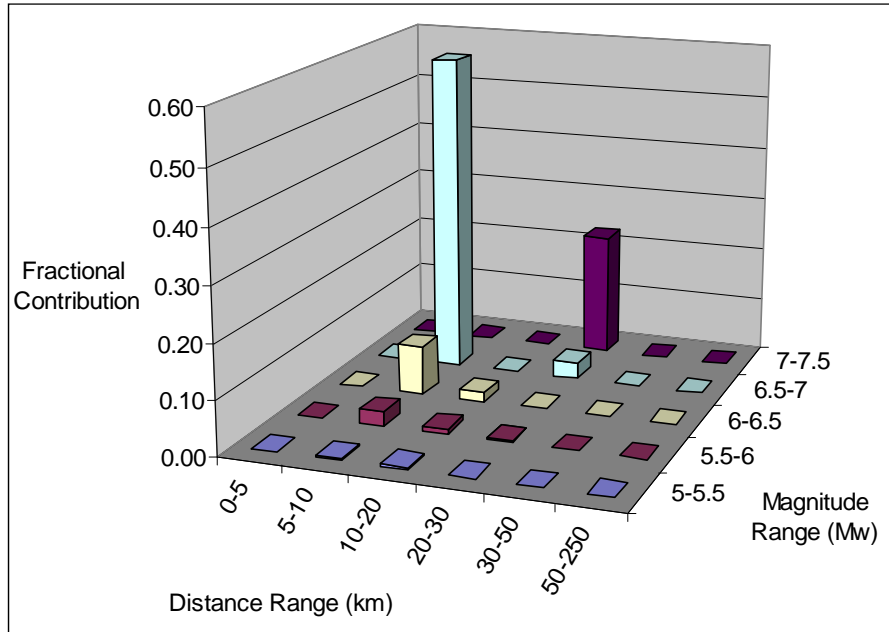


**Figure 24 Deaggregation of a UHS at a Period of 1.0 seconds**

Bridge designers should request the deaggregation of the UHS at the dominant periods of the structure from their geotechnical consultant and ensure the spectrum compatible ground motions originated from recordings of real earthquakes (not synthetic or numerically generated earthquakes) with a similar magnitude and distance to the earthquake scenario shown in the deaggregation. It is common for different earthquake scenarios to dominate the deaggregation at different periods in the UHS. If this is the case, at least one ground motion set should come from each ground motion scenario shown in the deaggregation of the UHS at critical periods.

### 4.5.3 Vertical Design Spectrum

The vertical design spectrum should be provided to the bridge design engineers by geotechnical engineers based on seismotectonic and geotechnical studies. A sample vertical design spectrum is shown in Figure 25. This vertical design spectrum will likely be based on vertical to horizontal (V/H) spectral ratios. In other words, the vertical design spectrum may be created by scaling the horizontal design spectrum. Historically a simple ratio of 2/3 was used for all periods. A number of studies (Niazi and Bozorgnia, 1989; Niazi and Bozorgnia, 1990; Niazi and Bozorgnia, 1991; Niazi and Bozorgnia, 1992; Bozorgnia and Campbell, 2004; Yilmaz et al., 2006; Kunnath et al., 2007) have shown

that a constant reduction factor is not accurate for near field seismic events. Typical V/H ratios vary depending on soil type, distance to fault, and magnitude with values ranging from about 1.5 down to 0.3 (see Figure 26). The peak V/H ratio is typically just below 0.1 seconds.

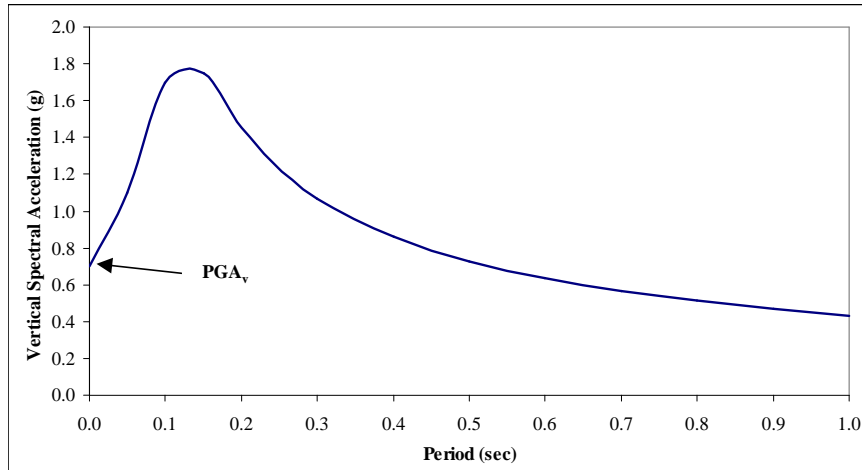


Figure 25 Sample Vertical Design Spectrum

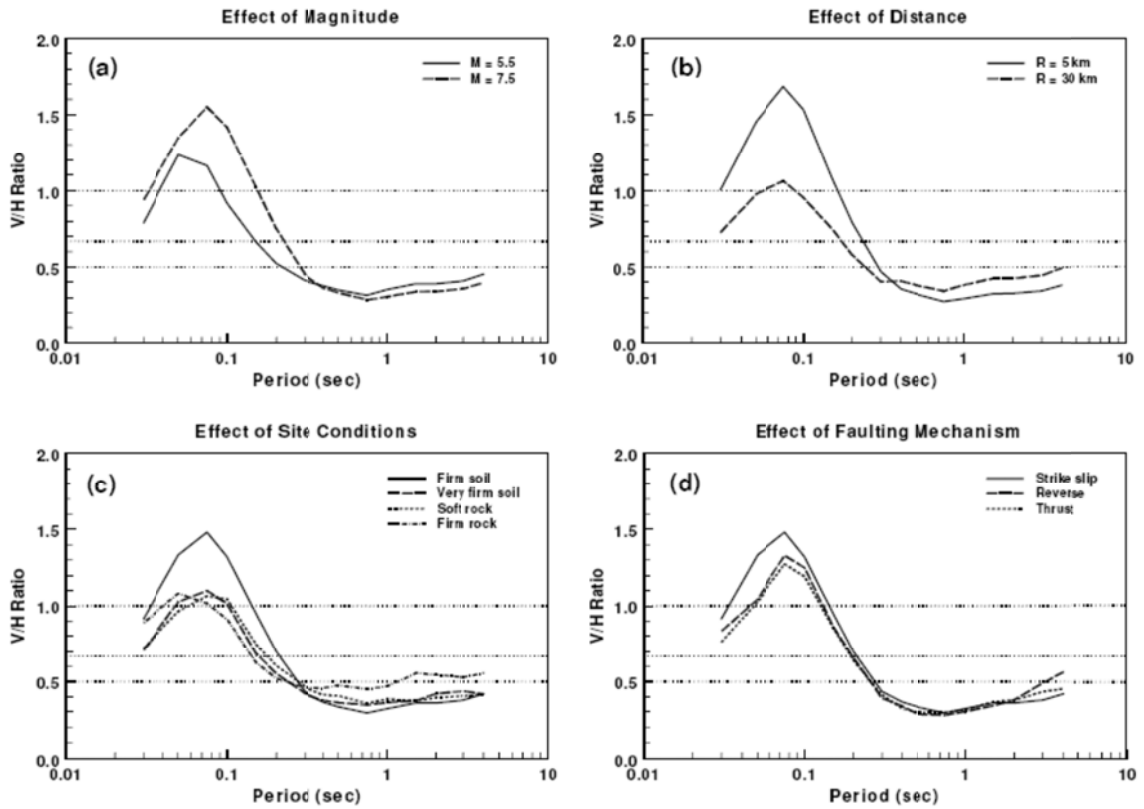


Figure 26 V/H ratio for Various Parameters (Bozorgnia and Campbell, 2004)

Design engineers should check the vertical design spectrum and make sure that a constant V/H ratio was not used for the generation of a near source vertical design spectrum.

It is important to note that the vertical peak ground acceleration,  $PGA_v$ , should be less than the peak spectral acceleration as illustrated in Figure 25. It may be the case that  $PGA_v$  is not indicated in this manner on the design spectrum. If this is the case, designers should confer with the geotechnical consultant on the project and obtain a more accurate estimate of the vertical peak ground acceleration. An accurate estimate of  $PGA_v$  is required for the safety evaluation earthquake design level of ‘Ordinary’ bridges, as discussed in Section 4.2.9.

## Chapter 5: STUDY OF EARTHQUAKE DEMAND METHODS

### 5.1 Objectives

The objective of the study of earthquake demand method was to determine the most appropriate method to estimate the vertical earthquake demands for both ‘Ordinary’ and ‘Important’ bridge structures.

### 5.2 Finite Element Models

Three two-dimensional analytical models were developed for a 91m (300 foot) span bridge. The first model simulated the superstructure using only linear elastic members. The second model simulated the superstructure using simple nonlinear elastic lumped plasticity members. The third model utilized numerous axial only gap-hook elements to explicitly model the behavior of concrete and post-tensioning tendons at critical superstructure segment joints.

#### 5.2.1 Linear Elastic Model

The linear elastic model (LEM) was developed using SAP2000 Version 14 with linear elastic members representing the superstructure (see Figure 27). Potential nonlinear response at the top and bottom of the piers was modeled using nonlinear Link elements. The pier hinging properties utilized a Takeda multi-linear plastic hysteretic model. This type of model is commonly used for the design of ‘Ordinary’ bridges.

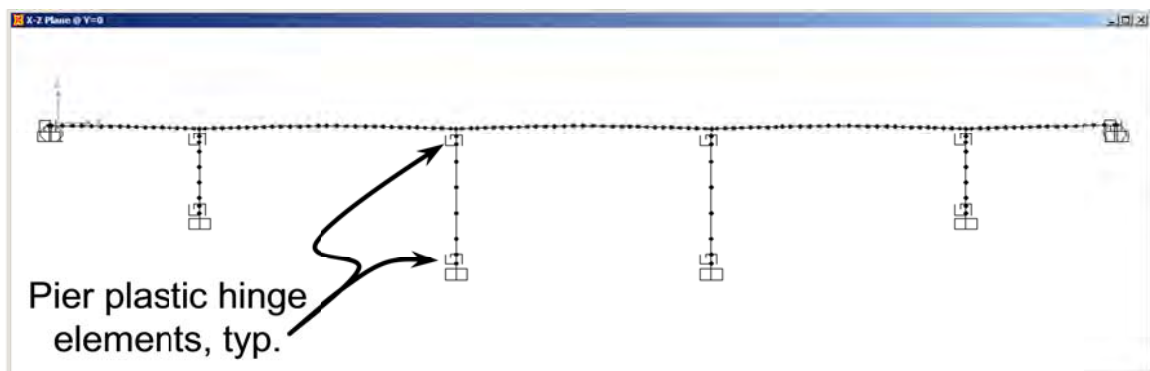
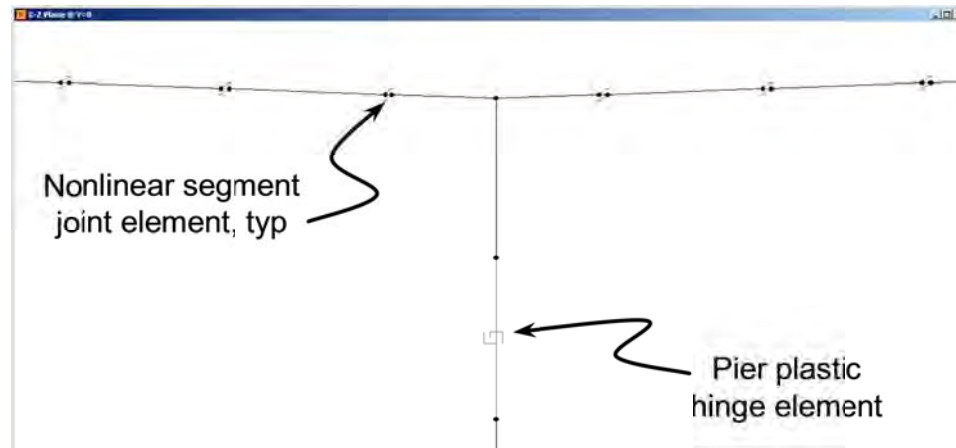


Figure 27 Schematic of the Linear Elastic Model

### 5.2.2 Nonlinear Elastic Model

The nonlinear elastic model (NEM) is exactly the same as the LEM, however select superstructure segment joints were modeled using nonlinear link elements to allow for potential joint opening (see Figure 28). These elements follow a multi-linear elastic rule, shown in Figure 31 and Figure 32, so they do not dissipate energy. This model is expected to be the most sophisticated approach that is likely to be used by practicing engineers for the design of 'Important' bridges.



**Figure 28 Detail of the Segment Joints Adjacent to eh Piers in the Nonlinear Elastic Model**

### 5.2.3 Nonlinear Inelastic Model

The nonlinear inelastic model (NIM) was developed using Ruaumoko (Carr, 2004) because of its large library of nonlinear hysteretic rules. The NIM utilized numerous axial only gap-hook elements to explicitly model the behavior of concrete and post-tensioning tendons at critical superstructure segment joints (see Figure 29 and Figure 30).

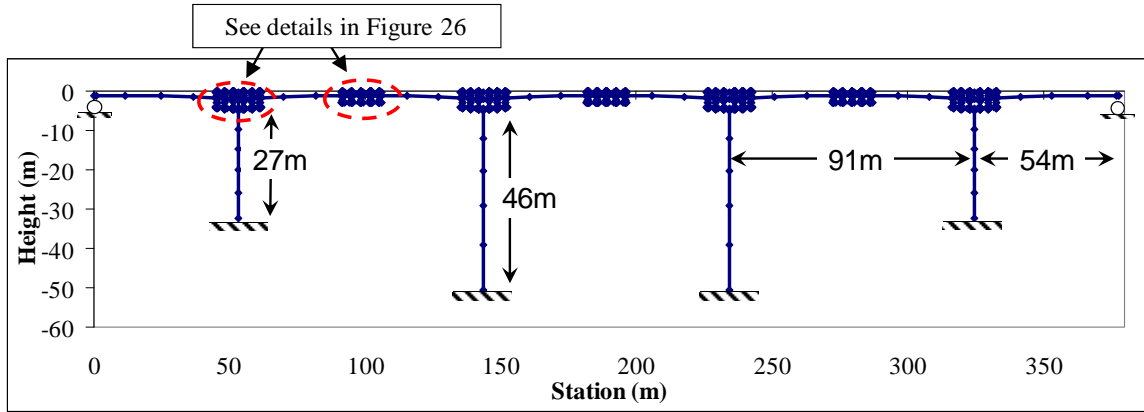


Figure 29 Schematic of the Nonlinear Inelastic Model

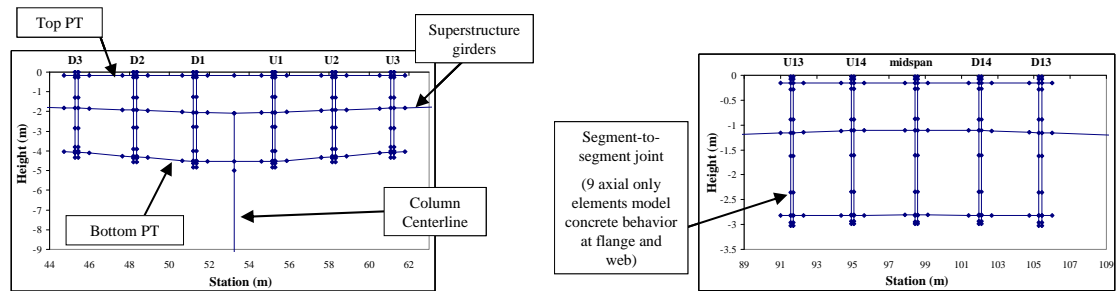


Figure 30 Details of the Segment Joints Adjacent to the Piers and Near Midspan

### 5.2.4 Moment Rotation Curves

A bi-linear moment-rotation curve was required for the SAP2000 NEM. This curve was based on a line from the origin to the decompression point, and a line from the decompression point through the lesser of the crushing point or the LP point. The curves for the first joint adjacent to the pier, joint D1/U1, and the midspan joint are shown in Figure 31 and Figure 32, respectively. Note that both of these figures include a moment offset discussed below and shown in Figure 33.

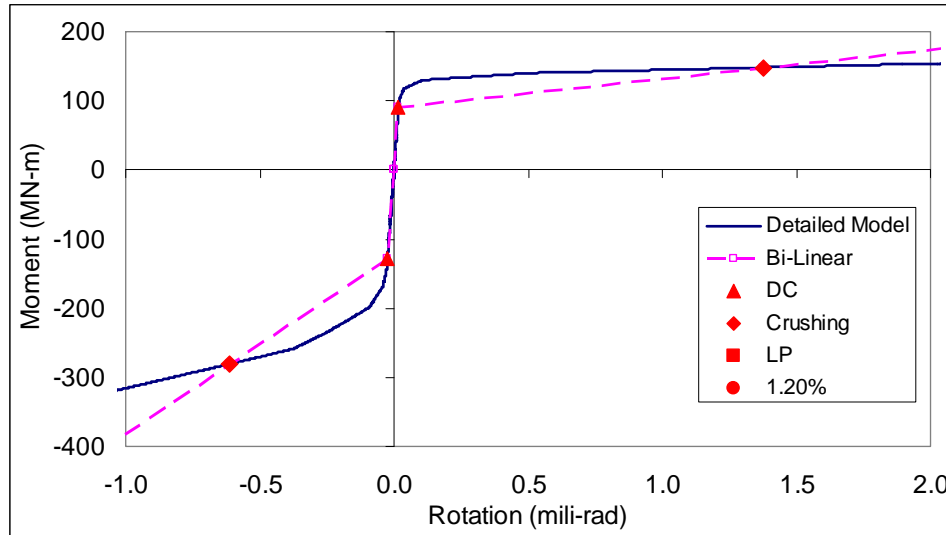


Figure 31 Moment-Rotation Curves for NEM with Moment Offset - Segment Joint D1/U1

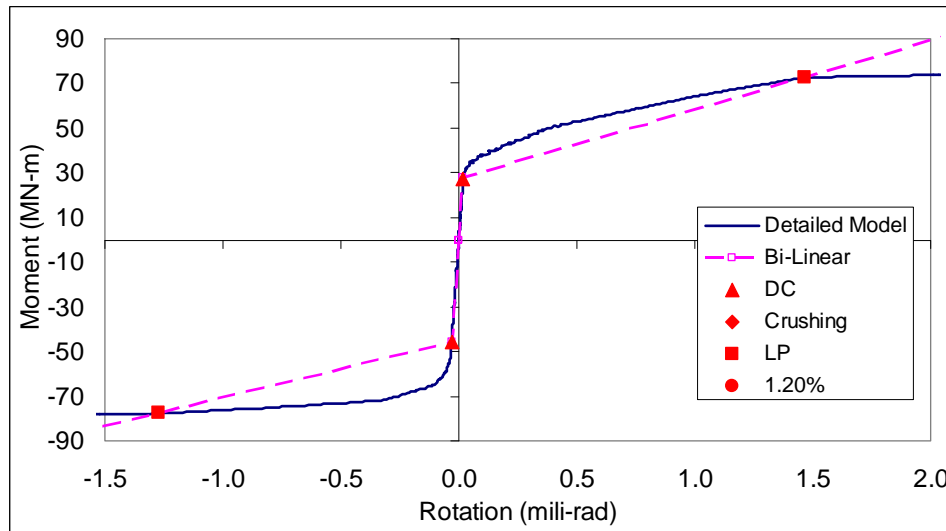
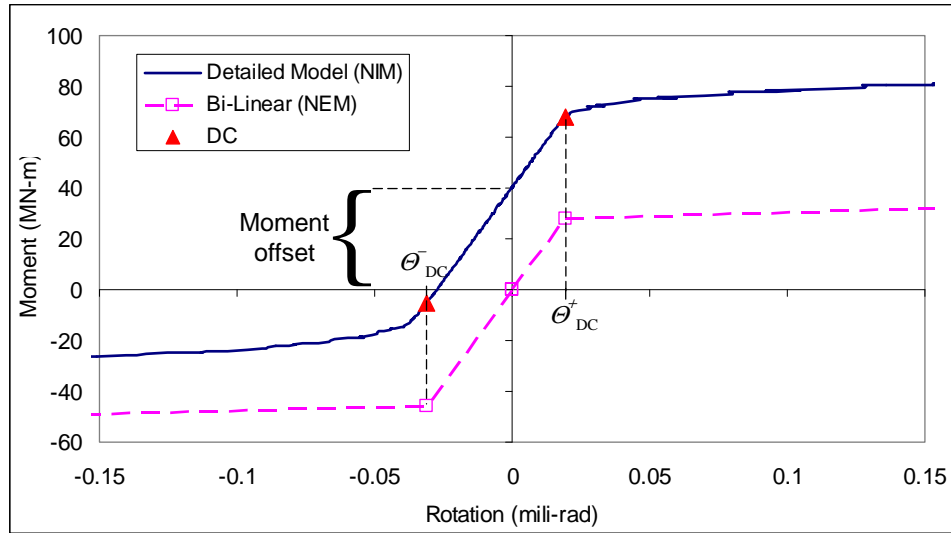


Figure 32 Moment-Rotation Curves for NEM with Moment Offset - Segment Joint at Midspan

It is important to note that SAP2000 requires that the nonlinear curves pass through the origin. Thus the bilinear curves needed to be offset as illustrated in Figure 33. This maintained the rotations at which limit states occurred, but shifted the moments. This is reasonable since the expected behavior does not pass through the origin because of the effects of PT on the section, which were not incorporated into the NEM.



**Figure 33. Offset in Moment-Rotation Curves required for SAP2000**

### 5.2.5 Calibration of Nonlinear Models

Previous research has indicated that the response of segment-to-segment joints can vary due to the state of stress on the joints prior to the earthquake (Veletzos and Restrepo, 2009). Both the NEM and NIM were calibrated to the end of construction (EOC) dead load stress state prior to earthquake time history analysis by applying moments and axial forces across the members at segment joints (see Figure 34). These EOC stresses were obtained from a full longitudinal construction staging analysis that included construction staging effects as well as creep and shrinkage that occurred during construction.

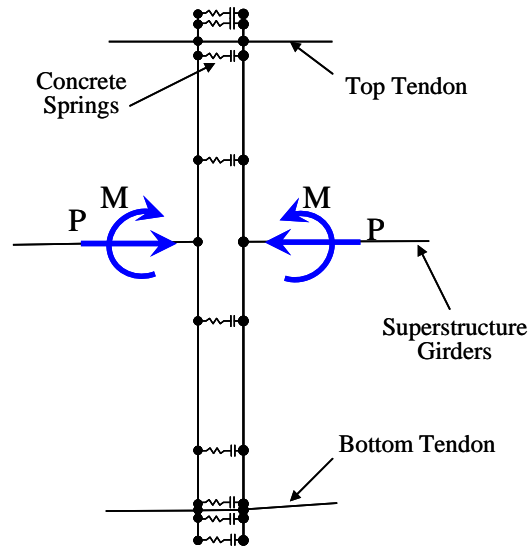


**Figure 34. Schematic of Segment Joint Forces Required to Calibrate the NIM and NEM. NIM shown, NEM similar.**

### 5.3 Model Validations

The dynamic characteristics and elastic response of the three models were compared to ensure consistent results

#### 5.3.1 Modal Properties

Table 8 compares the periods of the dominant modes from each model. The LEM and NEM are identical. Figure 35 compares the periods of the LEM and the NIM. Figure 36 and Figure 37 compare the longitudinal and vertical modal mass, respectively, of the NIM and the LEM. It is clear from these figures that the elastic dynamic properties of the three models are virtually identical.

**Table 8 Period Comparison**

Mode	Period (sec)		
	Linear Elastic Model	Nonlinear Elastic Model	Nonlinear Inelastic Model
1	2.04	2.04	2.04
2	0.99	0.99	0.97
3	0.71	0.71	0.70
4	0.54	0.54	0.53
5	0.39	0.39	0.39
8	0.32	0.32	0.32

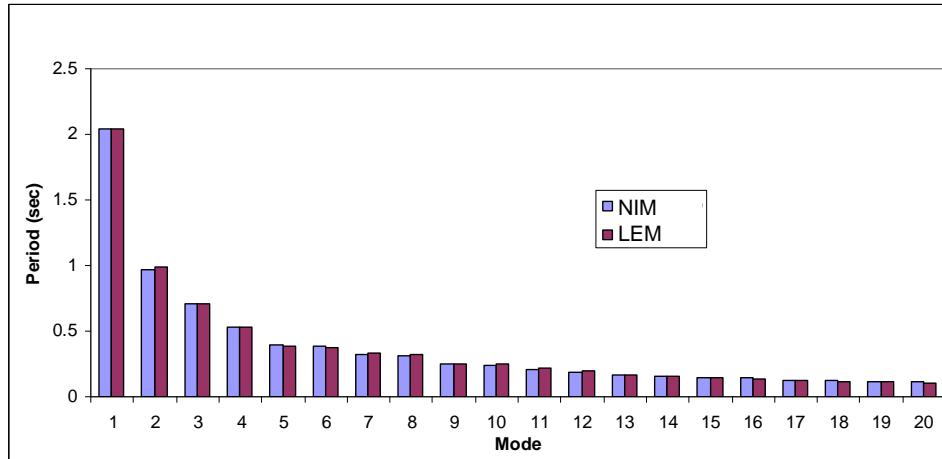


**Figure 35 Period Comparison**

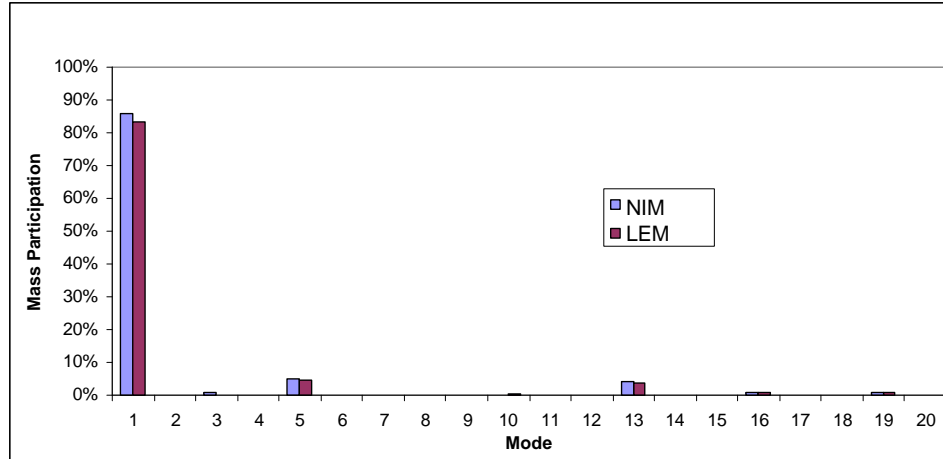


Figure 36 Longitudinal Modal Mass Participation Comparison

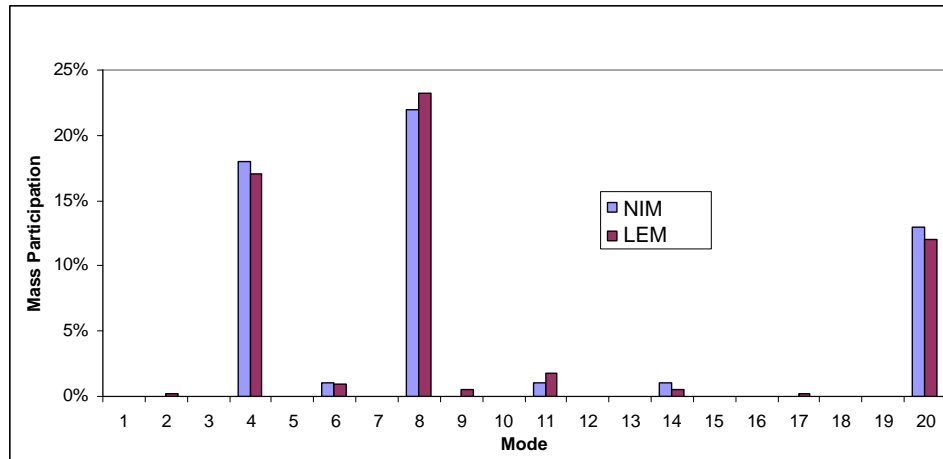
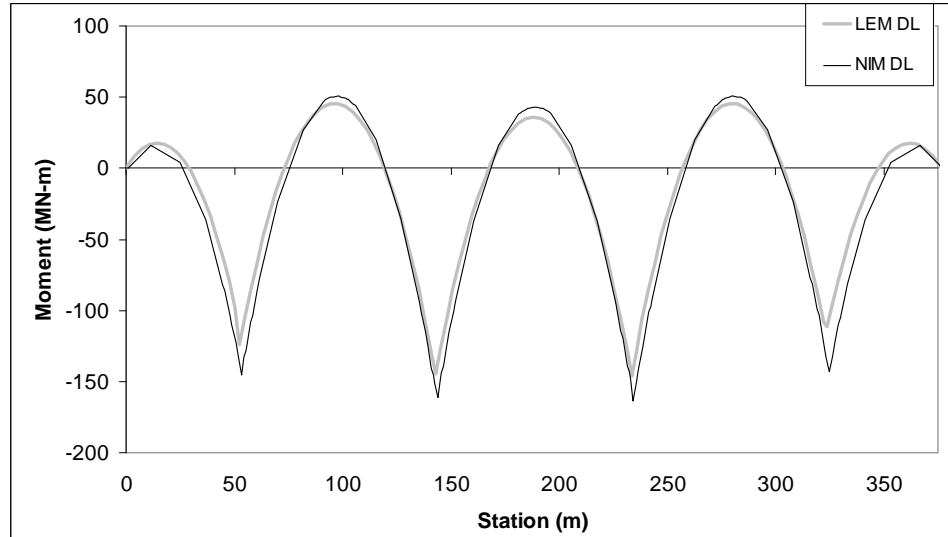


Figure 37 Vertical Modal Mass Participation Comparison

### 5.3.2 Elastic Superstructure Time History Comparison

The NEM and the NIM were modified slightly to prevent nonlinear behavior in the superstructure segment joints. These models were subjected to a single vertical time history analysis. The results of these new elastic superstructure models were compared with the LEM as a check. The dead load bending moments of the LEM and the elastic NIM are shown in Figure 38. The bending moments from the elastic NIM are slightly larger than the LEM. This is due to the effects of the tendons on the flexural behavior of the superstructure, which were not modeled in the LEM.



**Figure 38 Dead Load Bending Moment Comparison – LEM vs. Elastic version of NIM**

Figure 39 compares the superstructure bending moment envelopes for the LEM and the elastic version of the NEM and the NIM. The LEM and the NEM are identical. The bending moments from the NIM, however, are somewhat larger than the LEM and the NEM. This is due to the effects of the tendons.

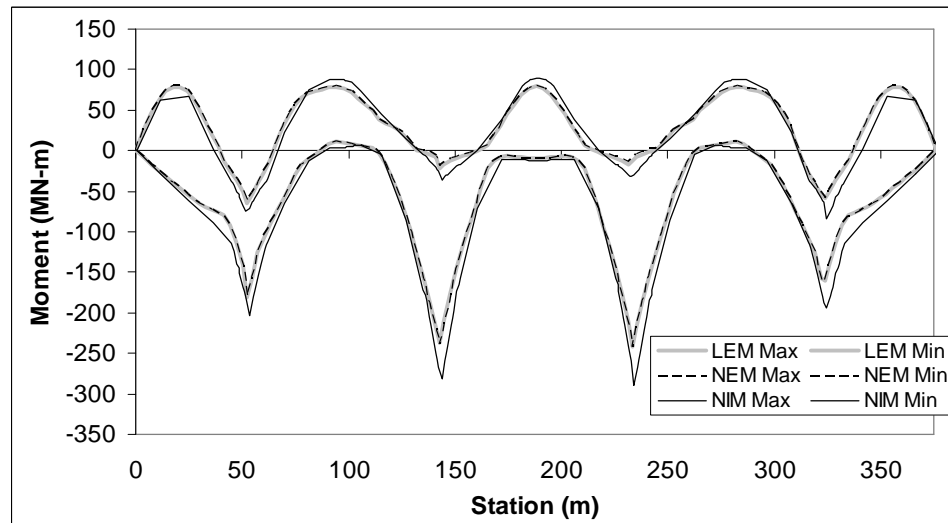


**Figure 39 Elastic Time History Comparison – LEM vs. Elastic NEM vs. Elastic NIM**

#### ***5.4 Design Spectra and Ground Motions***

The three models were subjected to vertical earthquakes representing five different hazard levels. The vertical design spectra (see Figure 40) were generated by scaling the horizontal design spectrum, based on recommendations by Kunnath et al.

2007. The horizontal design spectra (see Figure 41) were based on the uniform hazard spectra for an assumed site in California.

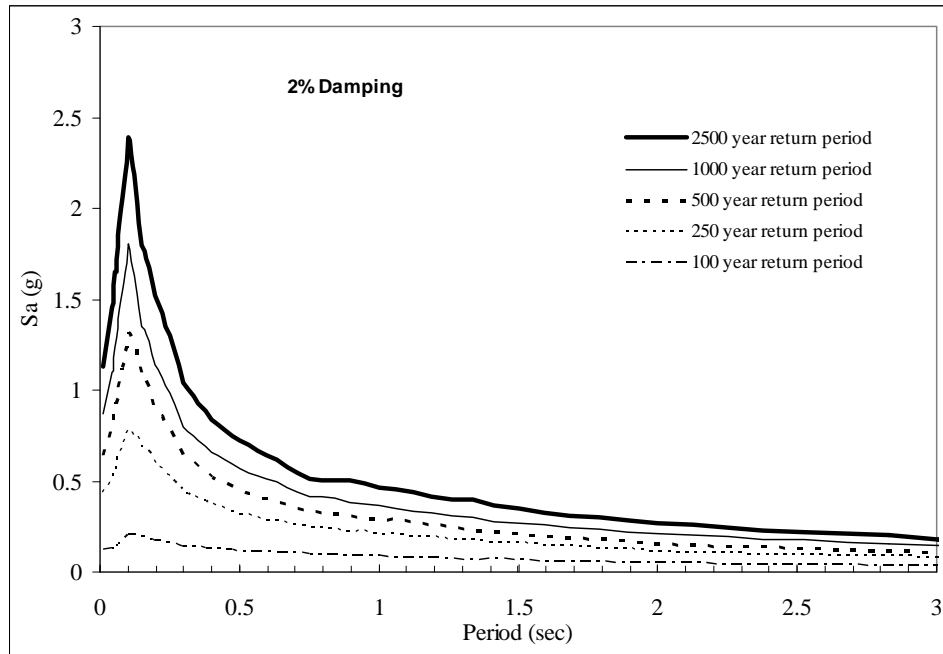


**Figure 40. Vertical Design Earthquake Spectrum**

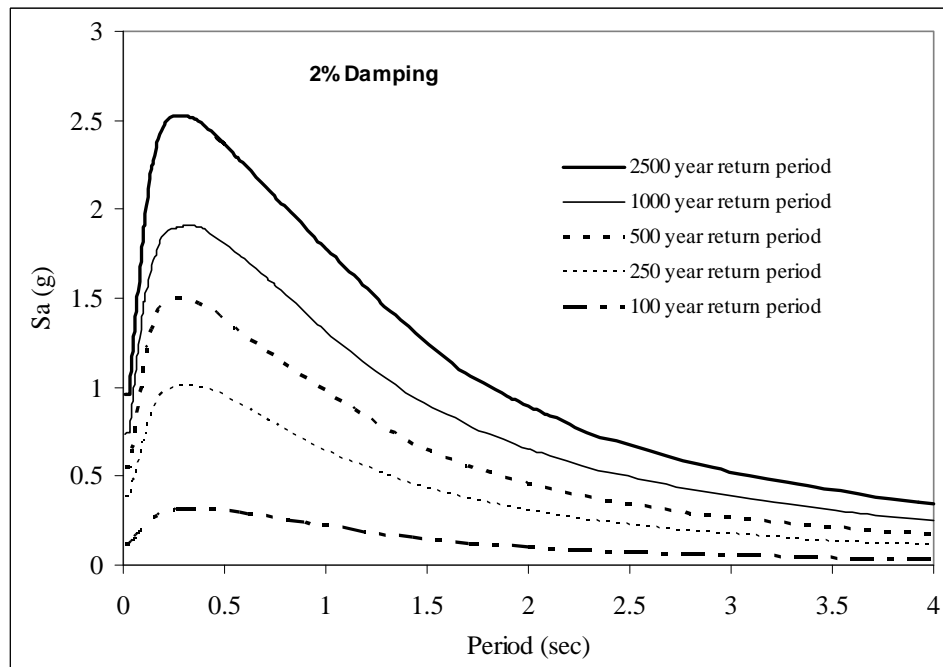


**Figure 41. Horizontal Design Earthquake Spectrum**

Ten ground motions were selected for each hazard level based on the deaggregation of the uniform hazard spectrum at the dominant modes. In general, the smaller hazards were dominated by Magnitude 7.0 to 7.5 at a distance of 20 to 30 km (12 to 18 miles), while the larger hazards were dominated by a Magnitude 6.5 to 7.0 at a distance of 5 to 10 km (3 to 6 miles). The records were made spectrum compatible using the program WAVGEN (Mukherjee and Gupta, 2002). The spectrum compatible motions were then baseline corrected to ensure that the velocity at the beginning and end of the motions were zero. The source ground motions for each hazard level are listed in Table 9.

**Table 9 Source Ground Motions**

Hazard	Earthquake	Station	Year	Moment Magnitude	Closest Distance (km)
100	Duzce, Turkey	Lamont 1058	1999	7.1	0.2
100	Irpinia, Italy-01	Bisaccia	1980	6.9	21.3
100	New Zealand-02	Matahina Dam	1987	6.6	16.1
100	Friuli, Italy-01	Tolmezzo	1976	6.5	15.8
100	Corinth, Greece	Corinth	1981	6.6	10.3
100	Tabas, Iran	Dayhook	1978	7.4	13.9
100	Landers	Desert Hot Springs	1992	7.3	21.8
100	Imperial Valley-06	SAHOP Casa Flores	1979	6.5	9.6
100	Northridge-01	LA - Hollywood Stor FF	1994	6.7	24.0
100	Northridge-01	Pacific Palisades - Sunset	1994	6.7	24.1
250	Cape Mendocino	Cape Mendocino	1992	7.0	7.0
250	Landers	Joshua Tree	1992	7.3	11.0
250	Northridge-01	Beverly Hills - 12520 Mulhol	1994	6.7	18.4
250	Northridge-01	Newhall - Fire Sta	1994	6.7	5.9
250	Cape Mendocino	Petrolia	1992	7.0	8.2
250	Northridge-01	Tarzana - Cedar Hill A	1994	6.7	15.6
250	Chi-Chi, Taiwan	TCU071	1999	7.6	5.3
250	Chi-Chi, Taiwan	TCU076	1999	7.6	2.8
250	Chi-Chi, Taiwan	TCU116	1999	7.6	12.4
250	Northridge-01	Newhall - W Pico Canyon Rd.	1994	6.7	5.5
500	Erzican, Turkey	Erzincan	1992	6.7	4.4
500	Gazli, USSR	Karakyr	1976	6.8	5.5
500	Kobe, Japan	KJMA	1995	6.9	1.0
500	Loma Prieta	Los Gatos - Lexington Dam	1989	6.9	5.0
500	Cape Mendocino	Petrolia	1992	7.0	8.2
500	San Fernando	Pacoima Dam (upper left abut)	1971	6.6	1.8
500	Northridge-01	Rinaldi Receiving Sta	1994	6.7	6.5
500	Kobe, Japan	Takatori	1995	6.9	1.5
500	Chi-Chi, Taiwan	TCU110	1999	7.6	11.6
500	Northridge-01	Newhall - W Pico Canyon Rd.	1994	6.7	5.5
1000	Erzican, Turkey	Erzincan	1992	6.7	4.4
1000	Gazli, USSR	Karakyr	1976	6.8	5.5
1000	Kobe, Japan	KJMA	1995	6.9	1.0
1000	Loma Prieta	Los Gatos - Lexington Dam	1989	6.9	5.0
1000	Northridge-01	Beverly Hills - 14145 Mulhol	1994	6.7	17.2
1000	San Fernando	Pacoima Dam (upper left abut)	1971	6.6	1.8
1000	Northridge-01	Sylmar - Olive View Med FF	1994	6.7	5.3
1000	Kobe, Japan	Takatori	1995	6.9	1.5
1000	Chi-Chi, Taiwan	TCU067	1999	7.6	0.6
1000	Chi-Chi, Taiwan	TCU072	1999	7.6	7.0
2500	Erzican, Turkey	Erzincan	1992	6.7	4.4
2500	Gazli, USSR	Karakyr	1976	6.8	5.5
2500	Kobe, Japan	KJMA	1995	6.9	1.0
2500	Loma Prieta	Los Gatos - Lexington Dam	1989	6.9	5.0
2500	Northridge-01	Beverly Hills - 14145 Mulhol	1994	6.7	17.2
2500	San Fernando	Pacoima Dam (upper left abut)	1971	6.6	1.8
2500	Northridge-01	Sylmar - Olive View Med FF	1994	6.7	5.3
2500	Kobe, Japan	Takatori	1995	6.9	1.5
2500	Chi-Chi, Taiwan	TCU067	1999	7.6	0.6
2500	Chi-Chi, Taiwan	TCU072	1999	7.6	7.0

Figure 42 compares the median vertical response spectra with the vertical design spectra for the 2500 year hazard. In general there is good agreement between the median

response and the design spectra, particularly at the dominant vertical periods of 0.54 and 0.32 seconds. The remaining four hazard levels compared similarly.

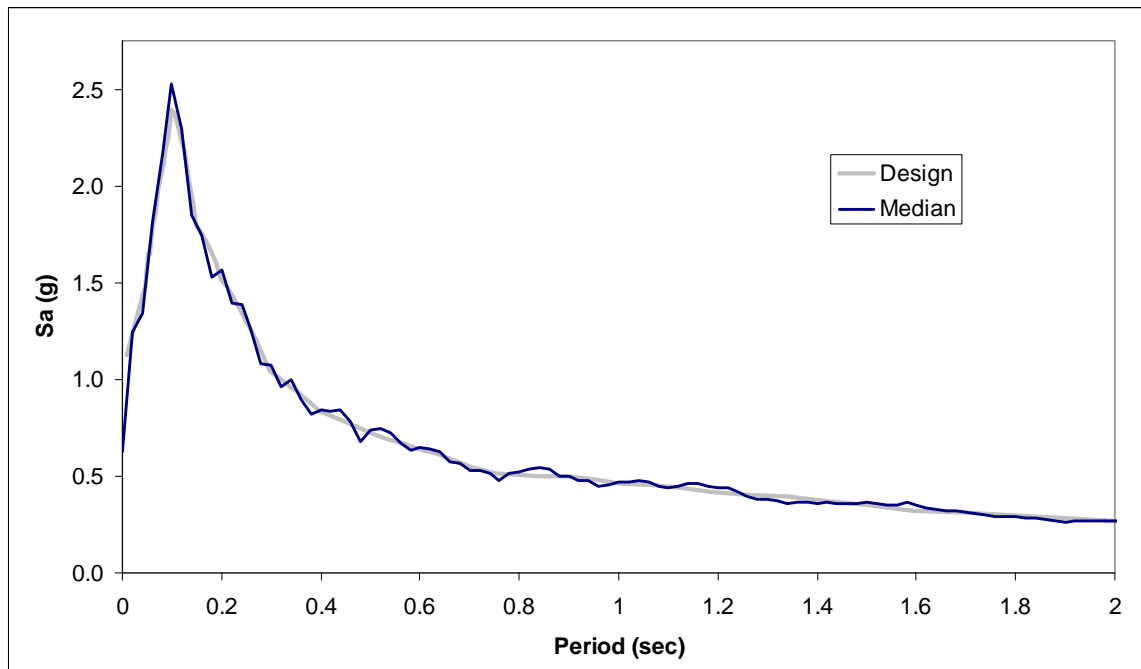


Figure 42 2500 Year Hazard Spectrum

### 5.5 Limit States

The limit states of interest in this study were decompression (DC) of the extreme concrete fibers, crushing of the extreme concrete fibers, the limit of proportionality (LP) of the main PT tendons and full yield of the PT tendons. The DC limit state was defined at 13% of the direct tensile strength of concrete, taken as  $4\sqrt{f'_c(\text{psi})}$ . This stress level approximates the residual tension stresses that act across the rough crack between precast segments. The crushing limit state was defined as the strain  $0.85 f'_c$ . The LP limit state was defined as the point at a stress of 215 ksi, which is eighty percent of the specified ultimate tensile strength. The tendon was considered to fully yield at a tensile strain of 1.2%.

The limit state that identifies when segment joints are fully opened is defined using with the effective moment and effective rotation (see Figure 43). These parameters are a critical point in a bi-linear curve that approximates the behavior of a segment-to-segment joint. The bi-linear curve follows the gross section stiffness until the effective moment is reached. At this point the curve will deviate towards the lesser of the point where the concrete strain reaches 0.003 or the tendon stress reaches 210 ksi. The effective moment and rotation are obtained by balancing the area between the bi-linear curve and the expected joint behavior.

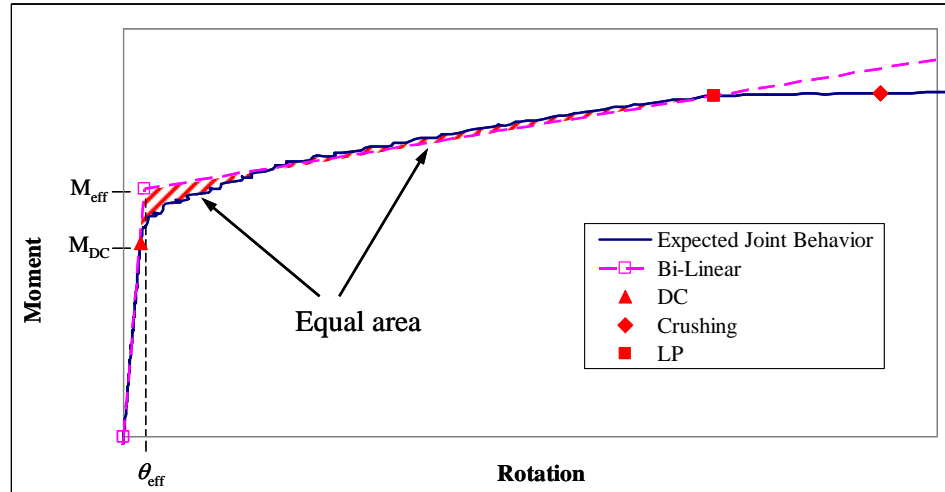


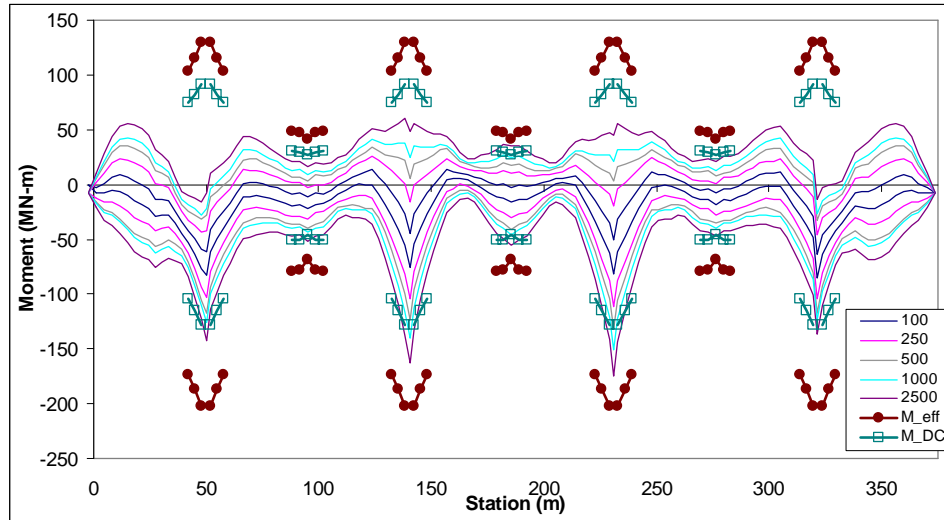
Figure 43. Definition of Effective Moment and Effective Rotation Capacities

## 5.6 Results

### 5.6.1 Elastic Time History vs. Elastic Modal Analysis

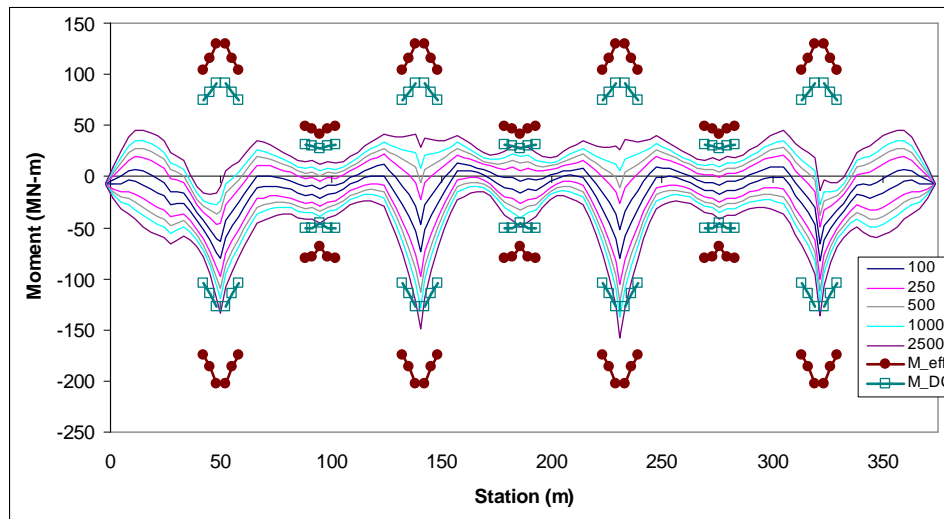
Modal analyses were performed for all five hazard levels using both the CQC and the SRSS combination rules. 200 modes carrying 100% of the vertical mass were used in the modal combinations. The results from these two modal combination rules were identical. In addition, vertical time history analyses were performed using the LEM for all five hazard levels. 2% damping was assumed for both the time history analyses and the modal analyses

Figure 44 shows the median bending moment envelopes for the time history analyses from the LEM. The superstructure moments were added to the EOC dead load moment as obtained from a full longitudinal construction staging analysis. Figure 45 indicates that all of the hazards remain below the effective moment of the segment joints indicating that all the segment joint are expected to remain essentially elastic. A few of the segment joints, particularly near the middle of the spans, exceed the decompression moment, indicating that joint opening is beginning to occur.



**Figure 44. Median Bending Moment Envelopes for the Time History Analyses from the LEM.**

Figure 45 shows the median bending moment envelopes for the modal analyses from the linear elastic model after adding in the EOC dead load moments. This figure is very similar to Figure 44 and the same conclusions can be drawn.



**Figure 45. Median Bending Moment Envelopes for the Modal Analyses from the LEM**

Figure 46 shows the ratio of the earthquake only bending moment envelopes from the time history and modal analyses for the 2500 year hazard. This figure illustrates that time history analyses generated moment demands that were 19% larger than the modal analyses on average for the 2500 year hazard. The ratios for the other hazards are indicated in Table 10. This difference is predominately due to damping. The damping ratio of two dominant vertical modes (i.e. periods of 0.3 and 0.5 seconds) is approximately 1% (see Figure 47) in the time history analyses while it is 2% in the modal

analyses. This should produce an average 18% larger response in the time history analyses than the modal analyses for these modes, according to scale factors determined by Kawashima and Aizawa (1986) (see Figure 48 for the scale factors relative to 5% damping).

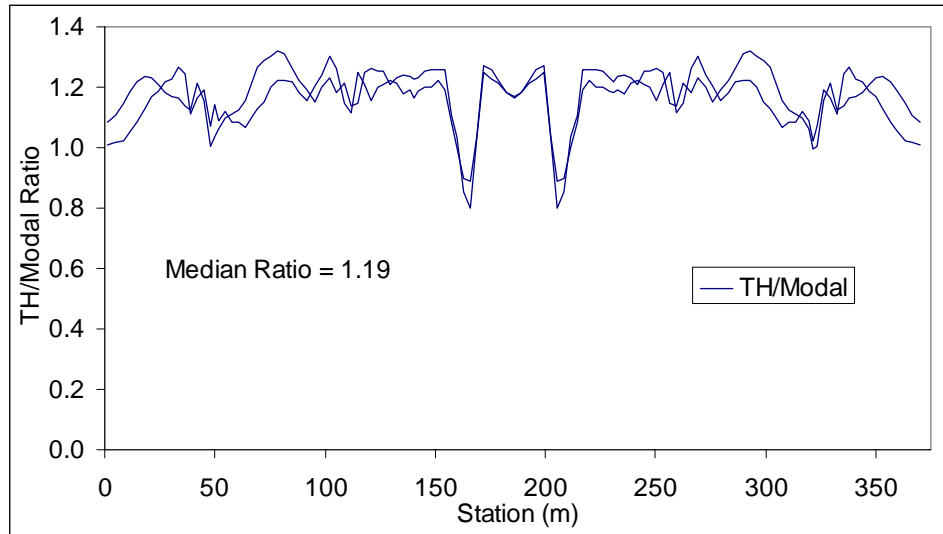
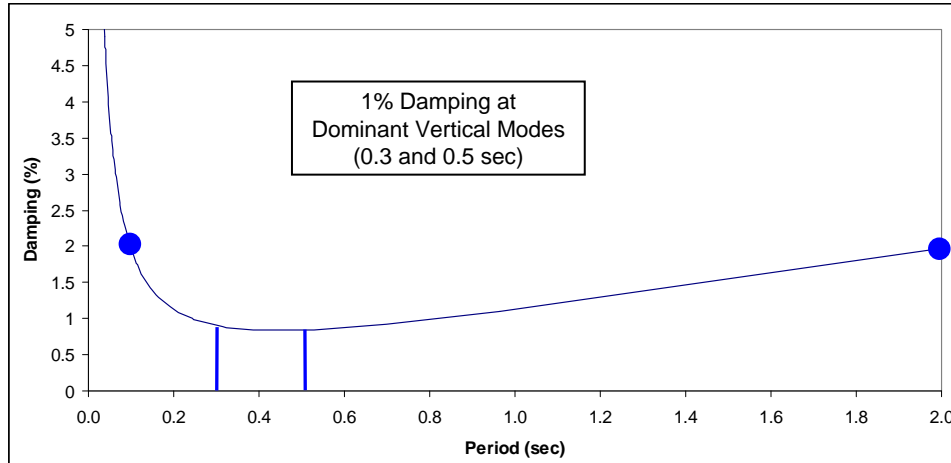


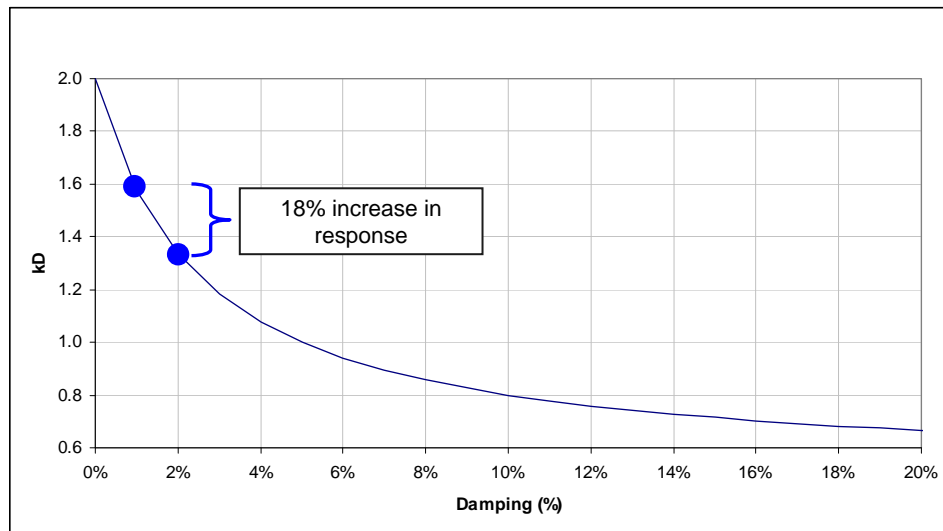
Figure 46. Ratio of Median Bending Moment Envelopes for the 2500 Year Hazard

Table 10 Summary of Median Time History to Modal Bending Moment Ratio

Hazard	Median TH to Modal Ratio
100	1.22
250	1.17
500	1.23
1000	1.19
2500	1.19



**Figure 47 2% Rayleigh Damping used for Time History Analyses**



**Figure 48 Kawashima and Aizawa (1986) Response Spectra Damping Scale Factors**

### 5.6.2 Collapse Mechanism Check

A check of the possible static collapse mechanism must be performed to satisfy the no collapse criteria. This approach assumes the first vertical mode carries all the vertical mass. In most scenarios this check can be easily satisfied as illustrated in Figure 49 and Figure 50.

Study of Earthquake Demand Methods

	D1/U1	D2/U2	D3/U3
M_pier(neg)	-467	-412	-361 MN-m
M_i(pos)	115	115	115 MN-m
L_i	30.5	28.8	27.2 m
L_end	50.9	48.1	45.3 m
w_end	1.27	1.31	1.35 MN/m
W_end	9.10	8.51	7.95 MN
Sc_end	6.10	6.37	6.68 g
PGA_v (2500 yr)	1.2	1.2	1.2 g
Sa(T=0.3sec)	1	1	1 g
Dvert	1.2	1.2	1.2 g
Dvert/Sc_end	0.20	0.19	0.18
	ok	ok	ok

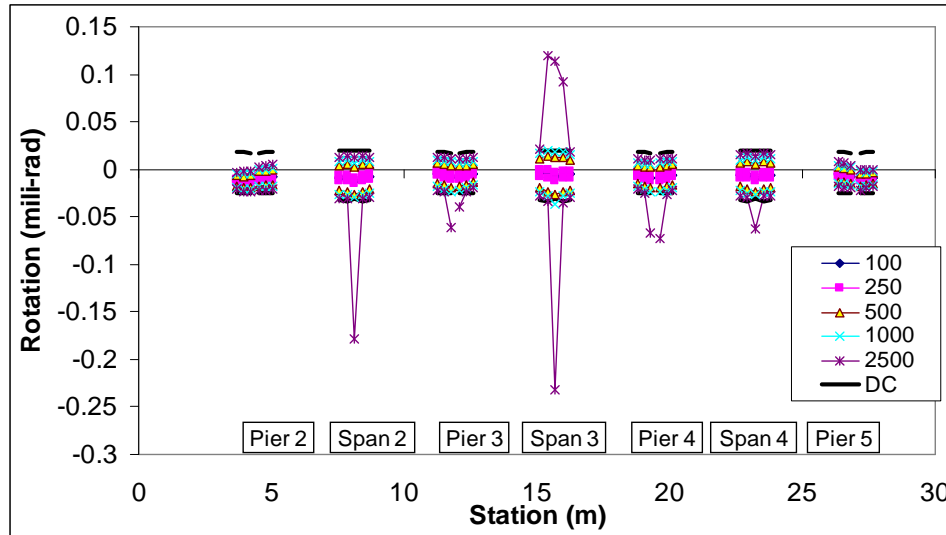
Figure 49 Sample Collapse Mechanism Calculations – 2500 Year Hazard – End Span

	D1/U1	D2/U2	D3/U3
M_pier(neg)	-467	-412	-361 MN-m
M_midspan(pos)	115	115	115 MN-m
L_int	85.1	79.3	73.8 m
w_int	0.643	0.669	0.699 MN/m
W_int	15.6	14.4	13.3 MN
Sc_int	2.51	2.68	2.88 g
PGA_v (2500 yr)	1.2	1.2	1.2 g
Sa(T=0.3sec)	1	1	1 g
Dvert	1.2	1.2	1.2 g
Dvert/Sc_end	0.48	0.45	0.42
	ok	ok	ok

Figure 50 Sample Collapse Mechanism Calculations – 2500 Year Hazard – Interior Spans

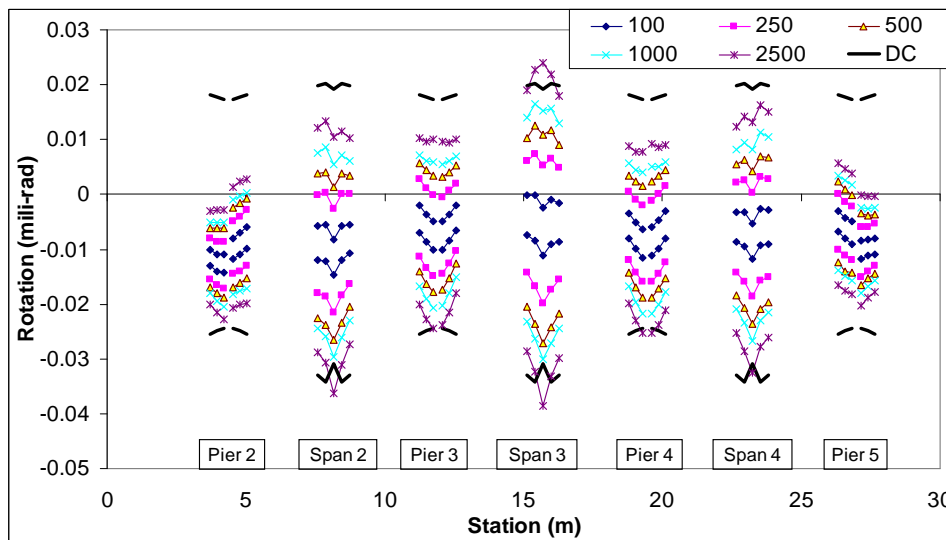
### 5.6.3 Nonlinear Elastic Model vs. Nonlinear Inelastic Model

Figure 51 shows the median segment joint rotation envelopes from the NEM as well as the rotation of the cracking limit state. This figure indicates that nonlinear response occurs near midspan, particularly due to negative bending. The response does not exceed the crushing or LP limit states indicating that permanent damage is unlikely. This is consistent with the results of the linear elastic models shown in Figure 44.



**Figure 51. Segment Joint Rotation Envelopes for the NEM**

Figure 52 shows the median segment joint rotation envelopes from the NIM as well as the rotation of the cracking limit state. This figure indicates that the majority of segments do not exceed the cracking limit state. A few segment joints, particularly at the middle of the spans, exceeded the DC limit state. This is consistent with the results of the linear elastic models shown in Figure 44. It is important to note that capacity design of the superstructure based on hinging of the top of the column, does not necessarily preclude joint opening.



**Figure 52. Segment Joint Rotation Envelopes for the NIM**

## 5.7 Recommendations

Based on the analyses performed and the results presented in this chapter, the following recommendations are made. These recommendations have been included in the complete design recommendations shown in Chapter 7.

### 5.7.1 ‘Ordinary’ Bridges

For the functional evaluation of ‘Ordinary’ bridges, a modal analysis using a linear elastic model is recommended. The results should be used to ensure that the superstructure does not exceed the effective moment, thus the joints will remain essentially elastic.

For the safety evaluation of ‘Ordinary’ bridges, it is recommended that designers satisfy the no collapse criteria by checking the capacity of all vertical collapse mechanisms relative to the vertical design spectrum. The capacity of the collapse mechanism for both interior and end spans must be greater than the larger of (i) the vertical peak ground acceleration in the vertical design spectrum and (ii) the vertical spectral acceleration at the dominant vertical mode. The collapse mechanism capacity,  $S_c$ , (see Figure 21 and Figure 22) can be determined based on Eq.4-5.

$$S_{c_{int}} = \frac{W_{int}}{W_{int}/L_{int}} - 1 \quad 4-5a$$

$$S_{c_{end}} = \frac{W_{end}}{W_{end}/L_{end}} - 1 \quad 4-5b$$

where,  $L_{end}$  = clear end span length,  $L_{int}$  = clear interior span length,  $w_{end}$  = uniform distributed load of the end span segment,  $w_{int}$  = uniform distributed load of the interior span segment,  $W_{end}$  = total weight of the end span segment,  $W_{int}$  = total weight of the interior span segment.

The uniform distributed loads  $w_{end}$  and  $w_{int}$  that will develop these collapse mechanisms can be determined from Eq. 4-4 for both end and interior spans.

$$w_{end} = \frac{8}{4L_{end}L_i - 4L_i^2} \left( \left| M_{Pier}^- \right| \frac{L_i}{L_{end}} + M_i^+ \right) \quad 4-4a$$

$$w_{int} = \frac{8}{L_{int}^2} \left( \left| M_{Pier}^- \right| + M_{Midspan}^+ \right) \quad 4-4b$$

where,  $M_{Pier}^-$  = ultimate negative bending capacity of the segment joint adjacent to the pier,  $M_{Midspan}^+$  = ultimate positive bending capacity of the midspan segment joint of interior spans,  $M_i^+$  is the ultimate positive bending capacity of the end span segment joint of interest,  $L_i$  = length from the abutment centerline to the segment joint of interest

### 5.7.2 'Important' Bridges

For both the functional and safety evaluation of 'Important' bridges, a time history analysis using a nonlinear elastic model is recommended. The results should be used to ensure that the superstructure does not exceed the crushing or limit of proportionality (LP) limit states, thus segment joints will remain essentially undamaged.

## **Chapter 6: LOAD COMBINATION INVESTIGATION**

### **6.1 Objectives**

The objectives of the load combination investigation were to:

- Study the probability of a strong thermal gradient occurring simultaneously with a strong seismic event.
- Estimate the probability of two pre-earthquake stress states (i.e. at end of construction and after creep and shrinkage considerations) occurring simultaneously with a strong earthquake.
- Recommend a vertical earthquake load combination

### **6.2 Introduction**

It has been shown that the superstructure pre-earthquake stress state can affect the response of segmental bridges (Veletzos and Restrepo, 2009).

The effects of thermal gradients can alter the pre-earthquake stress state in bridge superstructures. These effects cause daily stress variations and the magnitude of these stress variations follow an annual sinusoidal cycle, with the peak variations occurring during the summer months.

In addition, the pre-earthquake stress states are altered by volumetric changes (i.e. creep and shrinkage) which vary over the life of the bridge and are primarily a function of relative humidity and the effective thickness of the superstructure cross section.

### **6.3 Thermal Gradient**

The results from two separate multi-year studies on the effects of thermal gradients on bridge superstructures were reviewed. One study was on the San Antonio “Y” project in Texas, which measured thermal differences at multiple superstructure locations over a period of 2 ½ years. The second study measured thermal gradients on the North Halawa Valley Viaduct in Hawaii over a two year period.

Figure 53 and Figure 54 show peak positive and negative thermal differences on the San Antonio “Y” project and compare the measured differences to the code design value. These figures indicate that the AASHTO segmental guide specifications (AASHTO, 1999) appear to overestimate the positive thermal gradients, yet

underestimate the negative thermal gradients in 32 instances over a 2 ½ year period. There is clearly a sinusoidal pattern to the temperature difference data.

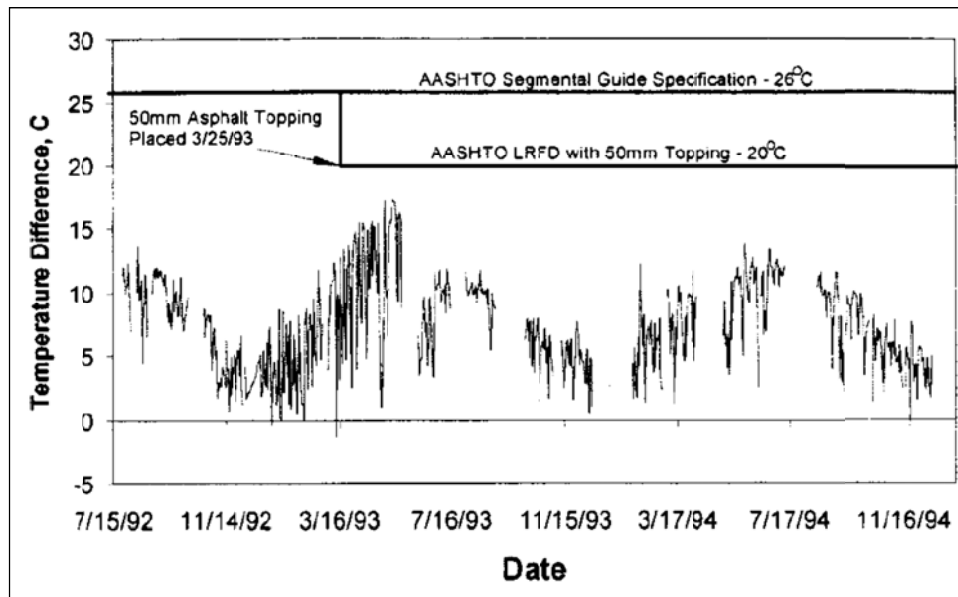


Figure 53: Maximum Positive Temperature Differences on the San Antonio “Y” Project (Roberts-Wollman et al., 2002)

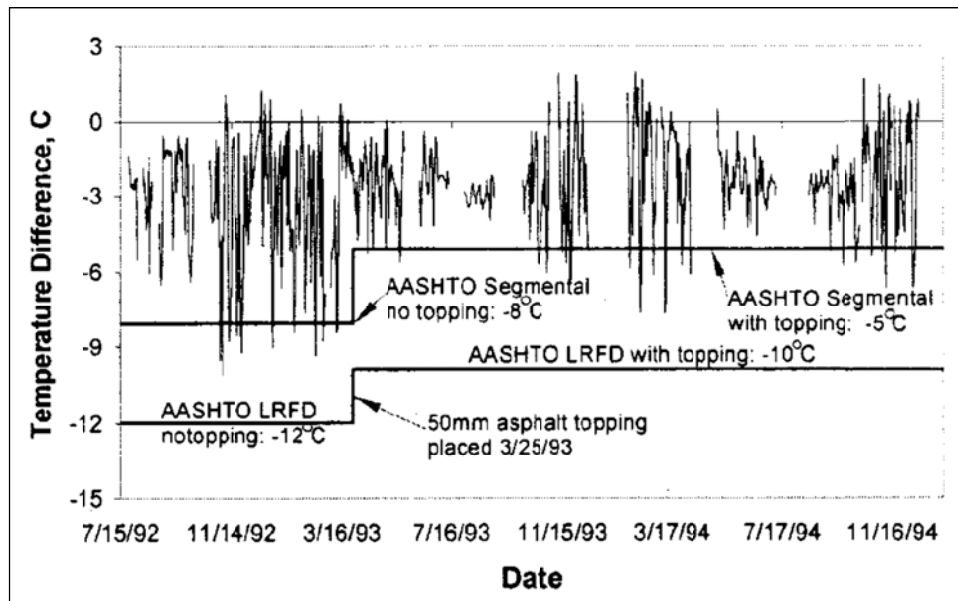
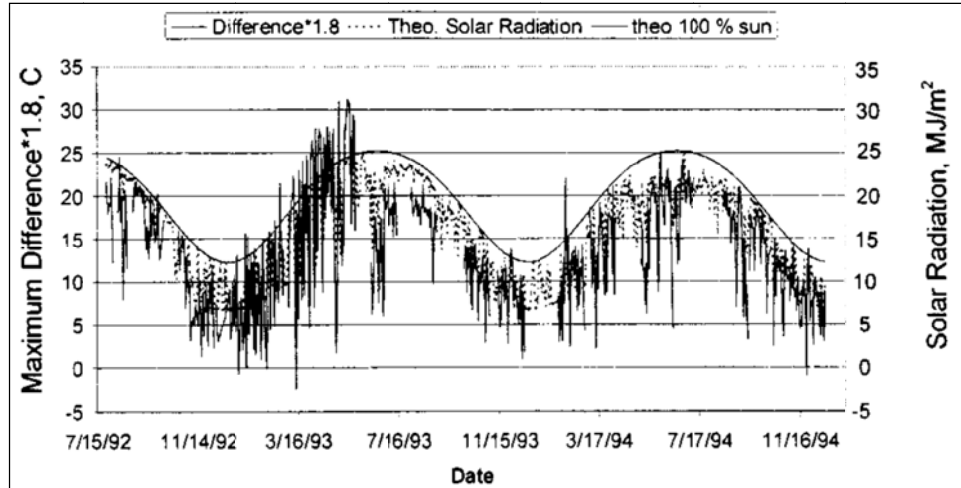


Figure 54: Maximum Negative Temperature Differences on the San Antonio “Y” Project (Roberts-Wollman et al., 2002)

Figure 55 compares the positive temperature difference times 1.8 with the theoretical solar radiation. This figure indicates that there is a strong correlation between temperature difference and solar radiation that follows an annual cycle.



**Figure 55: Comparison of Solar Radiation and the Maximum Positive Temperature Difference x 1.8 on the San Antonio “Y” Project (Roberts-Wollman et al., 2002)**

Figure 56 shows the measured deck temperatures for one location on the North Halawa Viaduct in 1995. This figure indicates a sinusoidal pattern to the peak deck temperatures that is similar to the data from the San Antonio “Y” Project. Figure 57 shows the deck and web temperatures for the month July 1995, which was the month with the largest measured deck temperatures. The largest deck temperatures during July occurred on the first day of the month. The temperature measurements over the course of the day were recorded at two hour increments and are shown in Figure 58. The thermocouple locations across the section are shown in Figure 59. By subtracting the deck measurements (i.e. location 14E) from the web measurements (location 22E), the temperature difference in the superstructure was obtained over the course of an extreme temperature day (see Figure 60). The temperature differenced exceeded 75% of the peak temperature difference for approximately 4.5 hours in the day (i.e. 19% of the day). The temperature difference exceeded 50% of the peak temperature difference for approximately 7 hours in the day (i.e. 29% of the day).

Load Combinations Investigation

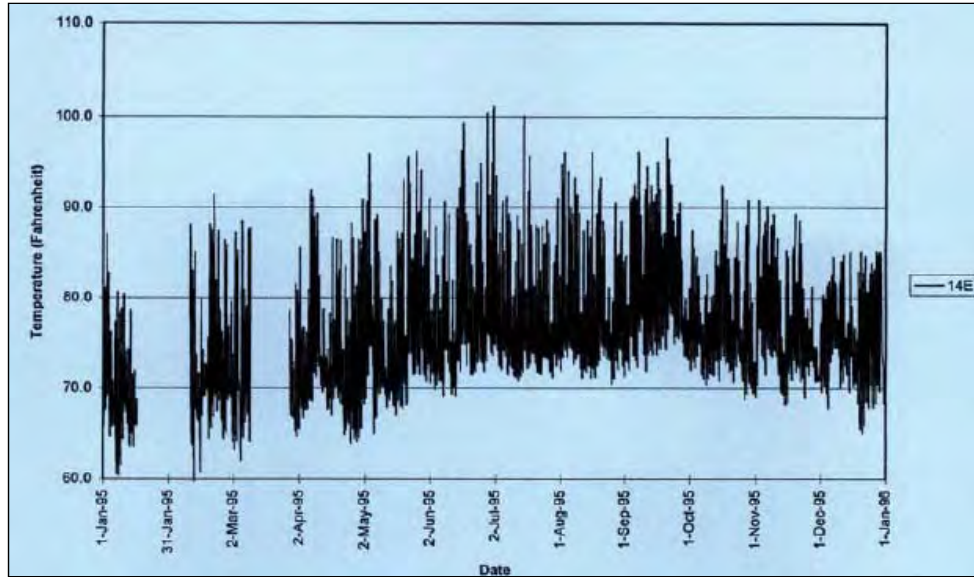


Figure 56: 1995, Thermocouple Readings on the North Halawa Valley Viaduct (Shushkewich, 1998)

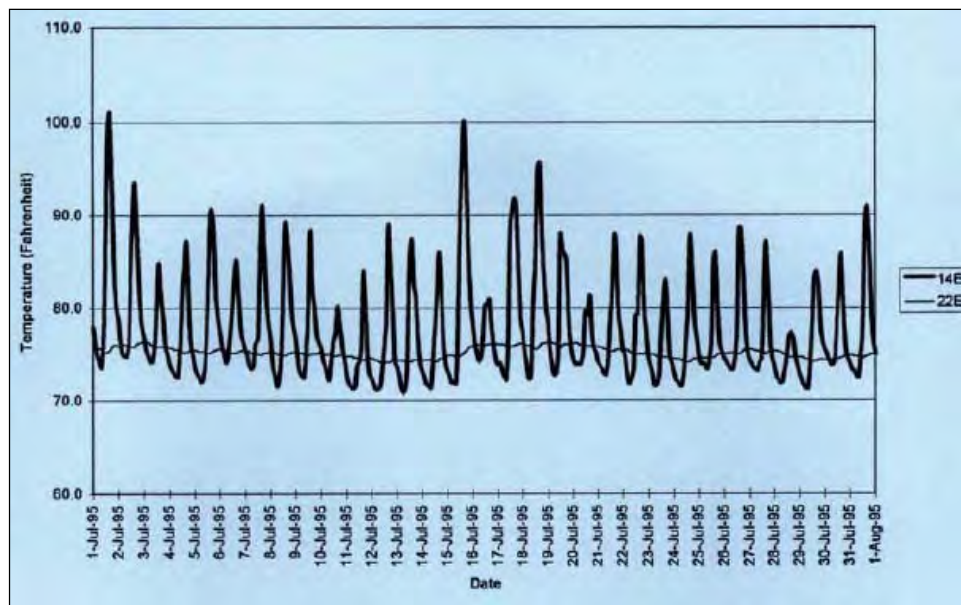


Figure 57: July 1995, Thermocouple Readings on the North Halawa Valley Viaduct (Shushkewich, 1998)

Load Combinations Investigation

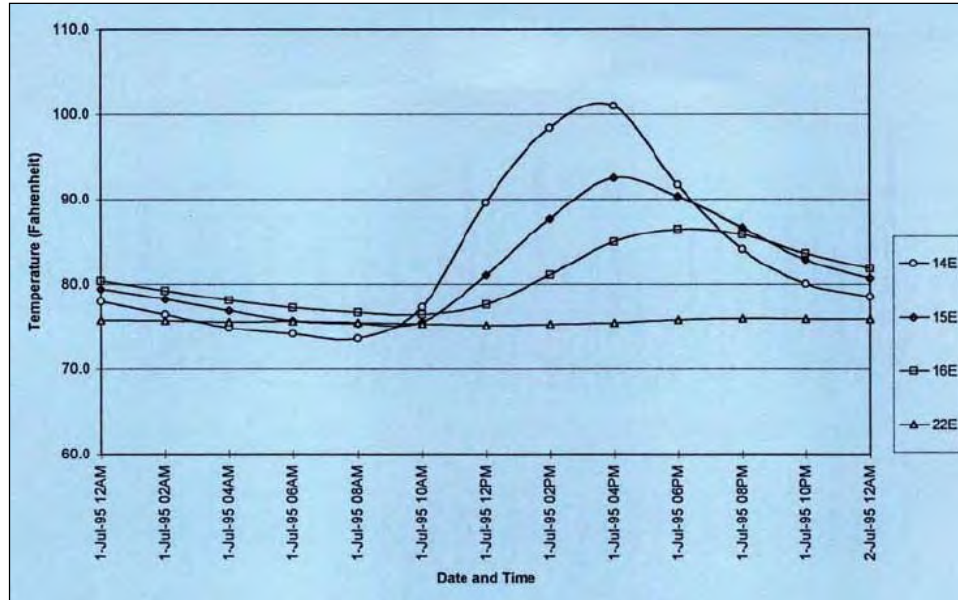


Figure 58: July 1, 1995, Thermocouple Readings on the North Halawa Valley Viaduct (Shushkewich, 1998)

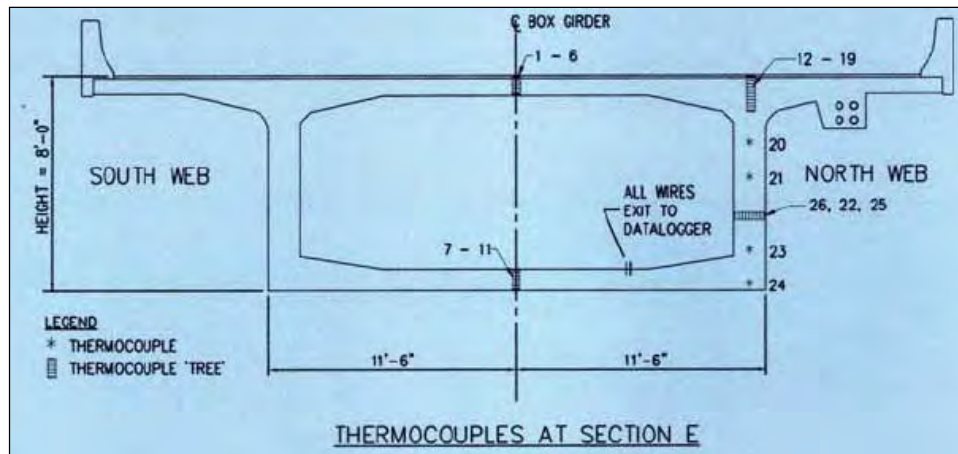


Figure 59: Thermocouple Locations on the North Halawa Valley Viaduct (Shushkewich, 1998)

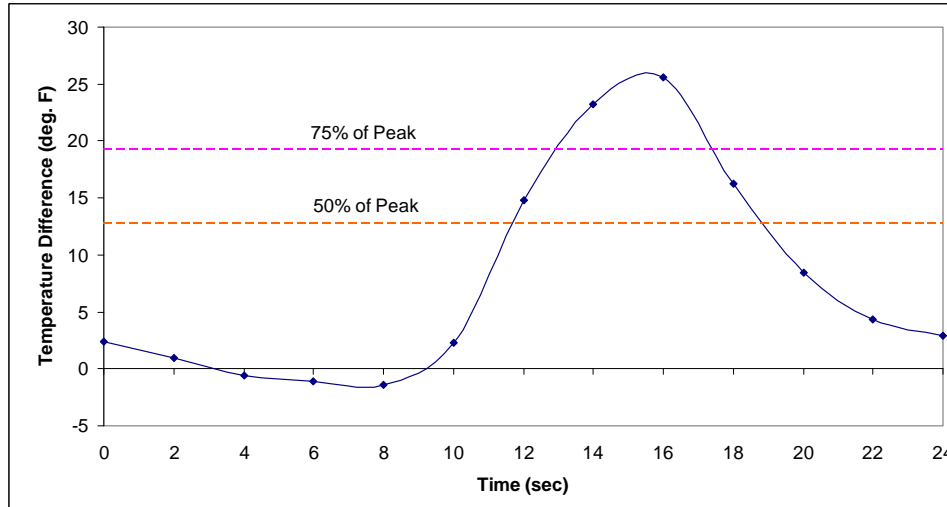


Figure 60: July 1, 1995, Temperature Differences between Thermocouple 14E and 22E on the North Halawa Valley Viaduct

## 6.4 Creep and Shrinkage

Several methods exist to estimate creep and shrinkage strains in concrete. One of the most prevalent in the bridge industry is the method from the CEB-FIP Model Code 1990 (Comité Euro-International du Béton, 1993). This method is applicable for concrete with compressive strengths up to 10,000 psi and relative humidities above 40% and is described below. The time dependant creep and shrinkage coefficients were determined based on expected parameters for segmental bridges in the span range of interest for this research project.

### 6.4.1 Shrinkage

The shrinkage strain,  $\epsilon_{cs}$ , of normal weight concrete is given by:

$$\epsilon_{cs}(t, t_s) = \epsilon_{cso} \beta_s(t, t_s) \quad 6-1$$

where  $\epsilon_{cso}$  is the basic shrinkage strain for a particular concrete and relative humidity, and  $\beta_s$  is a coefficient to describe the development of shrinkage with time and is given by:

$$\beta_s(t, t_s) = \left[ \frac{(t - t_s)}{350(h_e/h_o)^2 + (t - t_s)} \right]^{0.5} \quad 6-2$$

where  $t$  is the age of the concrete in days,  $t_s$  is the age of the concrete in days when shrinkage stated (i.e. the age at the end of moist-curing),  $h_o$  is taken as 4 inches,  $h_e$  is the effective thickness in inches to account for the volume/surface ratio and is given by:

$$h_e = 2A_c / u \quad 6-3$$

where  $A_c$  is the area of the cross section, and  $u$  is the perimeter of the cross section exposed to the atmosphere.

The effective thickness for the superstructures of the Otay River Bridge and the San Francisco-Oakland Bay Bridge Skyway at midspan and at the piers were calculated (see Table 11). These effective thicknesses were used as input for the time dependant shrinkage coefficient,  $\beta_s$  as shown in Figure 61.

**Table 11 Typical Effective Thickness for Precast Segmental Bridges**

Bridge	Location	Effective Thickness, $h_e$ (in)
Otay River Bridge	Pier	14.2
Otay River Bridge	Midspan	12.9
SFOBB Skyway	Pier	27.5
SFOBB Skyway	Midspan	19.3
Average →		<b>18.5</b>

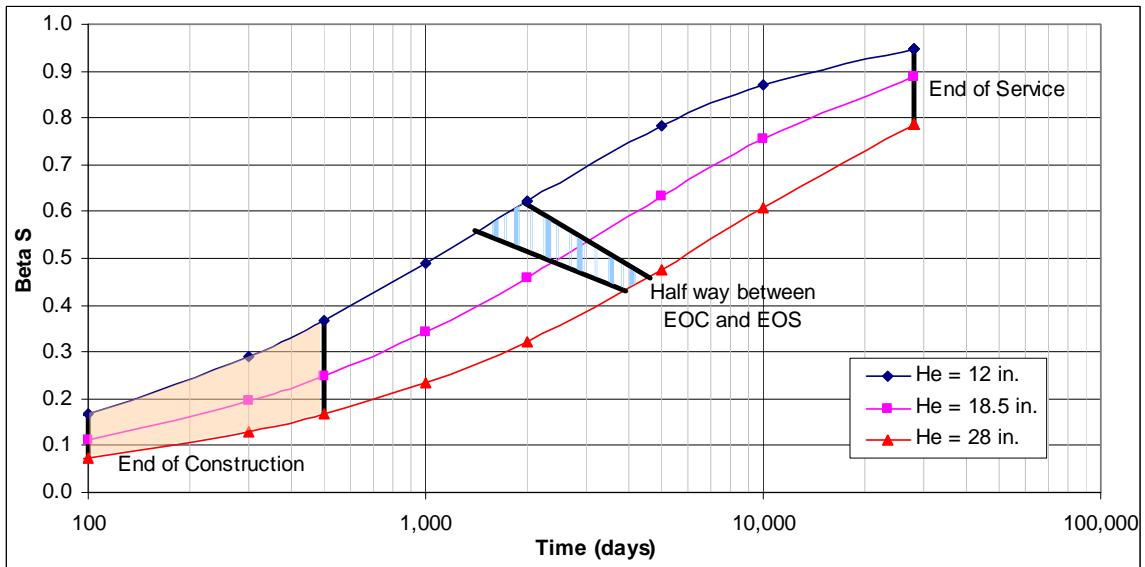


**Figure 61: Shrinkage vs Time**

#### 6.4.2 Creep

The creep strain,  $\epsilon_{cc}$ , of normal weight concrete is given by:

$$\epsilon_{cc}(t) = \frac{\sigma_c(t_o)}{E_c(28)} \phi(t, t_o) \tag{6-4}$$

where  $\sigma_c(t_o)$  is the stress in the concrete at the time of loading,  $t_o$ ,  $E_c(28)$  is the Young's modulus of concrete at 28 days, and  $\phi(t, t_o)$  is the creep coefficient given by:

$$\phi(t, t_o) = \phi_o \beta_c(t, t_o) \tag{6-5}$$

where  $\phi_o$  is the basic creep which is a function of the relative humidity, the composition of the concrete and the degree of hydration at the start of loading.  $\beta_c$  is a coefficient to account for the development of creep with time and is given by:

$$\beta_c(t, t_o) = \left[ \frac{(t - t_o)}{\beta_H + (t - t_o)} \right]^{0.3} \tag{6-6}$$

with

$$\beta_H = 150 \left[ 1 + \left( 1.2 \frac{RH}{RH_o} \right)^{18} \right] \frac{h_e}{h_o} + 250 \leq 1500 \tag{6-7}$$

where,  $t$  is the age of the concrete in days,  $t_o$  is the age of the concrete in days when the load is applied,  $RH$  is the relative humidity of the bridge site,  $RH_o$  is equal to 100 percent,  $h_o$  is taken as 4 inches,  $h_e$  is the effective thickness in inches (see Equation 3).

Figure 62 shows the time dependant creep coefficient,  $\beta_c$ , for expected relative humidities and effective thicknesses.

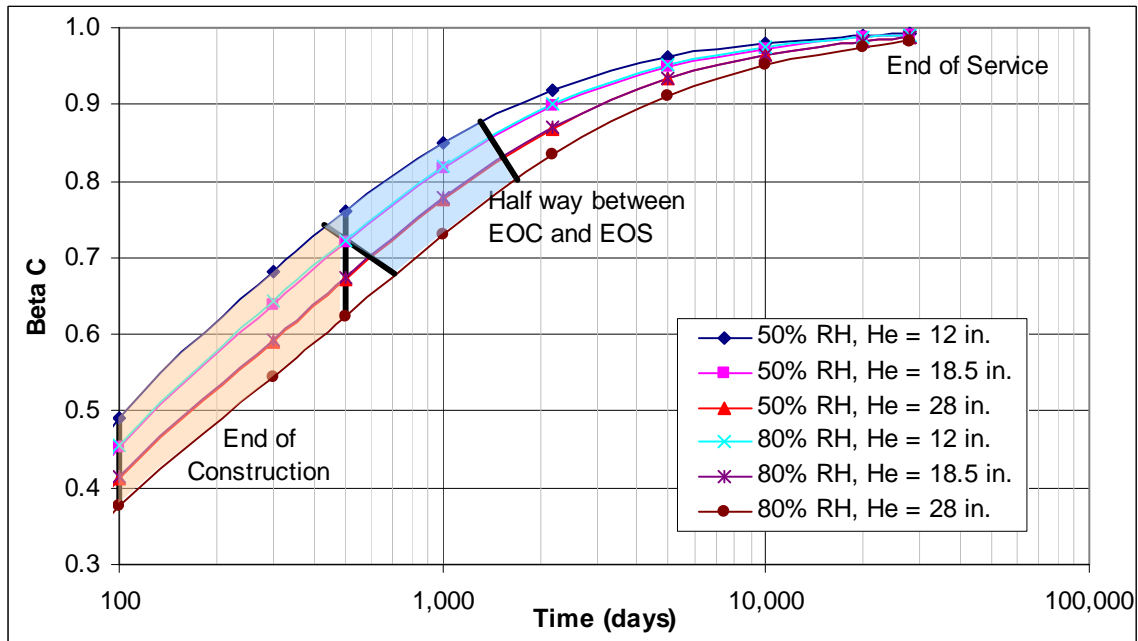


Figure 62: Creep vs Time

### 6.5 Discussion

To determine appropriate vertical earthquake load combinations, it is important to assess the likelihood of the considered load cases over the life of the bridge structure.

### 6.5.1 Thermal Gradient

If we assume, based on Figure 55 and Figure 56, that the days where the thermal difference between the top of the deck and the web exceed 75% of the peak thermal difference are of interest, we can conclude that on average, the thermal gradient load case will be of interest for approximately 25% of the year (i.e. during the summer months). In addition, the peak thermal gradient, defined at a thermal gradient that exceeds 75% of the maximum difference during the day, occurs only for a 4.5 hour period each day, i.e. for approximately 19% of the day. Thus there is only a 5% chance that a significant thermal load will exist on the bridge in a given year (i.e.  $0.25 \times 0.19 = 0.05$ ). Considering the effects of thermal gradients in addition to earthquakes will likely increase the return period by roughly a factor of 20.

### 6.5.2 Creep and Shrinkage

The age of each segment at the end of construction (EOC) will vary between approximately 100 and 500 days, depending on the construction rate, total number of bridge segments and order of segment placement. Assuming a bridge service life of 75 years, the concrete will be approximately 28000 days old at the end of service (EOS).

The shaded regions between 100 and 500 days in Figure 61 and Figure 62 indicate the amount of shrinkage and creep that has been removed from the concrete at the end of construction, respectively. The vertical line at 28000 days indicates the amount of shrinkage and creep removed from the system at the end of the service life of the bridge. The shaded regions in the middle of the figures represent the approximate half way point between the EOC and EOS stress states.

Figure 61 indicates that the half way point of shrinkage occurs between 1400 and 4600 days (4 to 13 years). This indicates that the shrinkage strains are below the half way point for approximately 5-17% of the bridges life and above the half way point for 83-95% of the bridges life.

Figure 62 indicates that the half way point of creep occurs between 430 and 1700 days (1 to 5 years). This indicates that the shrinkage strains are below the half way point for approximately 2-6% of the bridges life and above the half way point for 94-98% of the bridges life.

## 6.6 Recommendations

Based on the analyses performed and the results presented in this chapter, the following recommendations are made.

Do not consider temperature gradient effects in conjunction with earthquake loading as significant thermal gradients has at most a 5% chance of occurring simultaneously with a significant earthquake event.

## Load Combinations Investigation

Given the variability of creep and shrinkage due to the effective thickness, relative humidity, and construction rate of the project, it is difficult to accurately assess the likelihood that the pre-earthquake stresses being closer to EOC stresses or EOS stresses. Thus we recommend considering both EOC and EOS stress states in combination with vertical earthquake loads. This approach will provide reasonable bounds for the vertical earthquake response.

The recommended vertical earthquake load combinations are as follows:

$$DL_{EOC} \pm EQK_{vert} \quad \mathbf{6-8a}$$

$$DL_{EOS} \pm EQK_{vert} \quad \mathbf{6-8b}$$

These recommendations have been included in the complete design recommendations shown in Chapter 7.

## **Chapter 7: PEER REVIEWED DESIGN RECOMMENDATIONS**

### ***7.1 Objectives***

To develop a step-by-step design procedure that addressed the specific concerns of precast segmental bridges in seismic regions that incorporated appropriate: vertical load combinations (see Chapter 6); analysis techniques (see Chapter 5); and unbonded tendon lengths for the PT (see Chapter 2).

## 7.2 Detailed Design Procedure for 'Ordinary' Bridges

### 1 Seismic design spectra

#### 1.1 Design Spectra

- 1.1.1 Obtain a vertical and horizontal design spectrum from the geotechnical engineer. Confirm that the design spectrum was determined based on an appropriate return period.
- 1.1.2 Confirm that the vertical peak ground acceleration,  $PGA_v$ , is less than the peak spectral acceleration as illustrated in Figure 63. If this is not the case, designers should confer with the geotechnical consultant on the project and obtain a more accurate estimate of the vertical peak ground acceleration. An accurate estimate of  $PGA_v$  is required for the safety evaluation earthquake design level of 'Ordinary' bridges, as discussed in Section 7.1.2.

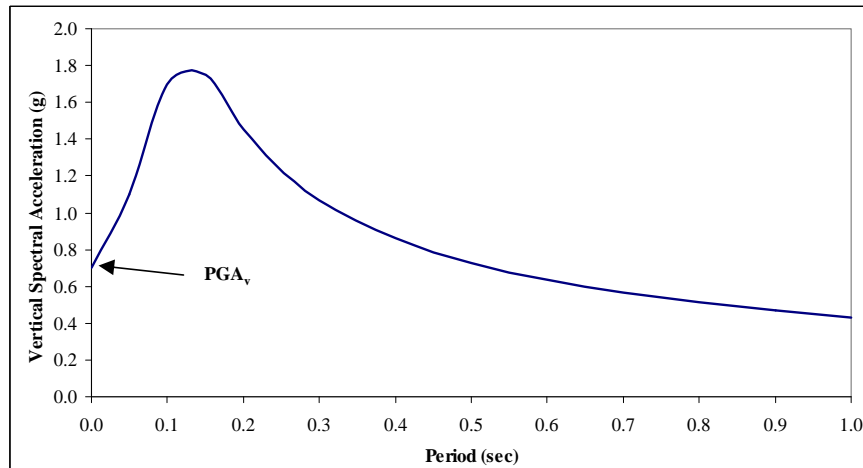


Figure 63 Sample Vertical Design Spectra

- 1.1.3 For bridges that are close to active faults, that is within approximately 10 km, check that the vertical design spectra was obtained from seismotectonic and geotechnical studies by determining the vertical to horizontal spectral ratio. For a given period divide the value on the vertical design spectra by the value on the horizontal design spectra. This ratio should vary from approximately 1.5 to 0.3 and should not be  $2/3$  for all periods, see Figure 64. If the V/H ratio is approximately equal to  $2/3$  and the site is within 10km of a fault, request a revised vertical spectra from the geotechnical engineer.

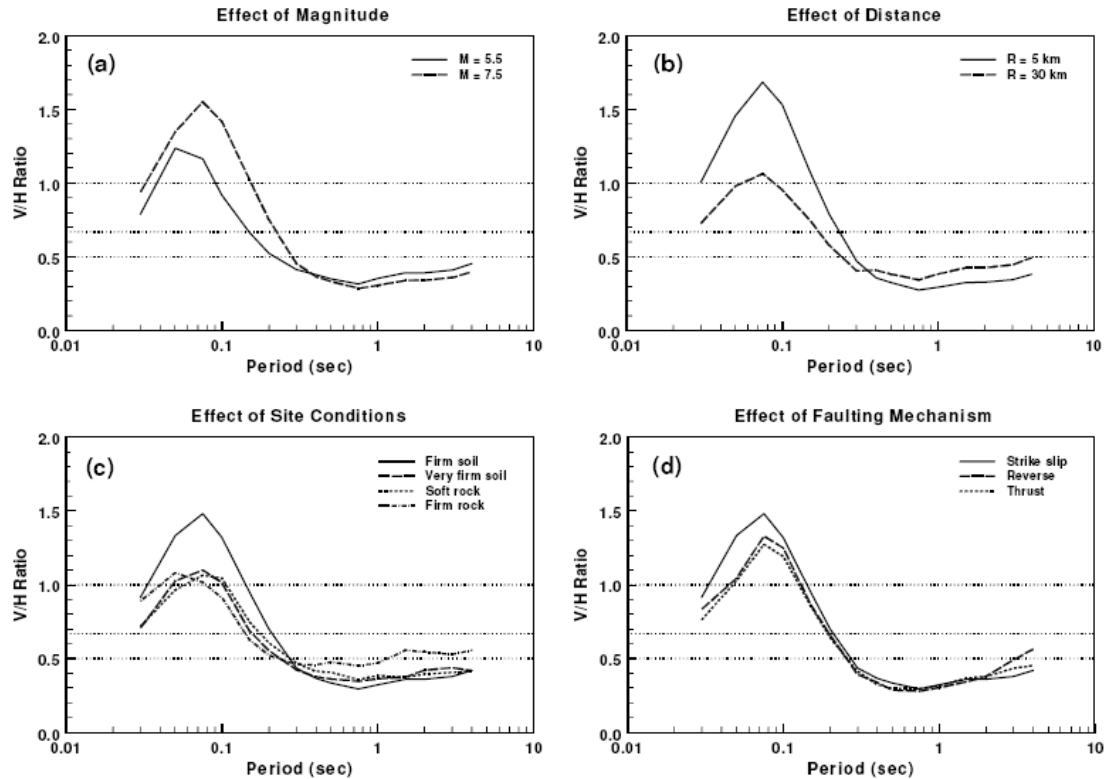


Figure 64 V/H ratio for Various Parameters (from Bozorgnia and Campbell, 2004)

## 2 Design for construction and service loads.

- 2.1 Design the bridge for service and construction loads. Ensure that the superstructure top and bottom flange thicknesses are large enough to support the large compression forces expected if the segment joints open. This will prevent the neutral axis from migrating into the webs.
- 2.2 The top flange at the piers and at midspan must be able to take the expected force of the top and continuity tendons after anchorage seating plus the yield force of the bottom tendons. Similarly, the bottom flange at the piers must be able to take the expected force of the bottom tendons after anchorage seating plus the yield force of the top and continuity tendons.

## 3 Column and superstructure capacities

- 3.1 Calculate the capacities of potential column plastic hinge regions using moment-curvature analysis as described in Section 3.3 of the Caltrans Seismic Design Criteria (Caltrans, 2009).
- 3.2 Superstructure Joints
  - 3.2.1 Calculate the capacities of at least the first two segment joints adjacent to the piers and at least three segment joints near midspan. Use moment-curvature analysis to

determine the moment capacity of the segment joints of 'Ordinary' bridges. Use expected concrete and pre-stressing material properties in these calculations as outlined in Section 3.3.1 of the Caltrans Seismic Design Criteria (SDC). Model the superstructure concrete as unconfined. Base the preload in the tendons on the expected tendon force at the end of construction and after considering losses due to creep, shrinkage and relaxation. Figure 65 shows a sample moment-curvature diagram of a superstructure segment joint for an 'Ordinary' bridge.

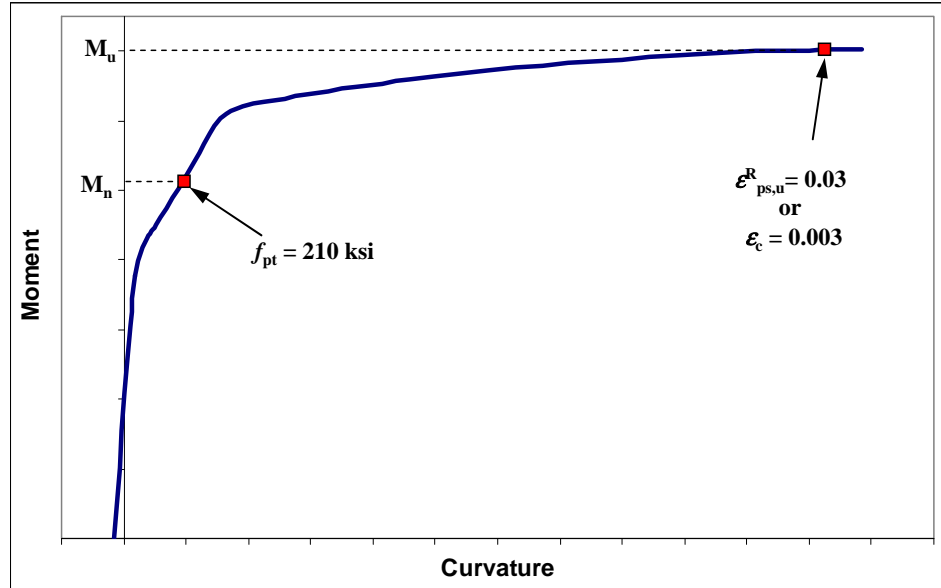


**Figure 65 Sample Moment-Curvature Diagram for 'Ordinary' Bridges**

- 3.2.2 Determine the ultimate moment capacity,  $M_u$ , based on a reduced ultimate prestressing steel strain,  $\epsilon_{ps,u}^R$ , of 0.03 or the strain in the extreme compression fibers  $\epsilon_c$  reaches 0.003.
- 3.2.3 Determine the nominal moment capacity,  $M_n$ , which is defined as the moment when the stress in the tendons reaches the limit of proportionality, defined as a stress of 210 ksi.
- 3.3 Superstructure Vertical Collapse Mechanism
- 3.3.1 Determine the uniform distributed load,  $w_{end}$  and  $w_{int}$ , that will develop the superstructure vertical collapse mechanisms using Equation 1.

$$\text{End Spans} \quad w_{end} = \frac{8}{4L_{end}L_i - 4L_i^2} \left( \left| M_{Pier}^- \right| \frac{L_i}{L_{end}} + M_i^+ \right) \quad \mathbf{1a}$$

$$\text{Interior Spans} \quad w_{int} = \frac{8}{L_{int}^2} \left( \left| M_{Pier}^- \right| + M_{Midspan}^+ \right) \quad \mathbf{1b}$$

$M_{Pier}^-$  is the ultimate negative bending capacity of the segment joint adjacent to the pier,  $M_{Midspan}^+$  is the ultimate positive bending capacity of the midspan segment joint of interior spans,  $M_i^+$  is the ultimate positive bending capacity of the end span segment joint of interest,  $L_i$  is the length from the abutment centerline to the segment joint of interest,  $L_{end}$  is the clear end span length and  $L_{int}$  is the clear interior span length. The likely vertical collapse mechanisms for end and interior spans are shown in Figure 66 and Figure 67, respectively.

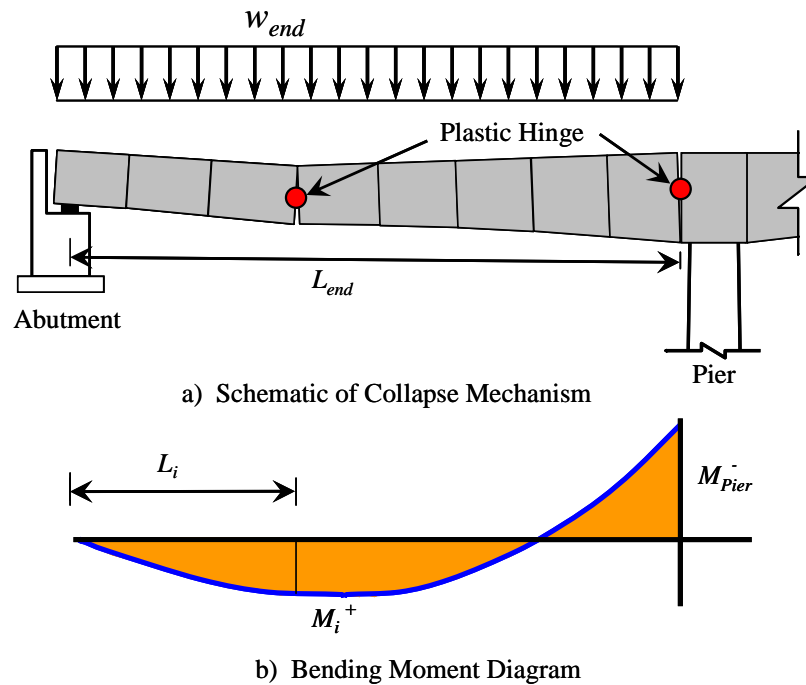


**Figure 66 End Span Collapse Mechanism**

## 'Ordinary' Bridges

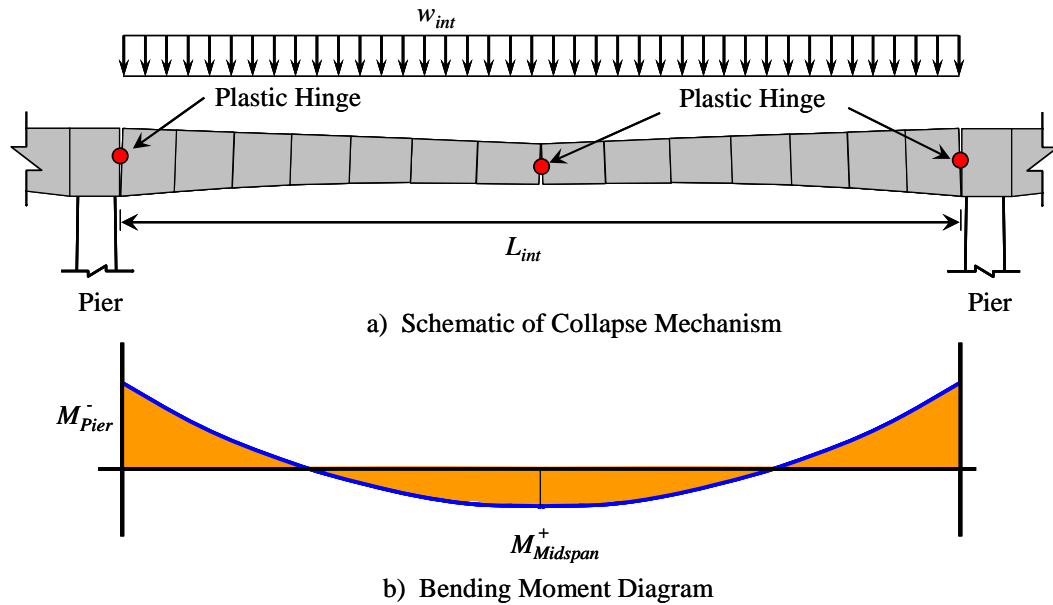


Figure 67 Interior Span Collapse Mechanism

- 3.3.2 Estimate the capacity of the collapse mechanism,  $S_c$ , in terms of vertical earthquake accelerations using Equation 2.

$$\text{Interior Spans} \quad S_{c_{int}} = \frac{W_{int}}{W_{int}/L_{int}} - 1 \quad 2a$$

$$\text{End Spans} \quad S_{c_{end}} = \frac{W_{end}}{W_{end}/L_{end}} - 1 \quad 2b$$

$W_{int}$  and  $W_{end}$  are the total weights of the interior and end span segments, respectively.

#### 4 Longitudinal construction staging analysis

- 4.1 Develop a construction staging model and perform a full longitudinal construction staging analysis (LCSA). This is common practice for segmental bridge construction and will not be discussed herein.
- 4.2 Obtain the bending moments at the location of critical superstructure segment joints at both the end of construction (EOC) and after the majority of creep and shrinkage (CS) has occurred.

#### 5 Longitudinal push over analysis

- 5.1 Perform a longitudinal push-over analysis. Use column flexural overstrengths based on the requirements of the Caltrans Seismic Design Criteria Section 4.3.1.

- 5.2 Design the superstructure for flexure to remain essentially elastic when the columns reach their flexural overstrength capacity. That is, the superstructure demands from the longitudinal push over must not exceed the nominal moment capacity,  $M_n$ .

## 6 Horizontal seismic demands and load combinations

- 6.1 Check the response of the bridge under horizontal (i.e. longitudinal and transverse) seismic demands. The peak vertical and horizontal earthquake demands are not likely to occur simultaneously due to the differences between the periods of the dominant modes and between the characteristics (i.e. frequency content and arrival time) of the vertical and horizontal input motions. Thus, the two effects can be considered independently.
- 6.2 Combine the horizontal earthquake demands based on the requirement of Section 2.1.2 of the Caltrans SDC. These requirements are appropriate for segmental bridges, thus special considerations are not provided herein.

## 7 Vertical seismic demands

### 7.1 FEE

- 7.1.1 Develop an elastic finite element model of the bridge. Linear elastic modeling is common practice, thus detailed guidelines will not be described herein.
- 7.1.2 Determine the vertical earthquake demands for the FEE design level of 'Ordinary' bridges from a vertical modal analysis using the complete quadratic combination (CQC) modal combination method (Clough and Penzien, 1993) based on a design spectrum per Section 1.1 above. Consider sufficient number of modes in the modal analysis to capture a minimum of 90% of the superstructure bridge mass in the vertical direction. Specify 2% modal damping to ensure consistency with the vertical design spectra.

### 7.2 SEE

Estimate the vertical earthquake demands,  $D_{vert}$ , using Equation 3.

$$D_{vert} = \max \left\{ \begin{array}{l} PGA_v \\ S_a(T_{v1}) \end{array} \right\} \quad 3$$

$S_a(T_{v1})$  is the vertical spectral acceleration at the dominant vertical mode. The dominant vertical mode is defined as the mode with the largest vertical modal participation factor. Note that pre-earthquake stress-states do not need to be considered in the capacity of the collapse mechanisms as they will not significantly affect the ultimate capacity of the superstructure.

## 8 Vertical earthquake load combinations

### 8.1 FEE

Combine the superstructure dead load demands at the end of construction and after the majority of creep and shrinkage has occurred, as determined from a full longitudinal construction staging analysis, with the vertical earthquake demands obtained from modal analysis. The vertical earthquake load combinations are as follows.

$$DL_{EOC} +/- EQ_{Vert} \quad \mathbf{4a}$$

$$DL_{CS} +/- EQ_{Vert} \quad \mathbf{4b}$$

$EQ_{Vert}$  are vertical earthquake demands and  $DL_{EOC}$  and  $DL_{CS}$  are dead load demands at the end of construction and after the majority of creep and shrinkage has occurred, respectively.

### 8.2 SEE

The vertical collapse mechanism is not strongly influenced by pre-earthquake stress states, thus no combinations are necessary for the safety evaluation of 'Ordinary' bridges.

## 9 Vertical demand/capacity ratios

### 9.1 FEE

Compare the segment joint moment demands obtained from Section 8 with the effective plastic moment capacity obtained from Section 3.1. Ensure that the moment demands are smaller than the nominal moment capacity for all superstructure segment joints.

### 9.2 SEE

Compare the capacity of the vertical collapse mechanisms,  $S_c$ , obtained from Section 3.3 with the estimated vertical earthquake demands,  $D_v$ , obtained from Section 7.1.2. Ensure that the demands are smaller than the capacities.

### 7.3 Detailed Design Procedure for "Important" Bridges

## 1 Seismic design spectra and ground motions

### 1.1 Design Spectra

- 1.1.1 Obtain a vertical and horizontal design spectrum from the geotechnical engineer. Confirm that the design spectrum was determined based on an appropriate return period.
- 1.1.2 Confirm that the vertical peak ground acceleration,  $PGA_v$ , is less than the peak spectral acceleration as illustrated in Figure 68. If this is not the case, designers should confer with the geotechnical consultant on the project and obtain a more accurate estimate of the vertical peak ground acceleration. An accurate estimate of  $PGA_v$  is required to ensure that the spectrum compatible ground motions are matched to an appropriate spectrum.

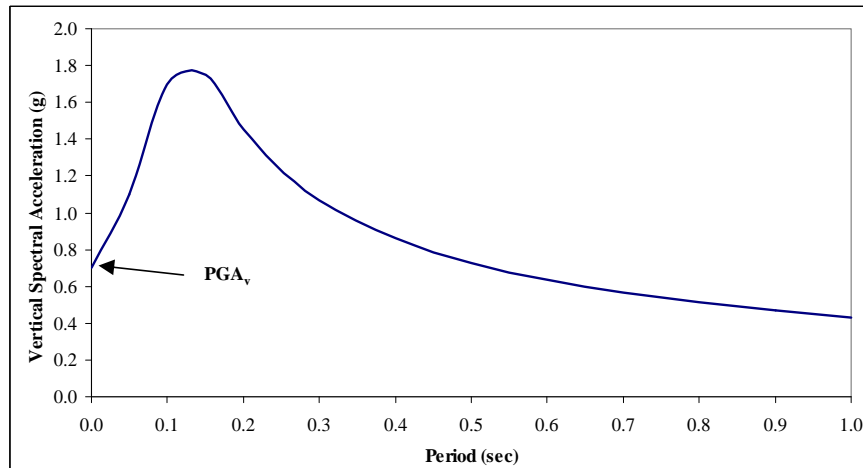
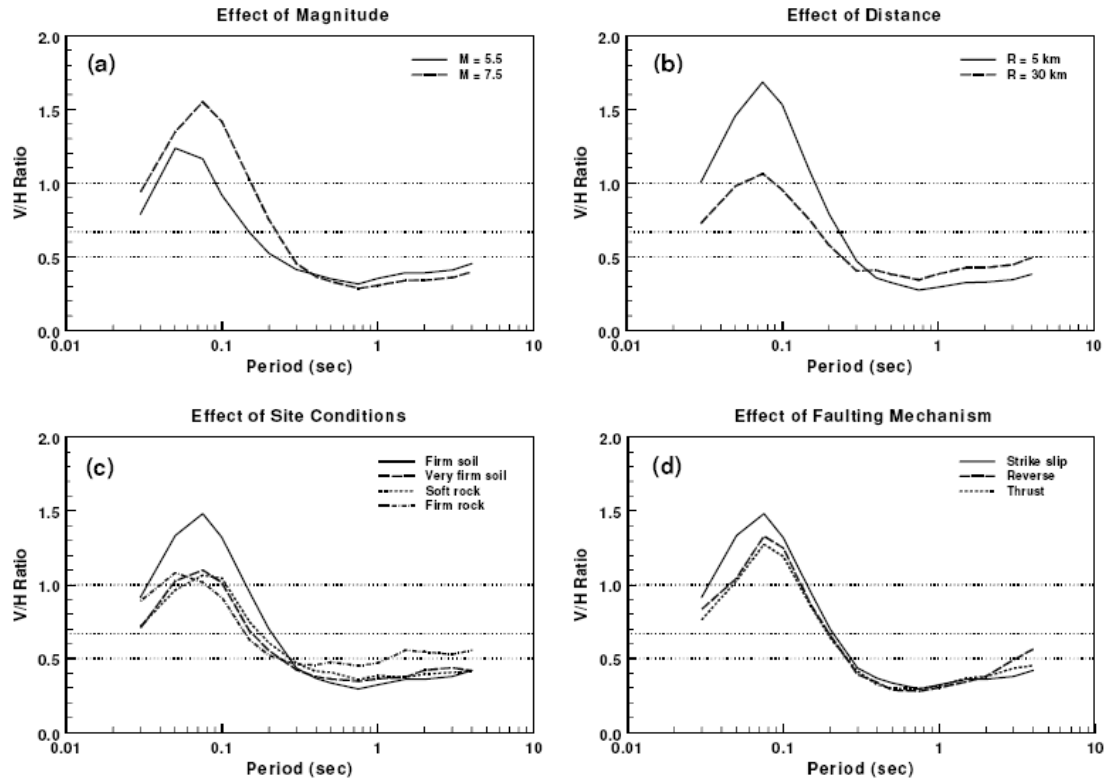


Figure 68 Sample Vertical Design Spectra

- 1.1.3 For bridges that are close to active faults, that is within approximately 10 km, check that the vertical design spectra was obtained from seismotectonic and geotechnical studies by determining the vertical to horizontal spectral ratio. For a given period divide the value on the vertical design spectra by the value on the horizontal design spectra. This ratio should vary from approximately 1.5 to 0.3 and should not be  $2/3$  for all periods, see Figure 64. If the V/H ratio is approximately equal to  $2/3$  and the site is within 10km of a fault, request a revised vertical spectrum from the geotechnical engineer.



**Figure 69 V/H ratio for Various Parameters (from Bozorgnia and Campbell, 2004)**

## 1.2 Time History Ground Motions

- 1.2.1 Obtain a minimum of three sets of spectrum compatible ground motions from the geotechnical engineer for each performance level being considered (i.e. safety evaluation earthquake and/or functional evaluation earthquake) to estimate the seismic demands on ‘Important’ bridges.
- 1.2.2 Obtain the deaggregation of the design spectra and the description of the earthquake scenario (that is, moment magnitude and distance to fault) of each spectrum compatible ground motion. Sample deaggregations are shown in Figure 70 and Figure 71.
- 1.2.3 Check that the ground motions are representative of the deaggregation near the dominant periods of the bridge. It is common for different earthquake scenarios to dominate the deaggregation at different periods. If this is the case, at least one ground motion set should come from a scenario shown in the deaggregation with a fractional contribution of greater than 0.4 at critical periods. For example, if the bridge has dominant modes at 0.5 seconds and 4.0 seconds and the deaggregations are shown in Figure 70 and Figure 71, respectively, then at least one ground motion set should be from an earthquake with a moment magnitude between 6.5 and 7.0 at a distance of 5 to 10 km and at least one set should be from an

'Important' Bridges

earthquake with a moment magnitude between 7.0 and 7.5 at a distance of 20 to 30 km.

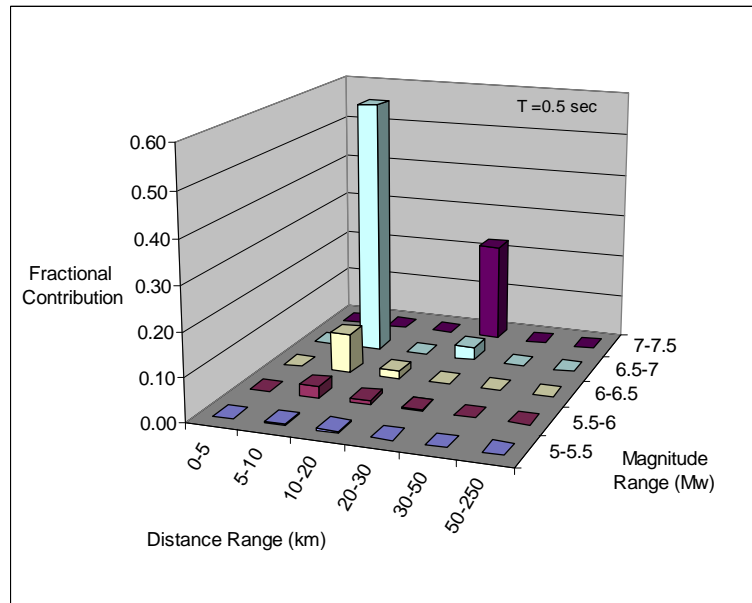


Figure 70 Deaggregation of a 2500 Year Return Design Spectra at a Period of 0.5 sec.

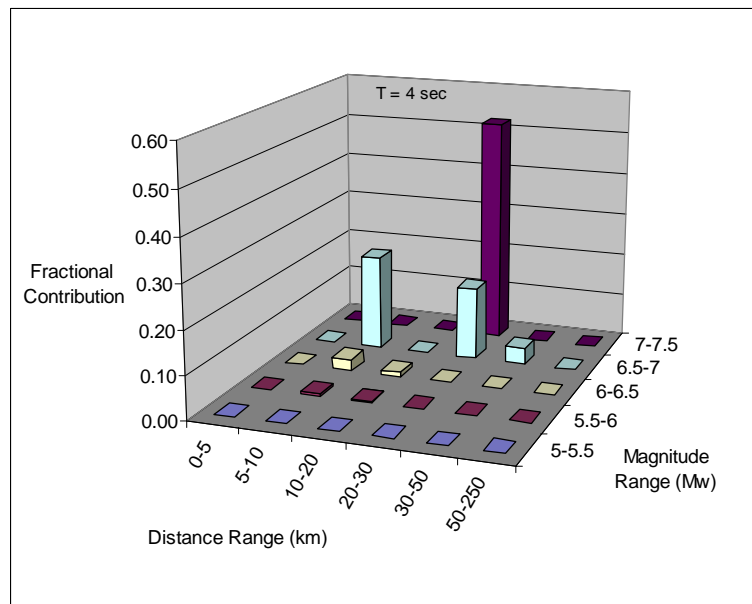


Figure 71 Deaggregation of a 2500 Year Return Design Spectra at a Period of 4.0 sec.

## 2 Design for construction and service loads.

- 2.1 Design the bridge for service and construction loads. Ensure that the superstructure top and bottom flange thicknesses are large enough to support the large compression forces expected if the segment joints open. This will prevent the neutral axis from migrating into the webs.
- 2.2 The top flange at the piers and at midspan must be able to take the expected force of the top and continuity tendons after anchorage seating plus the yield force of the bottom tendons. Similarly, the bottom flange at the piers must be able to take the expected force of the bottom tendons after anchorage seating plus the yield force of the top and continuity tendons.

## 3 Column and superstructure capacities

- 3.1 Calculate the capacities of potential column plastic hinge regions using moment-curvature analysis as described in Section 3.3 of the Caltrans Seismic Design Criteria (Caltrans, 2009).
- 3.2 Superstructure Joints
  - 3.2.1 Determine the moment capacity of segment joints of 'Important' bridges using detailed local non-linear finite element models based on the expected concrete and prestressing material properties per Section 3.2 of the Caltrans SDC. These models must capture the non-linear characteristics of the extreme concrete fibers in both tension and compression. In addition, the model must capture the non-linear characteristics of the PT tendons with accurate estimates of the pretension forces. Determine the moment-rotation characteristics of the segment joints by subjecting the models to monotonic rotational push demands. Cyclic push analyses are not required, thus the hysteretic rules used for the concrete and PT members are unimportant. Use an equivalent unbonded length for the PT tendons based on Equation 5.

$$L_u = 10.3\sqrt{A_{PT}} \quad 5$$

The reader is referred to Chapter 2: of this report, where the experimental results are discussed.

Figure 72 shows a sample moment-rotation diagram of a superstructure segment joint for an 'Important' bridge.

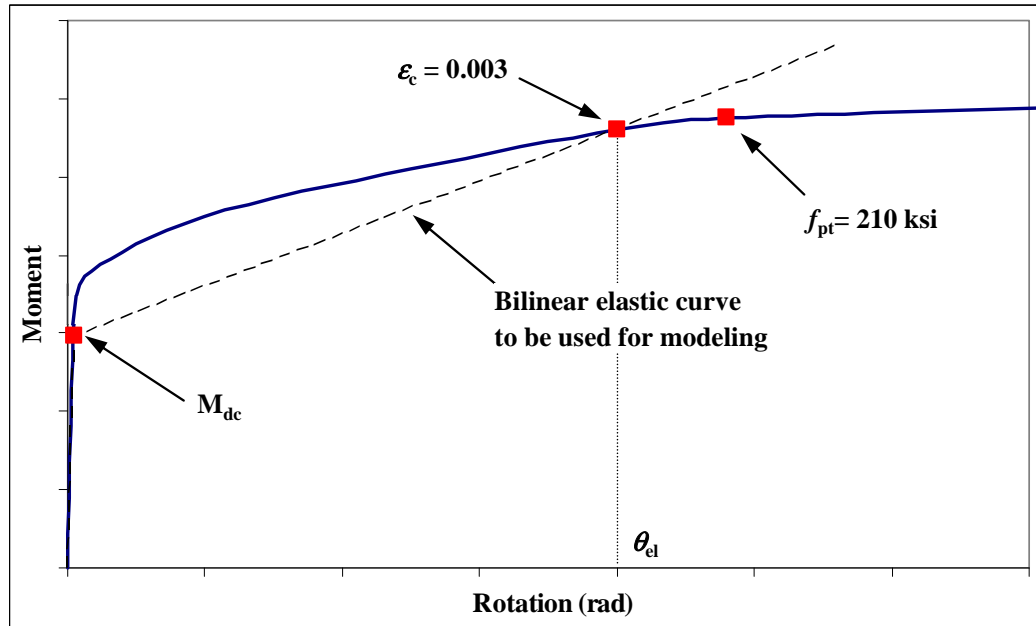


Figure 72 Sample Moment-Rotation Diagram for SEE of 'Important' Bridges

- 3.2.2 Determine the elastic rotation limit,  $\theta_{el}$ , based on a concrete strain,  $\epsilon_c$ , of 0.003, or a stress in the ASTM A416 prestressing tendon,  $f_{pt}$ , of 210 ksi, whichever generates the smaller rotation.
- 3.2.3 Obtain the decompression moment,  $M_{dc}$ , by observing the bending moment when the extreme concrete fiber stress exceeds the residual tension stress (taken as 13% of the direct tensile strength of concrete, i.e.  $0.13 * 4\sqrt{f'_c(\text{psi})} = 0.52\sqrt{f'_c(\text{psi})}$ )
- 3.2.4 Determine the bi-linear elastic curve to be used for the modeling of segment joints. The curve is characterized by the gross section stiffness until the decompression moment is reached. At this point the curve deviates towards the lesser of the point where the concrete strain reaches 0.003 or the tendon stress reaches 210 ksi (see Figure 72).

#### 4 Longitudinal construction staging analysis

- 4.1 Develop a construction staging model and perform a full longitudinal construction staging analysis (LCSA). This is common practice for segmental bridge construction and will not be discussed herein.
- 4.2 Obtain the bending moments at the location of critical superstructure segment joints at both the end of construction (EOC) and after the majority of creep and shrinkage (CS) has occurred.

## 5 Longitudinal push over analysis

- 5.1 Perform a longitudinal push-over analysis for all bridges regardless of importance classification. Use column flexural overstrengths based on the requirements of the Caltrans Seismic Design Criteria Section 4.3.1.
- 5.2 Design the superstructure for flexure to remain essentially elastic when the columns reach their flexural overstrength capacity. That is, the superstructure demands from the longitudinal push over must not exceed the elastic rotation capacity,  $\theta_{el}$ .

## 6 Seismic demands (FEE and SEE)

- 6.1 Develop a 3D nonlinear finite element model of the bridge. Model the superstructure with non-linear elastic moment-rotation hinging elements at a minimum of two segment joints adjacent to the piers and three segment joints near midspan (see Figure 73). The remainder of the superstructure may be modeled using elastic elements. The moment-rotation characteristics of select segment joints should be determined from local finite element models as outlined in Section 3.2. Pre-earthquake stress-states of the segment joints must be considered. Thus, forces must be applied across the non-linear segment joint members to calibrate the model to the EOC and CS stress-states obtained from a LCSA (see Section 4).

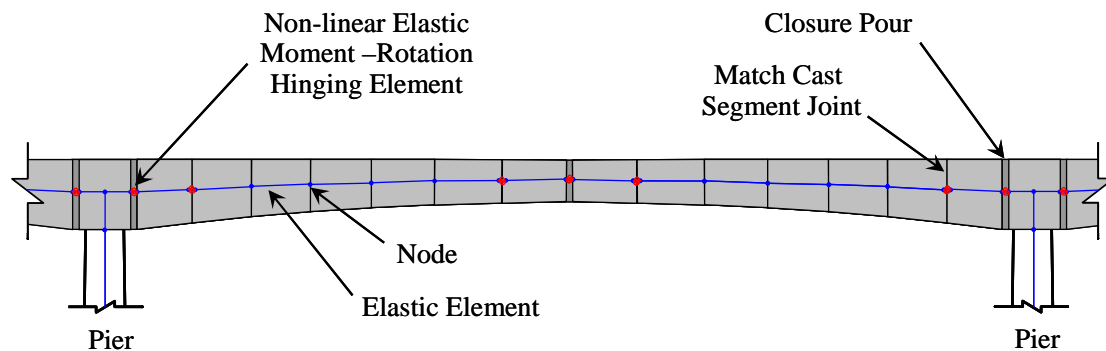


**Figure 73 Recommended Superstructure Modeling Approach for SEE Design Level of 'Important' Bridges**

It is important to note that many finite element programs including SAP2000 requires that the nonlinear curves pass through the origin. Thus the bilinear curves moment rotation curves for the superstructure segment joints need to be offset as illustrated in Figure 74. This will maintain the rotations at which limit states occurred, but will shift the moments. This is reasonable since the expected behavior does not pass through the origin because of the effects of PT on the section, which was not incorporated into the NEM.

## 'Important' Bridges

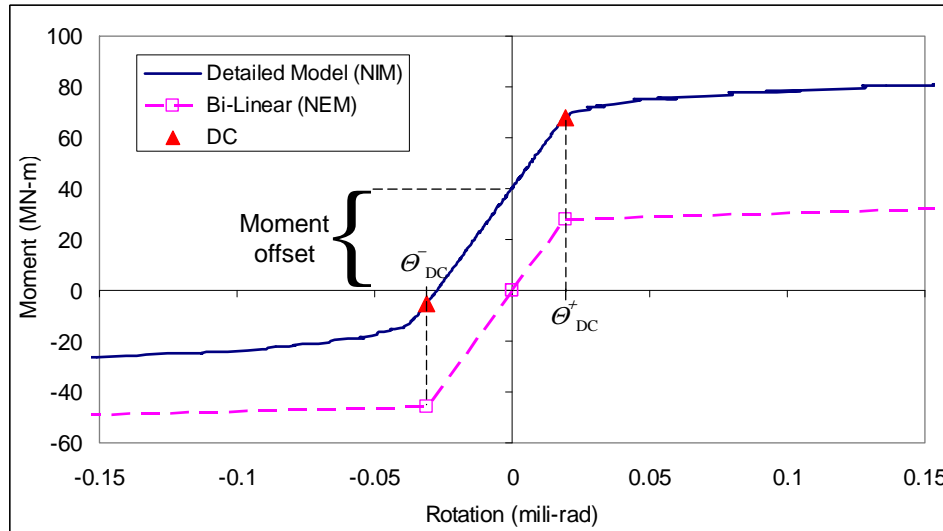


**Figure 74. Offset in Moment-Rotation Curves Required for Modeling of Segment Joints**

- 6.2 Use Rayleigh damping with as little damping as possible to ensure stability of the model. Damping coefficients not greater than 2% in the modes contributing to the first 90% of the vertical mass should be sufficient. For three-dimensional analyses, the damping coefficients in the three principal axes should, again, be maintained to no more than 2% for all the modes contributing to the first 90 percent of the mass in each axis.
- 6.3 Check the damping value at dominant horizontal and vertical modes to ensure that these modes are neither overdamped nor underdamped. A dominant mode is defined as a mode with at least 20% mass participation. Damping of all dominant modes should not exceed 2%. Adjust the specified Rayleigh damping periods to ensure these damping restrictions are achieved.
- 6.4 Obtain the vertical earthquake demands for the FEE and SEE design level of 'Important' bridges from 3D non-linear dynamic time history analysis, subjected to horizontal and vertical ground motions per Section 4.5.2. Use the maximum bridge response from the ground motion sets for design.

## 7 Vertical demand/capacity ratios

Compare the segment joints rotation demands obtained from Section 6 with the segment joints elastic rotation capacity obtained from Section 3.2. Ensure that the rotational demands are smaller than the elastic rotation capacity of the segment joints.

### 7.4 Design Flowcharts

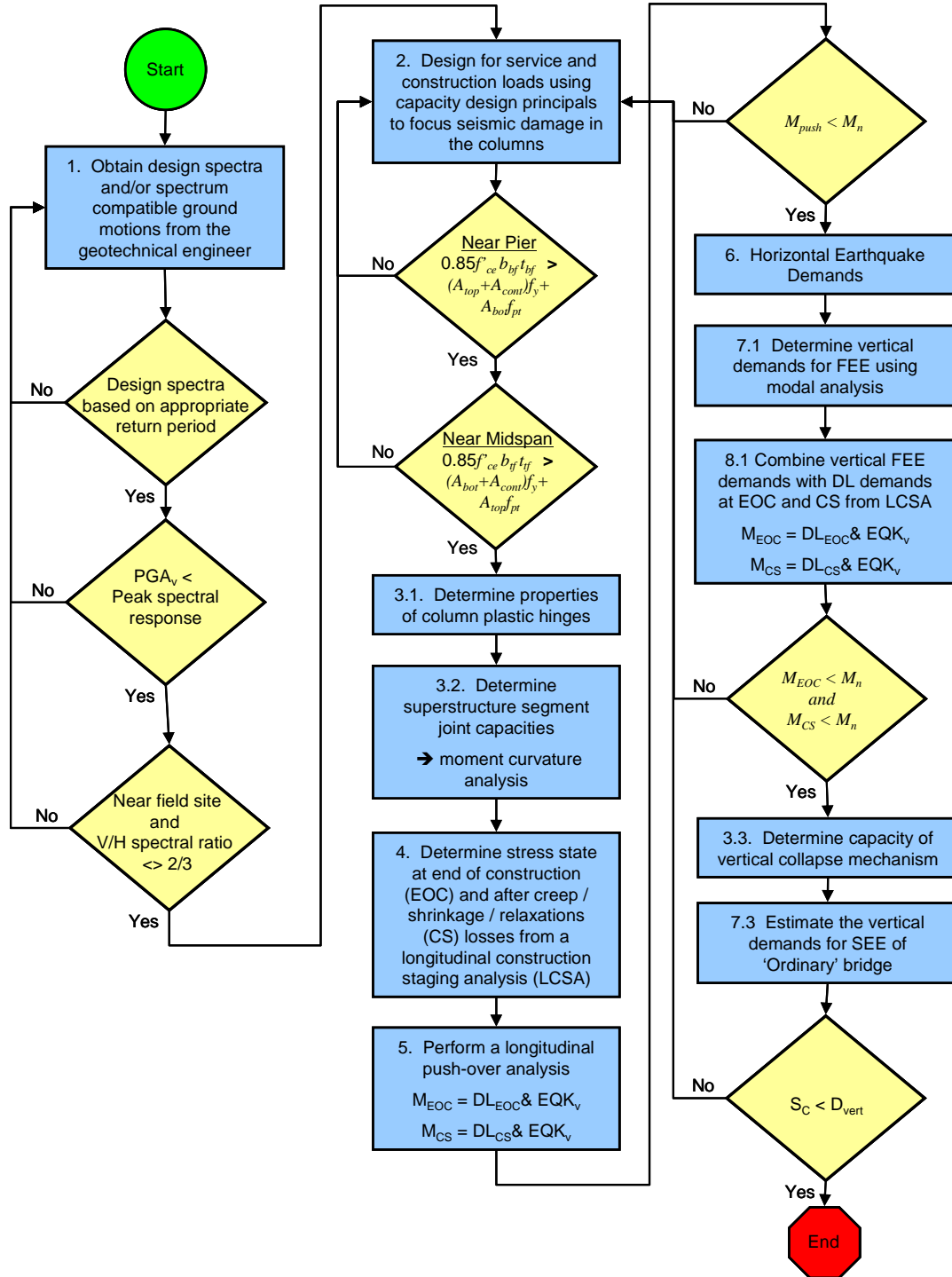


Figure 75 Design Flowchart for 'Ordinary' Bridges

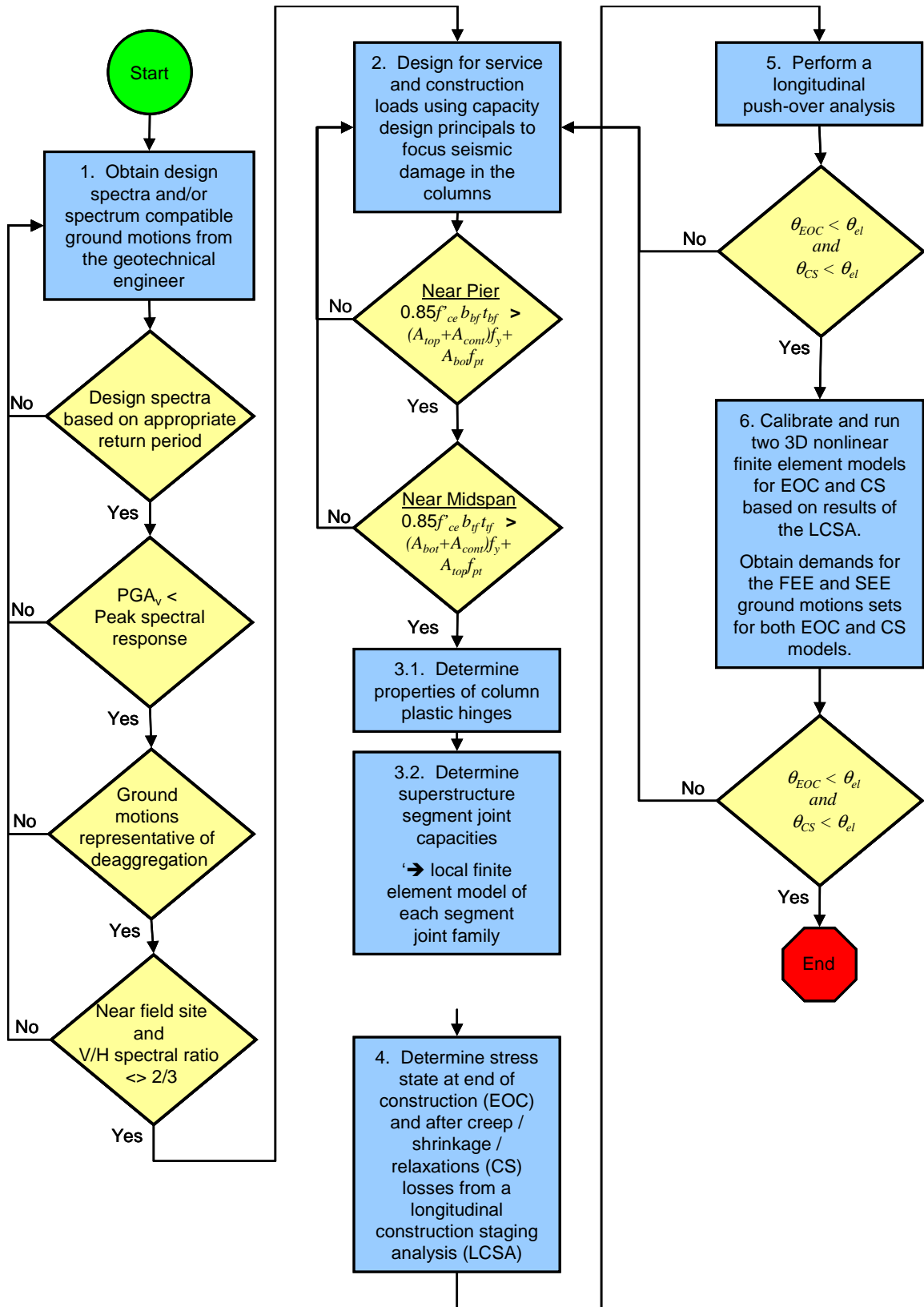


Figure 76 Design Flowchart for 'Important' bridges

## Chapter 8: CONCLUSIONS

The primary products of this research project include: a framework for the seismic design of precast segmental construction (see Chapter 4); a preliminary set of standard cross sections for precast concrete segmental bridge superstructures (see Chapter 3 and Appendix B); seismic design recommendations for segmental construction (see Chapter 7); and sample calculations that illustrate the use of the recommendations (see Appendix C). Specific conclusions based on the results of the experimental and analytical work presented in this project, and incorporated into the products listed above, include:

- Visual inspection of the tendon indicated that slip between the strands and the grout occurred primarily within the 12 inches (305 mm) adjacent to the segment joint.
- The tendon strands, and grouted duct behaved as a single entity and slipped relative to the surrounding concrete.
- The tendon yielded along the full length of the test region prior to failure. Such yielding, however, did not occur until strains of approximately 1.4% were observed in the joint region.
- The debond characteristics of multi-strand tendons are primarily influenced by the size of the tendon. The type or strength of grout showed no noticeable influence on bond characteristics of multi-strand tendons.
- An equation to evaluate the equivalent unbonded length of multi-strand tendons was developed and is valid up to full yielding of the tendon limit state, see Eqn. 2-2. The unbonded length of multi-strand tendons is proportional to the square root of the cross section area of the tendon. It is important to note that this equation was based on experiments that utilized corrugated metal ducts and mild steel longitudinal reinforcement ratio of 0.45% and may not accurately represent conditions that are significantly different from the experiments.
- Variations in the damping value of different modes due to Rayleigh damping caused the difference between elastic time history and modal analyses. The Rayleigh damping for vertical analyses should be based on the dominant vertical modes, not the dominant longitudinal mode, and 10Hz. It is recommended that Rayleigh damping be defined at frequencies where (i) the cumulative vertical

## Conclusions

modal mass exceeds 20% and (ii) the cumulative vertical modal mass exceeds 80%.

- The results from the linear elastic time history were consistent with the results from the nonlinear inelastic model. Both models indicate that the superstructure segments will exceed the decompression limit state at select segments, primarily at the midspan segments under negative bending and only due to the 2500 year hazard.
- The nonlinear elastic model predicted segment joint rotations that were up to five times larger than the rotations predicted by the nonlinear inelastic model. This is because the NEM used a bi-linear curve that assumed that the segment joint was already fully cracked.
- Do not consider temperature gradient effects in conjunction with earthquake loading as significant thermal gradients has at most a 5% chance of occurring simultaneously with a significant earthquake event.
- Given the variability of creep and shrinkage due to the effective thickness, relative humidity, and construction rate of the project, it is difficult to accurately assess the likelihood that the pre-earthquake stresses being closer to EOC stresses or EOS stresses. Thus we recommend considering both EOC and EOS stress states in combination with vertical earthquake loads. This approach will provide reasonable bounds for the vertical earthquake response.

## References

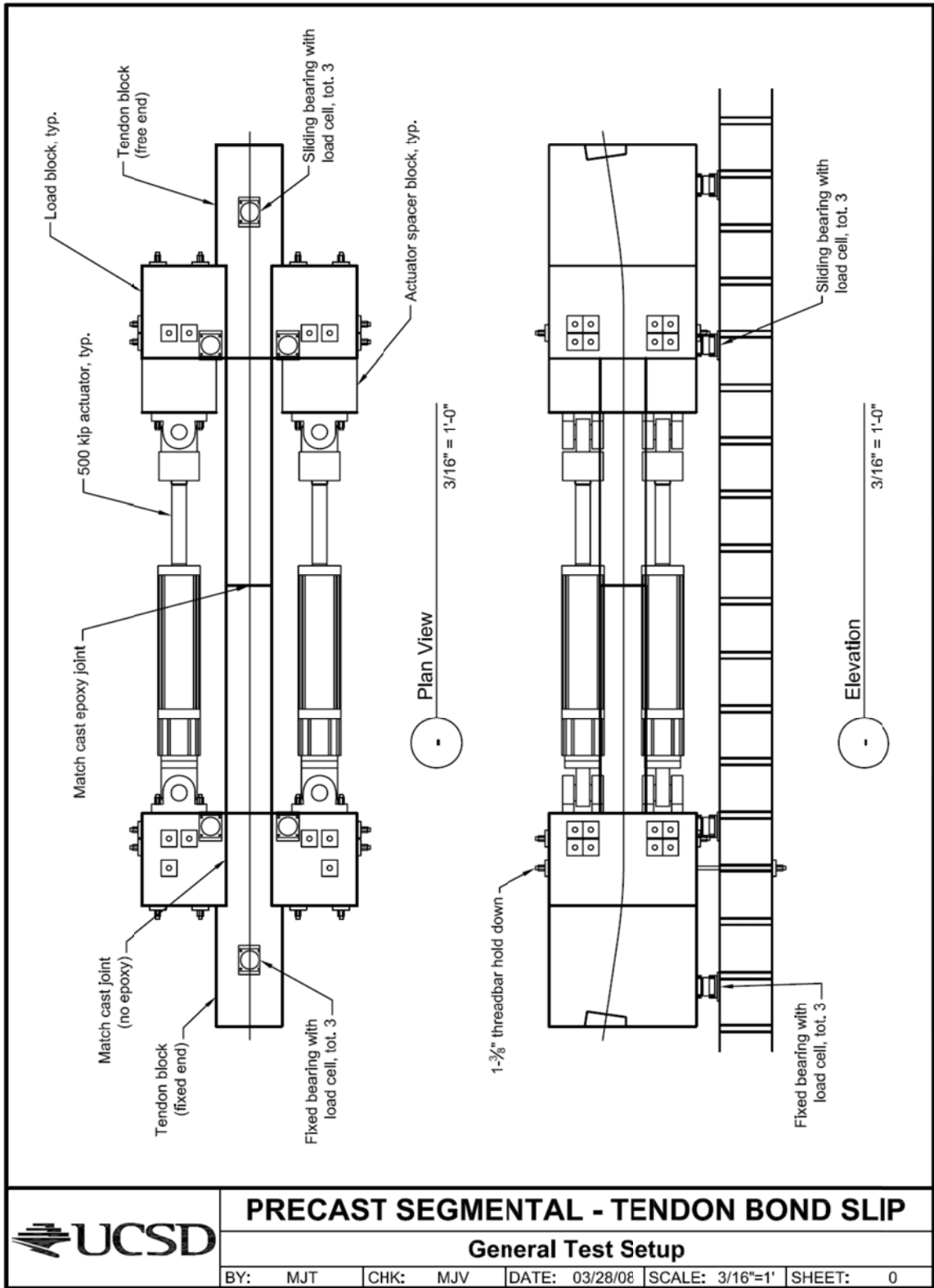
1. AASHTO, "AASHTO LRFD Bridge Design Specifications – Customary U.S Units - 2006 Interim Revisions", Third Edition, American Association of State Highway and Transportation Officials, Washington, D.C., 2006.
2. Abrahamson, N.A., "Non-Stationary Spectral Matching", Seismological Research Letters, Vol. 30, No. 1, 1992.
3. ACI, "Building Code Requirements for Structural Concrete (ACI 318-05) and Commentary (ACI 318R-05)" American Concrete Institute, Farmington Hills, Michigan, 2005.
4. Barnes, R.W., Burnes, N.H., and Kreger, M.E., "Development Length of 0.6 inch Prestressing Strand in Standard I-Shaped Pretensioned Concrete Beams", Center for Transportation Research, Bureau of Engineering Research, University of Texas at Austin, Research Report 1388-1, December, 1999.
5. Bozorgnia, Y., Campbell, K.W., "The Vertical-to-Horizontal Response Spectral Ratio and Tentative Procedures for Developing Simplified V/H Vertical Design Spectra", Journal of Earthquake Engineering, Vol. 8, No 2, pp 175-207, 2004.
6. Caltrans, "Seismic Design Criteria", Version 1.5, California Department of Transportation, Sacramento, CA, June 2009.
7. Carr, A.J., "RUAUMOKO – Users Manual". University of Canterbury, Christchurch, New Zealand, February 2004.
8. Clough, R.W., Penzein, J., "Dynamics of Structures", Second Edition, McGraw-Hill, Inc., New York, N.Y., 1993.
9. Kawashima, K, and Aizawa, K, "Modification of Earthquake Response Spectra with Respect to Damping Ratio", 3rd US National Conference on Earthquake Engineering, Charleston, SC, USA, 1986.
10. Kunnath, S., Abrahamson, N., Chai, Y.H., Erduran, E., Yilmaz, Z., "Effects of Vertical Ground Motions on the Seismic Behavior of Highway Bridge Structures", Draft Report Submitted to the California Department of Transportation, September, 2007.
11. Mattock, A.H., "Flexural Strength of Prestressed Concrete Sections by Programmable Calculator," PCI Journal, V. 24, No.1, pp. 32-54, Jan-Feb 1979.

## References

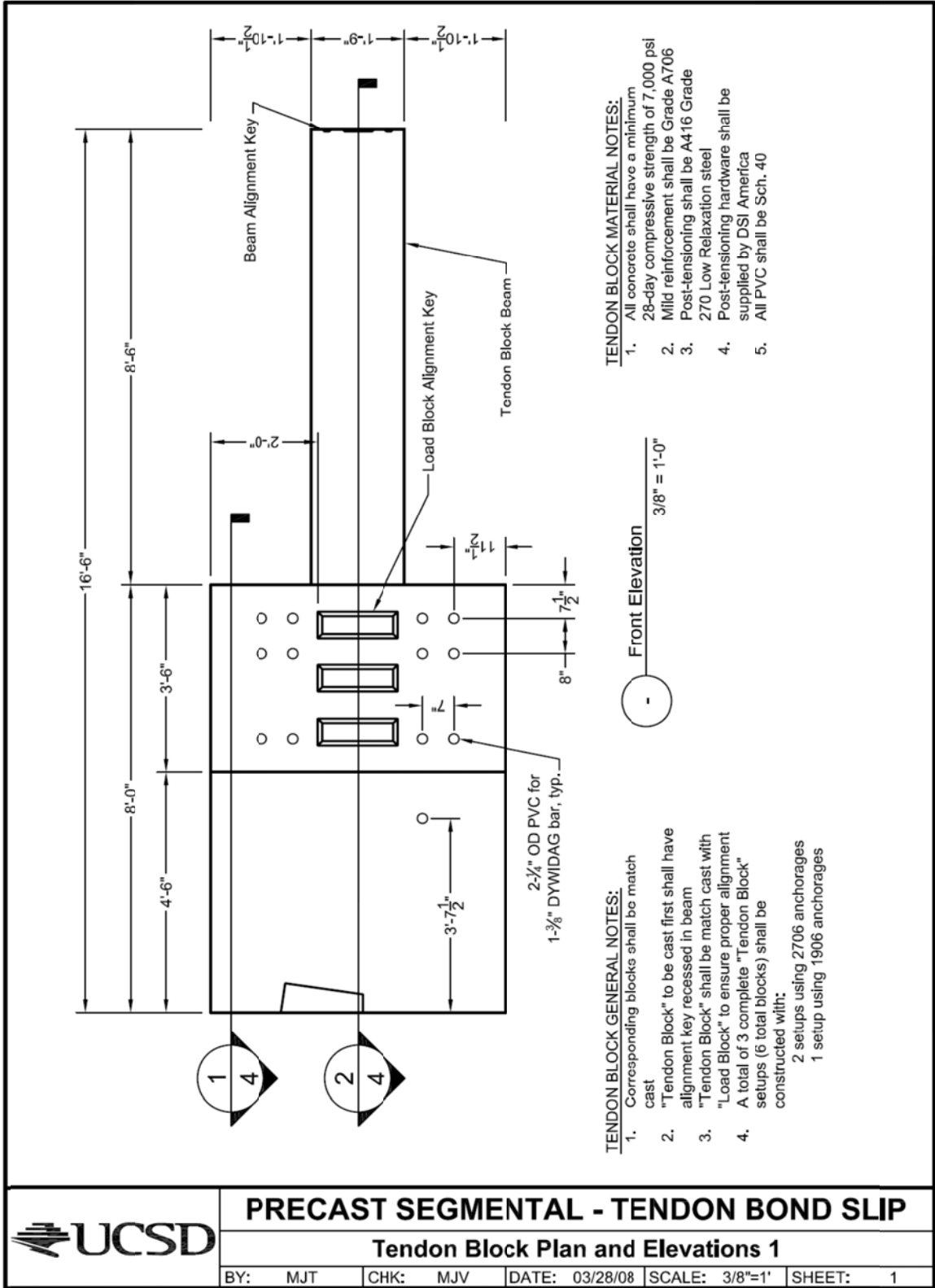
12. Megally, S., Veletzos, M.J., Burnell, K., Restrepo, J., and Seible, F., "Seismic Performance of Precast Concrete Segmental Bridges: Summary of Experimental Research on Segment-to-Segment Joints", Vol. 54, No. 2, pp. 116-142, Spring, 2009.
13. Mukherjee, S., and Gupta, V.K. "Wavelet-Based Generation of Spectrum-Compatible Time-Histories", Soil Dynamics and Earthquake Engineering, Vol. 22, No. 9, pp. 799-804, 2002.
14. Niazi, M. and Bozorgnia, Y., "Behavior of Near-Source Peak Vertical and Horizontal Ground Motions over SMART-1 Array, Taiwan", Bulletin of the Seismological Society of America, Vol. 81, pp 715-732, 1991.
15. Niazi, M. and Bozorgnia, Y., "Behavior of Near-Source Peak Vertical and Horizontal Response Spectra at SMART-1 Array, Taiwan", Earthquake Engineering and Structural Dynamics, Vol. 21, pp 37-50, 1992.
16. Niazi, M. and Bozorgnia, Y., "Behavior of Vertical Ground Motion Parameters in the Near-Field", Seismological Research Letters, Volume 60, pp 4, 1989.
17. Niazi, M. and Bozorgnia, Y., "Observed Ratios for PGV/PGA and PGD/PGA for Deep Soil Sites across SMART-1 Array, Taiwan", Proceeding of the Fourth US National Conference on Earthquake Engineering, Palm Springs, CA, 1990.
18. Ramirez, J.A., Russell, B.W. "Transfer, Development and Splice Length for Strand/Reinforcement in High-Strength Concrete", Final Report prepared for the National Cooperative Highway Research Program, NCHRP 12-60, July, 2007.
19. Veletzos, M.J., and Restrepo, J.I., "Modeling of Jointed Connections in Segmental Bridges", ASCE Journal of Bridge Engineering, Expected publication date January 2011.
20. Veletzos, M.J., and Restrepo, J.I., "Influence of vertical earthquake motion and pre-earthquake stress on joint response of precast concrete segmental bridges", PCI Journal, Vol. 54, No. 3, pp. 99-128, Summer 2009.
21. Wight, J.K., and MacGregor J.G., "Reinforced Concrete: Mechanics & Design", Pearson Education, Inc. New Jersey, 2009.
22. Yilmaz, Z., Zong, Z., Kunnath, S., Abrahamson, N., Chai, Y.H., "Assessment of the Effects of Vertical Ground Motions on Seismic Response of Highway Bridges", Proceedings of the 8th U.S. Conference on Earthquake Engineering, San Francisco, CA April, 2006.
23. Zia, P., and Mostafa, T., "Development Length of Prestressing Strands", PCI Journal, Vol. 22, No. 5, 1977.

## **Appendix A – Drawings of Experimental Program**

Appendix A – Drawings of Experimental Program

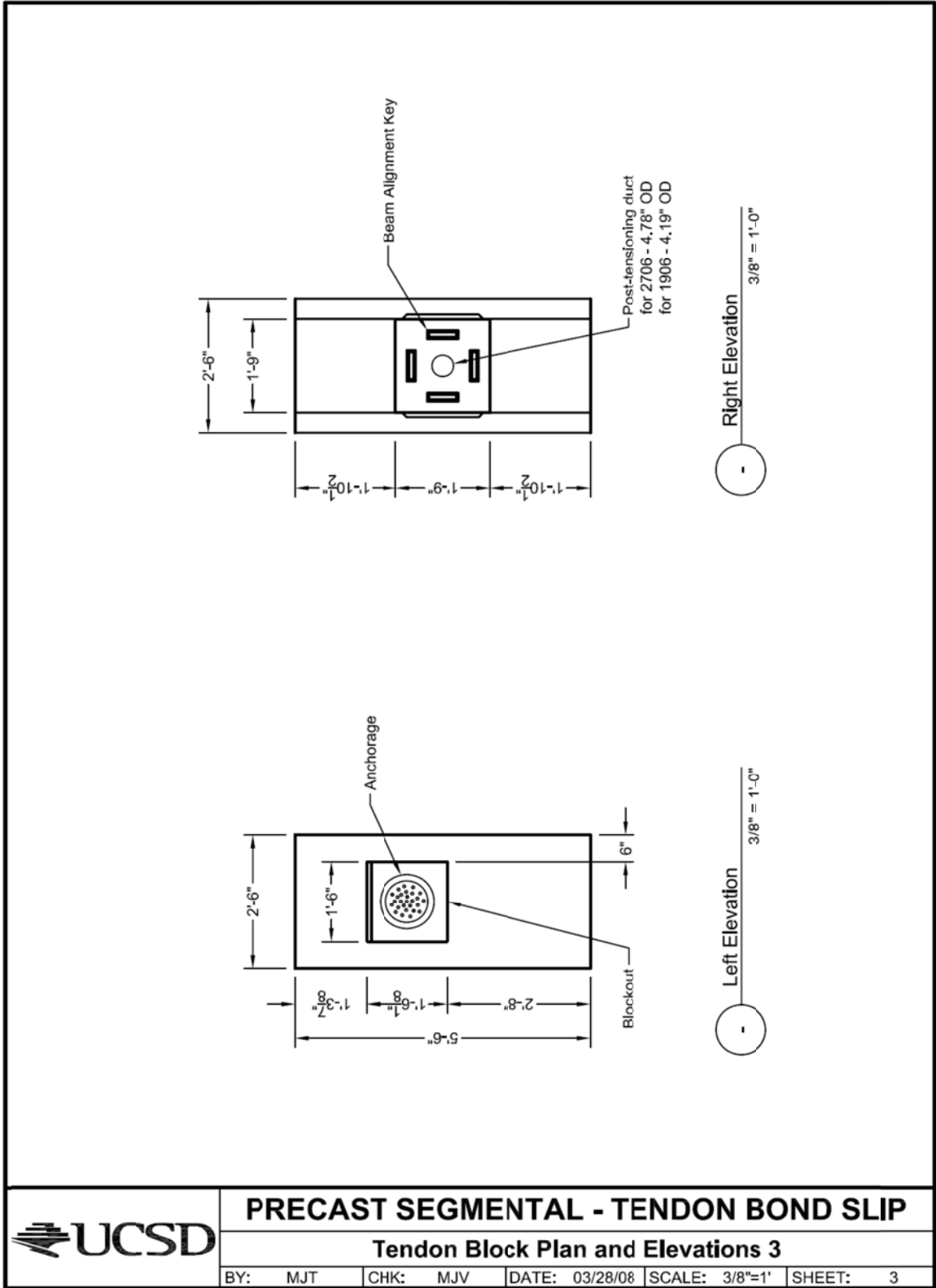


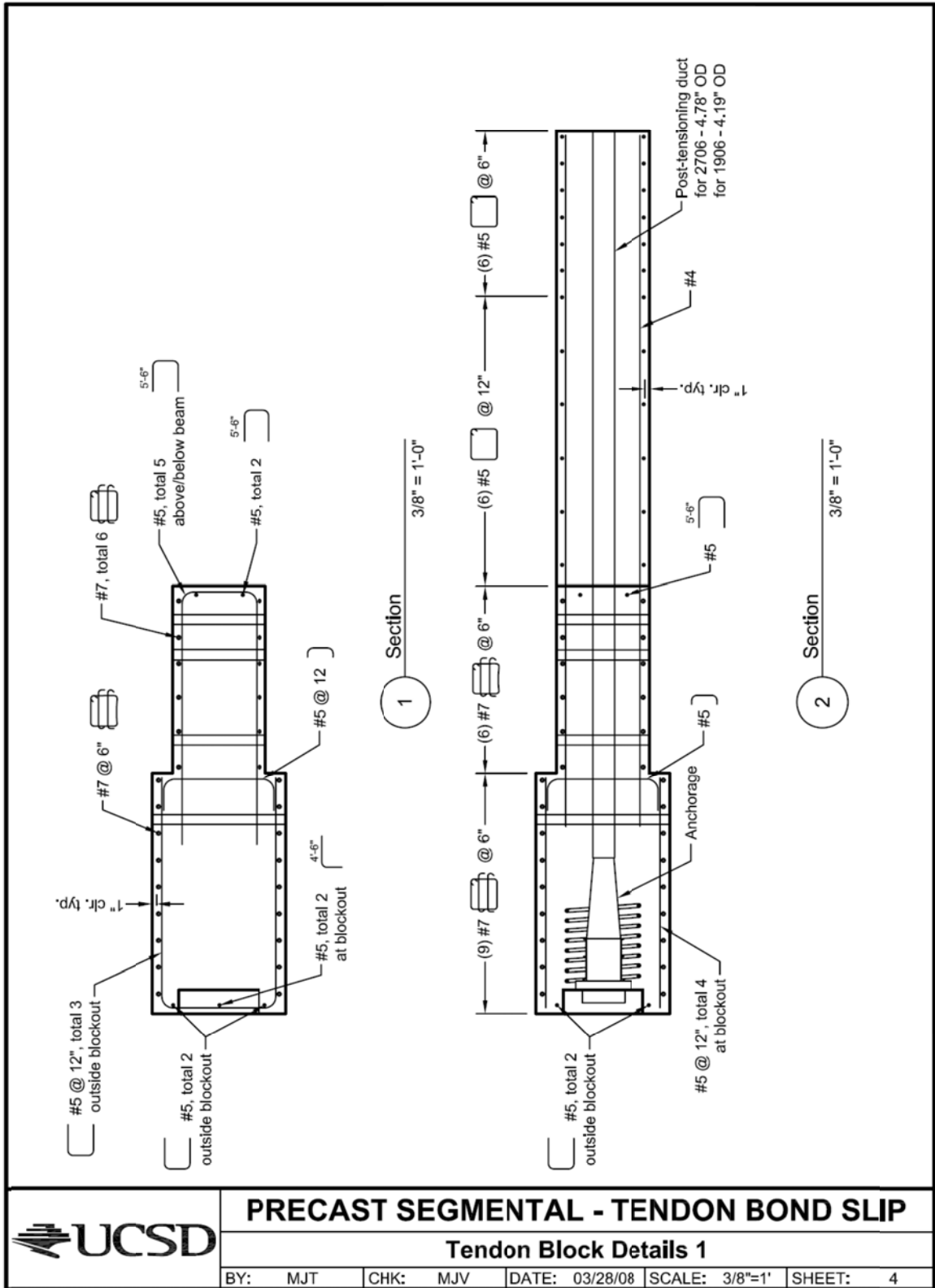
Appendix A – Drawings of Experimental Program

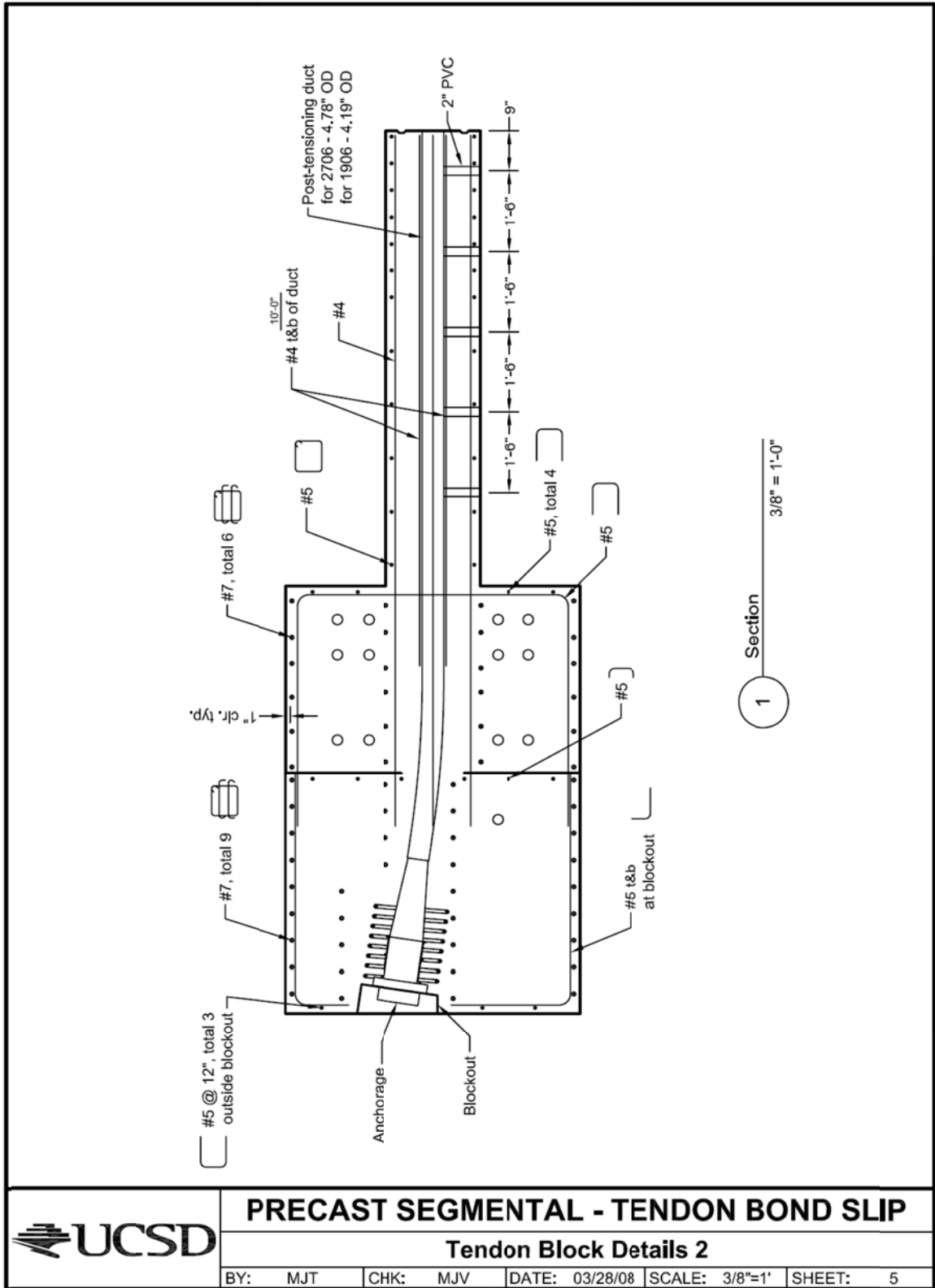




Appendix A – Drawings of Experimental Program





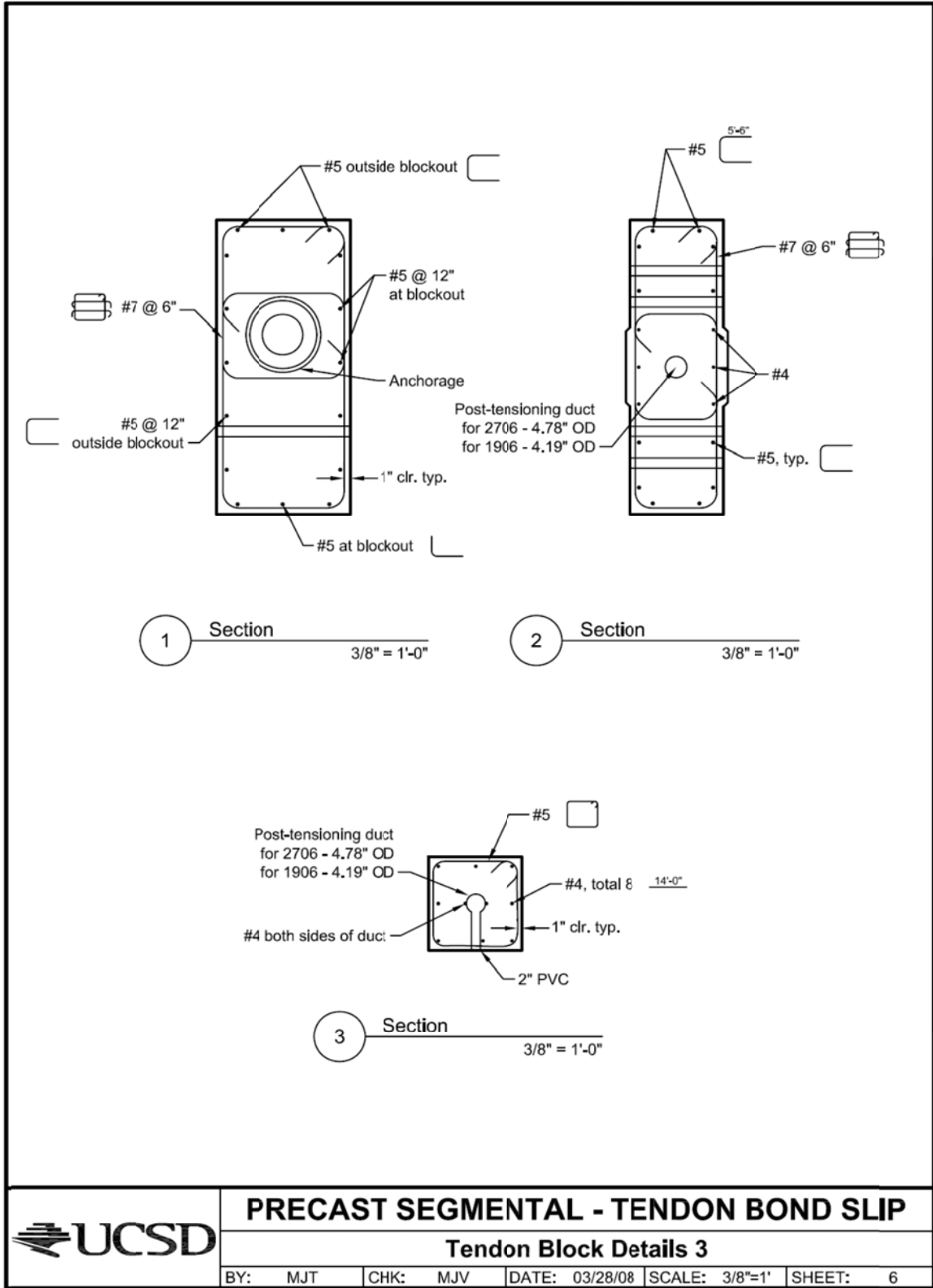


**PRECAST SEGMENTAL - TENDON BOND SLIP**

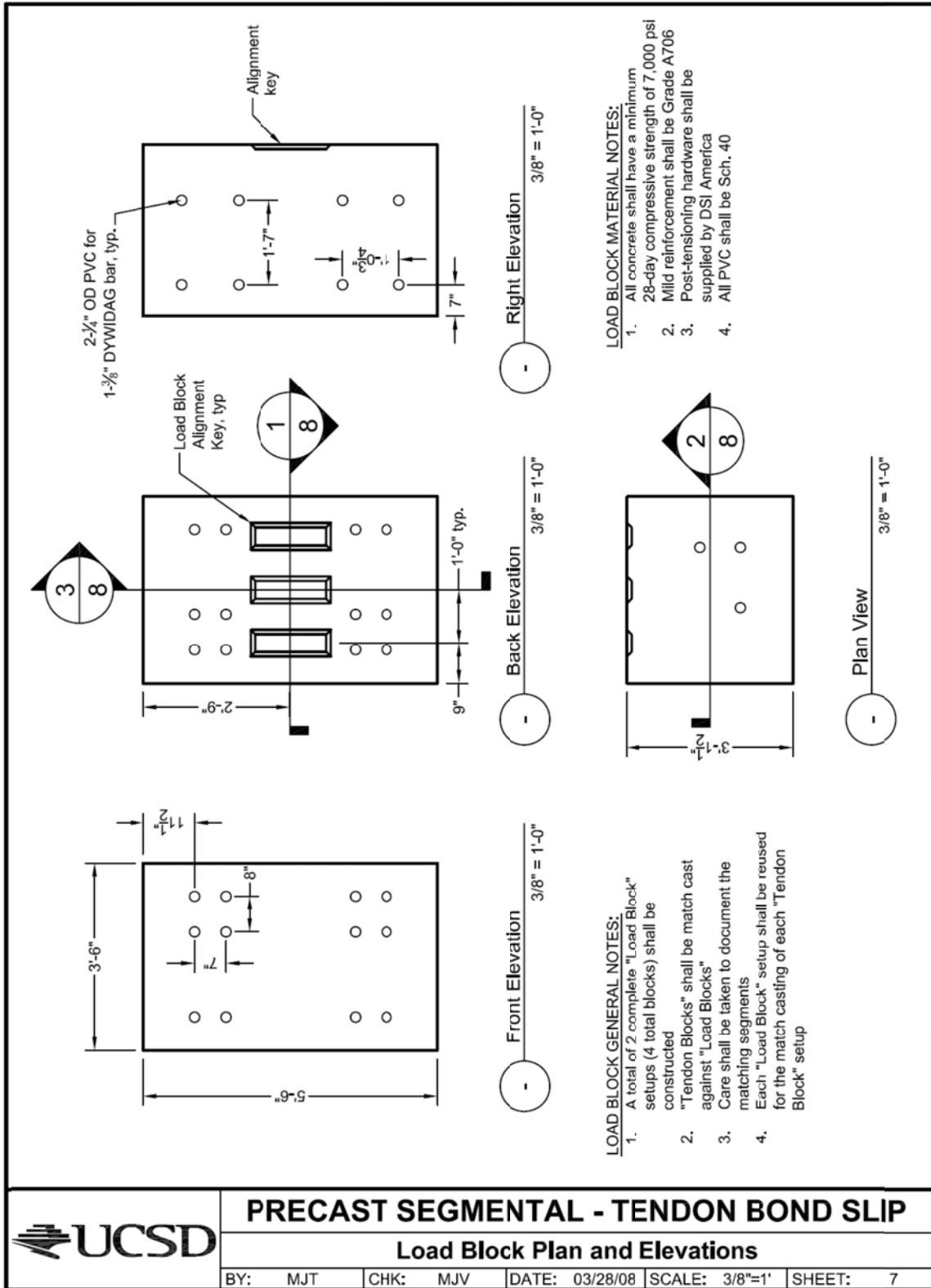
**Tendon Block Details 2**

BY: MJT	CHK: MJV	DATE: 03/28/08	SCALE: 3/8"=1'	SHEET: 5
---------	----------	----------------	----------------	----------

Appendix A – Drawings of Experimental Program



Appendix A – Drawings of Experimental Program

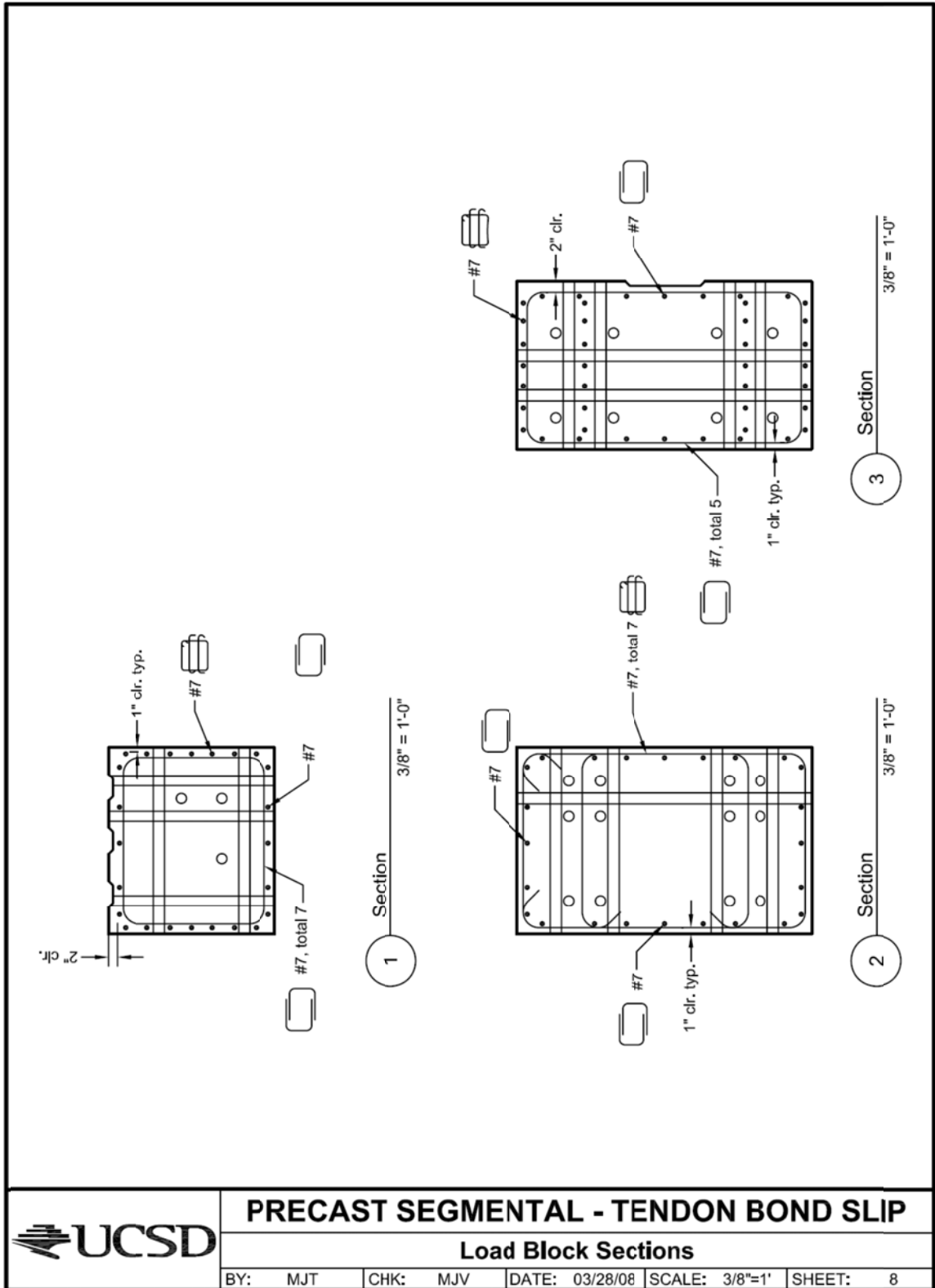


**PRECAST SEGMENTAL - TENDON BOND SLIP**

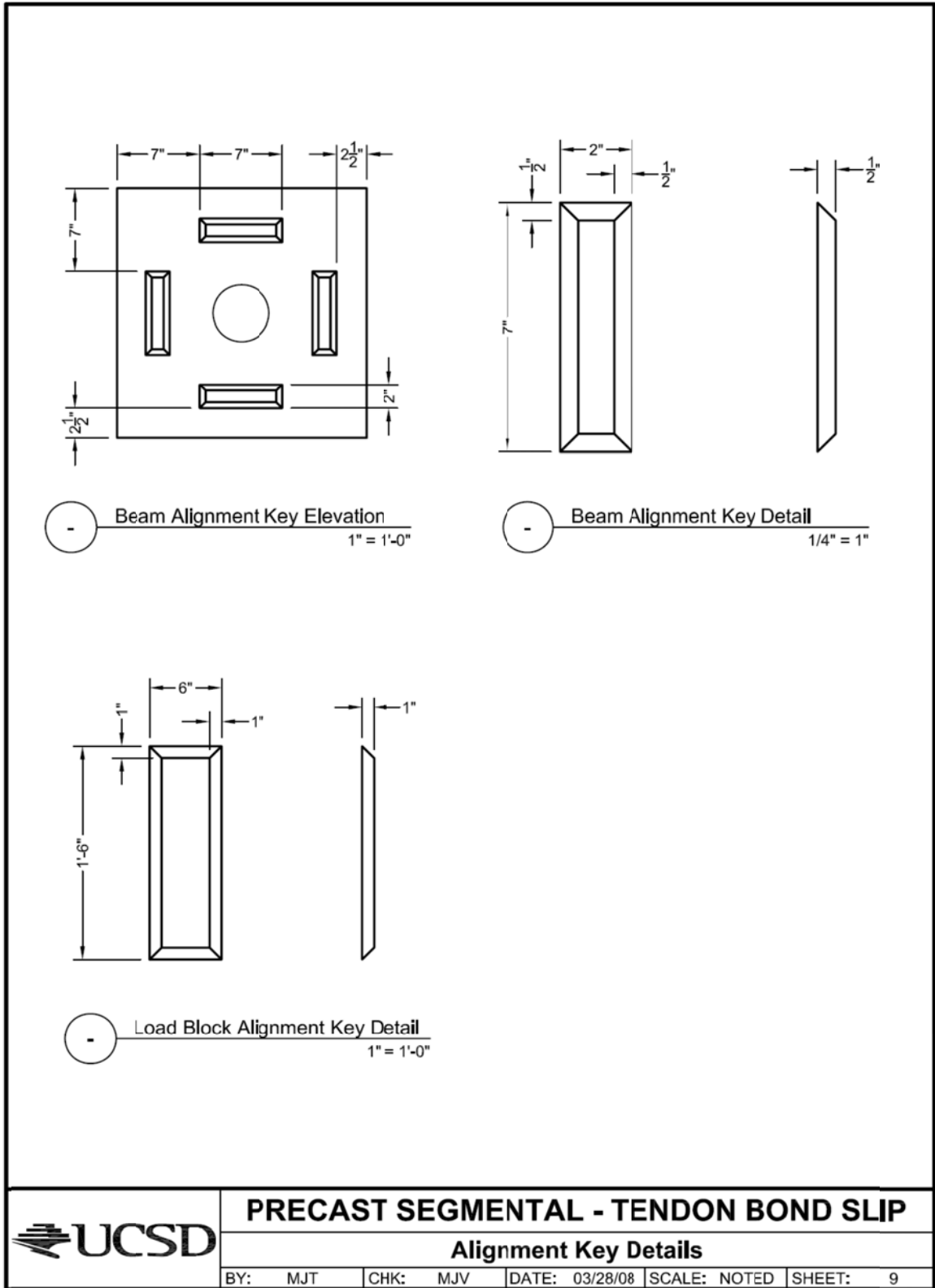
**Load Block Plan and Elevations**

BY: MJT | CHK: MJV | DATE: 03/28/08 | SCALE: 3/8"=1' | SHEET: 7

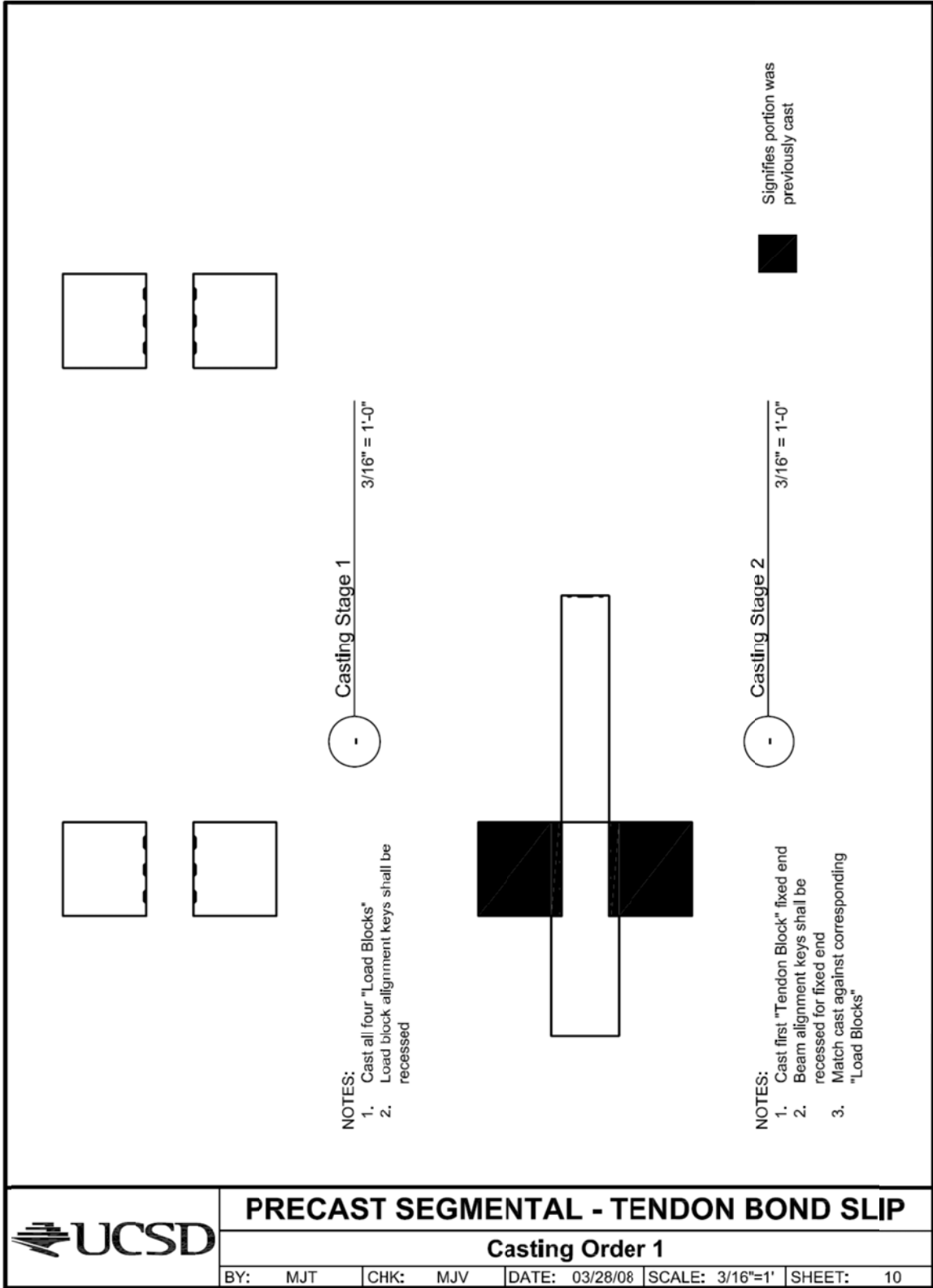
Appendix A – Drawings of Experimental Program

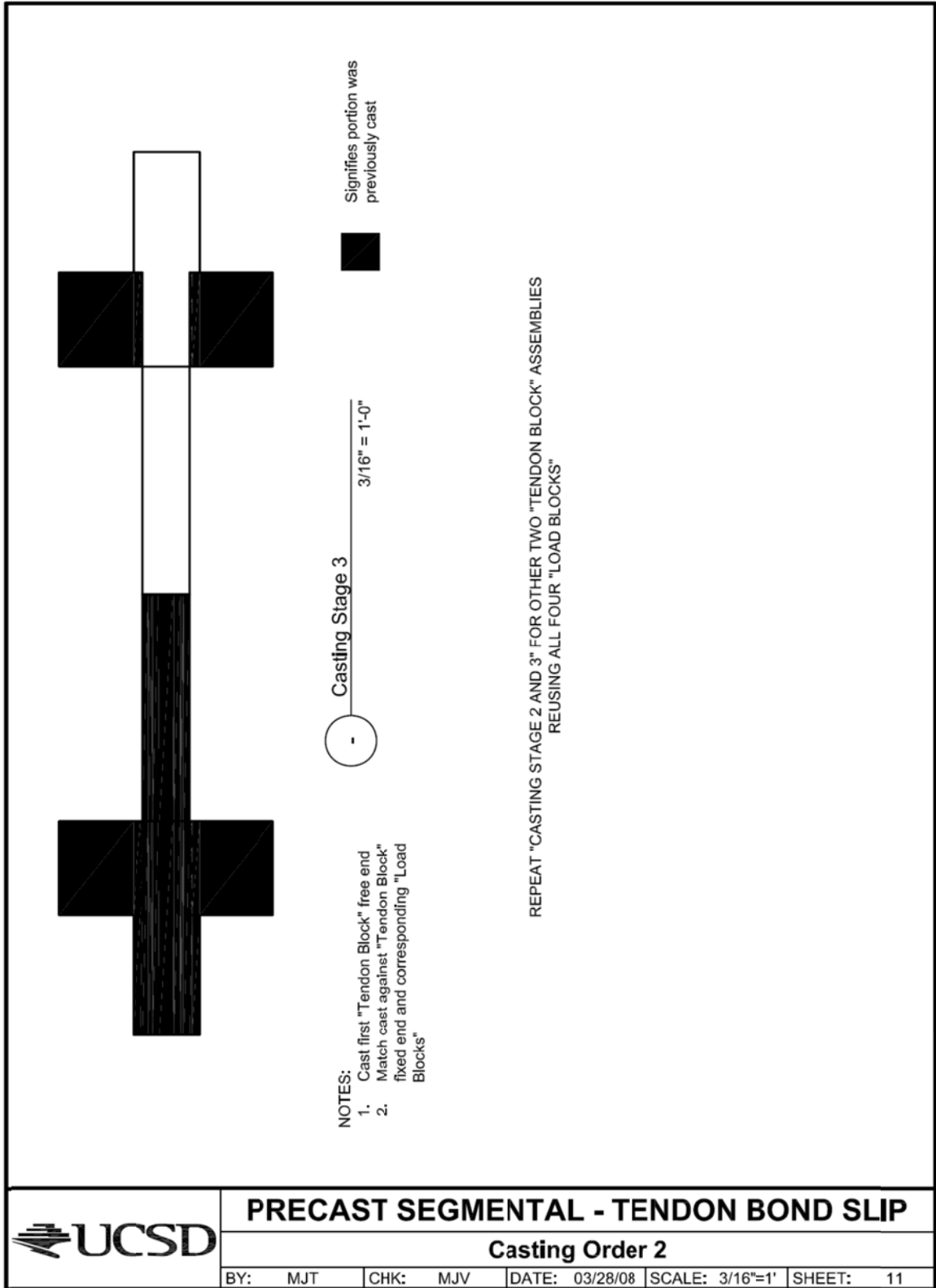


Appendix A – Drawings of Experimental Program

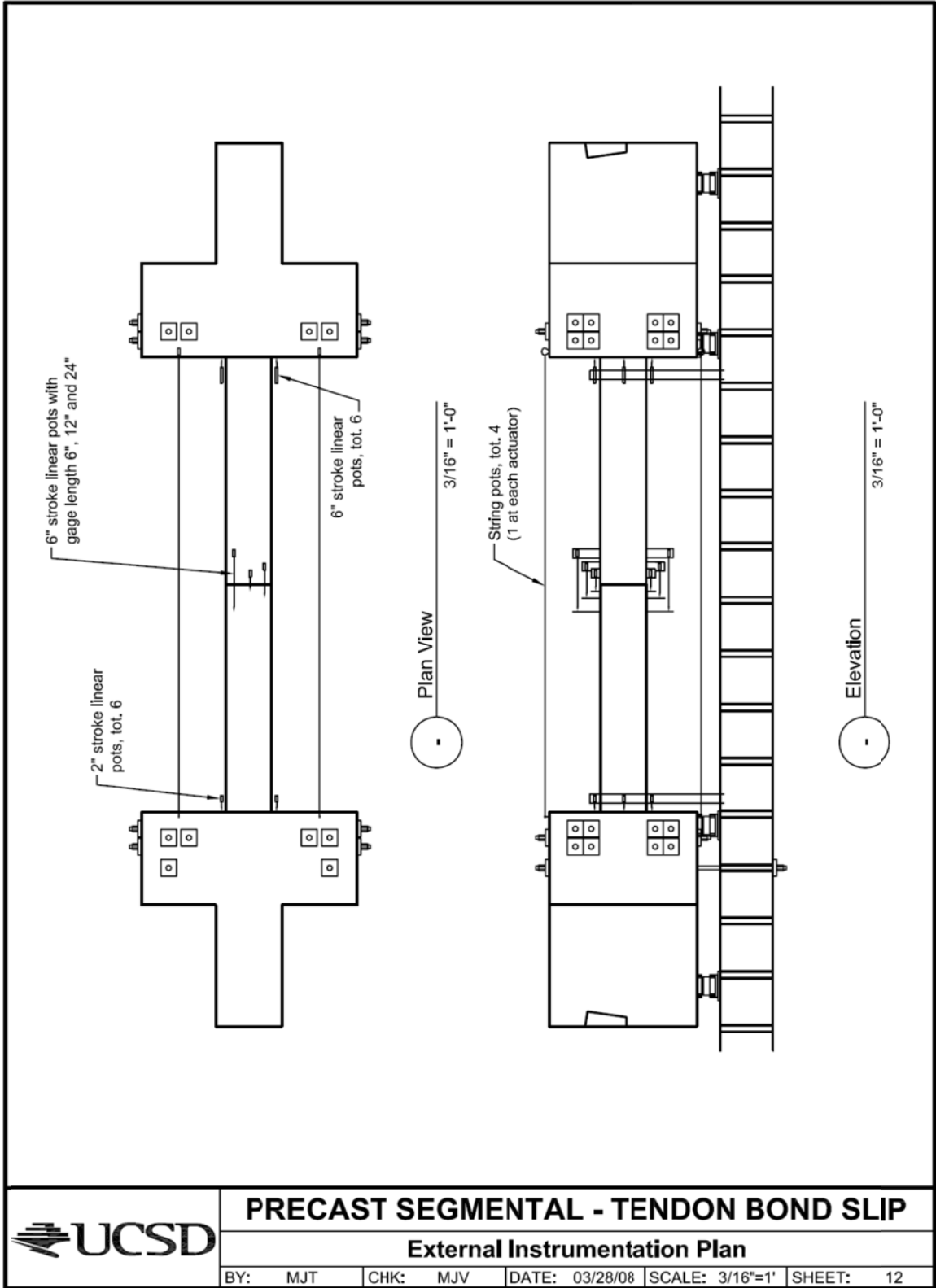


Appendix A – Drawings of Experimental Program





Appendix A – Drawings of Experimental Program

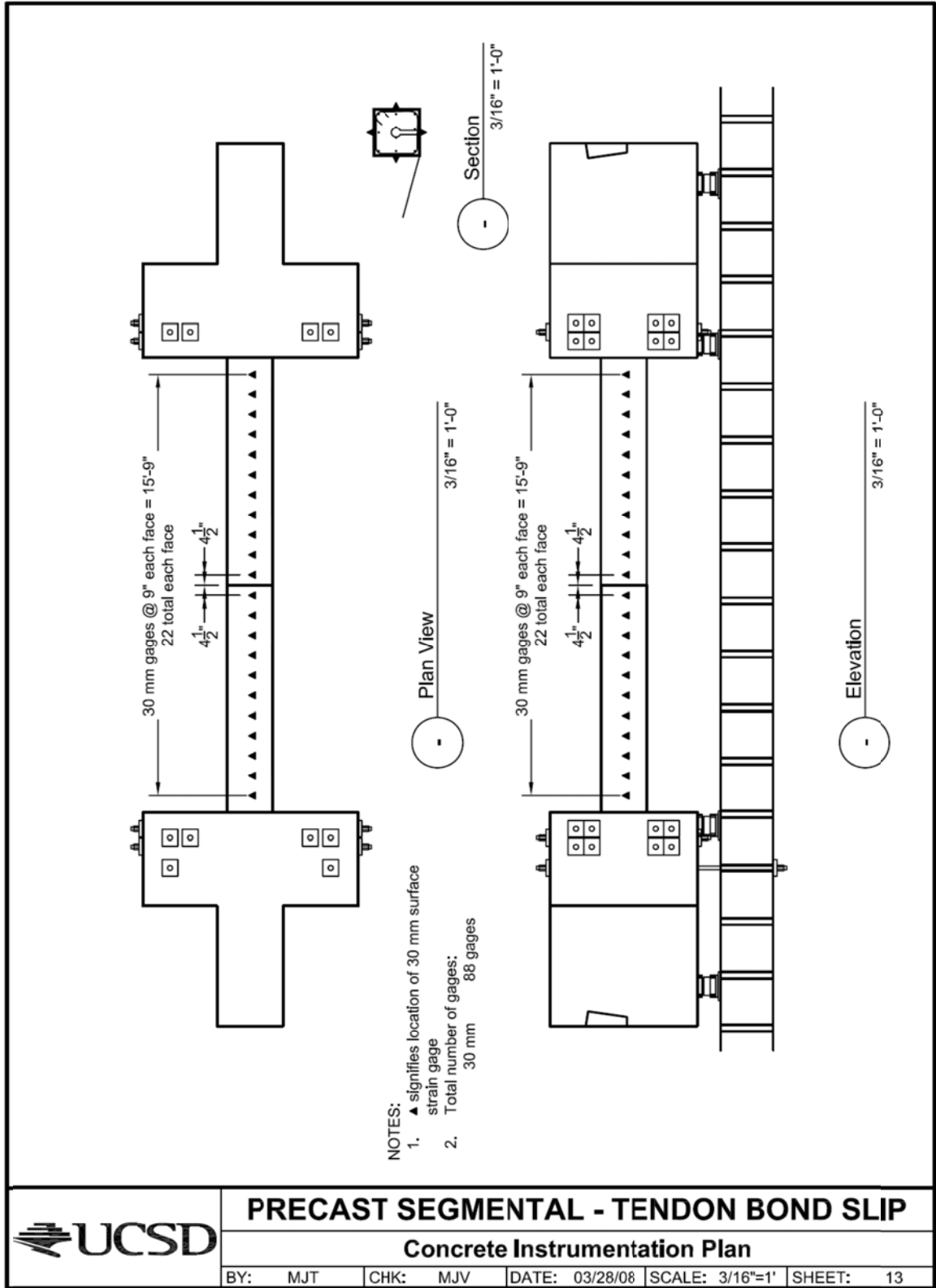


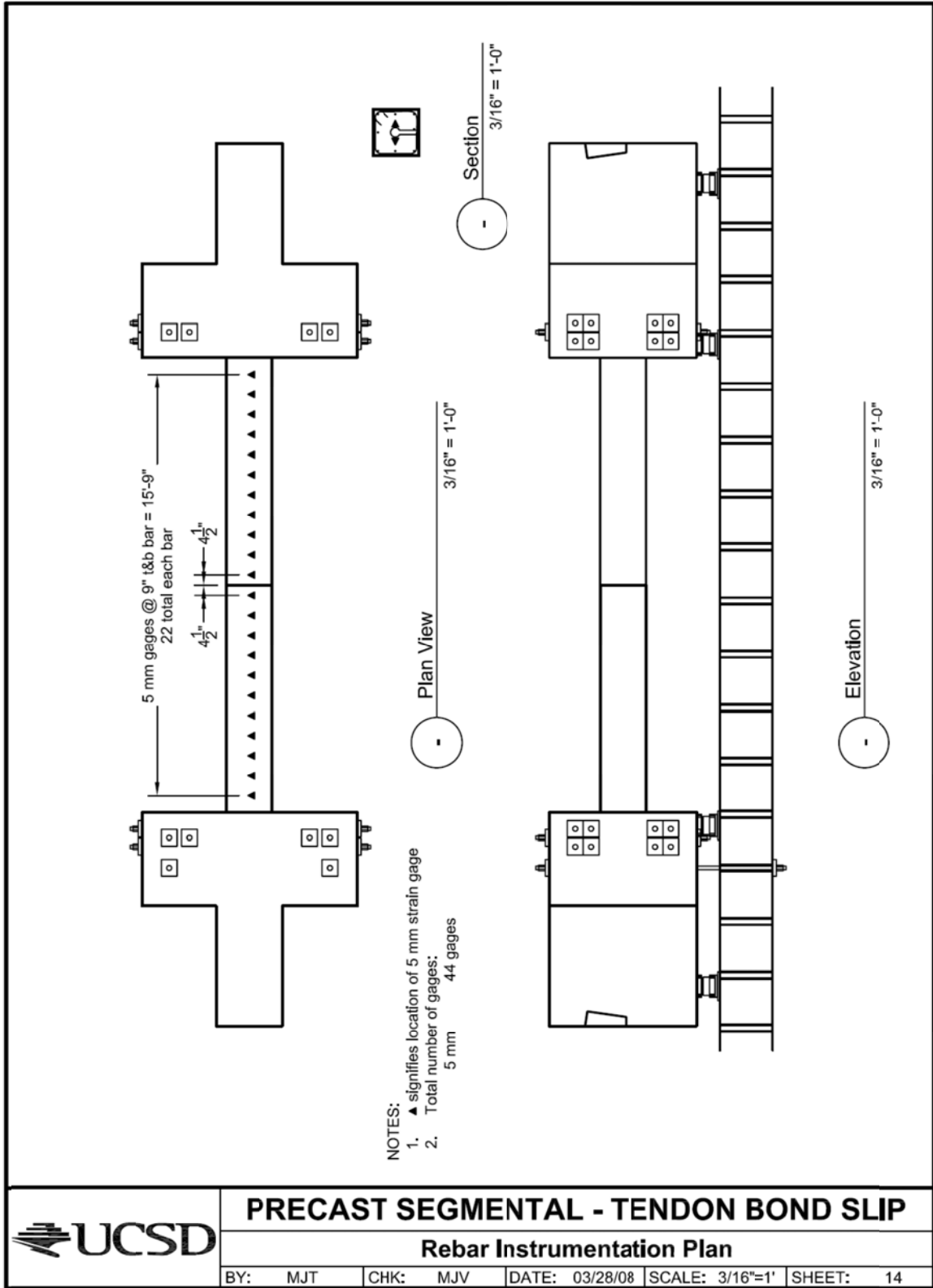
**PRECAST SEGMENTAL - TENDON BOND SLIP**

**External Instrumentation Plan**

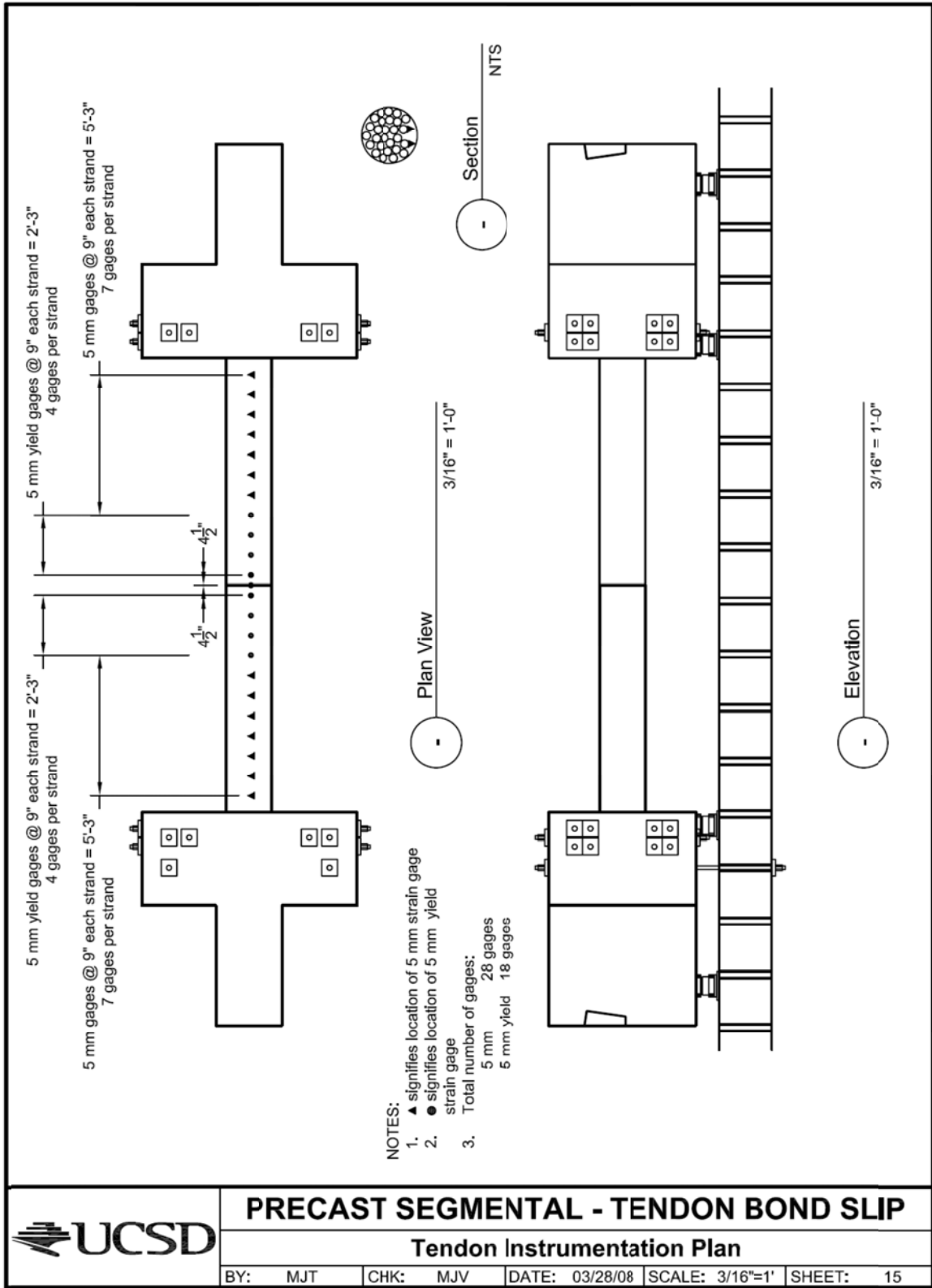
BY: MJT    CHK: MJV    DATE: 03/28/08    SCALE: 3/16"=1'    SHEET: 12

Appendix A – Drawings of Experimental Program

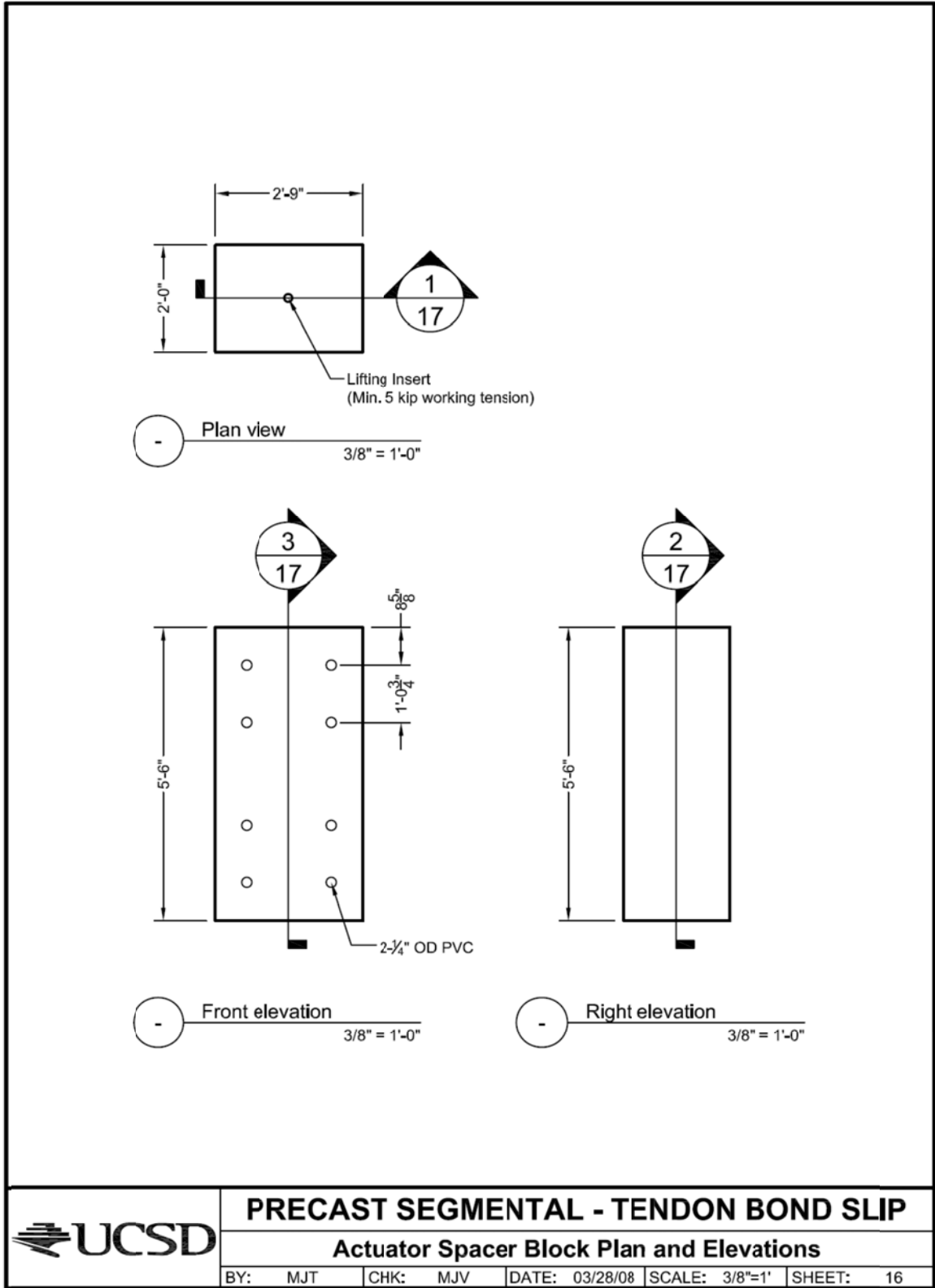




Appendix A – Drawings of Experimental Program

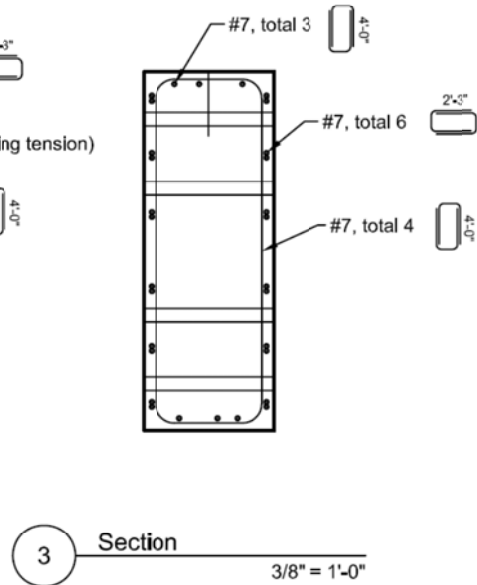
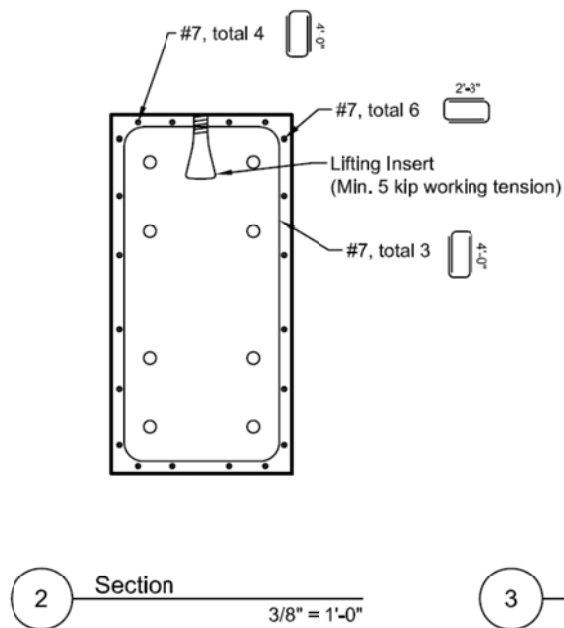
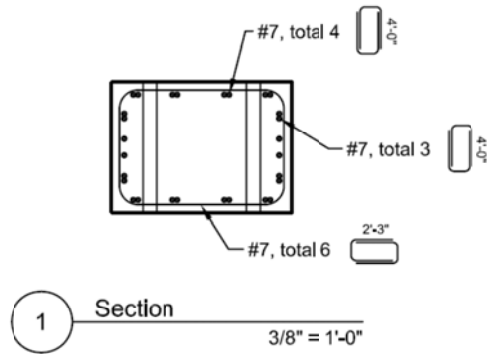


Appendix A – Drawings of Experimental Program



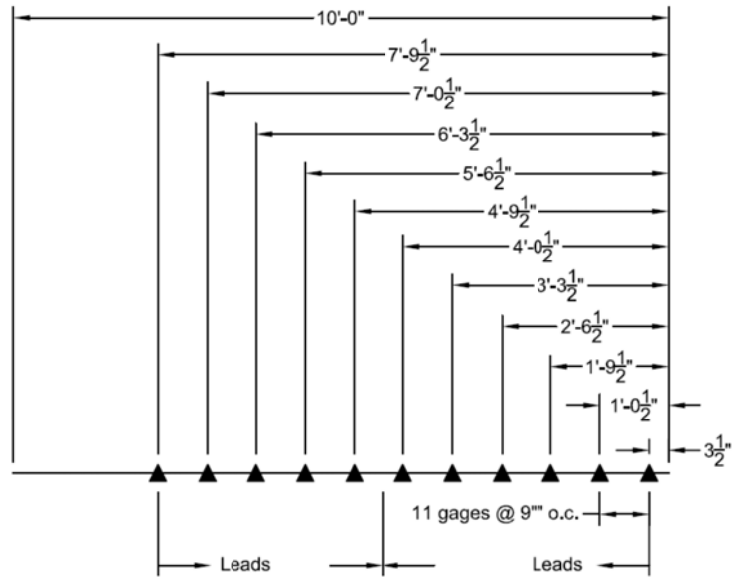
Appendix A – Drawings of Experimental Program

Qty	Units	Total	Size	Total
2x6	2	24	7	hold 1-10" 2'-3"
2x3	2	12	7	hold 2-5" 4'-0"
2x4	2	16	7	hold 1-6" 4'-0"



	<b>PRECAST SEGMENTAL - TENDON BOND SLIP</b>				
	<b>Actuator Spacer Block Sections</b>				
BY: MJT	CHK: MJV	DATE: 03/28/08	SCALE: 3/8"=1'	SHEET: 17	

Appendix A – Drawings of Experimental Program

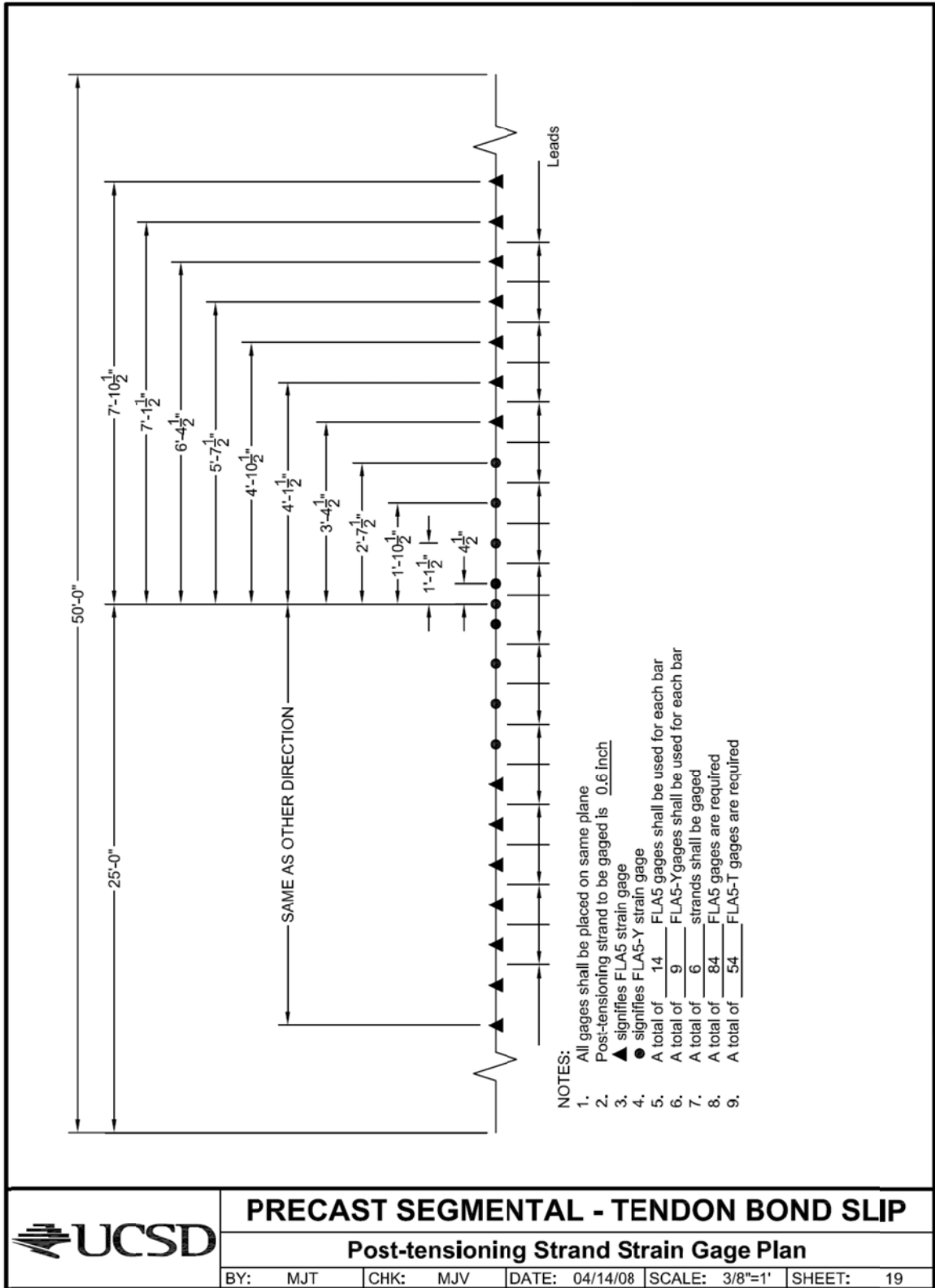


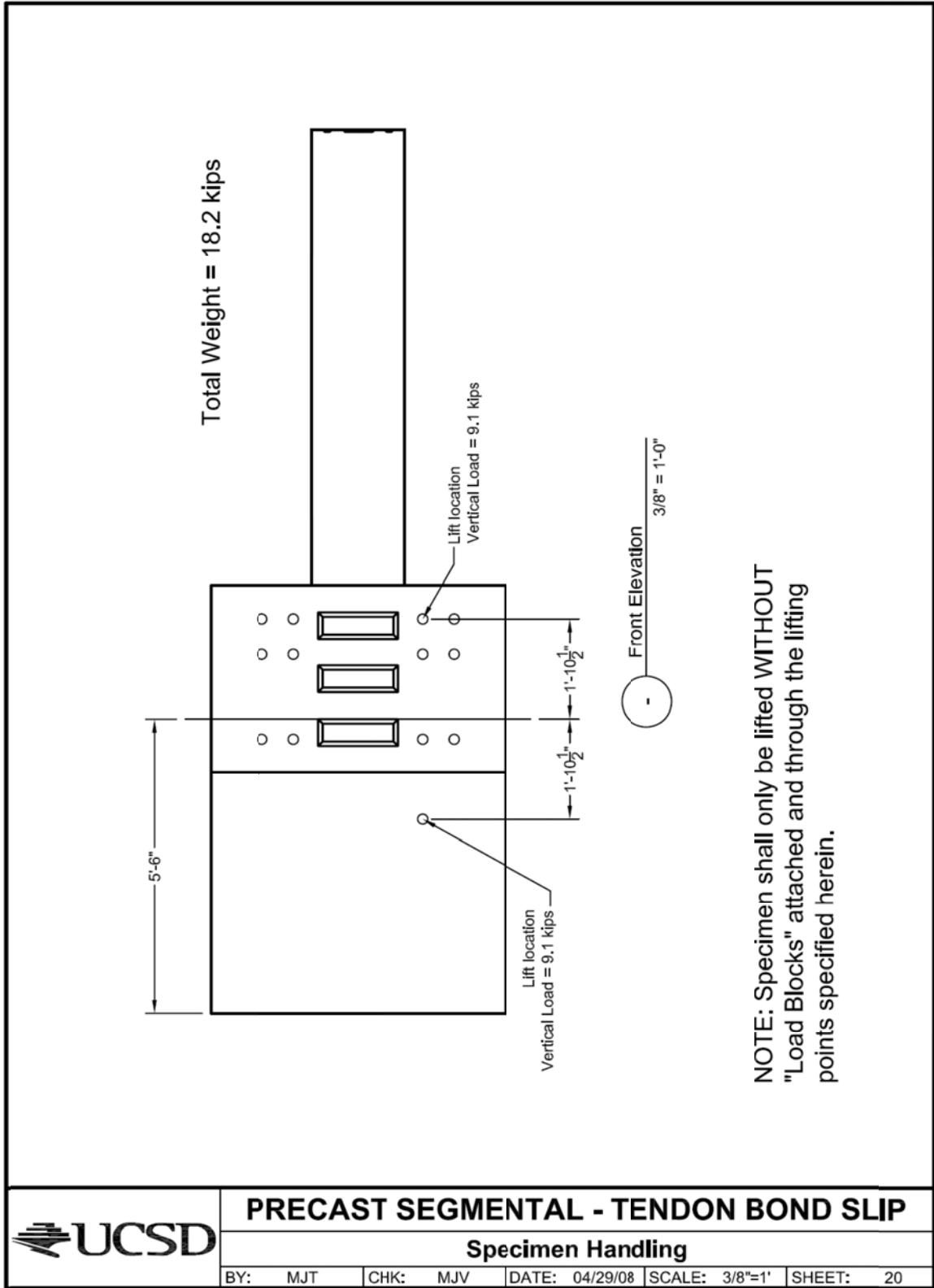
NOTES:

1. All gages shall be placed on same plane
2. Reinforcing bar to be gaged is No. 4
3. ▲ signifies FLA5 strain gage
4. A total of 11 FLA5 gages shall be used for each bar
5. A total of 12 bars shall be gaged
6. A total of 132 FLA5 gages are required

	<b>PRECAST SEGMENTAL - TENDON BOND SLIP</b>					
	<b>Rebar Strain Gage Plan</b>					
BY: MJT	CHK: MJV	DATE: 04/14/08	SCALE: 3/8"=1'	SHEET: 18		

Appendix A – Drawings of Experimental Program





## **Appendix B – Standard Sections**

# CALTRANS Segmental Box Girder Standard Sections for Balanced Cantilever Construction

Span Lengths 300 to 500 feet  
Deck Widths 28 to 45 feet

March 28, 2008



Department of  
Structural Engineering

CALTRANS - Segmental Box Girder Standard  
Sections for Balanced Cantilever Construction

Span Lengths from 300 to 500 feet

Cover Sheet

SECTION DATE (REVISIONS DATE ONLY)

SCALE

1

10

# Appendix B – Standard Sections

## Purpose

The standards sections shown on these sheets have been developed to establish a limited number of practical sections leading to uniformity and simplicity of forming and production methods. These standards are applicable to most conditions of highway bridge loading and usage within the approximate span limits indicated for the sections, and the design loads specified in the design specifications.

## Design Specifications

1. "Caltrans Bridge Design Specifications" (BDS), LFD Version, September 2004.
2. "Caltrans Seismic Design Criteria" (SDC), Version 1.4, June 2006.
3. "AASHTO Guide Specifications for Design and Construction of Segmental Bridges", 2nd edition, 1999, with interim revisions through 2003.

## Span Limits

The span limits shown on these sheets are approximate only and are not mandatory at either limit. The span limits shown contemplate the use of concrete weighing 155 pcf (including rebar) and concrete strength of not less than 5000 psi.

## Precast Concrete

Recommended minimum strength of concrete is 5000 psi. Concrete of greater compressive strength may be used, and may be required for structural considerations, in which case limiting stresses will be based on the concrete specifications for the actual project.

## Post-Tensioning Steel

Post-tensioning steel shall be 7-wire, 1/2 inch or 0.6 inch diameter strands, conforming to ASTM A416 (AASHTO M203), Grade 270. The maximum internal tendon size used for balanced cantilever construction under these standards shall not exceed 37-1/2 inch, or 31-0.6 inch diameter Grade 270 low relaxation strands. Unless otherwise stated in the contract special provisions, other aspects of furnishing, installing and grouting of prestressing steel shall be in accordance with the details shown on the plans, and the "Recommended Contract Administration Guidelines for Design and Construction of Segmental Concrete Bridges", March 1995, American Segmental Bridge Institute.

## Reinforcing Steel

All reinforcing steel shall conform to the requirements of the AASHTO Standard Specifications, and shall be ASTM A615, Grade 60, or ASTM A706. When permitted welded grillages shall be shop prepared. Field welding of reinforcing steel will be permitted at the discretion of the engineer.

## Shop Drawing Requirements

Shop drawing requirements shall be in accordance with the "Recommended Contract Administration Guidelines for Design and Construction of Segmental Concrete Bridges" published by the American Segmental Bridge Institute, March 1995, unless other provisions are stated in the contract special provisions.

## Fabrication, Formwork, Handling, Storage, Shipment and Erection

Fabrication, formwork, handling, storage and erection of precast segments shall be in accordance with the "Recommended Contract Administration Guidelines for Design and Construction of Segmental Concrete Bridges" published by the American Segmental Bridge Institute, March 1995, unless other provisions are stated in the Contract Special Provisions. Angular intersections of formwork shall have a minimum radius of 2 inches. Slab and box edges shall have a minimum chamfer of 3/4 inches.

## Epoxy Joining of Precast Concrete Segments

When required by the contract drawings, epoxy joining of precast segments shall be in accordance with the "Recommended Contract Administration Guidelines for Design and Construction of Segmental Concrete Bridges" published by the American Segmental Bridge Institute, March 1995, unless other provisions are stated in the contract special provisions.

## Temporary Post-Tensioning

Temporary post-tensioning required for construction of balanced cantilever bridges using these standards sections shall be internal bars or tendons in top and bottom slabs unless specifically detailed otherwise in the contract drawings.

## Camber Diagrams

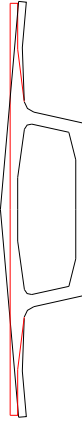
A final long term camber diagram which compensates for deflections in accordance with the assumed material properties shall be provided by the contractor and reviewed by the designer.

## Wearing Surfaces

For those regions in which deicing chemicals are used on roadways, a sacrificial wearing surface is recommended to protect the structural deck and thereby enhance the life of the structure. In regions where deicing chemicals are not used, as-cast riding surfaces without wearing surfaces may be used.

## Crown Roadway Cross Sections

Crown roadways should be accommodated by rotating the cantilever wings downward and building up the top slab between the webs. The shape of the inside void shall remain unchanged.



## Span-to-Depth Ratios

The standard sections shown on these sheets were developed based on span-to-depth ratios of approximately 35-50 for midspan sections and 15-18 for pier sections. The depth of the sections shall vary parabolically between the piers and midspan.

## Bottom Soffit Thickness

The bottom soffit thickness shall vary along the length of the span with the thickness at the pier larger than at midspan. The bottom soffit thickness must be large enough to balance the tensile load due to yielding of the cantilever and continuity tendons and the jacking force of bottom tendons.



Department of  
Structural Engineering

CALTRANS - Segmental Box Girder Standard  
Sections for Balanced Cantilever Construction

Span Lengths from 300 to 500 feet

General Notes

SECTION CASE (EXCLUDING SIZE (NO))

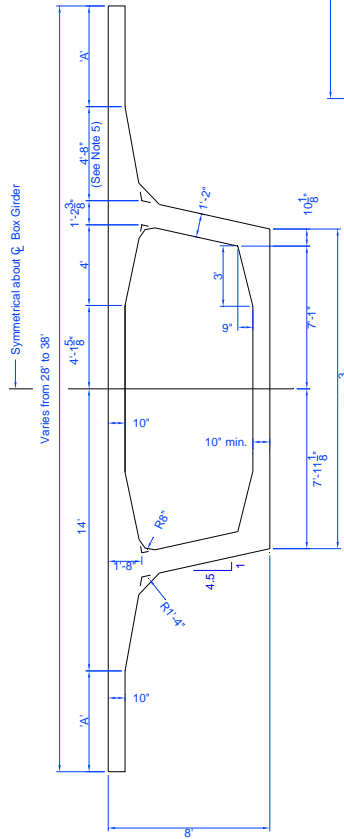
FORM

SECTION CASE (EXCLUDING SIZE (NO))

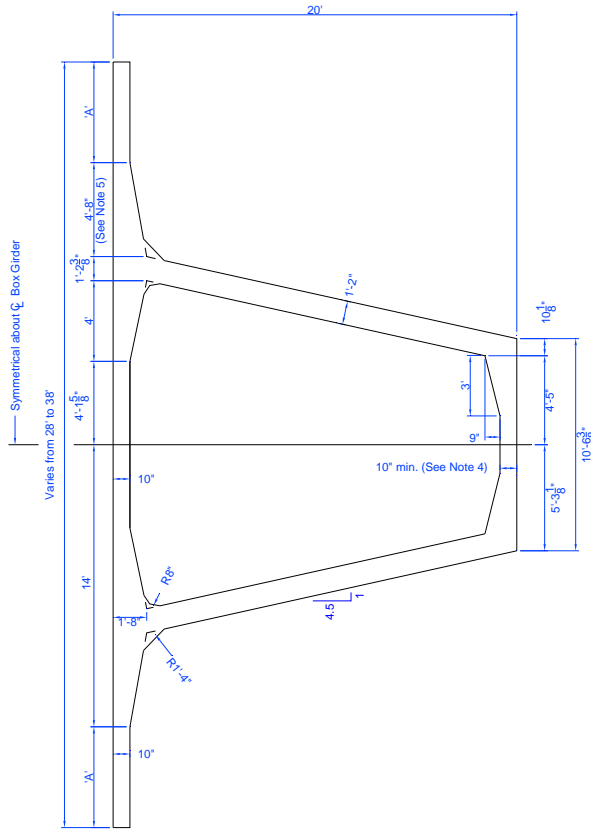
SHEET 2 OF 10

# Appendix B – Standard Sections

- NOTES:**
1. Area denotes cross-sectional area.
  2. Ix denotes bending moment of inertia.
  3. Yt denotes distance from the centroidal axis to the top of the section.
  4. Bottom soffit thickness shall increase at piers per General Notes. The 3'-0" dimension adjusts accordingly.
  5. For widths less than 28 feet, the 4'-8" dimension is decreased. The depth of the slab at the edge of the segment increases accordingly.



**Midspan**



**Pier**

Deck Width (ft)	Midspan				Pier				
	"A" (in)	Area (in <sup>2</sup> )	Unit Weight (kip/ft)	Ix (ft <sup>4</sup> )	Yt (in)	Area (in <sup>2</sup> )	Unit Weight (kip/ft)	Ix (ft <sup>4</sup> )	Yt (in)
28	0	8,821	9.19	561.8	38.2	12,317	12.83	4,542	94.3
29	6	8,941	9.31	568.1	37.7	12,437	12.96	4,588	93.4
30	12	9,061	9.44	574.3	37.3	12,557	13.08	4,633	92.6
31	18	9,181	9.56	580.3	36.9	12,677	13.21	4,677	91.8
32	24	9,301	9.69	586.1	36.4	12,797	13.33	4,720	90.9
33	30	9,421	9.81	591.8	36.0	12,917	13.46	4,763	90.1
34	36	9,541	9.94	597.4	35.7	13,037	13.58	4,804	89.4
35	42	9,661	10.06	602.8	35.3	13,157	13.71	4,845	88.6
36	48	9,781	10.19	608.1	34.9	13,277	13.83	4,885	87.8
37	54	9,901	10.31	613.2	34.5	13,397	13.96	4,925	87.1
38	60	10,021	10.44	618.3	34.2	13,517	14.08	4,963	86.4



Department of  
Structural Engineering

CAL TRANS - Segmental Box Girder Standard  
Sections for Balanced Cantilever Construction

Span Lengths from 300 to 350 feet

Deck Width 28 to 38 feet

PIER WIDTHS IN INCHES

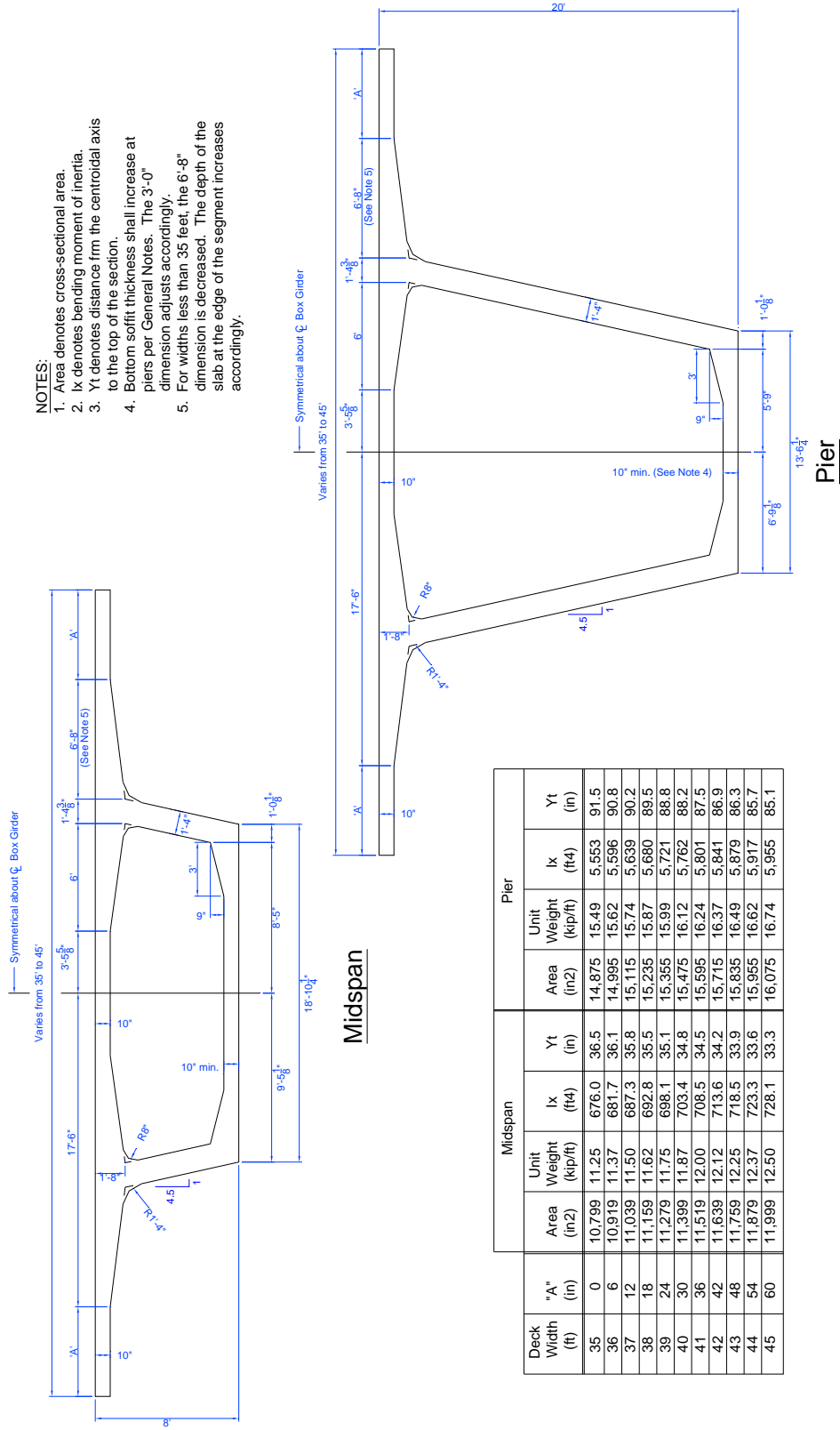
10 12 14 16 18 20 22 24 26 28 30 32 34 36 38

REVISIONS

NO.	DATE	DESCRIPTION	SCALE
1			
2			
3			

# Appendix B – Standard Sections

- NOTES:**
1. Area denotes cross-sectional area.
  2. Ix denotes bending moment of inertia.
  3. Yt denotes distance from the centroidal axis to the top of the section.
  4. Bottom soffit thickness shall increase at piers per General Notes. The 3'-0" dimension adjusts accordingly.
  5. For widths less than 35 feet, the 6'-8" dimension is decreased. The depth of the slab at the edge of the segment increases accordingly.



Deck Width (ft)	Midspan				Pier			
	Area (in <sup>2</sup> )	Unit Weight (kip/ft)	Ix (ft <sup>4</sup> )	Yt (in)	Area (in <sup>2</sup> )	Unit Weight (kip/ft)	Ix (ft <sup>4</sup> )	Yt (in)
35	10,799	11.25	676.0	36.5	14,875	15.49	5,553	91.5
36	10,919	11.37	681.7	36.1	14,995	15.62	5,596	90.8
37	11,039	11.50	687.3	35.8	15,115	15.74	5,639	90.2
38	11,159	11.62	692.8	35.5	15,235	15.87	5,680	89.5
39	11,279	11.75	698.1	35.1	15,355	15.99	5,721	88.8
40	11,399	11.87	703.4	34.8	15,475	16.12	5,762	88.2
41	11,519	12.00	708.5	34.5	15,595	16.24	5,801	87.5
42	11,639	12.12	713.6	34.2	15,715	16.37	5,841	86.9
43	11,759	12.25	718.5	33.9	15,835	16.49	5,879	86.3
44	11,879	12.37	723.3	33.6	15,955	16.62	5,917	85.7
45	11,999	12.50	728.1	33.3	16,075	16.74	5,955	85.1

Department of  
Structural Engineering

CAL TRANS - Segmental Box Girder Standard  
Sections for Balanced Cantilever Construction

Span Lengths from 300 to 350 feet

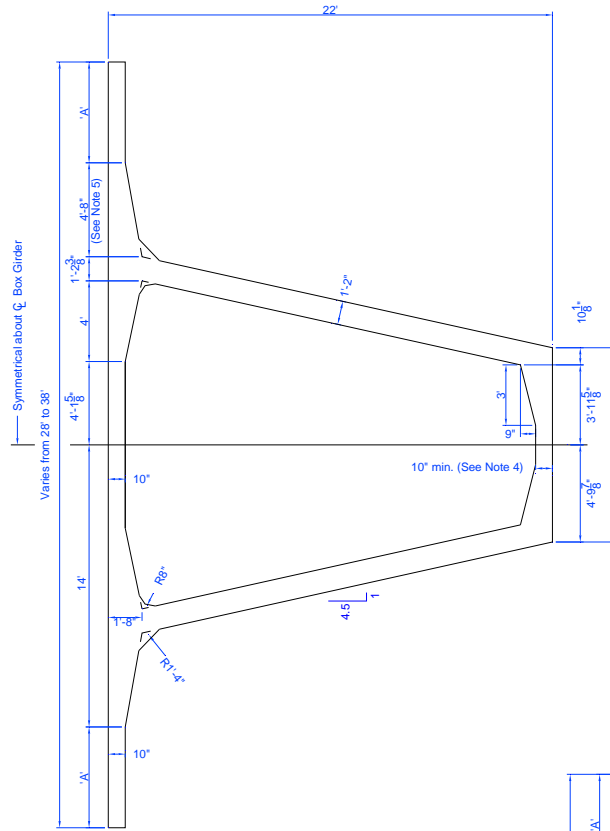
Deck Width 35 to 45 feet

SCALE: 1" = 1'-0"

SECTION: 1 OF 1

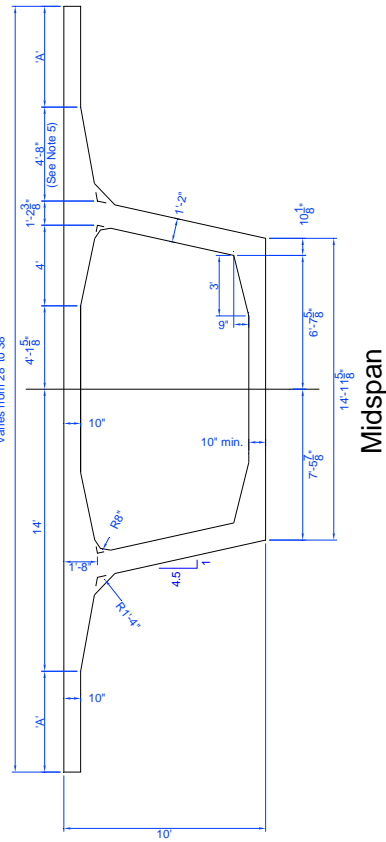
DATE: 10/10/10

# Appendix B – Standard Sections



- NOTES:**
1. Area denotes cross-sectional area.
  2. Ix denotes bending moment of inertia.
  3. Yt denotes distance from the centroidal axis to the top of the section.
  4. Bottom soffit thickness shall increase at piers per General Notes. The 3'-0" dimension adjusts accordingly.
  5. For widths less than 28 feet, the 4'-8" dimension is decreased. The depth of the slab at the edge of the segment increases accordingly.

Deck Width (ft)	Midspan				Pier				
	"A" (in)	Area (in <sup>2</sup> )	Unit Weight (kip/ft)	Ix (ft <sup>4</sup> )	Yt (in)	Area (in <sup>2</sup> )	Unit Weight (kip/ft)	Ix (ft <sup>4</sup> )	Yt (in)
28	0	9,402	9.79	942.9	47.4	12,902	13.44	5,633	103.8
29	6	9,462	9.86	948.1	47.1	13,022	13.56	5,689	102.9
30	12	9,522	9.92	953.2	46.8	13,142	13.69	5,744	102.0
31	18	9,582	9.98	958.3	46.6	13,262	13.81	5,798	101.1
32	24	9,642	10.04	963.3	46.3	13,382	13.94	5,851	100.3
33	30	9,702	10.11	968.2	46.1	13,502	14.06	5,903	99.4
34	36	9,762	10.17	973.1	45.8	13,622	14.19	5,954	98.6
35	42	9,822	10.23	977.9	45.5	13,742	14.31	6,005	97.8
36	48	9,882	10.29	982.6	45.3	13,862	14.44	6,054	97.0
37	54	9,942	10.36	987.3	45.1	13,982	14.56	6,103	96.2
38	60	10,002	10.42	992.0	44.8	14,102	14.69	6,150	95.4





Department of  
Structural Engineering

**CALTRANS - Segmental Box Girder Standard Sections for Balanced Cantilever Construction**

**Span Lengths from 350 to 400 feet**

**Deck Width 28 to 38 feet**

SECTION INDEX (SEE GENERAL NOTES)

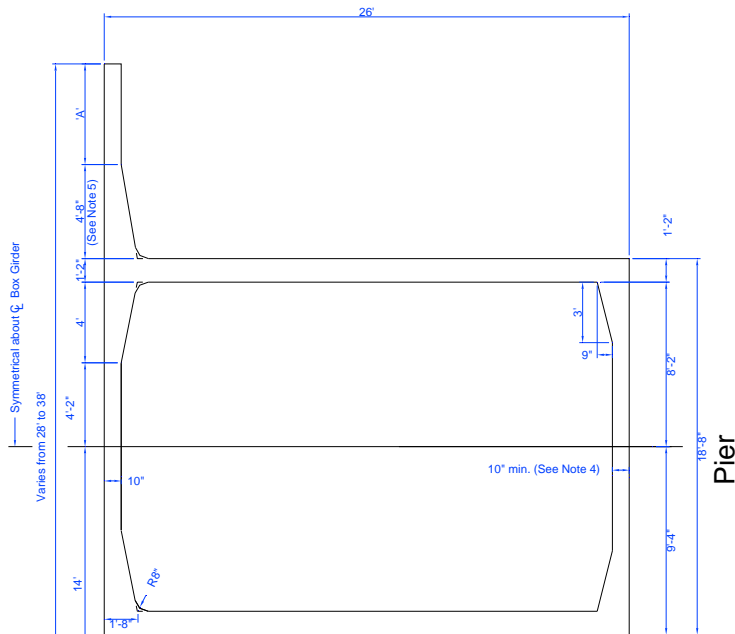
1	2	3	4	5	6	7	8	9	10
---	---	---	---	---	---	---	---	---	----

SECTION INDEX (SEE GENERAL NOTES)

1	2	3	4	5	6	7	8	9	10
---	---	---	---	---	---	---	---	---	----

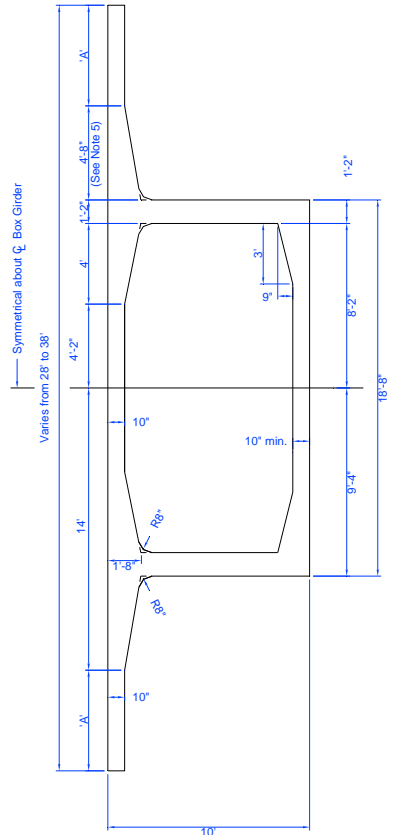


# Appendix B – Standard Sections



- NOTES:**
1. Area denotes cross-sectional area.
  2. Ix denotes bending moment of inertia.
  3. Yt denotes distance from the centroidal axis to the top of the section.
  4. Bottom soffit thickness shall increase at piers per General Notes. The 3'-0" dimension adjusts accordingly.
  5. For widths less than 28 feet, the 4'-8" dimension is decreased. The depth of the slab at the edge of the segment increases accordingly.

Deck Width (ft)	Midspan				Pier				
	"A" (in)	Area (in <sup>2</sup> )	Unit Weight (kip/ft)	Ix (ft <sup>4</sup> )	Yt (in)	Area (in <sup>2</sup> )	Unit Weight (kip/ft)	Ix (ft <sup>4</sup> )	Yt (in)
28	0	9,764	10.17	1,031	50.3	15,140	15.77	10,068	138.1
29	6	9,824	10.23	1,037	50.0	15,260	15.90	10,170	137.0
30	12	9,884	10.30	1,043	49.7	15,380	16.02	10,270	136.0
31	18	9,944	10.36	1,049	49.5	15,500	16.15	10,368	135.0
32	24	10,004	10.42	1,055	49.2	15,620	16.27	10,466	134.0
33	30	10,064	10.48	1,060	48.9	15,740	16.40	10,561	133.0
34	36	10,124	10.55	1,066	48.7	15,860	16.52	10,655	132.0
35	42	10,184	10.61	1,071	48.4	15,980	16.65	10,748	131.1
36	48	10,244	10.67	1,077	48.2	16,100	16.77	10,840	130.2
37	54	10,304	10.73	1,082	47.9	16,220	16.90	10,930	129.2
38	60	10,364	10.80	1,087	47.7	16,340	17.02	11,018	128.3



## Midspan



Department of  
Structural Engineering

**CAL TRANS - Segmental Box Girder Standard Sections for Balanced Cantilever Construction**

**Span Lengths from 400 to 450 feet**

**Deck Width 28 to 38 feet**

FOR SPAN LENGTHS FROM 400 TO 450 FEET, INCHES

FOR DECK WIDTHS FROM 28 TO 38 FEET, INCHES

SCALE: 1/4" = 1'-0"



# Appendix B – Standard Sections

Deck Width (ft)	Midspan				Pier				
	"A" (in)	Area (in <sup>2</sup> )	Unit Weight (kip/ft)	I <sub>x</sub> (ft <sup>4</sup> )	Y <sub>t</sub> (in)	Area (in <sup>2</sup> )	Unit Weight (kip/ft)	I <sub>x</sub> (ft <sup>4</sup> )	Y <sub>t</sub> (in)
28	0	9,764	10.17	1,031	50.3	16,484	17.17	14,234	160.9
29	6	9,824	10.23	1,037	50.0	16,604	17.30	14,374	159.8
30	12	9,884	10.30	1,043	49.7	16,724	17.42	14,511	158.6
31	18	9,944	10.36	1,049	49.5	16,844	17.55	14,647	157.5
32	24	10,004	10.42	1,055	49.2	16,964	17.67	14,781	156.5
33	30	10,064	10.48	1,060	48.9	17,084	17.80	14,913	155.4
34	36	10,124	10.55	1,066	48.7	17,204	17.92	15,043	154.4
35	42	10,184	10.61	1,071	48.4	17,324	18.05	15,171	153.3
36	48	10,244	10.67	1,077	48.2	17,444	18.17	15,298	152.3
37	54	10,304	10.73	1,082	47.9	17,564	18.30	15,422	151.3
38	60	10,364	10.80	1,087	47.7	17,684	18.42	15,545	150.3

**NOTES:**

1. Area denotes cross-sectional area.
2. I<sub>x</sub> denotes bending moment of inertia.
3. Y<sub>t</sub> denotes distance from the centroidal axis to the top of the section.
4. Bottom soffit thickness shall increase at piers per General Notes. The 3'-0" dimension adjusts accordingly.
5. For widths less than 28 feet, the 4'-8" dimension is decreased. The depth of the slab at the edge of the segment increases accordingly.

**Midspan**

Department of Structural Engineering

CALTRANS - Segmental Box Girder Standard Sections for Balanced Cantilever Construction

**Pier**

Department of Structural Engineering

CALTRANS - Segmental Box Girder Standard Sections for Balanced Cantilever Construction

Deck Width 28 to 38 feet

Span Lengths from 450 to 500 feet

Scale: 1/8" = 1'-0"

Sheet: 9 of 10

# Appendix B – Standard Sections

**NOTES:**

1. Area denotes cross-sectional area.
2. Ix denotes bending moment of inertia.
3. Yt denotes distance from the centroidal axis to the top of the section.
4. Bottom soffit thickness shall increase at piers per General Notes. The 3'-0" dimension adjusts accordingly.
5. For widths less than 35 feet, the 6'-8" dimension is decreased. The depth of the slab at the edge of the segment increases accordingly.

**NOTES:**

1. Area denotes cross-sectional area.
2. Ix denotes bending moment of inertia.
3. Yt denotes distance from the centroidal axis to the top of the section.
4. Bottom soffit thickness shall increase at piers per General Notes. The 3'-0" dimension adjusts accordingly.
5. For widths less than 35 feet, the 6'-8" dimension is decreased. The depth of the slab at the edge of the segment increases accordingly.

**Midspan**

Deck Width (ft)	Midspan				Pier				
	"A" (in)	Area (m <sup>2</sup> )	Unit Weight (kip/ft)	Ix (ft <sup>4</sup> )	Yt (in)	Area (m <sup>2</sup> )	Unit Weight (kip/ft)	Ix (ft <sup>4</sup> )	Yt (in)
35	0	11,844	12.34	1,234	47.9	19,524	20.34	17,005	155.5
36	6	11,964	12.46	1,244	47.4	19,644	20.46	17,136	154.5
37	12	12,084	12.59	1,255	47.0	19,764	20.59	17,264	153.6
38	18	12,204	12.71	1,265	46.6	19,884	20.71	17,391	152.7
39	24	12,324	12.84	1,275	46.2	20,004	20.84	17,517	151.8
40	30	12,444	12.96	1,285	45.8	20,124	20.96	17,641	151.0
41	36	12,564	13.09	1,294	45.4	20,244	21.09	17,764	150.1
42	42	12,684	13.21	1,304	45.0	20,364	21.21	17,885	149.2
43	48	12,804	13.34	1,313	44.7	20,484	21.34	18,005	148.4
44	54	12,924	13.46	1,322	44.3	20,604	21.46	18,123	147.6
45	60	13,044	13.59	1,331	43.9	20,724	21.59	18,240	146.7

**Span Lengths from 450 to 500 feet**

**Deck Width 35 to 45 feet**

Department of  
Structural Engineering

CALTRANS - Segmental Box Girder Standard  
Sections for Balanced Cantilever Construction

Scale: 1" = 10'-0"

Appendix B – Standard Sections

**Document:** Caltrans - Segmental Box Girder Standard Sections for Balanced Cantilever Construction

**Document Date:** March 28, 2008

**Response Date:** July 8, 2008

<b>Reviewer</b>	<b>Item #</b>	<b>Sheet</b>	<b>Comment</b>	<b>Response</b>
Caltrans	1		Design Specifications: need to reference LRFD.	Will do.
Caltrans	2		Wearing surface: It would be beneficial if we included sacrificial wearing surface for all the areas including those where we do not use deicing chemicals because the deck is not replaceable for this type of structure. Usually the deck service life becomes the bridge service life, which is around 40 years or so. Our design life is 75 years. This is especially true where we have high truck traffic. This may be something we need to discuss with the Bridge Deck Protection Committee.	Will do.
Caltrans	3		Span-to-Depth ratio. We use Depth-to-Span ratio. Recommend the ratios be changed for consistency. Example, "35 to 50" to "0.029 to 0.020".	Will do.
Caltrans	4		Keep maximum cantilever length within AASHTO Segmental Guide Specifications (max cantilever ratio = 0.45).	Will do.
Caltrans	5		Consider handling the width variation by changing the top and bottom slab length at the centerline of the Box Girder. Benefit: the top slab depth (1'-8" over the web) would not have to be as thick if the maximum overhang length was reduced. This idea would need input from form fabricators to discuss feasibility.	Disagree. Altering the cell dimension is very difficult from a construction point of view as it requires a different set of internal forms, which are a very complicated and costly piece of machinery. It is more cost effective to adjust the external cantilever forms.
Caltrans	6		Modify radius' to simple fillets.	Will do.
Caltrans	7		Specs require a unit weight of concrete to be 155pcf. The charts are using 150pcf.	Will do.
PBS&J	1		Section width 28 ft seems to be too narrow. If your bridge width is 28 ft, this will be only one lane as we have shoulder(s) and two barriers at the end. To build a bridge with more lanes, the 28 ft wide section cannot be used unless there will be two precast box girders	We will revise the minimum widths.

Appendix B – Standard Sections

			joined together by a CIP deck closure. Is this your intention?	
PBS&J	2		In the General Notes sheet, reference should be made to the AASHTO LRFD Specifications instead of the AASHTO Standard Specifications. We are currently using the LRFD specs in California as you know and no one will be allowed to use the Standard Specs (LFD) unless this is exceptionally allowed by Caltrans.	Will do
PBS&J	3		General Notes (Wearing Surfaces): Sacrificial wearing surface may be required even if no deicing chemicals are used. For example, I do not think deicing chemicals are used in Florida, but they always require 1/2" sacrificial wearing surface.	Will revise.
PBS&J	4		Web thickness: I could be wrong, but I am not sure web thickness will be sufficient for shear-torsion design as well as concrete principal stresses at sections near the piers. I feel the web is thin for deep sections (like the 30 ft deep sections).	These standard sections cover a wide range of design options and are not intended to be fully designed sections. There are simply far too many parameters to consider at this stage. The intent is to develop general cross section shapes that will help standardize the equipment necessary to construct these section. If thicker webs are required based on detailed design calculations, the contractor can simply push out the external forms with out much difficulty.
PBS&J	5		Unit weight values in tables in all sheets are calculated based on 150 pcf concrete density, whereas 155 pcf is mentioned in the General Notes sheet (to account for weight of rebars).	Will do.
PBS&J	6		Other editorial comments are in the attached markups.	Noted. Thank you.
IBT	7	1	The cover page's title should read "Precast Segmental Box.." to differentiate from cast-in-place segmental construction.	Will revise.

## Appendix B – Standard Sections

IBT	8		<p>We understand that the standard sections presented in Appendix A have been developed in the hope of reducing the cost of segmental superstructures in the long term by lowering the fixed overhead associated with segment production. However it should be recognized that cast-in-place rather than precast segmental construction is more often used for the span range under consideration for the following reasons:</p> <p>For construction over land, there is a limitation on both segment height and segment weight: it is not practical to transport segments in excess of 80 tons or 16 ft in height. Using a span to depth ratio of 18 at the pier, the practical span length limitation is therefore around 300 ft for bridges built over land.</p> <p>This would limit the applicability of these standard sections to bridges that are built with water access to the alignment, with a sufficient number of spans to justify precasting. This was the case for the SFOBB project.</p>	Noted. Thank you for your comments.
IBT	9		<p>The deck width of 28 ft would normally be applicable to bridge ramps and would not typically be used for long span bridges. There may be difficulties fitting the post-tensioning tendons in the top slab of such a narrow section.</p>	We will revise the minimum widths.
IBT	10	2	<p>General Notes, general. There are several items here that are essentially the domain of the Owner and Designer, and would be generated for each individual project. For example, the design standards, material types and strengths, shop drawing and camber requirements are all things that would be decided by an Owner. We recommend instead using these General Notes only to clarify the assumptions made in the development of these plans, and then noting that the actual values used are the responsibility of the Designer.</p>	Thank you. We will consider your recommendation and discuss with Caltrans.

## Appendix B – Standard Sections

IBT	11	2	General Notes – Under “Post-Tensioning”, the largest tendon referenced is a 31-strand 0.6” tendon. Care should be exercised when using such large units due to large local forces at the anchorages and at the deviation points. For the bottom slab tendons, using tendon sizes above 19 – 0.6” strands is risky because of the large radial forces due to the vertical curvature of the slab.	We will remove this note.
IBT	12	2	General Notes – “Temporary Post-Tensioning”, if the PT is internal, it is not temporary, as it will remain in the structure. This is often considered to be the more expensive option (as opposed to external blocks) due to the “lost” PT bars. In addition, the PT bars take up space within the top and bottom flanges that may be needed for the permanent ducts – space that can be at a premium for long span bridges.	We will remove this note.
IBT	13	2	General Notes – “Crown Roadway Cross Sections”, the variation in the bottom surface of the wing would require a form with adjustable wing if it is to be re-used. This would have an impact on the form design, and is typical of the type of challenge that section standardization has faced in the past.	Noted.
IBT	14	2	General Notes – “Bottom Soffit Thickness”, the bottom flange does not necessarily need to carry the full compression, as the webs can be mobilized to carry a portion of this load under most design codes.	Disagree. It is not recommended to mobilize the web for seismic loads.
IBT	15	3-10	Sections, General – The top flange in the vicinity of the webs should be investigated as an anchorage zone. Larger tendons, like those anticipated in the General Notes, many not easily fit into the space provided.	Noted. See response to PBS&J comment #4
IBT	16	3-10	A preliminary post-tensioning design should be performed for representative spans. A major challenge for long spans can be accommodating the number of ducts required in the top flanges at the piers, and in the bottom flanges near center span. Particularly for long spans with narrow widths, the actual PT layout and corresponding bulkheads should be estimated.	Noted. See response to PBS&J comment #4

## Appendix B – Standard Sections

IBT	17	3-10	The bottom flanges shown are misleading for the deeper sections. Typically, there would be no haunch when the flange is deeper, and the flange thickness near the piers could be between 2-3' for the longer spans.	Will revise.
IBT	18	3-10	Nothing is shown regarding the continuity anchorage blisters, upper or lower. These are typically a fixed part of the core form, and standardization of their size and location would be beneficial.	Will revise.
IBT	19	3-10	A preliminary check of the transverse post-tensioning in the deck should be performed to ensure that the dimensions shown are feasible. In addition, the preliminary bulkhead layout anticipated in comment 6 should take into account the conflicts with the anticipated transverse PT profile, as it relates to cover and reinforcement.	Noted. See response to PBS&J comment #4
IBT	20	3-10	It is unclear how the section properties shown could be reasonably calculated if the bottom flange is to be adjusted. They should be based on reasonable bottom flange thickness values – otherwise an estimate based on these numbers would be artificially low.	Will revise.
IBT	21	3-10	The webs shown appear somewhat slender for the longer spans. They should be checked for principal stresses at service, as well as for ultimate shear stress limitations. If vertical post-tensioning is intended to reduce the web thickness, it should be noted.	Noted. See response to PBS&J comment #4
IBT	22	3-10	The 10 inch minimum bottom and top slab thickness seems conservative and will result into heavy sections. In the past, a minimum thickness of 8 inch has been used with 9 inch at the wing tips to accommodate transverse PT anchorages.	Will revise.

## Appendix B – Standard Sections

TY Lin	1		<p>What is the range of applicability of this framework? The sections all deal with precast box girders for balanced cantilever construction. What about:</p> <ul style="list-style-type: none"> <li>- Cast in place segmental</li> <li>- Span by span</li> <li>- External Prestressing</li> <li>- Dry joints vs. epoxy joints</li> <li>- Widths other than those from 28' to 45'</li> <li>- Spans other than 300' to 500'</li> <li>- Multi-cell boxes</li> <li>- Multiple box systems (twin boxes)</li> <li>- Sections for heavy rail rather than vehicle loading</li> </ul> <p>These do not need to be covered by the recommendations but they should be explicitly included or excluded from the framework.</p>	Will revise.
TY Lin	2	2	Note typos under the following sections: Purpose, Post-Tensioning Steel, Shop Drawing Requirements, Epoxy Joining of Precast Concrete Segments	Will revise. Thank you.
TY Lin	3	2	Under Reinforcing Steel - Insert "A706" between "of" and "reinforcing" for last sentence.	Will revise
TY Lin	4	2	Under Shop Drawing Requirements - It is preferable to use the LRFD Construction Specifications, 2006 for this reference. They are more current than ASBI's.	Will revise
TY Lin	5	2	Under Epoxy Joining of Precast Concrete Segments - It is preferable to use the LRFD Construction Specifications, 2006 for this reference. They are more current than ASBI's. Should use LRFD reference here as well.	Will revise
TY Lin	6	2	Under Temporary Post-Tensioning - This is not necessary, and in some cases not the best solution. Why not leave this open? External bars in blisters can be recovered, and can be more economical. Also, considering the application here, it may be better to avoid bonded PT bars in segments with external PT as the primary reinforcing.	Will revise
TY Lin	7	2	Under Crown Roadway Cross Sections - This is a limited case. The main point of holding the core is key. But depending on the crown conditions, it is best to hold the overhand soffit if possible. Also, for twin roadways or twin boxes, it is best to rotate each box for the crossfall rather than crown boxes.	Noted.

## Appendix B – Standard Sections

TY Lin	8	3	For Pier - These soffit slabs are shown too small. They should be shown as about 1/3 (or more) of the segment area at the pier.	Will revise
TY Lin	9	3-10	Midspace - Why are the sections at midspace using a 10" bottom slab? Is it necessary to deviate from the ASBI standard sections which have a 9" bottom slab?	Will revise
TY Lin	10	4	For Pier - For these large boxes and spans, deck widths for a single box can go larger than 45 feet. You can show a width 6-8 times the minimum depth	Will revise
TY Lin	11	5	For Pier - While sloped webs are preferred in general, I would use vertical webs for such a narrow long span bridge (don't see many 400' spans at 28 ft width).	Noted.
TY Lin	12	10	For Pier - See earlier comments on widths. Should show up to 70 ft +/- with single cell at this span (and use sloping webs). You do not want user to assume this is maximum standard width for a single cell box.	Will revise

## **Appendix C - Verification of Proposed Design Approach**

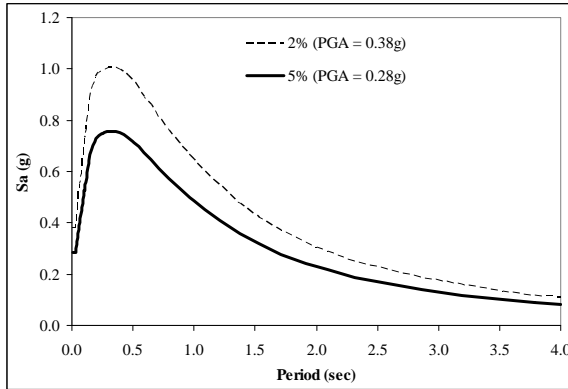
Sample calculations illustrating the use of the complete design recommendations (see Chapter 7) are presented on the following pages.

'Ordinary' Bridge

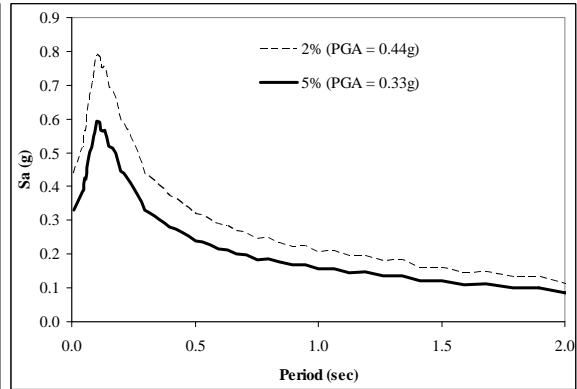
# 'Ordinary' Bridge – Sample Design Calculations

## 1. Seismic Design Spectra

### Horizontal FEE Design Spectra

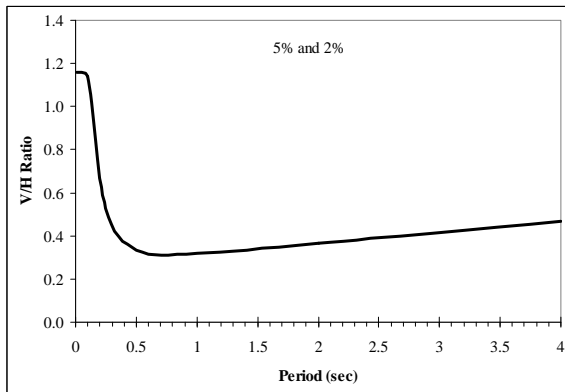


### Vertical FEE Design Spectra



The vertical peak ground acceleration,  $PGA_v$ , is less than the peak spectral acceleration → OK

### FEE V/H Spectral Ratio



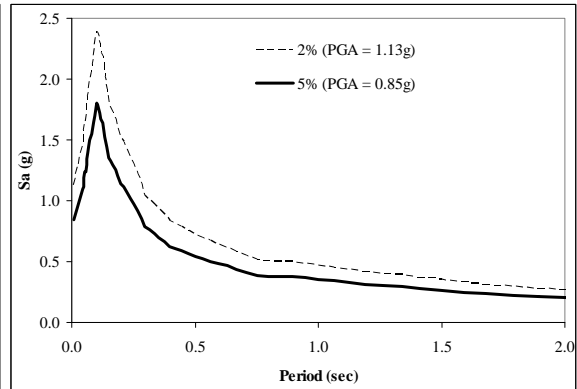
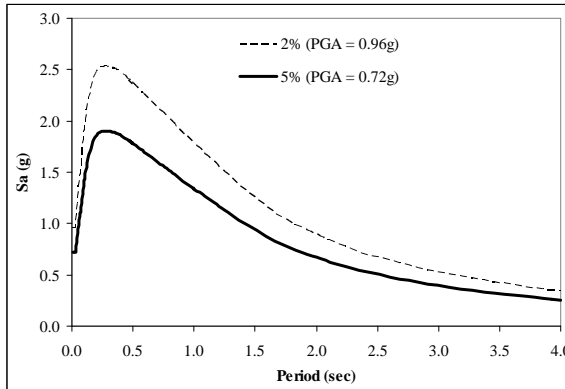
The vertical to horizontal spectral ratio is not equal to 2/3 for all periods → OK

Appendix C - Verification of Proposed Design Approach

'Ordinary' Bridge

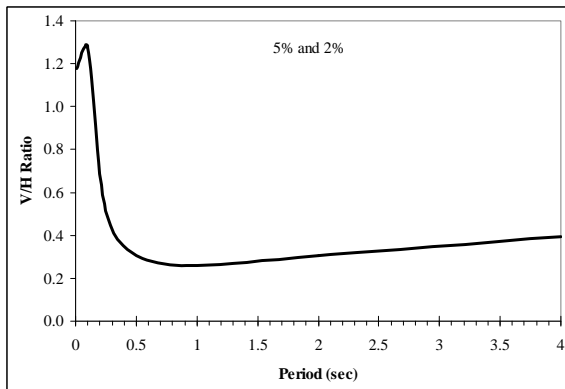
**Horizontal SEE Design Spectra**

**Vertical SEE Design Spectra**



The vertical peak ground acceleration,  $PGA_v$ , is less than the peak spectral acceleration → OK

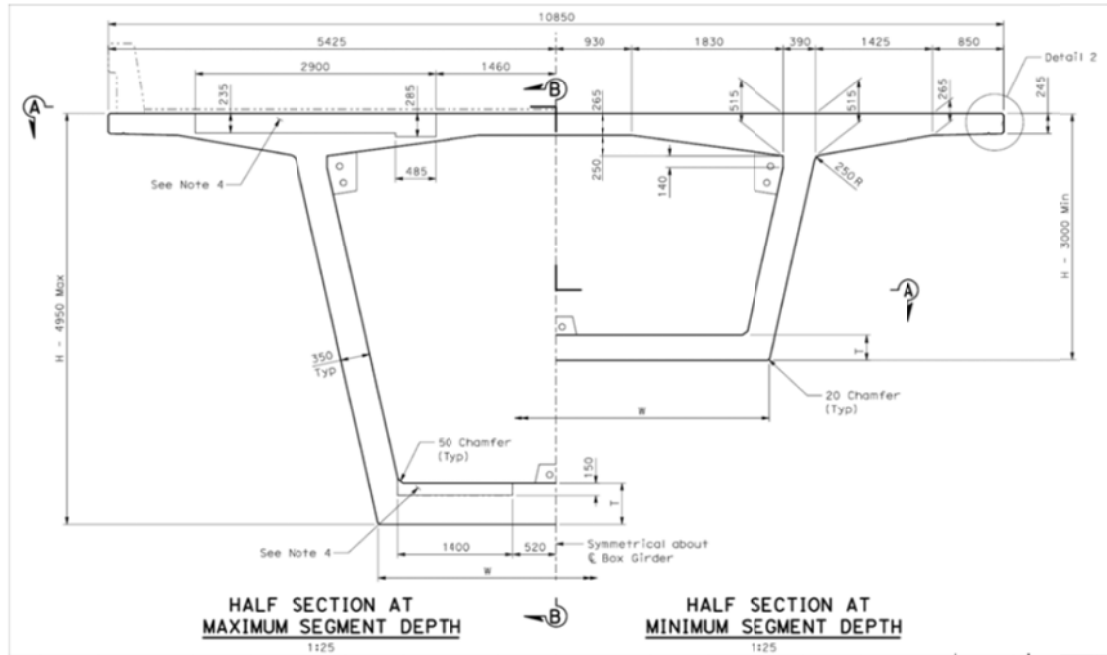
**SEE V/H Spectral Ratio**



The vertical to horizontal spectral ratio is not equal to 2/3 for all periods → OK

## 2. Design for Construction and Service Loads

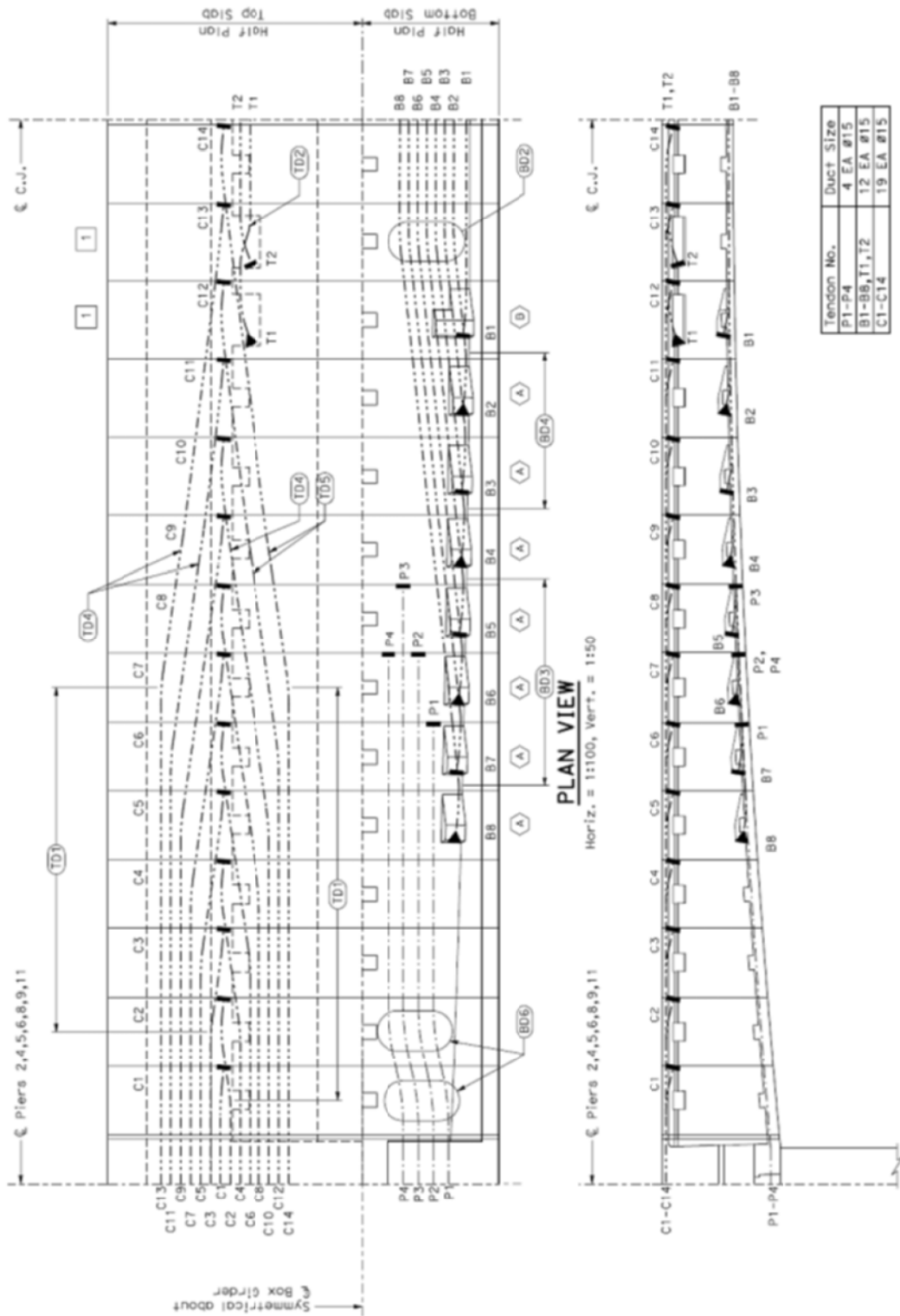
### Typical Cross Sections



TYPICAL AND ABUTMENT CANTILEVER SEGMENT DIMENSIONS			
Joint No.	H	T	W
1	4950	497	4322
2	4693	484	4437
3	4455	471	4543
4	4234	457	4642
5	4032	444	4732
6	3847	430	4814
7	3681	417	4888
8	3533	403	4954
9	3403	390	5012
10	3292	376	5062
11	3187	361	5109
12	3105	346	5145
13	3047	331	5171
14	3012	300	5187
15	3000	300	5192

Appendix C - Verification of Proposed Design Approach  
 'Ordinary' Bridge

**PT Layout**



**2.1 Ensure that the superstructure top and bottom flange thicknesses are large enough to support the large compression forces experienced when the segment joints open.**

$f_{ce} := 1.3 \cdot 6.0 \text{ksi}$	$f_{ce} = 7.8 \text{ksi}$	Expected concrete compressive strength
$F_y := 245 \text{ksi}$		Yield stress of PT
$F_{pt} := .55 \cdot 270 \cdot \text{ksi}$	$F_{pt} = 148.5 \cdot \text{ksi}$	Expected stress of PT after seating
$A_{strand} := .217 \text{in}^2$		Area of single PT strand

**Segment Joint Adjacent to Pier**

$b_{tf} := 10.85 \text{m}$	$b_{tf} = 35.597 \text{-ft}$	Width of top flange
$t_{tf} := 0.3 \text{m}$	$t_{tf} = 11.811 \text{-in}$	Average thickness of top flange
$A_{tf} := b_{tf} \cdot t_{tf}$	$A_{tf} = 35.037 \cdot \text{ft}^2$	Top flange area
$b_{bf} := 4.322 \text{m}$	$b_{bf} = 14.18 \text{-ft}$	Width of bottom flange
$t_{bf} := .656 \text{m}$	$t_{bf} = 25.827 \text{-in}$	Thickness of bottom flange
$A_{bf} := b_{bf} \cdot t_{bf}$	$A_{bf} = 30.518 \cdot \text{ft}^2$	Bottom flange area
$n_t := 15$		Number of strands per TOP tendon
$N_t := 2 \cdot 14$	$N_t = 28$	Number of TOP tendons
$A_{pt\_top} := n_t \cdot N_t \cdot A_{strand}$		TOP tendon area
	$A_{pt\_top} = 91.14 \cdot \text{in}^2$	
$n_b := 4$		Number of strands per BOTTOM tendon
$N_b := 4$		Number of BOTTOM tendons
$A_{pt\_bot} := n_b \cdot N_b \cdot A_{strand}$		BOTTOM tendon area
	$A_{pt\_bot} = 3.472 \cdot \text{in}^2$	

**Positive Bending (i.e. tension on bottom, compression on top)**

$T_{demand} := A_{pt\_bot} \cdot F_y + A_{pt\_top} \cdot F_{pt}$		Under positive bending the bottom tendons will yield while the top tendons will likely not exceed their stress after seating.
$T_{demand} = 1.438 \times 10^4 \cdot \text{kip}$		
$C_{capacity} := 0.85 \cdot f_{ce} \cdot A_{tf}$		
$C_{capacity} = 3.345 \times 10^4 \cdot \text{kip}$		
$DC := \frac{T_{demand}}{C_{capacity}}$	$DC = 0.43$	$D/C < 1.0 \quad \Rightarrow \text{OK}$

**Negative Bending (i.e. tension on top, compression on bottom)**

$T_{demand} := A_{pt\_top} \cdot F_y$		Under negative bending the top tendons will yield. The bottom tendons are jacked just enough to seat the anchorages and can be neglected.
$T_{demand} = 2.233 \times 10^4 \cdot \text{kip}$		
$C_{capacity} := 0.85 \cdot f_{ce} \cdot A_{bf}$		
$C_{capacity} = 2.914 \times 10^4 \cdot \text{kip}$		
$DC := \frac{T_{demand}}{C_{capacity}}$	$DC = 0.766$	$D/C < 1.0 \quad \Rightarrow \text{OK}$

Appendix C - Verification of Proposed Design Approach  
'Ordinary' Bridge

Segment Joint at Midspan

$b_{tf} := 10.85\text{m}$	$b_{tf} = 35.597\text{-ft}$	Width of top flange
$t_{tf} := 0.3\text{m}$	$t_{tf} = 11.811\text{-in}$	Average thickness of top flange
$A_{tf} := b_{tf} \cdot t_{tf}$	$A_{tf} = 35.037\text{-ft}^2$	Top flange area
$b_{bf} := 5.192\text{m}$	$b_{bf} = 17.034\text{-ft}$	Width of bottom flange
$t_{bf} := .300\text{m}$	$t_{bf} = 11.811\text{-in}$	Thickness of bottom flange
$A_{bf} := b_{bf} \cdot t_{bf}$	$A_{bf} = 16.766\text{-ft}^2$	Bottom flange area
$n_t := 12$		Number of strands per TOP tendon
$N_t := 4$		Number of TOP tendons
$A_{pt\_top} := n_t \cdot N_t \cdot A_{strand}$		TOP tendon area
	$A_{pt\_top} = 10.416\text{-in}^2$	
$n_b := 12$		Number of strands per BOTTOM tendon
$N_b := 2 \cdot 8$	$N_b = 16$	Number of BOTTOM tendons
$A_{pt\_bot} := n_b \cdot N_b \cdot A_{strand}$		BOTTOM tendon area
	$A_{pt\_bot} = 41.664\text{-in}^2$	

Positive Bending (i.e. tension on bottom, compression on top)

$T_{demand} := A_{pt\_bot} \cdot F_y + A_{pt\_top} \cdot F_{pt}$		Under positive bending the bottom tendons will reach their ultimate capacities while the top tendons will likely not exceed their stress after seating.
$T_{demand} = 1.175 \times 10^4 \cdot \text{kip}$		
$C_{capacity} := 0.85 \cdot f_{ce} \cdot A_{bf}$		
$C_{capacity} = 3.345 \times 10^4 \cdot \text{kip}$		
$DC := \frac{T_{demand}}{C_{capacity}}$	$DC = 0.351$	$D/C < 1.0 \quad \implies \text{OK}$

Negative Bending (i.e. tension on top, compression on bottom)

$T_{demand} := A_{pt\_top} \cdot F_y + A_{pt\_bot} \cdot F_{pt}$		Under negative bending the top tendons will reach their ultimate capacities while the bottom tendons will likely not exceed their stress after seating.
$T_{demand} = 8.739 \times 10^3 \cdot \text{kip}$		
$C_{capacity} := 0.85 \cdot f_{ce} \cdot A_{bf}$		
$C_{capacity} = 1.601 \times 10^4 \cdot \text{kip}$		
$DC := \frac{T_{demand}}{C_{capacity}}$	$DC = 0.546$	$D/C < 1.0 \quad \implies \text{OK}$

### **3. Column and Superstructure Capacities**

#### ***3.1 Column Capacities (Moment Curvature Analysis)***

Calculate the capacities of potential column plastic hinge regions using moment-curvature analysis as described in Section 3.3 of the Caltrans Seismic Design Criteria. This is standard practice in the industry, thus sample calculations are not shown herein.

### 3.2 Superstructure Joint Capacities (Moment-Curvature Analysis)

#### XTRACT Material Report - Educational

For use only in an academic or research setting

Material Name: Unconfined1

Material Type: Unconfined Concrete

MJV

Merrimack College

3/10/2010

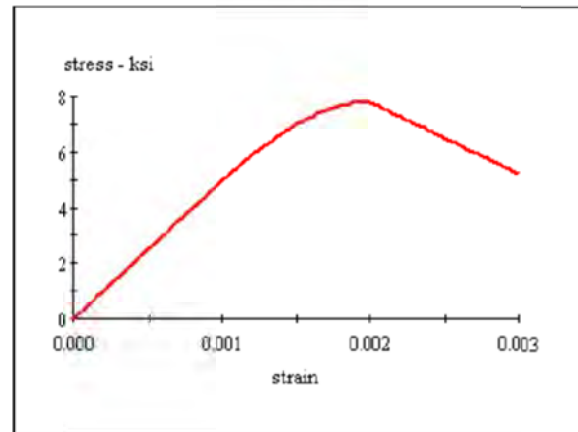
Task 5

300 ft Superstructure - Near Pier

Page \_\_ of \_\_

#### Input Parameters:

Tension Strength:	0 ksi
28 Day Strength:	7.800 ksi
Post Crushing Strength:	0 ksi
Tension Strain Capacity:	0 Ten
Spalling Strain:	5.000E-3 Comp
Failure Strain:	3.000E-3 Comp
Elastic Modulus:	5034 ksi
Secant Modulus:	3900 ksi



#### Model Details:

For Strain -  $\epsilon < 2 \epsilon_t$   $f_c = 0$

For Strain -  $\epsilon < 0$   $f_c = \epsilon \cdot E_c$

For Strain -  $\epsilon < \epsilon_{cu}$   $f_c = \frac{f_c \cdot x}{r - 1 + x^r}$

For Strain -  $\epsilon < \epsilon_{sp}$   $f_c = f_{cu} + (f_{cp} - f_{cu}) \cdot \frac{(\epsilon - \epsilon_{cu})}{(\epsilon_{sp} - \epsilon_{cu})}$

$$x = \frac{\epsilon}{\epsilon_{cc}}$$

$$r = \frac{E_c}{E_c - E_{sec}}$$

$$E_{sec} = \frac{f_c}{\epsilon_{cc}}$$

$\epsilon$  = Concrete Strain

$f_c$  = Concrete Stress

$E_c$  = Elastic Modulus

$E_{sec}$  = Secant Modulus

$\epsilon_t$  = Tension Strain Capacity

$\epsilon_{cu}$  = Ultimate Concrete Strain

$\epsilon_{cc}$  = Strain at Peak Stress = .002

$\epsilon_{sp}$  = Spalling Strain

$f_c$  = 28 Day Compressive Strength

$f_{cu}$  = Stress at  $\epsilon_{cu}$

$f_{cp}$  = Post Spalling Strength

#### Material Color States:

- Tension strain after tension capacity
- Tension strain before tension capacity
- Initial state
- Compression before crushing strain
- Compression before end of spalling
- Compression after spalling

#### Reference:

Mander, J.B., Priestley, M. J. N., "Observed Stress-Strain Behavior of Confined Concrete", Journal of Structural Engineering, ASCE, Vol. 114, No. 8, August 1988, pp. 1827-1849

Appendix C - Verification of Proposed Design Approach  
 'Ordinary' Bridge

**XTRACT Material Report - Educational**

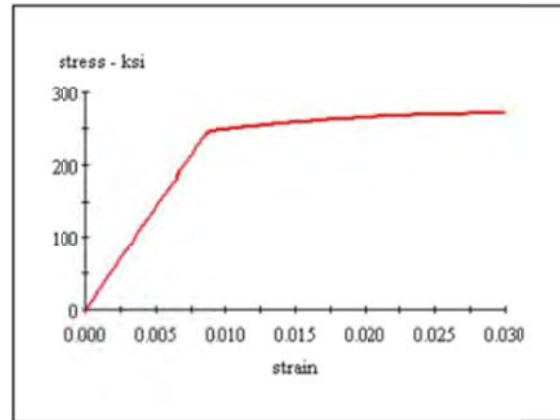
For use only in an academic or research setting.

Material Name: PreStress1  
 Material Type: Prestressing Steel

MJV  
 Merrimack College  
 3/10/2010  
 Task 5  
 300 ft Superstructure - Near Pier  
 Page \_\_ of \_\_

**Input Parameters:**

Yield Stress: 245.1 ksi  
 Peak Stress: 270.0 ksi  
 Yield Strain: 8.600E-3  
 Strain at Peak Stress: 30.00E-3  
 Failure Strain: 30.00E-3  
 Elastic Modulus: 28.50E+3 ksi  
 Additional Information: Symetric Tension and Comp.



**Model Details:**

$$\text{For Strain - } \varepsilon < \varepsilon_y \quad f_s = E \cdot \varepsilon$$

$$\text{For Strain - } \varepsilon < \varepsilon_{su} \quad f_s = f_u - (f_u - f_y) \cdot \left( \frac{\varepsilon_{sp} - \varepsilon}{\varepsilon_{sp} - \varepsilon_{sh}} \right)^2$$

- ε = Steel Strain
- fs = Steel Stress
- f<sub>y</sub> = Yield Stress
- f<sub>u</sub> = Fracture Stress
- ε<sub>y</sub> = Yield Strain
- ε<sub>sp</sub> = Strain at Peak Stress
- ε<sub>su</sub> = Failure Strain
- E = Elastic Modulus

**Material Color States:**

- Tension force after yield
- Initial state
- Compression force after yield

Appendix C - Verification of Proposed Design Approach  
 'Ordinary' Bridge

<b>XTRACT Section Report - Educational</b> For use only in an academic or research setting. Section Name: J1 (near Pier) - 656mm Bot. Flange		MJV Merrimack College 3/10/2010 Task 5 300 ft Superstructure - Near Pier Page __ of __	
<hr/>			
<b>Section Details:</b>			
X Centroid:	-3.551E-3 in		
Y Centroid:	111.4 in		
Section Area:	14.74E+3 in^2		
EI gross about X:	4.57E+11 kip-in^2		
EI gross about Y:	7.55E+11 kip-in^2		
I trans (Unconfined1) about X:	9.09E+7 in^4		
I trans (Unconfined1) about Y:	1.50E+8 in^4		
Reinforcing Bar Area:	127.8 in^2		
Percent Longitudinal Steel:	.8667 %		
Overall Width:	427.2 in		
Overall Height:	194.9 in		
Number of Fibers:	1039		
Number of Bars:	36		
Number of Materials:	2		
<b>Material Types and Names:</b>			
Unconfined Concrete:	<input type="checkbox"/> Unconfined1		
Prestressing Steel:	<input checked="" type="checkbox"/> PreStress1		

Appendix C - Verification of Proposed Design Approach  
'Ordinary' Bridge

## XTRACT Analysis Report - Educational

For use only in an academic or research setting.

Section Name: J1 (near Pier) - 656mm Bot. Flange  
 Loading Name: Negative  
 Analysis Type: Moment Curvature

MJV  
 Merrimack College  
 3/10/2010  
 Task 5  
 300 ft Superstructure - Near Pier  
 Page \_\_ of \_\_

### Section Details:

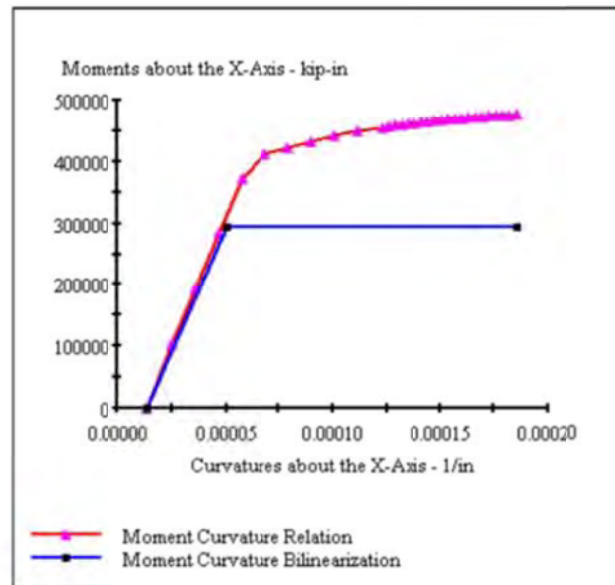
X Centroid: -3.551E-3 in  
 Y Centroid: 111.4 in  
 Section Area: 14.74E+3 in<sup>2</sup>

### Loading Details:

Incrementing Loads: Mxx Only  
 Number of Points: 31  
 Analysis Strategy: Displacement Control

### Analysis Results:

Failing Material: PreStress1  
 Failure Strain: 30.00E-3 Tension  
 Curvature at Initial Load: -14.01E-6 1/in  
 Curvature at First Yield: -61.33E-6 1/in  
 Ultimate Curvature: -1.855E-3 1/in  
 Moment at First Yield: -386.0E+3 kip-in  
 Ultimate Moment: -476.5E+3 kip-in  
 Centroid Strain at Yield: 3.998E-3 Ten  
 Centroid Strain at Ultimate: 13.55E-3 Ten  
 N.A. at First Yield: -65.19 in  
 N.A. at Ultimate: -73.08 in  
 Energy per Length: 65.66 kips  
 Effective Yield Curvature: 50.20E-6 1/in  
 Effective Yield Moment: 295.2E+3 kip-in  
 Over Strength Factor: -1.614  
 EI Effective: 8.16E+9 kip-in<sup>2</sup>  
 Yield EI Effective: 0 kip-in<sup>2</sup>  
 Bilinear Hardening Slope: 0 %  
 Curvature Ductility: 3.694



Appendix C - Verification of Proposed Design Approach  
'Ordinary' Bridge

## XTRACT Analysis Report - Educational

For use only in an academic or research setting.

Section Name: J1 (near Pier) - 656mm Bot. Flange

Loading Name: Negative

Analysis Type: Moment Curvature

MJV

Merrimack College

3/10/2010

Task 5

300 ft Superstructure - Near Pier

Page \_\_\_ of \_\_\_

Min. Unconfined Strain (strain)	Max. PreStress1 Strain (strain)	Min. Unconfined Stress (ksi)	Max. PreStress1 Stress (ksi)	Mxx (kip-in)	Kxx (1/in)
-0.6587E-3	5.222E-3	-3.309	148.8	0	-14.01E-6
-0.7538E-3	5.199E-3	-3.780	148.2	-102.1E+3	-24.88E-6
-0.8376E-3	5.188E-3	-4.191	147.8	-193.9E+3	-35.75E-6
-0.9177E-3	6.094E-3	-4.578	173.7	-283.3E+3	-46.62E-6
-0.9965E-3	7.942E-3	-4.951	226.4	-372.1E+3	-57.48E-6
-1.064E-3	9.801E-3	-5.263	247.8	-411.3E+3	-68.35E-6
-1.125E-3	11.67E-3	-5.538	251.7	-422.7E+3	-79.22E-6
-1.185E-3	13.53E-3	-5.800	255.3	-433.2E+3	-90.09E-6
-1.240E-3	15.41E-3	-6.033	258.4	-441.8E+3	-1010E-3
-1.295E-3	17.28E-3	-6.255	261.2	-449.6E+3	-1118E-3
-1.345E-3	19.15E-3	-6.450	263.6	-455.9E+3	-1227E-3
-1.359E-3	19.70E-3	-6.503	264.2	-457.6E+3	-1258E-3
-1.373E-3	20.24E-3	-6.554	264.8	-459.0E+3	-1290E-3
-1.387E-3	20.78E-3	-6.604	265.4	-460.5E+3	-1321E-3
-1.401E-3	21.32E-3	-6.653	265.9	-461.9E+3	-1353E-3
-1.414E-3	21.87E-3	-6.701	266.4	-463.2E+3	-1384E-3
-1.428E-3	22.41E-3	-6.749	266.9	-464.6E+3	-1415E-3
-1.442E-3	22.95E-3	-6.795	267.3	-465.7E+3	-1447E-3
-1.455E-3	23.49E-3	-6.841	267.7	-466.9E+3	-1478E-3
-1.469E-3	24.04E-3	-6.886	268.1	-467.9E+3	-1509E-3
-1.483E-3	24.58E-3	-6.930	268.4	-469.0E+3	-1541E-3
-1.496E-3	25.12E-3	-6.974	268.7	-470.0E+3	-1572E-3
-1.510E-3	25.66E-3	-7.016	269.0	-471.0E+3	-1604E-3
-1.524E-3	26.20E-3	-7.058	269.2	-471.9E+3	-1635E-3
-1.538E-3	26.75E-3	-7.099	269.4	-472.7E+3	-1666E-3
-1.552E-3	27.29E-3	-7.139	269.6	-473.4E+3	-1698E-3
-1.566E-3	27.83E-3	-7.178	269.7	-474.2E+3	-1729E-3
-1.580E-3	28.37E-3	-7.216	269.9	-474.9E+3	-1760E-3
-1.594E-3	28.92E-3	-7.253	269.9	-475.5E+3	-1792E-3
-1.608E-3	29.46E-3	-7.289	270.0	-476.0E+3	-1823E-3
-1.622E-3	30.00E-3	-7.324	270.0	-476.5E+3	-1855E-3
-1.622E-3	30.00E-3	-7.324	270.0	-476.5E+3	-1855E-3

Appendix C - Verification of Proposed Design Approach  
 'Ordinary' Bridge

**XTRACT Analysis Report - Educational**

For use only in an academic or research setting.

Section Name: J1 (near Pier) - 656mm Bot. Flange  
 Loading Name: Positive  
 Analysis Type: Moment Curvature

MJV  
 Merrimack College  
 3/10/2010  
 Task 5  
 300 ft Superstructure - Near Pier  
 Page \_\_ of \_\_

**Section Details:**

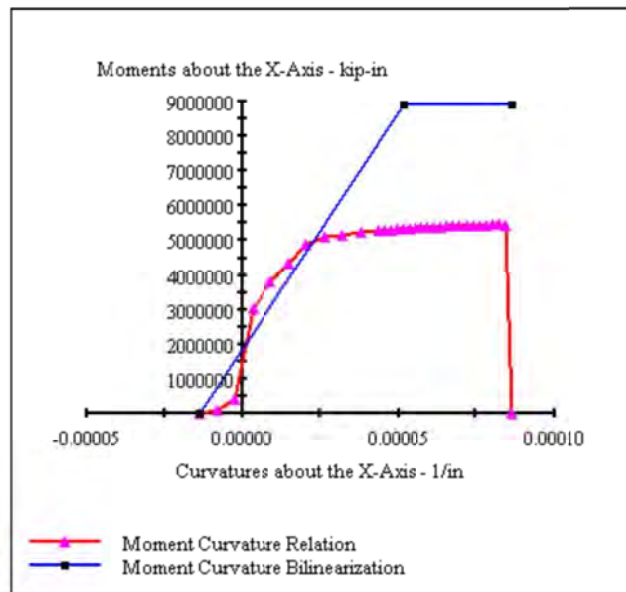
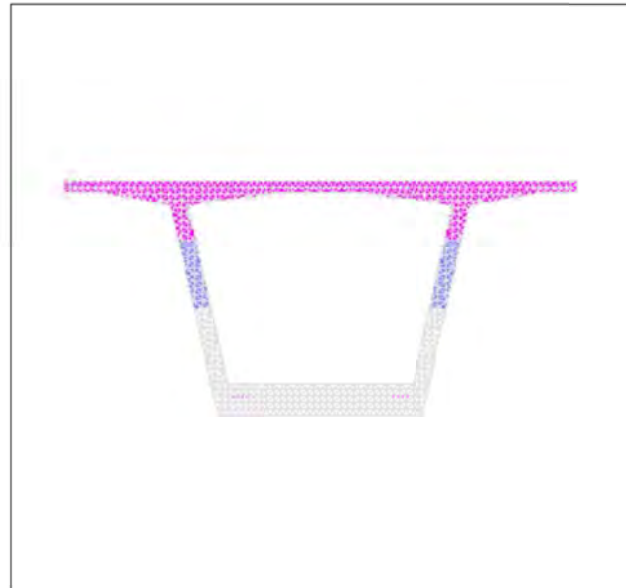
X Centroid: -3.551E-3 in  
 Y Centroid: 111.4 in  
 Section Area: 14.74E+3 in<sup>2</sup>

**Loading Details:**

Incrementing Loads: Mxx Only  
 Number of Points: 31  
 Analysis Strategy: Displacement Control

**Analysis Results:**

Failing Material: Not Available  
 Failure Strain: -----  
 Curvature at Initial Load: -14.01E-6 1/in  
 Curvature at First Yield: 22.34E-6 1/in  
 Ultimate Curvature: 86.29E-6 1/in  
 Moment at First Yield: 4.944E+6 kip-in  
 Ultimate Moment: 0 kip-in  
 Centroid Strain at Yield: 1.049E-3 Ten  
 Centroid Strain at Ultimate: 3.000E-3 Comp  
 N.A. at First Yield: 46.93 in  
 N.A. at Ultimate: -34.77 in  
 Energy per Length: 424.3 kips  
 Effective Yield Curvature: 51.56E-6 1/in  
 Effective Yield Moment: 8.917E+6 kip-in  
 Over Strength Factor: 0  
 EI Effective: 1.36E+11 kip-in<sup>2</sup>  
 Yield EI Effective: 0 kip-in<sup>2</sup>  
 Bilinear Hardening Slope: 0 %  
 Curvature Ductility: 1.674



Appendix C - Verification of Proposed Design Approach

'Ordinary' Bridge

**XTRACT Analysis Report - Educational**

For use only in an academic or research setting.

Section Name: J1 (near Pier) - 656mm Bot. Flange

Loading Name: Positive

Analysis Type: Moment Curvature

MTV

Merrimack College

3/10/2010

Task 5

300 ft Superstructure - Near Pier

Page \_\_\_ of \_\_\_

Min. Unconfined Strain (strain)	Max. PreStress1 Strain (strain)	Min. Unconfined Stress (ksi)	Max. PreStress1 Stress (ksi)	Mxx (kip-in)	Kxx (1/in)
-0.6587E-3	5.222E-3	-3.309	148.8	0	-14.01E-6
-0.5916E-3	5.262E-3	-2.974	150.0	78.64E+3	-8.244E-6
-0.4520E-3	5.375E-3	-2.274	153.2	421.6E+3	-2.482E-6
-0.6076E-3	5.820E-3	-3.054	165.9	3.025E+6	3.280E-6
-0.9002E-3	6.603E-3	-4.494	188.2	3.783E+6	9.042E-6
-1.131E-3	7.449E-3	-5.563	212.3	4.341E+6	14.80E-6
-1.352E-3	8.303E-3	-6.475	236.6	4.871E+6	20.57E-6
-1.508E-3	9.224E-3	-7.008	246.5	5.105E+6	26.33E-6
-1.619E-3	10.19E-3	-7.317	248.7	5.169E+6	32.09E-6
-1.726E-3	11.16E-3	-7.549	250.7	5.224E+6	37.85E-6
-1.833E-3	12.13E-3	-7.706	252.6	5.274E+6	43.62E-6
-1.871E-3	12.47E-3	-7.744	253.3	5.290E+6	45.65E-6
-1.910E-3	12.81E-3	-7.773	253.9	5.306E+6	47.68E-6
-1.948E-3	13.15E-3	-7.791	254.6	5.321E+6	49.71E-6
-1.987E-3	13.49E-3	-7.800	255.2	5.336E+6	51.74E-6
-2.028E-3	13.83E-3	-7.727	255.8	5.349E+6	53.78E-6
-2.071E-3	14.16E-3	-7.615	256.4	5.361E+6	55.81E-6
-2.116E-3	14.50E-3	-7.500	256.9	5.373E+6	57.84E-6
-2.164E-3	14.83E-3	-7.374	257.5	5.383E+6	59.87E-6
-2.213E-3	15.16E-3	-7.246	258.0	5.394E+6	61.90E-6
-2.263E-3	15.49E-3	-7.115	258.6	5.403E+6	63.94E-6
-2.314E-3	15.82E-3	-6.983	259.1	5.412E+6	65.97E-6
-2.366E-3	16.15E-3	-6.848	259.6	5.421E+6	68.00E-6
-2.423E-3	16.47E-3	-6.700	260.0	5.428E+6	70.03E-6
-2.484E-3	16.79E-3	-6.543	260.5	5.435E+6	72.06E-6
-2.546E-3	17.10E-3	-6.380	261.0	5.441E+6	74.10E-6
-2.620E-3	17.41E-3	-6.188	261.4	5.445E+6	76.13E-6
-2.699E-3	17.71E-3	-5.983	261.8	5.448E+6	78.16E-6
-2.782E-3	18.01E-3	-5.766	262.2	5.450E+6	80.19E-6
-2.874E-3	18.29E-3	-5.527	262.5	5.451E+6	82.23E-6
-3.000E-3	18.55E-3	-5.201	262.9	5.446E+6	84.26E-6

0	0	0	0	0	86.29E-6
---	---	---	---	---	----------

Appendix C - Verification of Proposed Design Approach  
'Ordinary' Bridge

### XTRACT Section Report - Educational

For use only in an academic or research setting.

Section Name: J2 (near Pier) 61mm Bot. Flange

MJV

Merrimack College

3/11/2010

Task 5

300 ft Superstructure - Near Pier

Page \_\_ of \_\_

#### Section Details:

X Centroid:	1.354E-3 in
Y Centroid:	106.6 in
Section Area:	14.30E+3 in <sup>2</sup>
EI gross about X:	3.98E+11 kip-in <sup>2</sup>
EI gross about Y:	7.45E+11 kip-in <sup>2</sup>
I trans (Unconfined1) about X:	7.91E+7 in <sup>4</sup>
I trans (Unconfined1) about Y:	1.48E+8 in <sup>4</sup>
Reinforcing Bar Area:	119.4 in <sup>2</sup>
Percent Longitudinal Steel:	.8345 %
Overall Width:	427.2 in
Overall Height:	184.8 in
Number of Fibers:	1040
Number of Bars:	143
Number of Materials:	2



#### Material Types and Names:

Unconfined Concrete:	<input type="checkbox"/> Unconfined1
Prestressing Steel:	<input checked="" type="checkbox"/> PreStress1

#### Comments:

User Comments

# XTRACT Analysis Report - Educational

For use only in an academic or research setting.

Section Name: J2 (near Pier) 61mm Bot. Flange

Loading Name: Positive

Analysis Type: Moment Curvature

MJV

Merrimack College

3/11/2010

Task 5

300 ft Superstructure - Near Pier

Page \_\_ of \_\_

## Section Details:

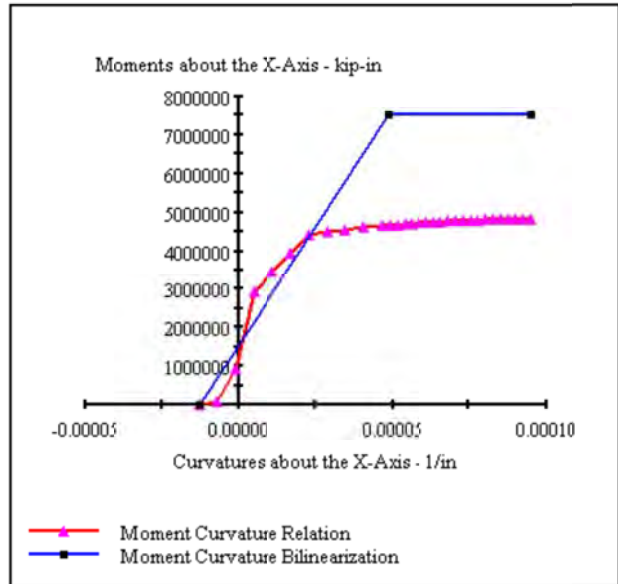
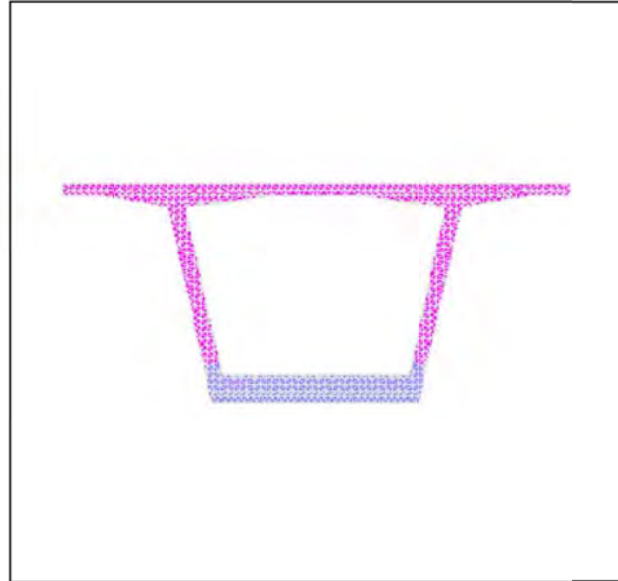
X Centroid: 1.354E-3 in  
 Y Centroid: 106.6 in  
 Section Area: 14.30E+3 in<sup>2</sup>

## Loading Details:

Incrementing Loads: Mxx Only  
 Number of Points: 30  
 Analysis Strategy: Displacement Control

## Analysis Results:

Failing Material: Unconfined1  
 Failure Strain: 3.000E-3 Compression  
 Curvature at Initial Load: -12.93E-6 1/in  
 Curvature at First Yield: 23.31E-6 1/in  
 Ultimate Curvature: 94.89E-6 1/in  
 Moment at First Yield: 4.415E+6 kip-in  
 Ultimate Moment: 4.822E+6 kip-in  
 Centroid Strain at Yield: 1.064E-3 Ten  
 Centroid Strain at Ultimate: 6.941E-3 Ten  
 N.A. at First Yield: 45.63 in  
 N.A. at Ultimate: 73.15 in  
 Energy per Length: 419.1 kips  
 Effective Yield Curvature: 48.79E-6 1/in  
 Effective Yield Moment: 7.520E+6 kip-in  
 Over Strength Factor: .6413  
 EI Effective: 1.22E+11 kip-in<sup>2</sup>  
 Yield EI Effective: 0 kip-in<sup>2</sup>  
 Bilinear Harding Slope: 0 %  
 Curvature Ductility: 1.945



Appendix C - Verification of Proposed Design Approach

'Ordinary' Bridge

<b>XTRACT Analysis Report - Educational</b>					
<small>For use only in an academic or research setting.</small>					
Section Name:		J2 (near Pier) 611mm Bot. Flange			
Loading Name:		Positive			
Analysis Type:		Moment Curvature			
MJV Merrimack College 3/11/2010 Task 5 300 ft Superstructure - Near Pier Page __ of __					
Min. Unconfined Strain (strain)	Max. PreStress1 Strain (strain)	Min. Unconfined Stress (ksf)	Max. PreStress1 Stress (ksf)	Mxx (kip-in)	Kxx (1/in)
-6.173E-3	5.303E-3	-3.103	151.1	0	-12.93E-6
-5.453E-3	5.348E-3	-2.742	152.4	82.43E+3	-6.964E-6
-3.194E-3	5.546E-3	-1.608	158.0	942.3E+3	-9.993E-6
-6.878E-3	6.050E-3	-3.454	172.4	2.916E+6	4.965E-6
-9.408E-3	6.850E-3	-4.688	195.2	3.475E+6	10.93E-6
-1.158E-3	7.687E-3	-5.681	219.1	3.950E+6	16.89E-6
-1.369E-3	8.530E-3	-6.539	243.1	4.407E+6	22.86E-6
-1.489E-3	9.464E-3	-6.950	247.1	4.507E+6	28.82E-6
-1.593E-3	10.41E-3	-7.250	249.1	4.561E+6	34.79E-6
-1.693E-3	11.37E-3	-7.484	251.1	4.608E+6	40.75E-6
-1.793E-3	12.32E-3	-7.656	253.0	4.651E+6	46.72E-6
-1.833E-3	12.71E-3	-7.706	253.7	4.667E+6	49.13E-6
-1.874E-3	13.09E-3	-7.746	254.5	4.682E+6	51.53E-6
-1.915E-3	13.48E-3	-7.775	255.2	4.697E+6	53.94E-6
-1.956E-3	13.86E-3	-7.794	255.8	4.711E+6	56.35E-6
-1.998E-3	14.24E-3	-7.800	256.5	4.725E+6	58.76E-6
-2.044E-3	14.62E-3	-7.685	257.1	4.737E+6	61.17E-6
-2.091E-3	15.00E-3	-7.564	257.8	4.749E+6	63.58E-6
-2.140E-3	15.38E-3	-7.435	258.4	4.759E+6	65.99E-6
-2.193E-3	15.75E-3	-7.299	259.0	4.769E+6	68.40E-6
-2.246E-3	16.12E-3	-7.160	259.5	4.778E+6	70.81E-6
-2.300E-3	16.49E-3	-7.019	260.1	4.786E+6	73.22E-6
-2.356E-3	16.86E-3	-6.874	260.6	4.795E+6	75.62E-6
-2.413E-3	17.23E-3	-6.726	261.1	4.802E+6	78.03E-6
-2.477E-3	17.60E-3	-6.561	261.6	4.809E+6	80.44E-6
-2.544E-3	17.95E-3	-6.386	262.1	4.814E+6	82.85E-6
-2.614E-3	18.31E-3	-6.203	262.6	4.819E+6	85.26E-6
-2.699E-3	18.65E-3	-5.983	263.0	4.822E+6	87.67E-6
-2.789E-3	18.98E-3	-5.747	263.4	4.823E+6	90.08E-6
-2.888E-3	19.31E-3	-5.491	263.8	4.824E+6	92.49E-6
-3.000E-3	19.62E-3	-5.200	264.1	4.822E+6	94.89E-6

# XTRACT Analysis Report - Educational

For use only in an academic or research setting.

Section Name: J2 (near Pier) 611mm Bot. Flange

Loading Name: Negative

Analysis Type: Moment Curvature

MJV

Merrimack College

3/11/2010

Task 5

300 ft Superstructure - Near Pier

Page \_\_ of \_\_

## Section Details:

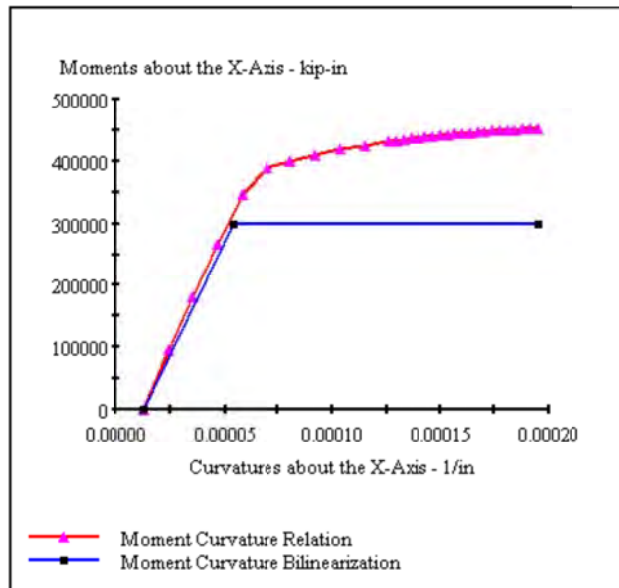
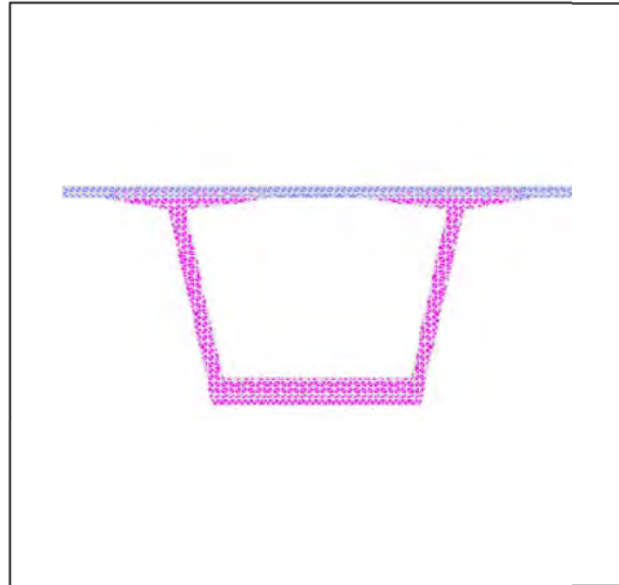
X Centroid: 1.354E-3 in  
 Y Centroid: 106.6 in  
 Section Area: 14.30E+3 in<sup>2</sup>

## Loading Details:

Incrementing Loads: Mxx Only  
 Number of Points: 31  
 Analysis Strategy: Displacement Control

## Analysis Results:

Failing Material: PreStress1  
 Failure Strain: 30.00E-3 Tension  
 Curvature at Initial Load: -12.93E-6 1/in  
 Curvature at First Yield: -63.09E-6 1/in  
 Ultimate Curvature: -.1948E-3 1/in  
 Moment at First Yield: -365.6E+3 kip-in  
 Ultimate Moment: -452.7E+3 kip-in  
 Centroid Strain at Yield: 3.838E-3 Ten  
 Centroid Strain at Ultimate: 13.31E-3 Ten  
 N.A. at First Yield: -60.84 in  
 N.A. at Ultimate: -68.32 in  
 Energy per Length: 66.17 kips  
 Effective Yield Curvature: 54.11E-6 1/in  
 Effective Yield Moment: 300.2E+3 kip-in  
 Over Strength Factor: -1.508  
 EI Effective: 7.29E+9 kip-in<sup>2</sup>  
 Yield EI Effective: 0 kip-in<sup>2</sup>  
 Bilinear Harding Slope: 0 %  
 Curvature Ductility: 3.601



Appendix C - Verification of Proposed Design Approach

'Ordinary' Bridge

**XTRACT Analysis Report - Educational**

For use only in an academic or research setting.

Section Name: J2 (near Pier) 611mm Bot. Flange

Loading Name: Negative

Analysis Type: Moment Curvature

MJV

Merrimack College

3/11/2010

Task 5

300 ft Superstructure - Near Pier

Page \_\_ of \_\_

Min. Unconfined Strain (strain)	Max. PreStress1 Strain (strain)	Min. Unconfined Stress (ksi)	Max. PreStress1 Stress (ksi)	Mxx (kip-in)	Kxx (1/in)
-6.173E-3	5.303E-3	-3.103	151.1	0	-12.93E-6
-7.154E-3	5.281E-3	-3.590	150.5	-96.46E+3	-24.26E-6
-8.011E-3	5.271E-3	-4.013	150.2	-182.0E+3	-35.59E-6
-8.832E-3	6.007E-3	-4.412	171.2	-265.3E+3	-46.92E-6
-9.636E-3	7.820E-3	-4.796	222.9	-347.8E+3	-58.25E-6
-1.033E-3	9.645E-3	-5.121	247.5	-389.5E+3	-69.58E-6
-1.095E-3	11.48E-3	-5.405	251.3	-400.4E+3	-80.91E-6
-1.155E-3	13.31E-3	-5.671	254.9	-410.2E+3	-92.24E-6
-1.211E-3	15.15E-3	-5.912	258.0	-418.4E+3	-1036E-3
-1.266E-3	16.99E-3	-6.140	260.8	-425.8E+3	-1149E-3
-1.315E-3	18.83E-3	-6.335	263.2	-431.6E+3	-1262E-3
-1.330E-3	19.39E-3	-6.392	263.9	-433.2E+3	-1297E-3
-1.345E-3	19.95E-3	-6.447	264.5	-434.8E+3	-1331E-3
-1.359E-3	20.51E-3	-6.502	265.1	-436.3E+3	-1365E-3
-1.374E-3	21.06E-3	-6.555	265.7	-437.7E+3	-1399E-3
-1.388E-3	21.62E-3	-6.608	266.2	-439.1E+3	-1434E-3
-1.403E-3	22.18E-3	-6.660	266.7	-440.3E+3	-1468E-3
-1.417E-3	22.74E-3	-6.711	267.1	-441.5E+3	-1502E-3
-1.432E-3	23.30E-3	-6.761	267.6	-442.7E+3	-1537E-3
-1.446E-3	23.86E-3	-6.811	267.9	-443.9E+3	-1571E-3
-1.461E-3	24.42E-3	-6.860	268.3	-444.9E+3	-1605E-3
-1.476E-3	24.98E-3	-6.907	268.6	-446.0E+3	-1640E-3
-1.490E-3	25.53E-3	-6.954	268.9	-446.9E+3	-1674E-3
-1.505E-3	26.09E-3	-7.000	269.2	-447.9E+3	-1708E-3
-1.520E-3	26.65E-3	-7.045	269.4	-448.7E+3	-1742E-3
-1.535E-3	27.21E-3	-7.089	269.6	-449.5E+3	-1777E-3
-1.550E-3	27.77E-3	-7.132	269.7	-450.3E+3	-1811E-3
-1.565E-3	28.33E-3	-7.175	269.8	-451.0E+3	-1845E-3
-1.580E-3	28.88E-3	-7.215	269.9	-451.6E+3	-1880E-3
-1.595E-3	29.44E-3	-7.255	270.0	-452.2E+3	-1914E-3
-1.610E-3	30.00E-3	-7.294	270.0	-452.7E+3	-1948E-3
-1.610E-3	30.00E-3	-7.294	270.0	-452.7E+3	-1948E-3

Appendix C - Verification of Proposed Design Approach  
'Ordinary' Bridge

**XTRACT Section Report - Educational**

For use only in an academic or research setting.

Section Name: J14 (adj to midspan)

MJV

Merrimack College

3/11/2010

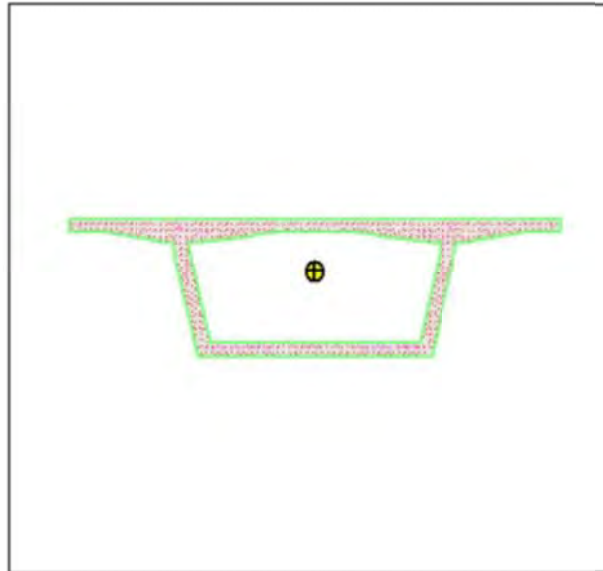
Task 5

300 ft Superstructure - Near Midspan

Page \_\_ of \_\_

**Section Details:**

X Centroid: -.8853E-14 in  
Y Centroid: 73.89 in  
Section Area: 10.86E+3 in<sup>2</sup>  
EI gross about X: 1.17E+11 kip-in<sup>2</sup>  
EI gross about Y: 6.36E+11 kip-in<sup>2</sup>  
I trans (Unconfined1) about X: 2.32E+7 in<sup>4</sup>  
I trans (Unconfined1) about Y: 1.26E+8 in<sup>4</sup>  
Reinforcing Bar Area: 69.56 in<sup>2</sup>  
Percent Longitudinal Steel: .6402 %  
Overall Width: 427.2 in  
Overall Height: 118.6 in  
Number of Fibers: 811  
Number of Bars: 56  
Number of Materials: 2



**Material Types and Names:**

Unconfined Concrete:  Unconfined1  
Prestressing Steel:  PreStress1

**Comments:**

User Comments

## XTRACT Analysis Report - Educational

For use only in an academic or research setting.

Section Name: J14 (adj to midspan)

Loading Name: Positive

Analysis Type: Moment Curvature

MJV

Merrimack College

3/11/2010

Task 5

300 ft Superstructure - Near Midspan

Page \_\_ of \_\_

### Section Details:

X Centroid: - .8853E-14 in

Y Centroid: 73.89 in

Section Area: 10.86E+3 in<sup>2</sup>

### Loading Details:

Incrementing Loads: Mxx Only

Number of Points: 30

Analysis Strategy: Displacement Control

### Analysis Results:

Failing Material: PreStressI

Failure Strain: 30.00E-3 Tension

Curvature at Initial Load: 3.353E-6 1/in

Curvature at First Yield: 38.83E-6 1/in

Ultimate Curvature: .2439E-3 1/in

Moment at First Yield: 550.9E+3 kip-in

Ultimate Moment: 644.5E+3 kip-in

Centroid Strain at Yield: 1.721E-3 Ten

Centroid Strain at Ultimate: 15.24E-3 Ten

N.A. at First Yield: 44.32 in

N.A. at Ultimate: 62.51 in

Energy per Length: 141.0 kips

Effective Yield Curvature: 44.45E-6 1/in

Effective Yield Moment: 638.2E+3 kip-in

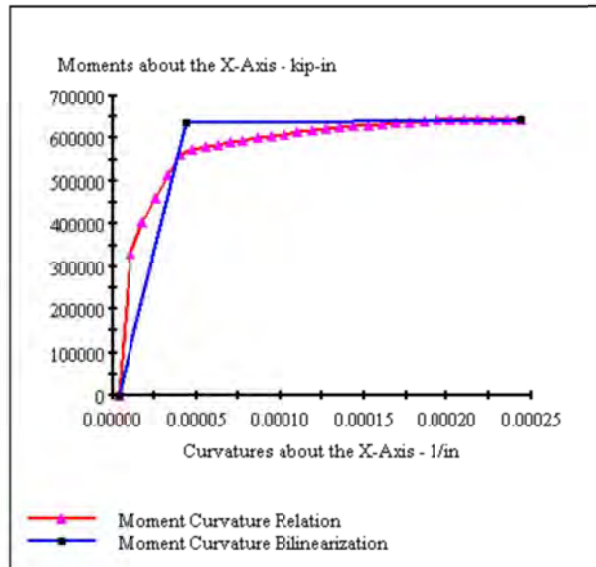
Over Strength Factor: 1.010

EI Effective: 1.55E+10 kip-in<sup>2</sup>

Yield EI Effective: 3.19E+7 kip-in<sup>2</sup>

Bilinear Harding Slope: .2055 %

Curvature Ductility: 5.487



Appendix C - Verification of Proposed Design Approach  
'Ordinary' Bridge

**XTRACT Analysis Report - Educational**

For use only in an academic or research setting.

Section Name: J14 (adj to midspan)

Loading Name: Positive

Analysis Type: Moment Curvature

MJV

Merrimack College

3/11/2010

Task 5

300 ft Superstructure - Near Midspan

Page \_\_ of \_\_

Min. Unconfined Strain (strain)	Max. PreStress1 Strain (strain)	Min. Unconfined Stress (ksi)	Max. PreStress1 Stress (ksi)	Mxx (kip-in)	Kxx (1/in)
-.4380E-3	5.320E-3	-2.204	151.6	0	3.353E-6
-.7137E-3	5.866E-3	-3.582	167.2	329.8E+3	10.79E-6
-.8348E-3	6.566E-3	-4.177	187.1	404.3E+3	18.22E-6
-.9312E-3	7.292E-3	-4.642	207.8	462.0E+3	25.66E-6
-1.017E-3	8.027E-3	-5.048	228.8	514.6E+3	33.09E-6
-1.096E-3	8.770E-3	-5.410	245.5	561.7E+3	40.53E-6
-1.149E-3	9.539E-3	-5.644	247.2	573.4E+3	47.97E-6
-1.196E-3	10.31E-3	-5.847	248.9	579.9E+3	55.40E-6
-1.240E-3	11.09E-3	-6.031	250.6	585.5E+3	62.84E-6
-1.284E-3	11.87E-3	-6.209	252.1	590.9E+3	70.27E-6
-1.326E-3	12.65E-3	-6.375	253.6	595.8E+3	77.71E-6
-1.372E-3	13.52E-3	-6.551	255.2	601.0E+3	86.02E-6
-1.417E-3	14.39E-3	-6.712	256.8	605.7E+3	94.33E-6
-1.461E-3	15.27E-3	-6.861	258.2	610.0E+3	.1026E-3
-1.506E-3	16.14E-3	-7.003	259.6	614.2E+3	.1109E-3
-1.551E-3	17.01E-3	-7.136	260.8	618.0E+3	.1193E-3
-1.596E-3	17.89E-3	-7.259	262.0	621.7E+3	.1276E-3
-1.641E-3	18.76E-3	-7.370	263.1	625.1E+3	.1359E-3
-1.686E-3	19.63E-3	-7.470	264.2	628.2E+3	.1442E-3
-1.732E-3	20.51E-3	-7.559	265.1	631.1E+3	.1525E-3
-1.779E-3	21.38E-3	-7.636	266.0	633.9E+3	.1608E-3
-1.827E-3	22.25E-3	-7.699	266.7	636.3E+3	.1691E-3
-1.874E-3	23.12E-3	-7.746	267.4	638.4E+3	.1774E-3
-1.922E-3	23.99E-3	-7.780	268.0	640.4E+3	.1857E-3
-1.971E-3	24.86E-3	-7.797	268.6	642.0E+3	.1940E-3
-2.026E-3	25.72E-3	-7.733	269.0	643.3E+3	.2023E-3
-2.087E-3	26.58E-3	-7.575	269.4	644.0E+3	.2107E-3
-2.148E-3	27.44E-3	-7.414	269.6	644.5E+3	.2190E-3
-2.211E-3	28.29E-3	-7.251	269.8	644.7E+3	.2273E-3
-2.275E-3	29.15E-3	-7.086	270.0	644.8E+3	.2356E-3
-2.338E-3	30.00E-3	-6.920	270.0	644.5E+3	.2439E-3

Appendix C - Verification of Proposed Design Approach  
'Ordinary' Bridge

## XTRACT Analysis Report - Educational

For use only in an academic or research setting.

Section Name: J14 (adj to midspan)

Loading Name: Negative

Analysis Type: Moment Curvature

MJV

Merrimack College

3/11/2010

Task 5

300 ft Superstructure - Near Midspan

Page \_\_ of \_\_

### Section Details:

X Centroid:  $-8.853 \times 10^{-14}$  in

Y Centroid: 73.89 in

Section Area:  $10.86 \times 10^3$  in<sup>2</sup>

### Loading Details:

Incrementing Loads: Mxx Only

Number of Points: 31

Analysis Strategy: Displacement Control

### Analysis Results:

Failing Material: PreStressI

Failure Strain:  $30.00 \times 10^{-3}$  Tension

Curvature at Initial Load:  $3.353 \times 10^{-6}$  1/in

Curvature at First Yield:  $-32.81 \times 10^{-6}$  1/in

Ultimate Curvature:  $-2.371 \times 10^{-3}$  1/in

Moment at First Yield:  $-1.214 \times 10^6$  kip-in

Ultimate Moment:  $-1.405 \times 10^6$  kip-in

Centroid Strain at Yield:  $.7354 \times 10^{-3}$  Ten

Centroid Strain at Ultimate:  $8.610 \times 10^{-3}$  Ten

N.A. at First Yield: -22.41 in

N.A. at Ultimate: -36.32 in

Energy per Length: 307.1 kips

Effective Yield Curvature:  $38.08 \times 10^{-6}$  1/in

Effective Yield Moment:  $1.392 \times 10^6$  kip-in

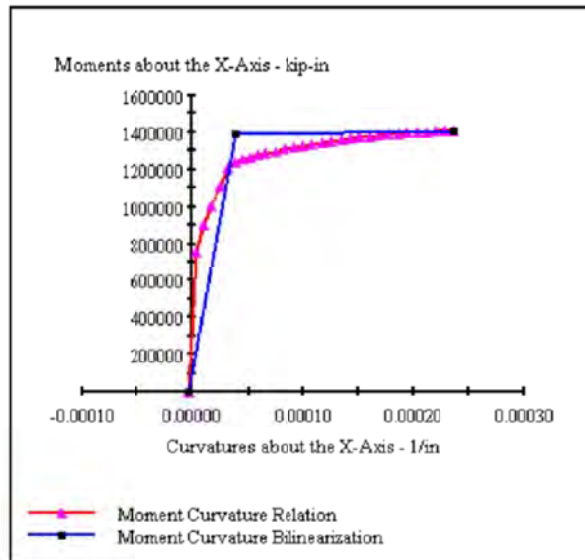
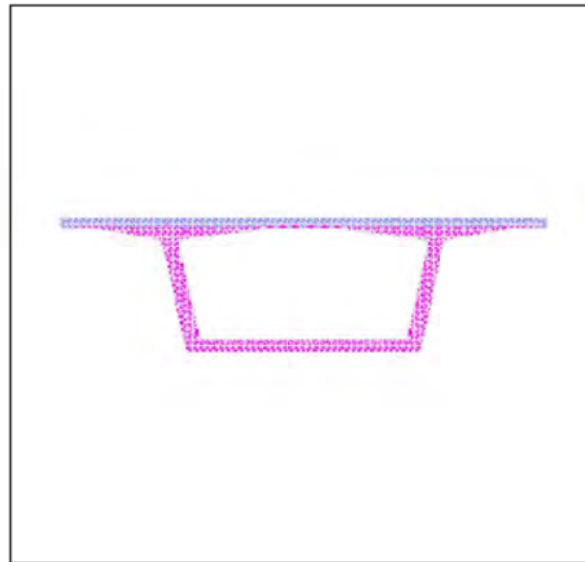
Over Strength Factor: -1.010

EI Effective:  $3.36 \times 10^{10}$  kip-in<sup>2</sup>

Yield EI Effective:  $7.03 \times 10^7$  kip-in<sup>2</sup>

Bilinear Hardening Slope: .2092 %

Curvature Ductility: 6.226



Appendix C - Verification of Proposed Design Approach  
'Ordinary' Bridge

**XTRACT Analysis Report - Educational**

For use only in an academic or research setting.

Section Name: J14 (adj to midspan)

Loading Name: Negative

Analysis Type: Moment Curvature

MJV

Merrimack College

3/11/2010

Task 5

300 ft Superstructure - Near Midspan

Page \_\_ of \_\_

Min. Unconfined Strain (strain)	Max. PreStress1 Strain (strain)	Min. Unconfined Stress (ksi)	Max. PreStress1 Stress (ksi)	Mxx (kip-in)	Kxx (1/in)
-0.4380E-3	5.320E-3	-2.204	151.6	0	3.353E-6
-0.3364E-3	5.744E-3	-1.693	163.7	-756.4E+3	-3.555E-6
-0.4403E-3	6.395E-3	-2.216	182.3	-899.1E+3	-10.46E-6
-0.5194E-3	7.071E-3	-2.613	201.5	-1.004E+6	-17.37E-6
-0.5937E-3	7.752E-3	-2.985	220.9	-1.106E+6	-24.28E-6
-0.6664E-3	8.434E-3	-3.347	240.4	-1.206E+6	-31.18E-6
-0.7173E-3	9.138E-3	-3.600	246.3	-1.241E+6	-38.09E-6
-0.7605E-3	9.850E-3	-3.813	247.9	-1.253E+6	-45.00E-6
-0.8018E-3	10.56E-3	-4.016	249.5	-1.264E+6	-51.91E-6
-0.8414E-3	11.28E-3	-4.209	250.9	-1.275E+6	-58.81E-6
-0.8809E-3	11.99E-3	-4.401	252.4	-1.285E+6	-65.72E-6
-0.9280E-3	12.88E-3	-4.627	254.1	-1.297E+6	-74.29E-6
-0.9718E-3	13.78E-3	-4.835	255.7	-1.308E+6	-82.86E-6
-1.015E-3	14.67E-3	-5.036	257.2	-1.318E+6	-91.42E-6
-1.054E-3	15.57E-3	-5.217	258.7	-1.327E+6	-99.99E-6
-1.091E-3	16.47E-3	-5.386	260.0	-1.336E+6	-1086E-3
-1.128E-3	17.37E-3	-5.549	261.3	-1.344E+6	-1171E-3
-1.164E-3	18.27E-3	-5.709	262.5	-1.352E+6	-1257E-3
-1.200E-3	19.17E-3	-5.866	263.6	-1.359E+6	-1343E-3
-1.237E-3	20.07E-3	-6.019	264.6	-1.365E+6	-1428E-3
-1.273E-3	20.97E-3	-6.167	265.6	-1.371E+6	-1514E-3
-1.310E-3	21.87E-3	-6.312	266.4	-1.377E+6	-1600E-3
-1.346E-3	22.77E-3	-6.452	267.2	-1.382E+6	-1685E-3
-1.382E-3	23.67E-3	-6.586	267.8	-1.387E+6	-1771E-3
-1.418E-3	24.57E-3	-6.714	268.4	-1.391E+6	-1857E-3
-1.454E-3	25.47E-3	-6.837	268.9	-1.395E+6	-1942E-3
-1.489E-3	26.37E-3	-6.950	269.3	-1.399E+6	-2028E-3
-1.520E-3	27.28E-3	-7.045	269.6	-1.401E+6	-2114E-3
-1.549E-3	28.18E-3	-7.132	269.8	-1.403E+6	-2199E-3
-1.578E-3	29.09E-3	-7.211	270.0	-1.405E+6	-2285E-3
-1.606E-3	30.00E-3	-7.285	270.0	-1.405E+6	-2371E-3
-1.606E-3	30.00E-3	-7.285	270.0	-1.405E+6	-2371E-3

Appendix C - Verification of Proposed Design Approach  
'Ordinary' Bridge

### XTRACT Section Report - Educational

For use only in an academic or research setting.

Section Name: J15 (midspan)

MJV

Merrimack College

3/10/2010

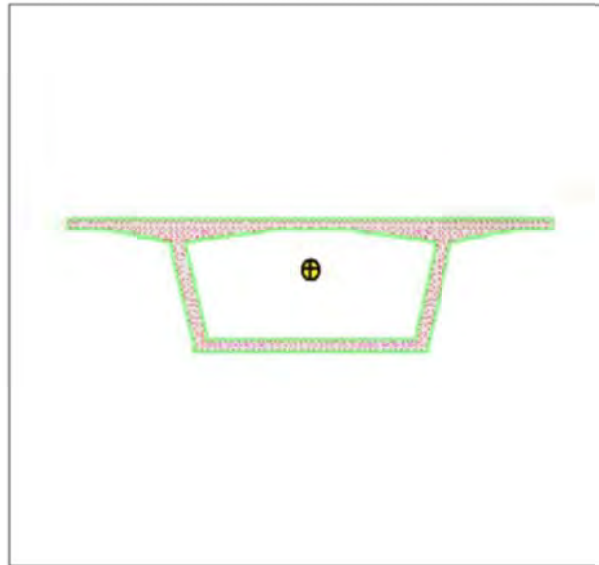
Task 5

300 ft Superstructure - Near Midspan

Page \_\_ of \_\_

#### Section Details:

X Centroid:	.7218E-14 in
Y Centroid:	73.46 in
Section Area:	10.88E+3 in <sup>2</sup>
EI gross about X:	1.16E+11 kip-in <sup>2</sup>
EI gross about Y:	6.34E+11 kip-in <sup>2</sup>
I trans (UnconfinedI) about X:	2.30E+7 in <sup>4</sup>
I trans (UnconfinedI) about Y:	1.26E+8 in <sup>4</sup>
Reinforcing Bar Area:	61.07 in <sup>2</sup>
Percent Longitudinal Steel:	.5615 %
Overall Width:	427.2 in
Overall Height:	118.1 in
Number of Fibers:	801
Number of Bars:	90
Number of Materials:	2



#### Material Types and Names:

Unconfined Concrete:	<input type="checkbox"/> UnconfinedI
Prestressng Steel:	<input checked="" type="checkbox"/> PreStressI

## XTRACT Analysis Report - Educational

For use only in an academic or research setting.

Section Name: J15 (midspan)

Loading Name: Positive

Analysis Type: Moment Curvature

MJV

Merrimack College

3/10/2010

Task 5

300 ft Superstructure - Near Midspan

Page \_\_ of \_\_

### Section Details:

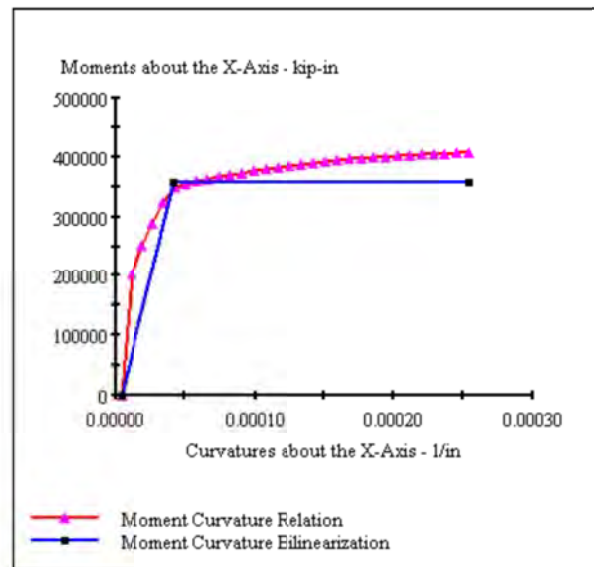
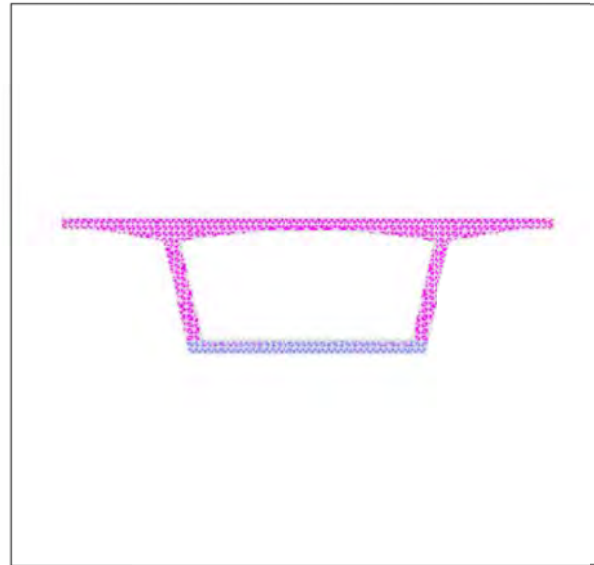
X Centroid: .7218E-14 in  
 Y Centroid: 73.46 in  
 Section Area: 10.88E+3 in<sup>2</sup>

### Loading Details:

Incrementing Loads: Mxx Only  
 Number of Points: 31  
 Analysis Strategy: Displacement Control

### Analysis Results:

Failing Material: PreStress1  
 Failure Strain: 30.00E-3 Tension  
 Curvature at Initial Load: 3.801E-6 1/in  
 Curvature at First Yield: 40.95E-6 1/in  
 Ultimate Curvature: .2547E-3 1/in  
 Moment at First Yield: 342.8E+3 kip-in  
 Ultimate Moment: 406.0E+3 kip-in  
 Centroid Strain at Yield: 1.975E-3 Ten  
 Centroid Strain at Ultimate: 16.19E-3 Ten  
 N.A. at First Yield: 48.23 in  
 N.A. at Ultimate: 63.56 in  
 Energy per Length: 91.66 kips  
 Effective Yield Curvature: 42.56E-6 1/in  
 Effective Yield Moment: 357.7E+3 kip-in  
 Over Strength Factor: 1.135  
 EI Effective: 9.23E+9 kip-in<sup>2</sup>  
 Yield EI Effective: 0 kip-in<sup>2</sup>  
 Bilinear Harding Slope: 0 %  
 Curvature Ductility: 5.984



Appendix C - Verification of Proposed Design Approach

'Ordinary' Bridge

**XTRACT Analysis Report - Educational**

For use only in an academic or research setting.

Section Name: J15 (midspan)

Loading Name: Positive

Analysis Type: Moment Curvature

MJV

Merrimack College

3/10/2010

Task 5

300 ft Superstructure - Near Midspan

Page \_\_ of \_\_

Min. Unconfined Strain (strain)	Max. PreStress1 Strain (strain)	Min. Unconfined Stress (ksi)	Max. PreStress1 Stress (ksi)	Mxx (kip-in)	Kxx (1/in)
-.4455E-3	5.274E-3	-2.242	150.3	0	3.801E-6
-.6577E-3	5.812E-3	-3.304	165.6	202.5E+3	11.62E-6
-.7591E-3	6.533E-3	-3.807	186.2	252.0E+3	19.44E-6
-.8388E-3	7.276E-3	-4.197	207.4	289.3E+3	27.25E-6
-.9096E-3	8.028E-3	-4.539	228.8	323.2E+3	35.07E-6
-.9716E-3	8.788E-3	-4.834	245.5	349.3E+3	42.89E-6
-1.016E-3	9.567E-3	-5.042	247.3	354.1E+3	50.71E-6
-1.059E-3	10.35E-3	-5.241	249.0	358.5E+3	58.52E-6
-1.100E-3	11.13E-3	-5.427	250.6	362.4E+3	66.34E-6
-1.139E-3	11.91E-3	-5.601	252.2	365.8E+3	74.16E-6
-1.178E-3	12.70E-3	-5.770	253.7	369.1E+3	81.98E-6
-1.221E-3	13.56E-3	-5.953	255.3	372.7E+3	90.61E-6
-1.263E-3	14.43E-3	-6.128	256.8	375.9E+3	99.24E-6
-1.305E-3	15.29E-3	-6.294	258.2	379.0E+3	.1079E-3
-1.347E-3	16.16E-3	-6.455	259.6	381.9E+3	.1165E-3
-1.388E-3	17.03E-3	-6.608	260.9	384.6E+3	.1251E-3
-1.429E-3	17.90E-3	-6.751	262.0	387.2E+3	.1338E-3
-1.470E-3	18.76E-3	-6.888	263.1	389.6E+3	.1424E-3
-1.511E-3	19.63E-3	-7.018	264.2	391.8E+3	.1510E-3
-1.552E-3	20.50E-3	-7.140	265.1	393.8E+3	.1597E-3
-1.593E-3	21.37E-3	-7.252	265.9	395.7E+3	.1683E-3
-1.634E-3	22.23E-3	-7.354	266.7	397.5E+3	.1770E-3
-1.676E-3	23.10E-3	-7.448	267.4	399.1E+3	.1856E-3
-1.718E-3	23.97E-3	-7.533	268.0	400.5E+3	.1942E-3
-1.761E-3	24.83E-3	-7.607	268.5	401.8E+3	.2029E-3
-1.804E-3	25.70E-3	-7.671	269.0	402.9E+3	.2115E-3
-1.849E-3	26.56E-3	-7.723	269.4	404.0E+3	.2201E-3
-1.894E-3	27.42E-3	-7.762	269.6	404.8E+3	.2288E-3
-1.940E-3	28.29E-3	-7.788	269.8	405.5E+3	.2374E-3
-1.988E-3	29.15E-3	-7.800	270.0	406.0E+3	.2460E-3
-2.044E-3	30.00E-3	-7.686	270.0	406.0E+3	.2547E-3
-2.044E-3	30.00E-3	-7.686	270.0	406.0E+3	.2547E-3

**XTRACT Analysis Report - Educational**

For use only in an academic or research setting.

Section Name: J15 (midspan)

Loading Name: Negative

Analysis Type: Moment Curvature

MJV

Merrimack College

3/10/2010

Task 5

300 ft Superstructure - Near Midspan

Page \_\_ of \_\_

**Section Details:**

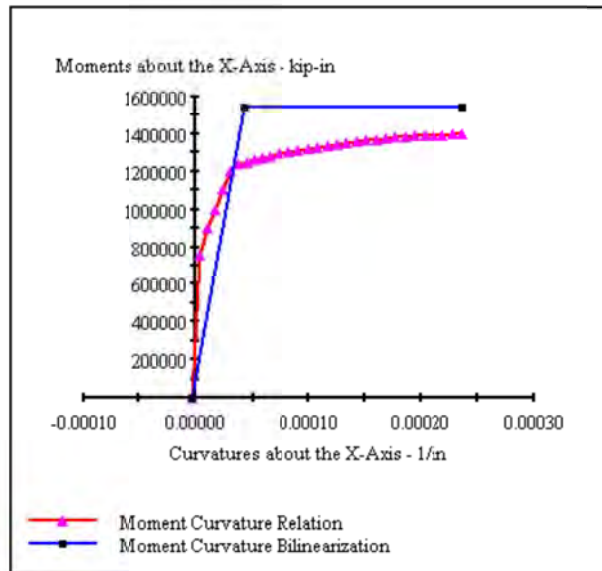
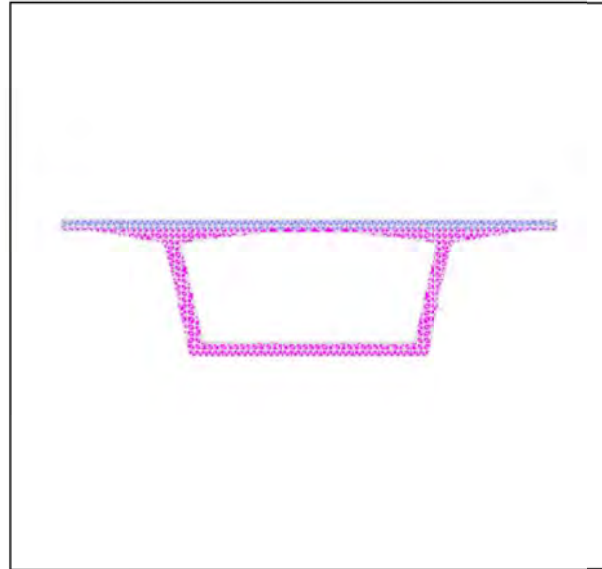
X Centroid: .7218E-14 in  
 Y Centroid: 73.46 in  
 Section Area: 10.88E+3 in<sup>2</sup>

**Loading Details:**

Incrementing Loads: Mxx Only  
 Number of Points: 31  
 Analysis Strategy: Displacement Control

**Analysis Results:**

Failing Material: PreStress1  
 Failure Strain: 30.00E-3 Tension  
 Curvature at Initial Load: 3.801E-6 1/in  
 Curvature at First Yield: -32.51E-6 1/in  
 Ultimate Curvature: -.2373E-3 1/in  
 Moment at First Yield: -1.209E+6 kip-in  
 Ultimate Moment: -1.397E+6 kip-in  
 Centroid Strain at Yield: .7638E-3 Ten  
 Centroid Strain at Ultimate: 8.692E-3 Ten  
 N.A. at First Yield: -23.49 in  
 N.A. at Ultimate: -36.63 in  
 Energy per Length: 306.5 kips  
 Effective Yield Curvature: 42.63E-6 1/in  
 Effective Yield Moment: 1.546E+6 kip-in  
 Over Strength Factor: -.9040  
 EI Effective: 3.33E+10 kip-in<sup>2</sup>  
 Yield EI Effective: 0 kip-in<sup>2</sup>  
 Bilinear Hardening Slope: 0 %  
 Curvature Ductility: 5.567



Appendix C - Verification of Proposed Design Approach

'Ordinary' Bridge

**XTRACT Analysis Report - Educational**

For use only in an academic or research setting.

Section Name: J15 (midspan)

Loading Name: Negative

Analysis Type: Moment Curvature

MJV

Merrimack College

3/10/2010

Task 5

300 ft Superstructure - Near Midspan

Page \_\_ of \_\_

Min. Unconfined Strain (strain)	Max. PreStress1 Strain (strain)	Min. Unconfined Stress (ksi)	Max. PreStress1 Stress (ksi)	Mxx (kip-in)	Kxx (1/in)
-4.455E-3	5.274E-3	-2.242	150.3	0	3.801E-6
-2.964E-3	5.738E-3	-1.492	163.5	-757.9E+3	-3.093E-6
-3.986E-3	6.386E-3	-2.006	182.0	-896.8E+3	-9.987E-6
-4.764E-3	7.058E-3	-2.397	201.2	-999.7E+3	-16.88E-6
-5.499E-3	7.735E-3	-2.766	220.4	-1.100E+6	-23.77E-6
-6.219E-3	8.413E-3	-3.126	239.8	-1.199E+6	-30.67E-6
-6.733E-3	9.112E-3	-3.382	246.3	-1.236E+6	-37.56E-6
-7.155E-3	9.820E-3	-3.591	247.9	-1.247E+6	-44.46E-6
-7.561E-3	10.53E-3	-3.792	249.4	-1.259E+6	-51.35E-6
-7.963E-3	11.24E-3	-3.989	250.9	-1.269E+6	-58.24E-6
-8.340E-3	11.95E-3	-4.173	252.3	-1.279E+6	-65.14E-6
-8.789E-3	12.84E-3	-4.392	254.0	-1.291E+6	-73.75E-6
-9.211E-3	13.74E-3	-4.594	255.6	-1.301E+6	-82.36E-6
-9.597E-3	14.64E-3	-4.778	257.2	-1.311E+6	-90.96E-6
-9.974E-3	15.54E-3	-4.956	258.6	-1.320E+6	-99.57E-6
-1.035E-3	16.44E-3	-5.130	260.0	-1.328E+6	-1082E-3
-1.072E-3	17.33E-3	-5.301	261.3	-1.337E+6	-1168E-3
-1.110E-3	18.23E-3	-5.470	262.5	-1.344E+6	-1254E-3
-1.147E-3	19.13E-3	-5.636	263.6	-1.351E+6	-1340E-3
-1.184E-3	20.03E-3	-5.798	264.6	-1.358E+6	-1426E-3
-1.222E-3	20.93E-3	-5.955	265.5	-1.365E+6	-1512E-3
-1.258E-3	21.83E-3	-6.108	266.4	-1.370E+6	-1598E-3
-1.293E-3	22.74E-3	-6.246	267.1	-1.376E+6	-1684E-3
-1.324E-3	23.64E-3	-6.369	267.8	-1.380E+6	-1771E-3
-1.355E-3	24.55E-3	-6.486	268.4	-1.384E+6	-1857E-3
-1.384E-3	25.45E-3	-6.595	268.9	-1.388E+6	-1943E-3
-1.413E-3	26.36E-3	-6.697	269.3	-1.390E+6	-2029E-3
-1.441E-3	27.27E-3	-6.793	269.6	-1.393E+6	-2115E-3
-1.468E-3	28.18E-3	-6.884	269.8	-1.395E+6	-2201E-3
-1.496E-3	29.09E-3	-6.972	270.0	-1.396E+6	-2287E-3
-1.523E-3	30.00E-3	-7.055	270.0	-1.397E+6	-2373E-3
-1.523E-3	30.00E-3	-7.055	270.0	-1.397E+6	-2373E-3

### Nominal Moment Capacity

Segment Joint	Positive Bending		Negative Bending	
	k-in	k-ft	k-in	k-ft
J1 (adj to Pier)	344,000	28,667	-4,290,000	-357,500
J2	327,000	27,250	-3,770,000	-314,167
J14	1,050,000	87,500	-468,000	-39,000
J15 (midspan)	1,050,000	87,500	-293,000	-24,417

Defined as the moment at which the stress in the PT is 210ksi

### Ultimate Moment Capacity

Segment Joint	Positive Bending		Negative Bending	
	k-in	k-ft	k-in	k-ft
J1 (adj to Pier)	477,000	39,750	-5,450,000	-454,167
J2	453,000	37,750	-4,820,000	-401,667
J14	1,410,000	117,500	-645,000	-53,750
J15 (midspan)	1,400,000	116,667	-406,000	-33,833

Note: The bending sign convention in XTRACT is not standard. The above table summarized the XTRACT results and changed to sign of the bending moments to the general standard, i.e. positive bending produces compression in the top flange.

### 3.3 Superstructure Vertical Collapse Mechanism

Several possible vertical collapse mechanisms are possible and were considered. The calculations below represent the critical mechanisms for end and interior spans.

#### End Spans

$$Li := 1203\text{-in} \qquad Lend := 2004\text{-in} \qquad Wend := 2047\text{-kip}$$

$$Mi\_pos := M\_J15\_pos \qquad Mpier\_neg := M\_J1\_neg$$

$$wend := \frac{8 \cdot \left( Mi\_pos + |M_{pier\_neg}| \cdot \frac{Li}{Lend} \right)}{4 \cdot Lend \cdot Li - 4 \cdot Li^2} \qquad wend = 9.696 \frac{\text{kip}}{\text{in}}$$

$$Sc\_end := \frac{wend}{\frac{Wend}{Lend}} - 1 \qquad Sc\_end = 8.492 \quad \text{in units of } g$$

#### Interior Spans

$$Lint := 3349\text{-in} \qquad Wint := 3507\text{-kip}$$

$$M\_pos := M\_J15\_pos \qquad M\_neg := M\_J1\_neg$$

$$wint := \frac{8 \cdot (M\_pos + |M\_neg|)}{Lint^2} \qquad wint = 4.885 \frac{\text{kip}}{\text{in}}$$

$$Sc\_int := \frac{wint}{\frac{Wint}{Lint}} - 1 \qquad Sc\_int = 3.666 \quad \text{in units of } g$$

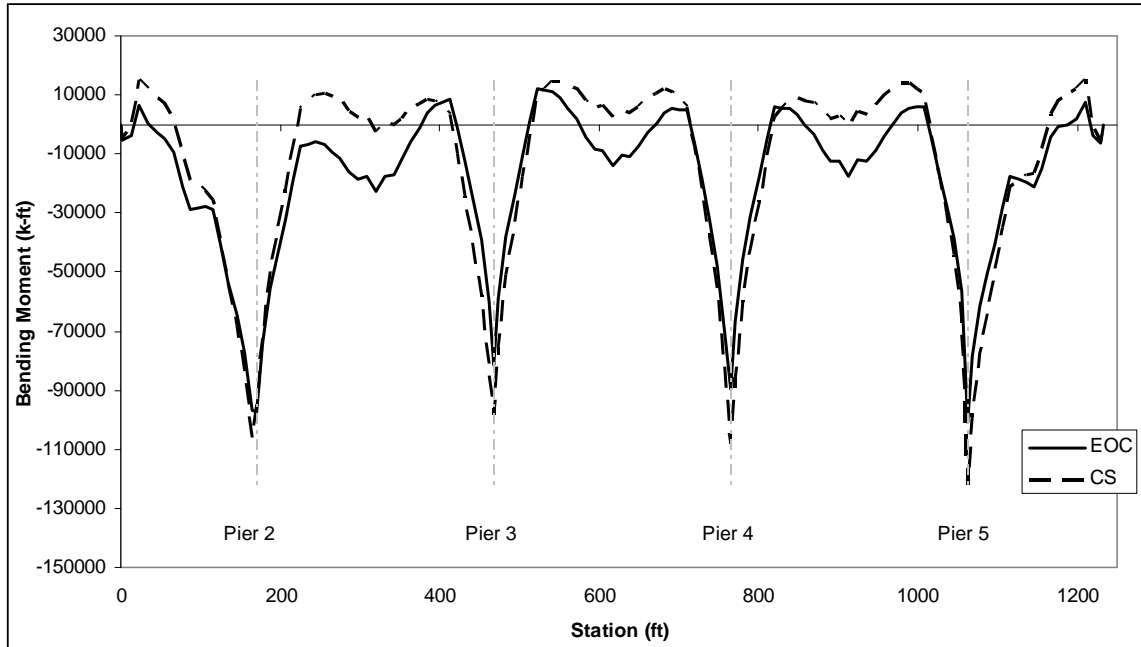
#### Superstructure Vertical Collapse Mechanism Capacity

$$Sc := \min(Sc\_end, Sc\_int) \qquad Sc = 3.666$$

A vertical collapse mechanism in the superstructure will develop if the bridge is subjected to a vertical acceleration of approximately 3.67g

#### 4. Longitudinal Construction Staging Analysis

A full longitudinal construction staging analysis (LCSA) was performed. The details of this analysis are not the focus of this report. Thus the end results are simply presented for simplicity. The dead load bending moment diagram at the end of construction (EOC) and after considering creep and shrinkage (CS) losses are shown below and includes the effects of the PT on the bridge.

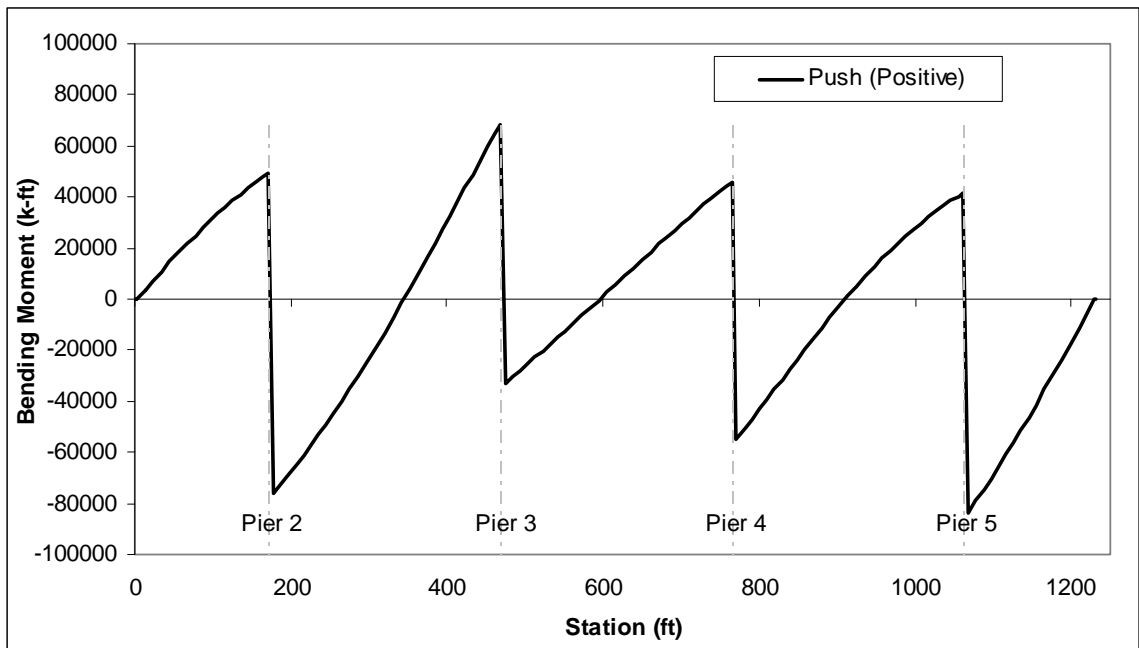


## 5. Longitudinal Push-Over Analysis

The finite element model was developed using SAP2000 Version 14 with linear elastic members representing the superstructure. Potential nonlinear response at the top and bottom of the piers was modeled using nonlinear Link elements. The pier hinging properties utilized a Takeda multi-linear plastic hysteretic model. For simplicity, it was assumed that the abutments will not be engaged during a longitudinal earthquake. This may not be the case in all structures and the need to include the effects of the abutments in a longitudinal push-over analysis should be considered.

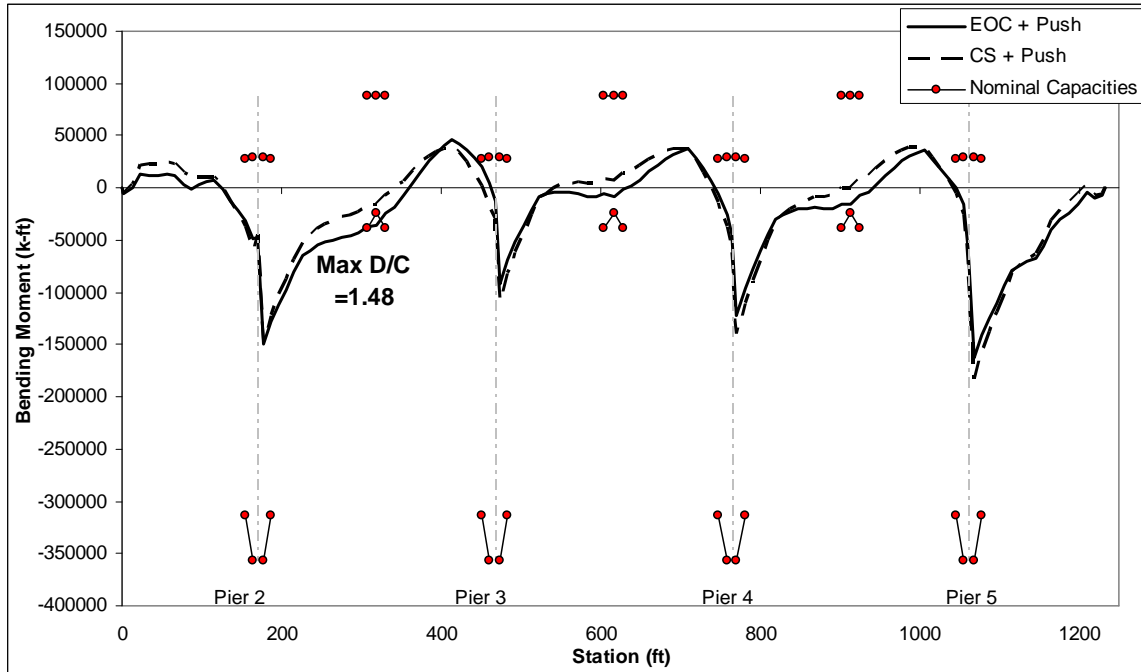
### **Positive Push Direction**

The superstructure moments from a push-over in the positive direction are shown below. This moment diagram does not include dead load moments.



The superstructure moments from the longitudinal push above were added to the EOC and CS superstructure moments from the LCSA. The resulting bending moment diagrams are shown below and compared with the nominal moment capacities of the superstructure.

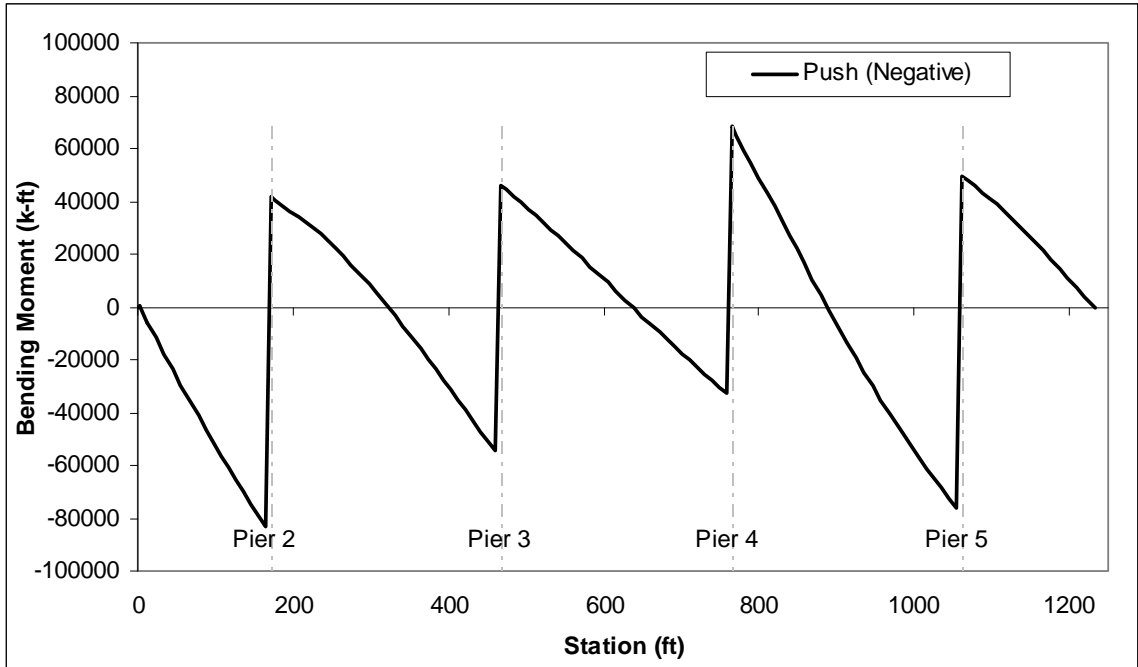
Appendix C - Verification of Proposed Design Approach  
'Ordinary' Bridge



The midspan joint of span 2 exceeds the nominal moment capacity in negative bending with end of construction stress state. This means that the tendons in the top flange of the midspan section will exceed 210 ksi.

**Negative Push Direction**

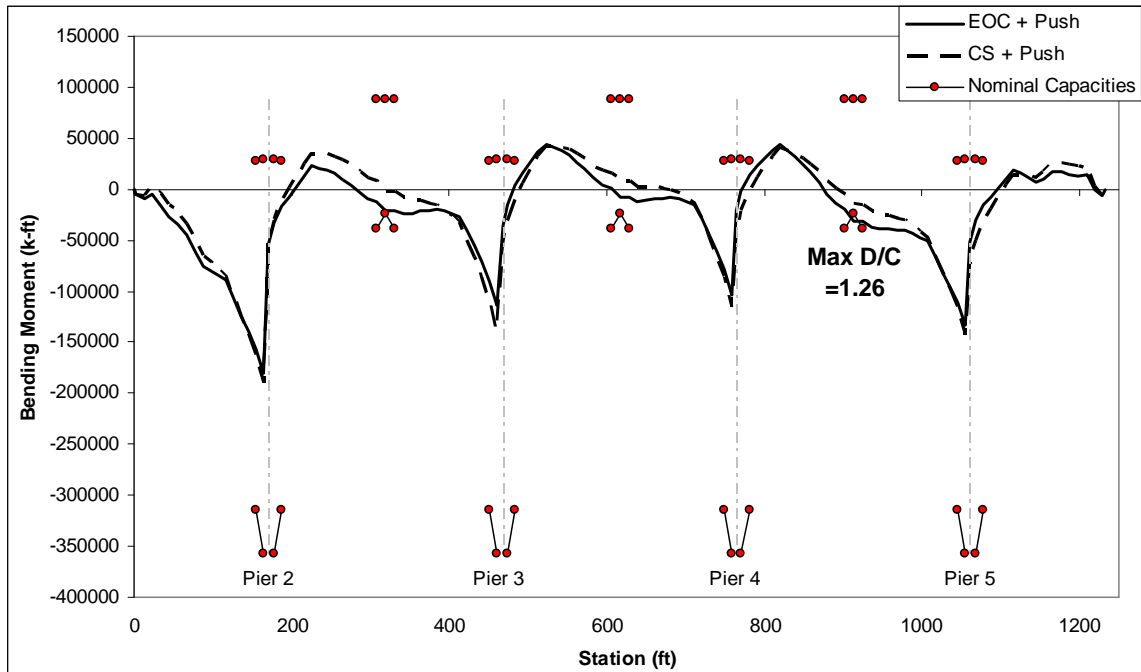
The superstructure moments from a push-over in the negative direction are shown below. This moment diagram does not included dead load moments.



The superstructure moments from the longitudinal push above were added to the EOC and CS superstructure moments from the LCSA. The resulting bending moment diagrams are shown below and compared with the nominal moment capacities of the superstructure.

## Appendix C - Verification of Proposed Design Approach

### 'Ordinary' Bridge



The midspan joint of span 2 exceeds the nominal moment capacity in negative bending with end of construction stress state. This means that the tendons in the top flange of the midspan section will exceed 210 ksi.

### ***Pushover Conclusions***

The midspan joints of spans 2 and 3 exceed the nominal moment capacity in negative bending with end of construction stress state. This means that the stresses in the top flange tendons at midspan will exceed 210 ksi. This is opposite the direction of gravity and will likely not cause collapse. Strictly speaking, however, it does not satisfy the proposed guidelines and the negative bending capacity should be increased. The joints adjacent to midspan experience similar demands and show D/C ratios of up to 0.95, thus the capacity of the midspan joints should be increased to match the capacity of the segment joints adjacent to midspan.

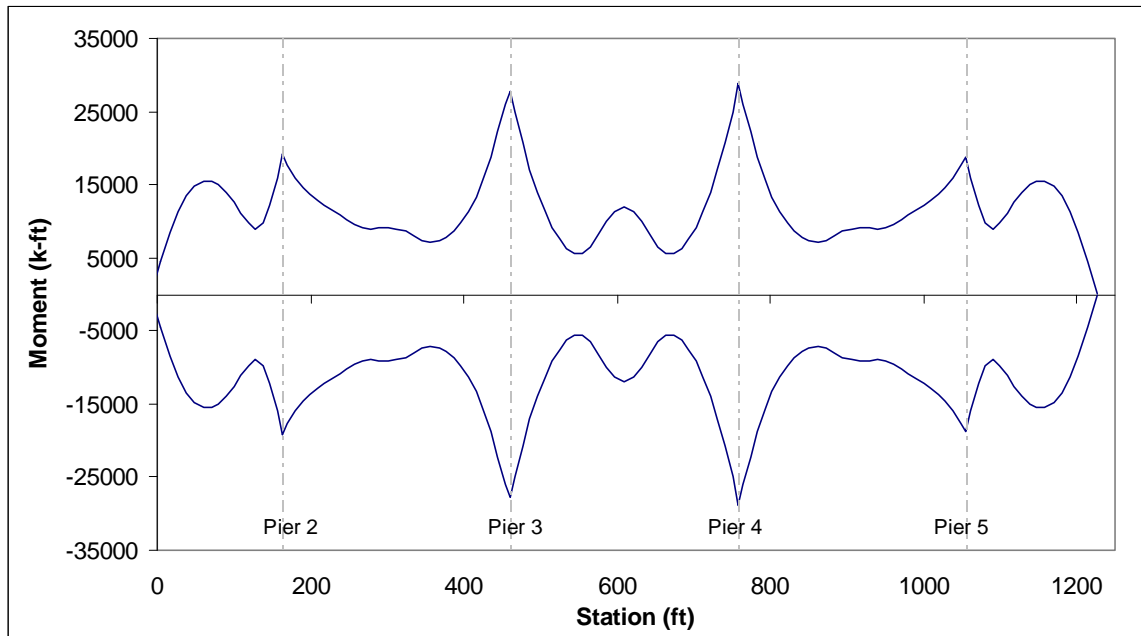
## **6. Horizontal Seismic Demands and Load Combinations**

Combine the horizontal earthquake demands based on the requirement of Section 2.1.2 of the Caltrans SDC. These requirements are appropriate for segmental bridges, thus special considerations are not provided herein.

## 7. Vertical Seismic Demands

### ***FEE (Modal Analysis)***

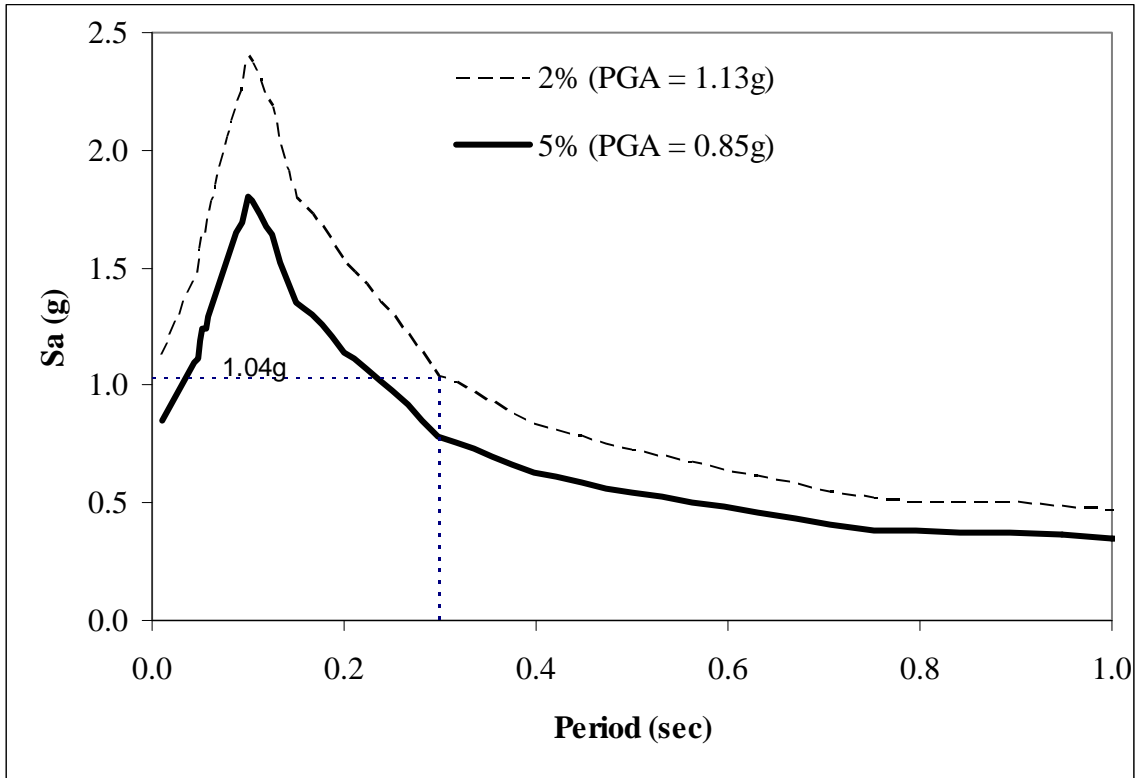
A finite element model was developed using the program SAP2000. This is the same model used for the longitudinal push-over analysis. A modal analysis was performed in the vertical (i.e. Z-direction) using 2% damping in the load case definition and vertical design spectrum based on 2% damping. The CQC modal combination method was used with 200 modes that captured 99% of the vertical mass in the superstructure. The moment diagram that resulted from this modal analysis is shown below. This diagram does not include dead load moments and mirror the horizontal axis to reflect the fact that the seismic motion can be either upward or downward.



### ***SEE (Collapse Mechanism)***

The vertical seismic demand,  $D_{vert}$ , for the collapse mechanism check is based on the maximum of the peak vertical ground acceleration,  $PGA_v$ , or the spectral acceleration of the dominant vertical superstructure mode. The superstructure contains two dominant modes: one at 0.30 seconds; the second at 0.50 seconds. Each mode captured approximately 20% of the superstructure mass. To obtain a conservative demand estimate, the dominant mode with the lowest period was used and compared with  $PGA_v$ .

Appendix C - Verification of Proposed Design Approach  
'Ordinary' Bridge

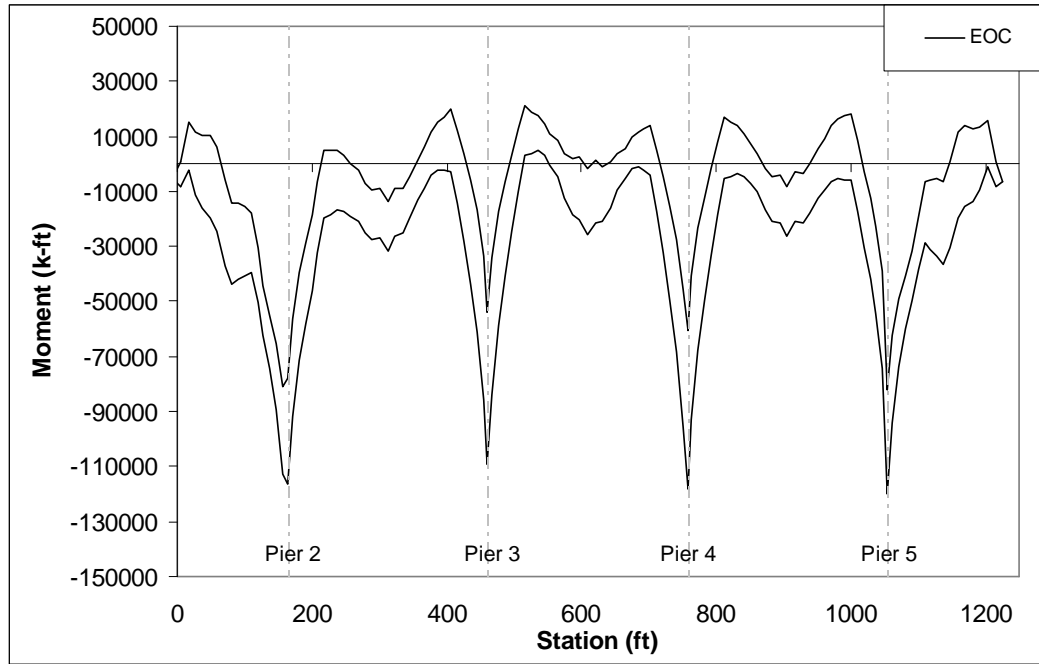


$$D_{\text{vert}} = \max(1.13, 1.04) = 1.13\text{g}.$$

## 8. Vertical Earthquake Load Combinations

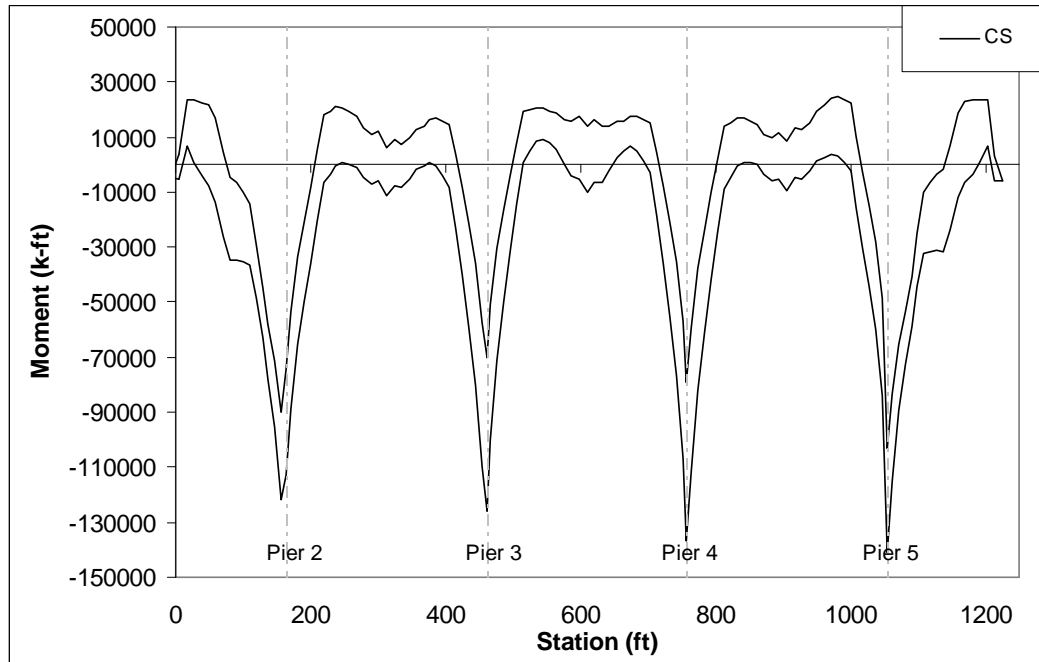
The superstructure moment demands obtained from the vertical modal demands were added to and subtracted from the EOC and CS superstructure moments. The resulting bending moment diagrams are shown below and represent both upward and downward vertical seismic demands.

### ***FEE - EOC***



Appendix C - Verification of Proposed Design Approach  
'Ordinary' Bridge

**FEE - CS**



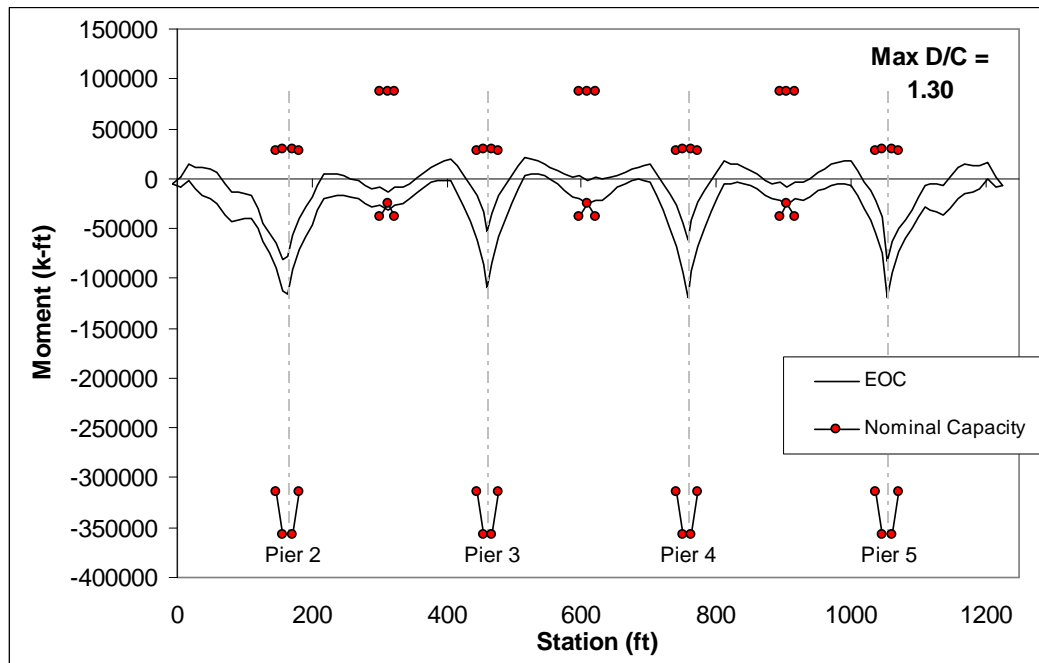
**SEE**

The vertical collapse mechanism is not strongly influenced by pre-earthquake stress states, thus no combinations are necessary for the safety evaluation of 'Ordinary' bridges.

## 9. Vertical Demand/Capacity Ratios

### FEE – EOC

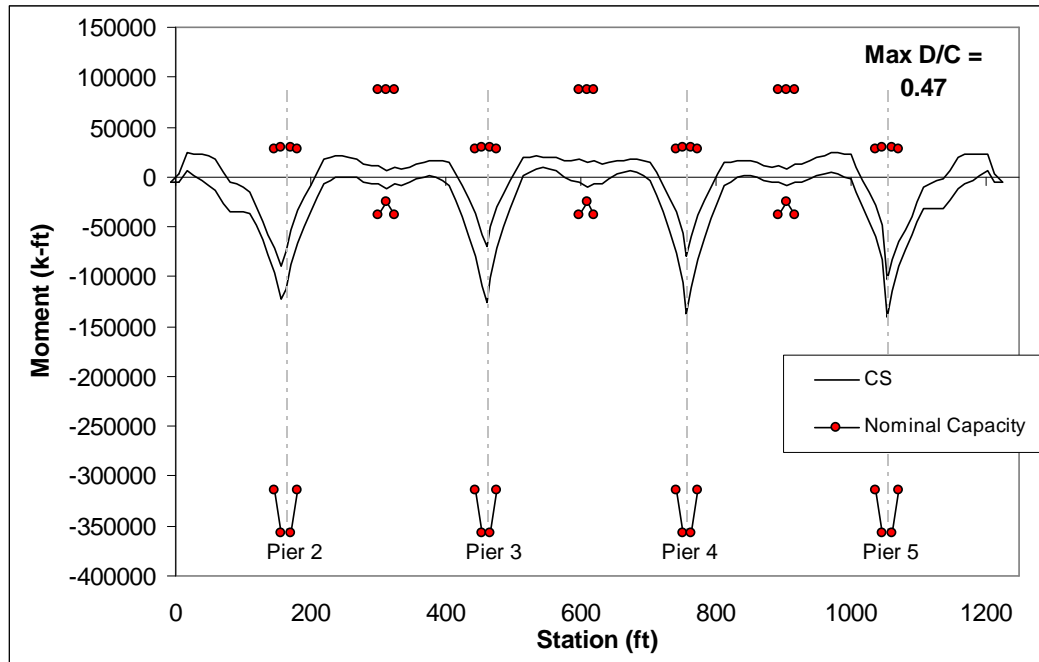
The vertical FEE superstructure bending moment demands based on EOC stress state are compared with the nominal bending moment capacities.



The midspan joint of spans 2, 3 and 4 exceed the nominal moment capacity in negative bending with end of construction stress state by up to 30%. Thus, the tendons in the top flange of the midspan section will exceed 210 ksi.

**FEE – CS**

The vertical FEE superstructure bending moment demands based on CS stress state are compared with the nominal bending moment capacities.



All superstructure moment demands based on CS stress state are less than nominal capacities.

**SEE**

Vertical collapse mechanisms capacity  $S_c = 3.66g$   
 Vertical earthquake demands  $D_v = 1.13g$

Demand/Capacity ratio  $D/C = 1.13g/3.66g = 0.31$   
 → OK

**Conclusions**

The negative bending capacity of the midspan segment joint should be increased to satisfy the FEE vertical seismic demands based on EOC stresses. This conclusion is consistent with results from the longitudinal push-over analysis.

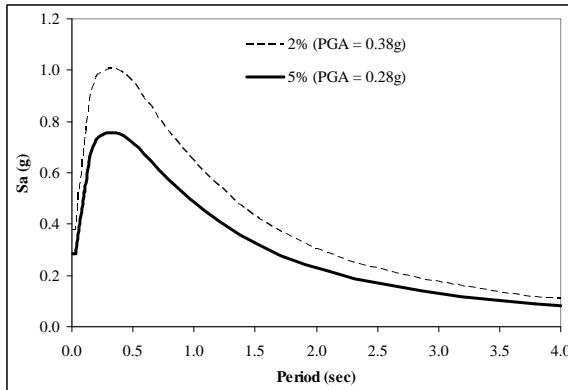
The SEE requirements are satisfied.

# 'Important' Bridge Sample Design Calculations

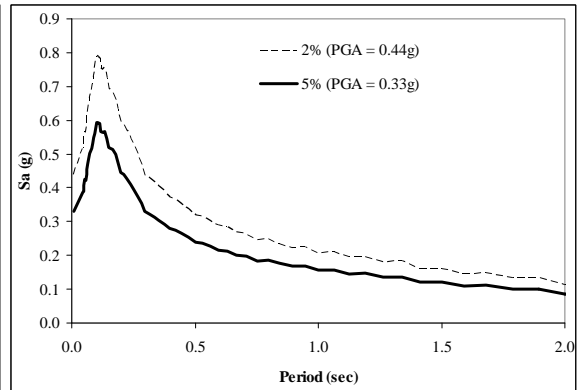
## 1. Seismic Design Spectra and Ground Motions

### 1.1 Design Spectra

#### Horizontal FEE Design Spectra

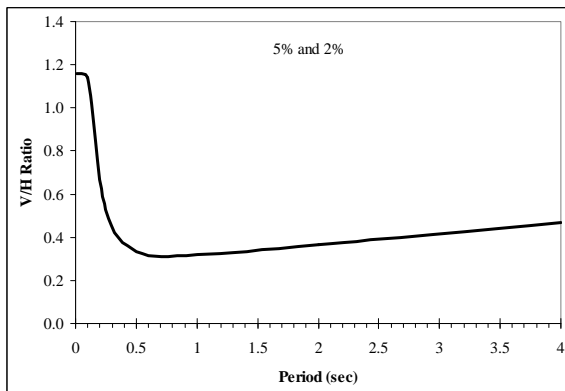


#### Vertical FEE Design Spectra



The vertical peak ground acceleration,  $PGA_v$ , is less than the peak spectral acceleration → OK

#### FEE V/H Spectral Ratio



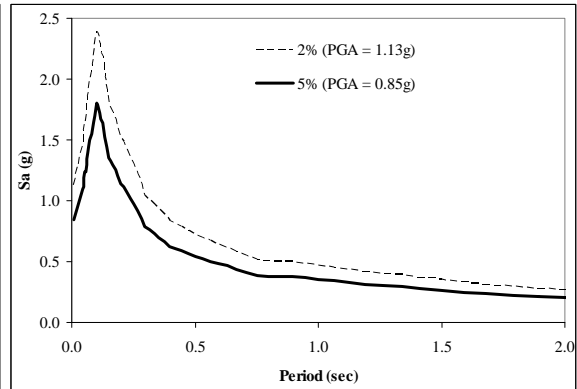
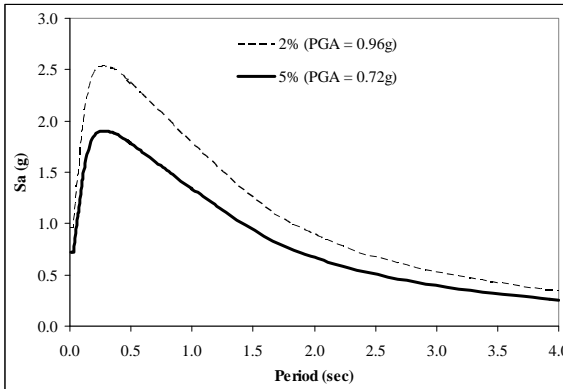
The vertical to horizontal spectral ratio is not equal to  $2/3$  for all periods → OK

Appendix C - Verification of Proposed Design Approach

'Important' Bridge

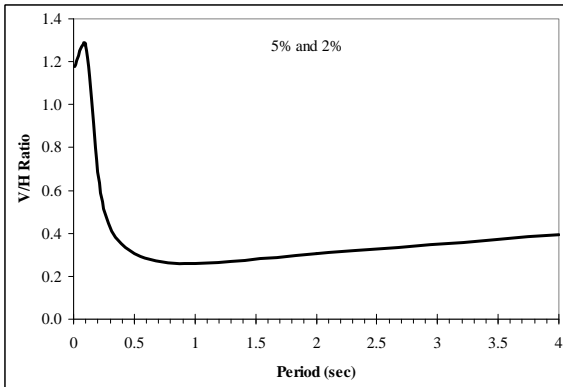
**Horizontal SEE Design Spectra**

**Vertical SEE Design Spectra**



The vertical peak ground acceleration,  $PGA_v$ , is less than the peak spectral acceleration → OK

**SEE V/H Spectral Ratio**



The vertical to horizontal spectral ratio is not equal to 2/3 for all periods → OK

**1.2 Time History Ground Motions**

Three spectrum compatible ground motions sets were obtained for the FEE and SEE design levels. The source ground motions for these spectrum compatible motions are indicated below.

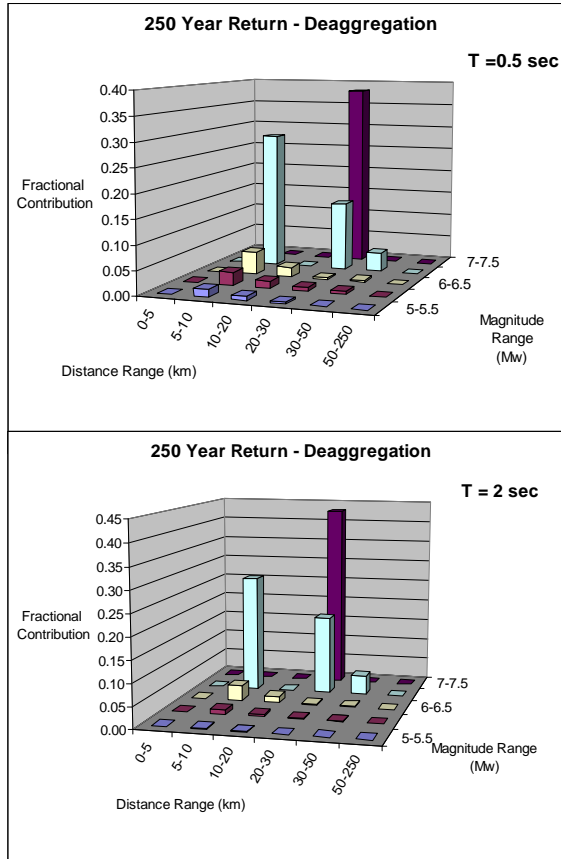
**FEE**

	<b>Earthquake</b>	<b>Station</b>	<b>Year</b>	<b>Mw</b>	<b>Closest Distance to Rupture Surface (km)</b>
1	Northridge	Sylmar	1994	6.7	6.40
2	Landers	Dessert Hot Spring	1992	7.3	21.8
3	Cape Mendocino	Shelter Cove Airport	1992	7.0	28.8

The deaggregation of the FEE hazard, shown below, indicates that a magnitude 7.0-7.5 event that is 20-30 km from the site contributes the most the hazard at the dominant periods (i.e. 0.66 and 2 seconds). The second most important event to the hazard is a magnitude 6.5-7.0 that is 5-10 km from the site. The source motions used match the deaggregation of the FEE hazard.

Appendix C - Verification of Proposed Design Approach

'Important' Bridge



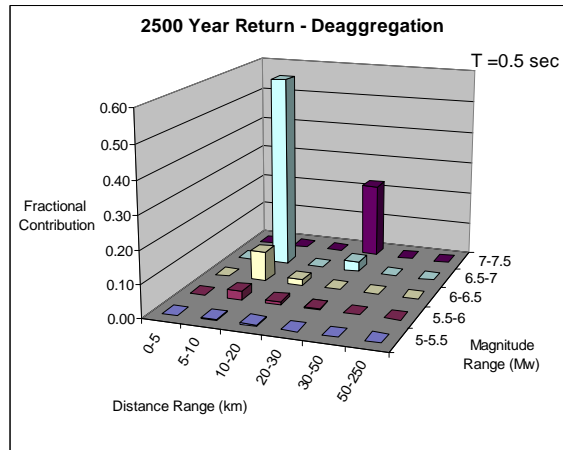
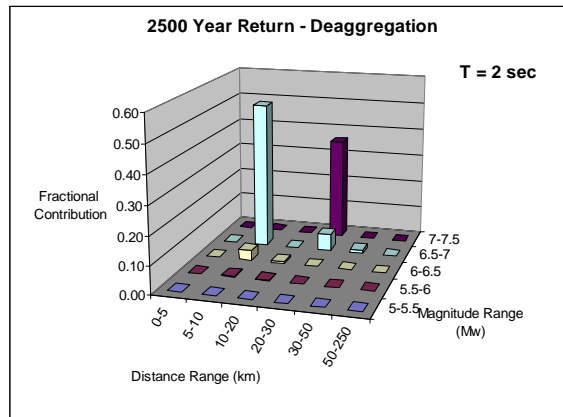
SEE

	Earthquake	Station	Year	Mw	Closest Distance to Rupture Surface (km)
1	Northridge	Sylmar	1994	6.7	6.40
2	Loma Prieta	Saratoga Aloha Ave	1989	7.0	8.30
3	Landers	Dessert Hot Spring	1992	7.3	21.8

Appendix C - Verification of Proposed Design Approach

'Important' Bridge

The deaggregation of the SEE hazard, shown below, indicates that a magnitude 6.5-7.0 event that is 5-10 km from the site contributes the most the hazard at the dominant periods (i.e. 0.66 and 2 seconds). The second most important event to the hazard is a magnitude 7.0-7.5 that is 20-30 km from the site. The source motions used match the deaggregation of the SEE hazard.



## 2. Design for Construction and Service Loads

### 2.1 Ensure that the superstructure top and bottom flange thicknesses are large enough to support the large compression forces experienced when the segment joints open.

$f_{ce} := 1.3 \cdot 8.0 \text{ksi}$	$f_{ce} = 10.4 \text{ksi}$	Expected concrete compressive strength
$F_y := 245 \text{ksi}$		Yield stress of PT
$F_{pt} := .55 \cdot 270 \text{ksi}$	$F_{pt} = 148.5 \text{ksi}$	Expected stress of PT after seating
$A_{strand} := .217 \text{in}^2$		Area of single PT strand

#### Segment Joint Adjacent to Pier

$b_{tf} := 987 \text{in}$	$b_{tf} = 82.25 \text{-ft}$	Width of top flange
$t_{tf} := 11.81 \text{in}$	$t_{tf} = 11.81 \text{-in}$	Average thickness of top flange
$A_{tf} := b_{tf} \cdot t_{tf}$	$A_{tf} = 80.948 \text{-ft}^2$	Top flange area
$b_{bf} := 335 \text{in}$	$b_{bf} = 27.917 \text{-ft}$	Width of bottom flange
$t_{bf} := 43.4 \text{in}$	$t_{bf} = 43.4 \text{-in}$	Thickness of bottom flange
$A_{bf} := b_{bf} \cdot t_{bf}$	$A_{bf} = 100.965 \text{-ft}^2$	Bottom flange area
$n_t := 1894$		Number of TOP strands
$A_{pt\_top} := n_t \cdot A_{strand}$		TOP tendon area
	$A_{pt\_top} = 410.998 \text{-in}^2$	
$n_b := 288$		Number of BOTTOM strands
$A_{pt\_bot} := n_b \cdot A_{strand}$		BOTTOM tendon area
	$A_{pt\_bot} = 62.496 \text{-in}^2$	
$n_c := 400$		Number of CONTINUITY strands
$A_{pt\_cont} := n_c \cdot A_{strand}$		CONTINUITY tendon area
	$A_{pt\_cont} = 86.8 \text{-in}^2$	

#### Positive Bending (i.e. tension on bottom, compression on top)

$T_{demand} := (A_{pt\_top} + A_{pt\_cont}) \cdot F_{pt} + A_{pt\_bot} \cdot F_y$		Under positive bending the bottom tendons will yield while the top and continuity tendons will likely not exceed their stress after seating.
$T_{demand} = 8.923 \times 10^4 \text{kip}$		
$C_{capacity} := 0.85 \cdot f_{ce} \cdot A_{tf}$		
$C_{capacity} = 1.03 \times 10^5 \text{kip}$		
$DC := \frac{T_{demand}}{C_{capacity}}$	$DC = 0.866$	$D/C < 1.0 \quad \implies \text{OK}$

#### Negative Bending (i.e. tension on top, compression on bottom)

$T_{demand} := (A_{pt\_top} + A_{pt\_cont}) \cdot F_y + A_{pt\_bot} \cdot F_{pt}$		Under negative bending the top and continuity tendons will yield while the bottom tendons will likely not exceed their stress after seating.
$T_{demand} = 1.312 \times 10^5 \text{kip}$		
$C_{capacity} := 0.85 \cdot f_{ce} \cdot A_{bf}$		
$C_{capacity} = 1.285 \times 10^5 \text{kip}$		
$DC := \frac{T_{demand}}{C_{capacity}}$	$DC = 1.021$	$D/C \sim 1.0 \quad \implies \text{Say, OK}$

Appendix C - Verification of Proposed Design Approach  
'Important' Bridge

Segment Joint at Midspan

$b_{tf} := 987\text{in}$	$b_{tf} = 82.25\text{-ft}$	Width of top flange
$t_{tf} := 11.81\text{in}$	$t_{tf} = 11.81\text{-in}$	Average thickness of top flange
$A_{tf} := b_{tf} \cdot t_{tf}$	$A_{tf} = 80.948\text{-ft}^2$	Top flange area
$b_{bf} := 335\text{in}$	$b_{bf} = 27.917\text{-ft}$	Width of bottom flange
$t_{bf} := 16.5\text{in}$	$t_{bf} = 16.5\text{-in}$	Thickness of bottom flange
$A_{bf} := b_{bf} \cdot t_{bf}$	$A_{bf} = 38.385\text{-ft}^2$	Bottom flange area
$n_t := 304$		Number of TOP strands
$A_{pt\_top} := n_t \cdot A_{strand}$		TOP tendon area
	$A_{pt\_top} = 65.968\text{-in}^2$	
$n_b := 354$		Number of BOTTOM strands
$A_{pt\_bot} := n_b \cdot A_{strand}$		BOTTOM tendon area
	$A_{pt\_bot} = 76.818\text{-in}^2$	
$n_c := 400$		Number of CONTINUITY strands
$A_{pt\_cont} := n_c \cdot A_{strand}$		CONTINUITY tendon area
	$A_{pt\_cont} = 86.8\text{-in}^2$	

Positive Bending (i.e. tension on bottom, compression on top)

$T_{demand} := (A_{pt\_top} + A_{pt\_cont}) \cdot F_{pt} + A_{pt\_bot} \cdot F_y$		Under positive bending the bottom tendons will yield while the top and continuity tendons will likely not exceed their stress after seating.
$T_{demand} = 4.151 \times 10^4 \cdot \text{kip}$		
$C_{capacity} := 0.85 \cdot f_{ce} \cdot A_{tf}$		
$C_{capacity} = 1.03 \times 10^5 \cdot \text{kip}$		
$DC := \frac{T_{demand}}{C_{capacity}}$	$DC = 0.403$	$D/C < 1.0 \quad \Rightarrow \text{OK}$

Negative Bending (i.e. tension on top, compression on bottom)

$T_{demand} := (A_{pt\_top} + A_{pt\_cont}) \cdot F_y + A_{pt\_bot} \cdot F_{pt}$		Under negative bending the top and continuity tendons will yield while the bottom tendons will likely not exceed their stress after seating.
$T_{demand} = 4.884 \times 10^4 \cdot \text{kip}$		
$C_{capacity} := 0.85 \cdot f_{ce} \cdot A_{bf}$		
$C_{capacity} = 4.886 \times 10^4 \cdot \text{kip}$		
$DC := \frac{T_{demand}}{C_{capacity}}$	$DC = 0.999$	$D/C \sim 1.0 \quad \Rightarrow \text{OK}$

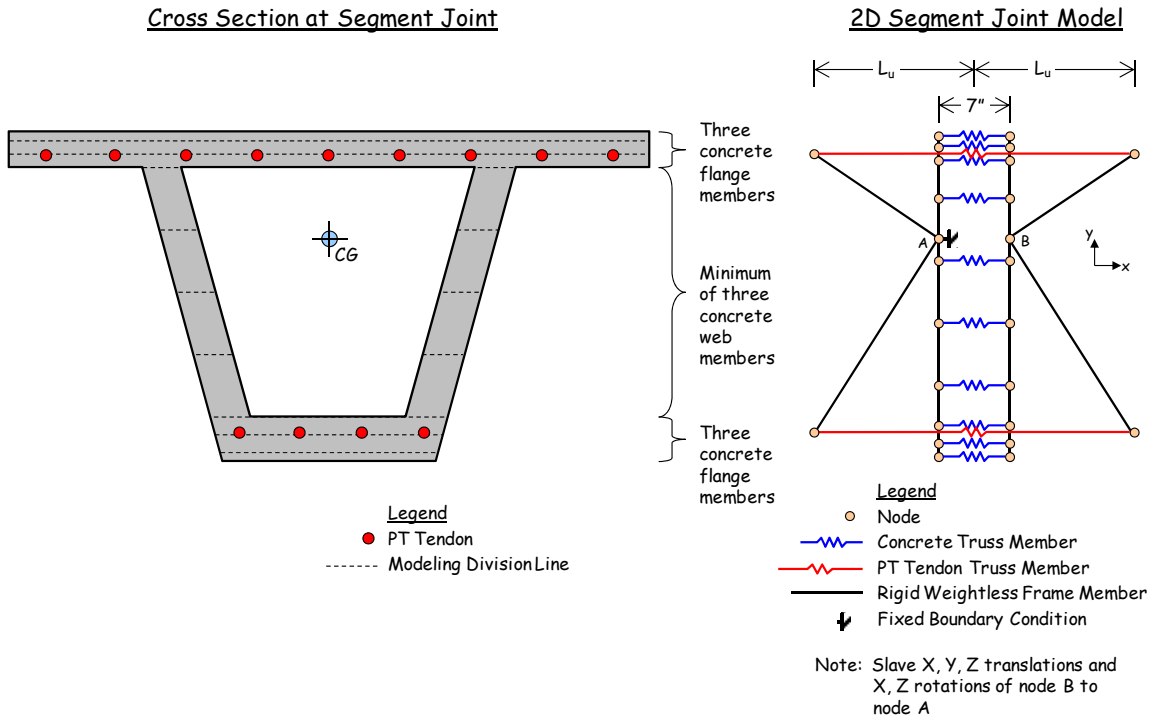
### 3. Column and Superstructure Capacities

#### 3.1 Column Capacities (Moment Curvature Analysis)

Calculate the capacities of potential column plastic hinge regions using moment-curvature analysis as described in Section 3.3 of the Caltrans Seismic Design Criteria. This is standard practice in the industry, thus sample calculations are not shown herein.

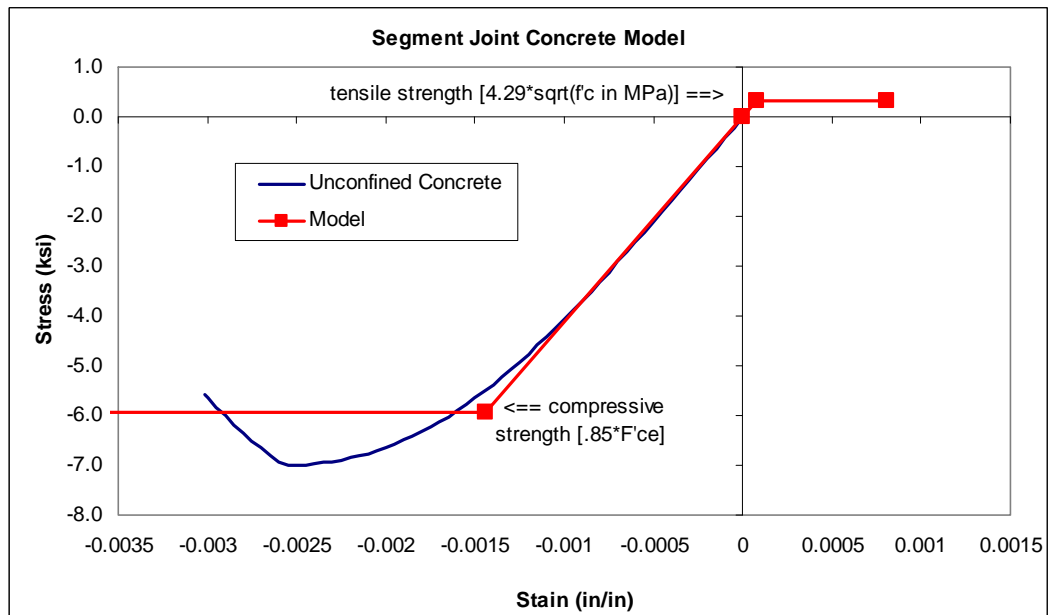
#### 3.2 Superstructure Joint Capacities

A detailed local nonlinear finite element model was created of each segment joint of interest. The flanges were divided into three segments. The webs were divided into a four segments. The moment of inertia of the joint model (based solely on the  $A*d^2$  terms of the parallel axis theorem) was within 5% of real section. If this was not the case, further subdivide would be required. All rigid members are weightless and connected as a frame. All concrete and PT tendon members were connected with pinned ends. One node at the centroid (node A) of the section had a fully fixed boundary condition. The other node at the centroid (node B) was slaved to node A in all directions except longitudinal rotations (i.e. rotation about the Z axis). The 2D segment joint model was loaded by applying monotonic rotations to node B.



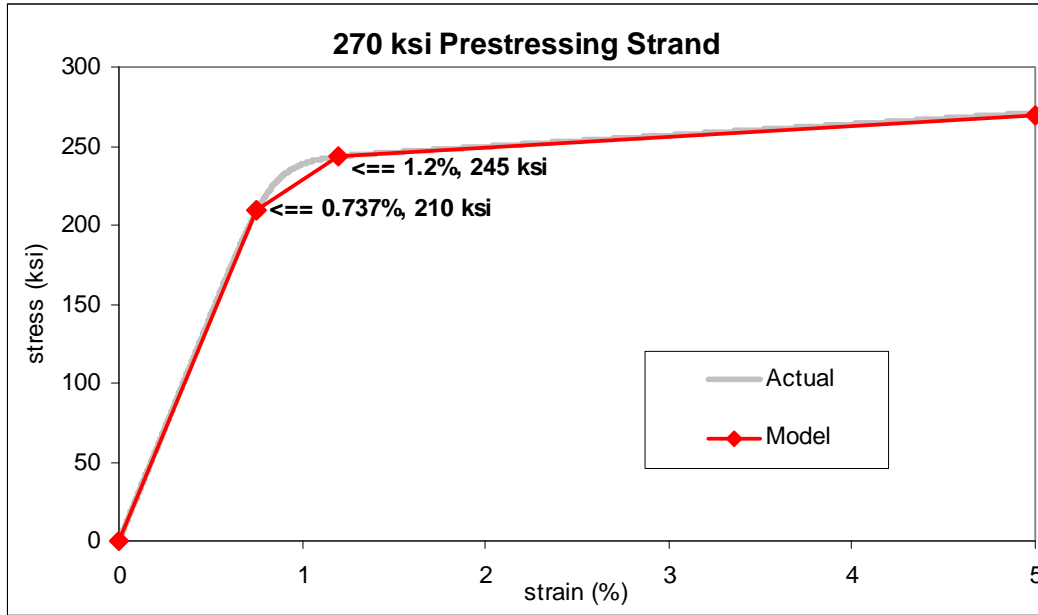
## 'Important' Bridge

The properties of the nonlinear concrete truss members were based on the stresses shown below and the cross section area of the member defined by the division lines above. The unconfined concrete stress-strain curve was determined using Thorenfeldt, Tomaszewicz and Jenson equation (Wight and Macgregor, 2009). The initial stiffness of the model curve was based on the stiffness obtained from the unconfined concrete stress-strain curve at 50% of  $f'_{ce}$ . The tensile and compressive capacities were based on 13% of the concrete direct tensile strength and 85% of the expected concrete strength,  $f'_{ce}$ , respectively. The expected concrete compressive strength was taken to be 1.3 times the design compressive strength (i.e.  $f'_{ce} = 1.3f'_c$ ), and the direct tensile strength was taken as  $0.33\sqrt{f'_{ce}} (MPa)$ . This tensile strength was used to approximate residual tensile stresses across the joints caused by particle contact across the rough crack between segments (see Veletzos and Restrepo, 2011).

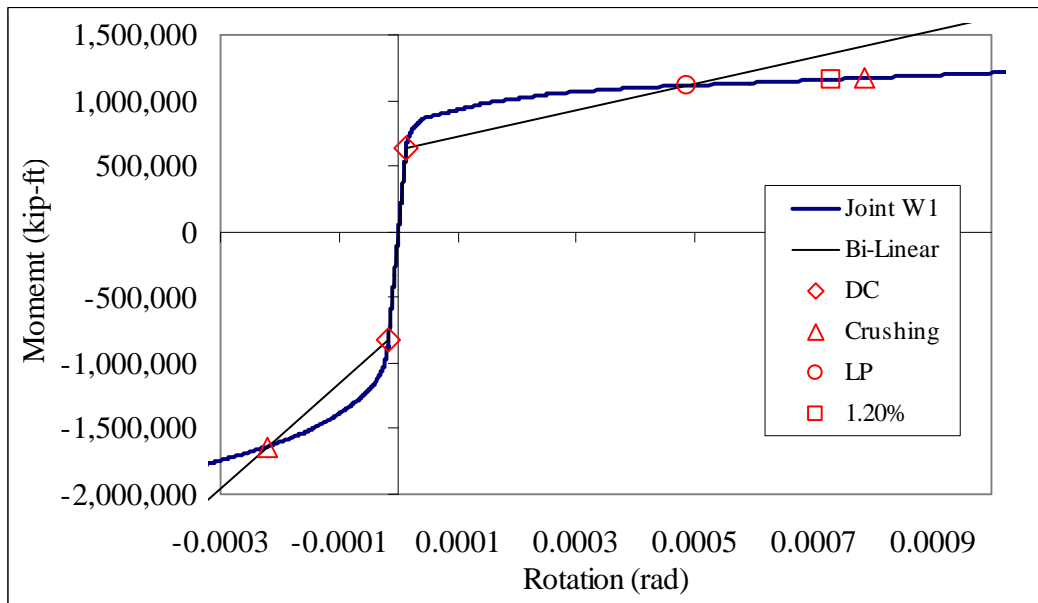


The properties of the nonlinear PT tendon truss members were based on the stresses shown below and the sum of all the tendons areas at the location. The tendons were preloaded to their expected stress during service which was calculated to be 55% GUTS.

Appendix C - Verification of Proposed Design Approach  
 'Important' Bridge

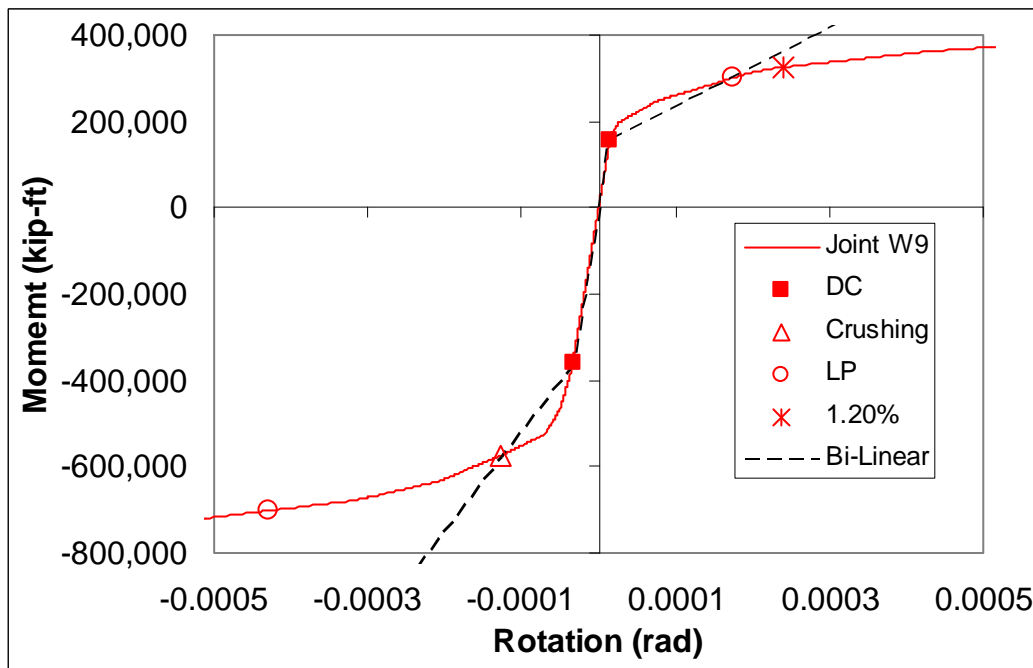
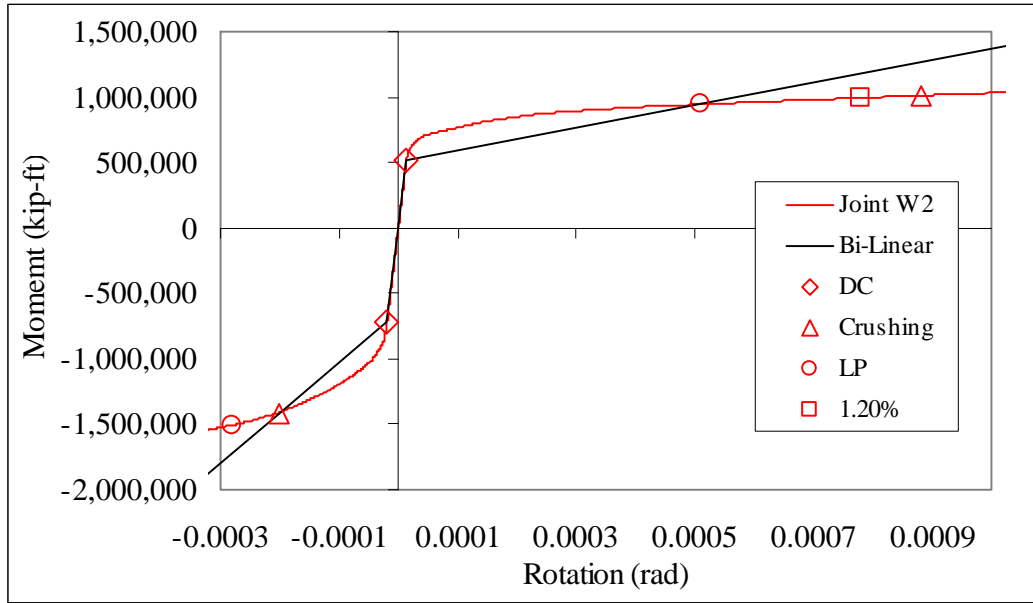


The moment rotation results from two joints adjacent to the pier (joints W1 and W2) and two joints near midspan (joints W9 and midspan) are shown below with bi-linear approximations. These results include a moment shift so that the bi-linear curve is centered on the origin. The bi-linear approximation is what will be used as the nonlinear behavior of the superstructure segment joints in the SAP model.



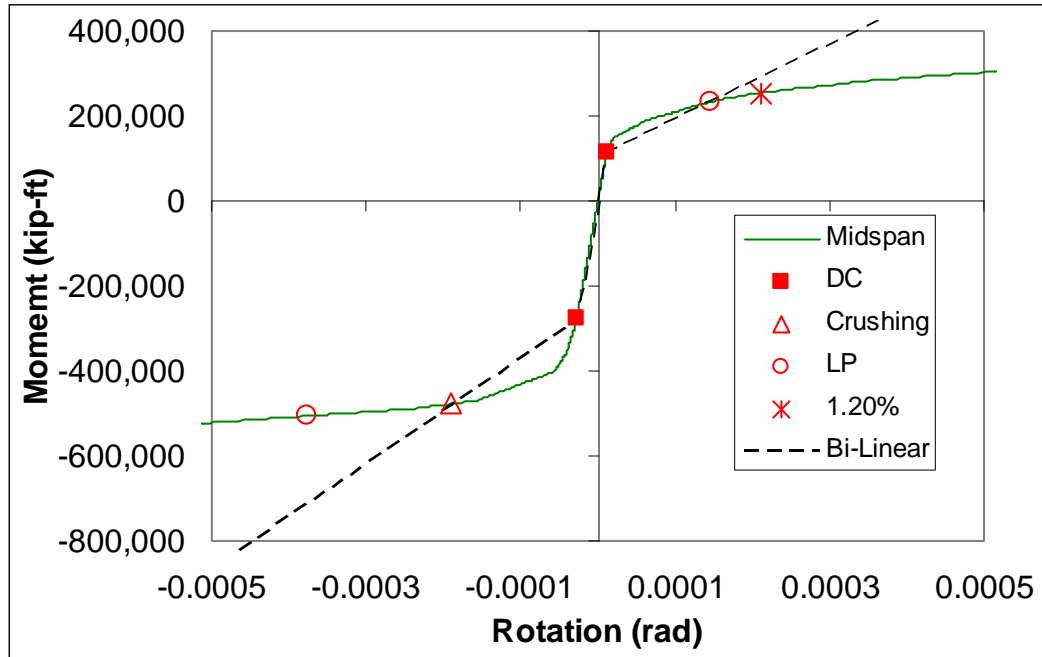
Appendix C - Verification of Proposed Design Approach

'Important' Bridge



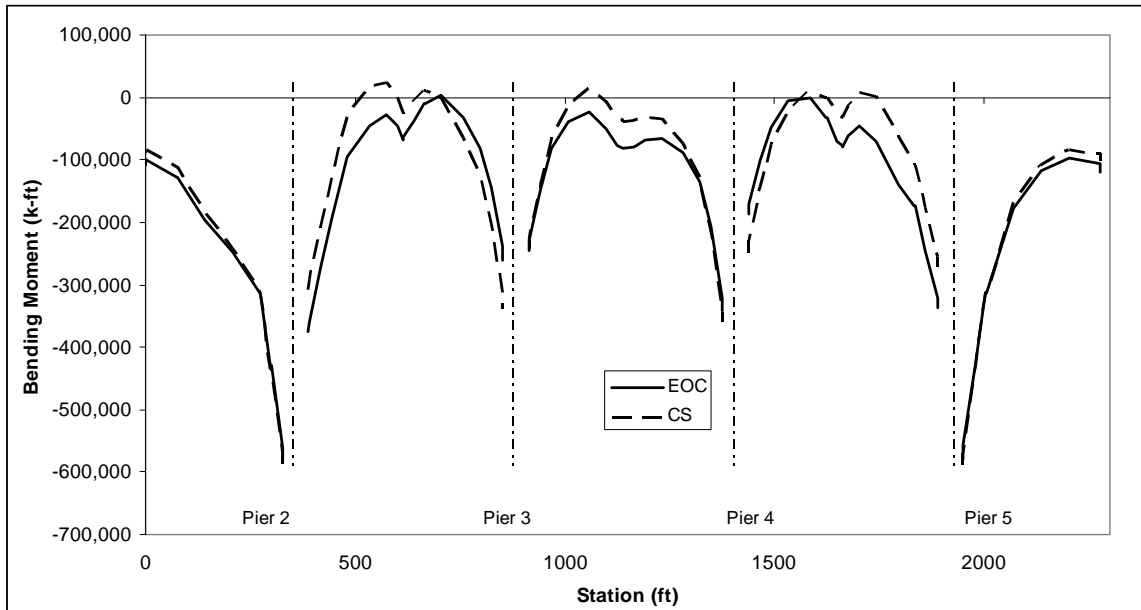
Appendix C - Verification of Proposed Design Approach

'Important' Bridge



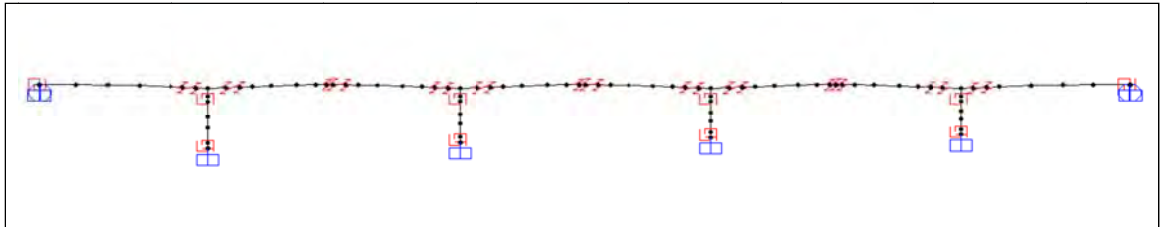
#### 4. Longitudinal Construction Staging Analysis

A full longitudinal construction staging analysis (LCSA) was performed. The details of this analysis are not the focus of this report, thus the end results are presented for simplicity. The dead load bending moment diagram at the end of construction (EOC) and after considering creep and shrinkage (CS) losses are shown below and include the effects of the PT on the bridge.

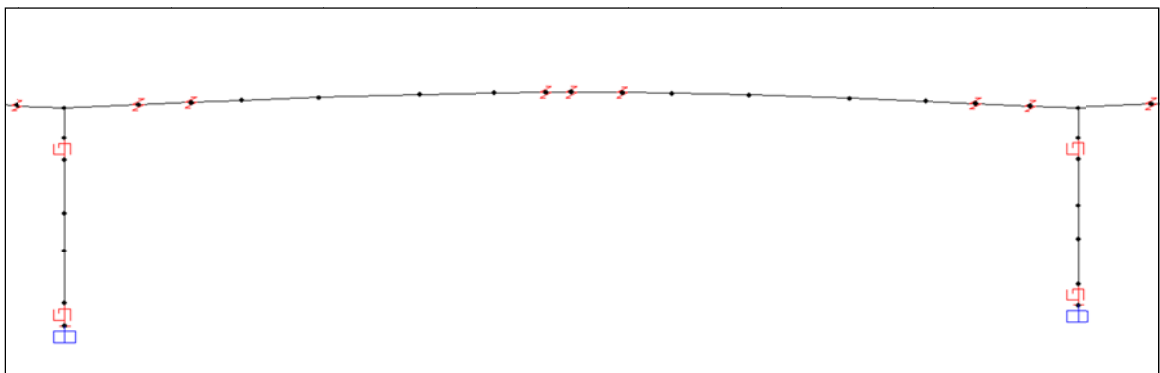


## 5. Longitudinal Push-Over Analysis

The finite element model was developed using SAP2000 Version 14 with linear elastic members representing the superstructure. Potential nonlinear response at the top and bottom of the piers was modeled using nonlinear Link elements. The pier hinging properties utilized a Takeda multi-linear plastic hysteretic model. Two models were developed and each model was calibrated to a different pre-earthquake stress state: end of construction (EOC); and after considering creep, shrinkage and relaxation losses (CS). Foundation springs were included in the model to account for soil structure interaction.



Three nonlinear elastic segment joints were modeled near midspan and four segment joints near the piers (two on each side). The joint behavior was modeled with nonlinear elastic bi-linear springs. The properties of these joints were based on the results of the detailed local non-linear models used to determine the capacities of the superstructure segment joints. These members were only capable of non-linear behavior in the vertical (longitudinal) moment direction. Nonlinear behavior was prohibited in the transverse moment direction.

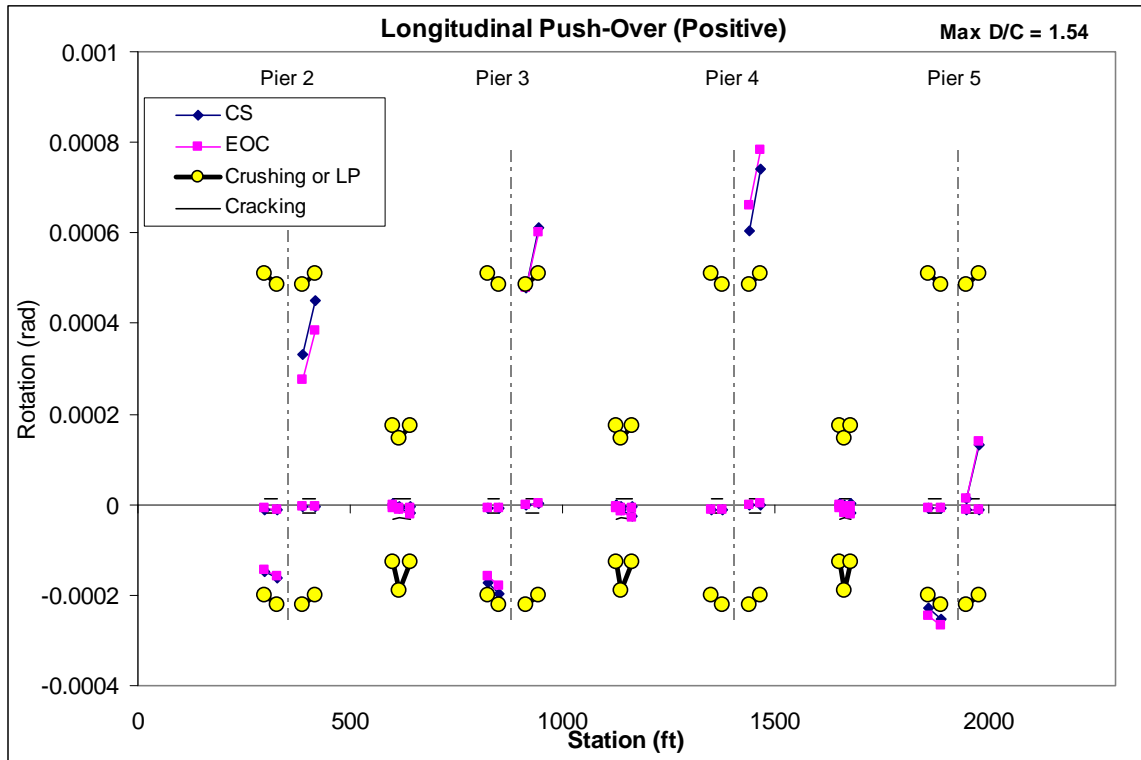


### ***Positive Push Direction***

The rotation in the nonlinear elastic superstructure segment joints members due to a push-over in the positive direction are shown below for both pre-earthquake stress states. The results are compared with the elastic rotation, defined as the rotation at which

'Important' Bridge

the extreme compression fibers reach a strain of 0.003 or the stress in the tendons exceed the limit of proportionality (taken as 210 ksi).

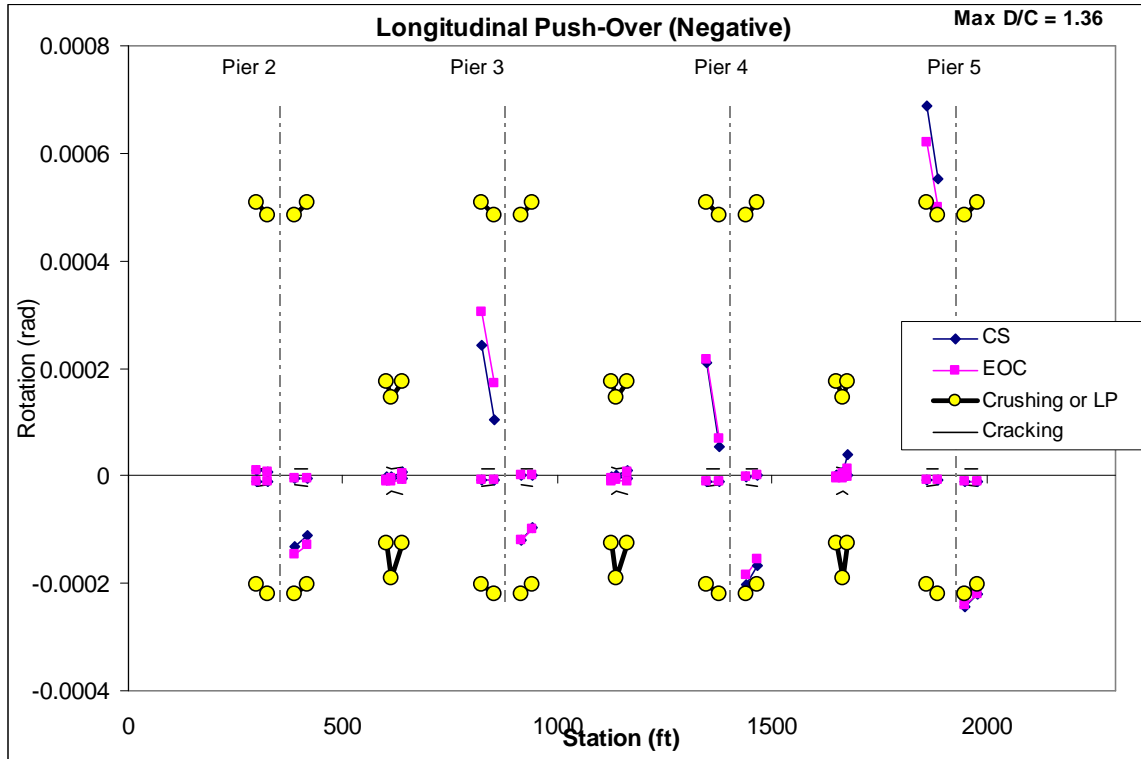


The results indicate that the pier segment joints will exceed the elastic rotation limit by up to 54%. This primarily occurs due to positive bending, although it is observed due to negative bending as well. The midspan segment joints remain within the elastic limit.

**Negative Push Direction**

The rotation in the nonlinear elastic superstructure segment joints members due to a push-over in the negative direction are shown below for both pre-earthquake stress states. The results are compared with the elastic rotation, defined as the rotation at which the extreme compression fibers reach a strain of 0.003 or the stress in the tendons exceed the limit of proportionality (taken as 210 ksi).

Appendix C - Verification of Proposed Design Approach  
 'Important' Bridge



The results indicate that the pier segment joints will exceed the elastic rotation limit by up to 36%. This primarily occurs due to positive bending, although it is observed due to negative bending as well. The midspan segment joints remain within the elastic limit.

**Pushover Conclusions**

The segment joints near the piers exceed the elastic rotation capacity primarily in positive bending. This means that the stresses in the bottom flange tendons near the piers will exceed 210 ksi. The capacity of the pier segment joints should be increased to ensure that the superstructure segment joints remain elastic. To reduce the demands on the superstructure the designer should consider reducing the reinforcement in the piers, provided the piers maintain sufficient ductility to accommodate increased displacements.

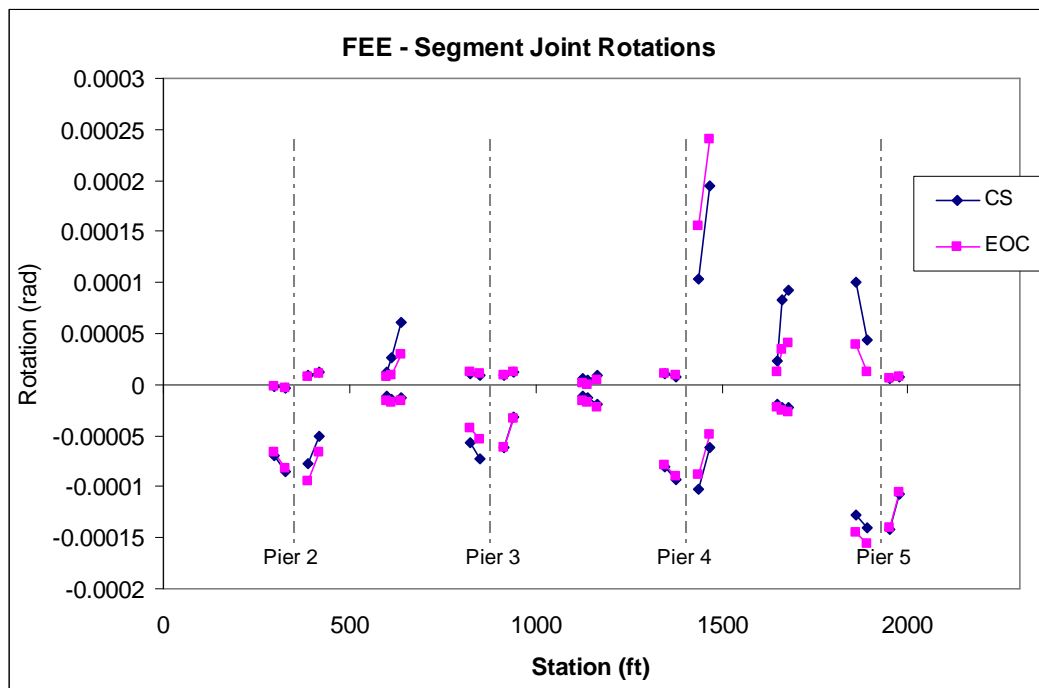
## 6. Seismic Demands

A 3D finite element model was developed using the program SAP2000. This was the same model used for the longitudinal push-over analysis. Non-linear elastic members were placed at select segment joints in the superstructure. The properties of these joints were based on the results of the detailed local non-linear models used to determine the capacities of the superstructure segment joints. These members were only capable of non-linear behavior in the vertical (longitudinal) moment direction. Nonlinear behavior was prohibited in the transverse moment direction.

2% Rayleigh damping was defined at the dominant longitudinal period (3.0 seconds) and at a period that included approximately 80 percent of the total vertical mass participation (0.35 sec).

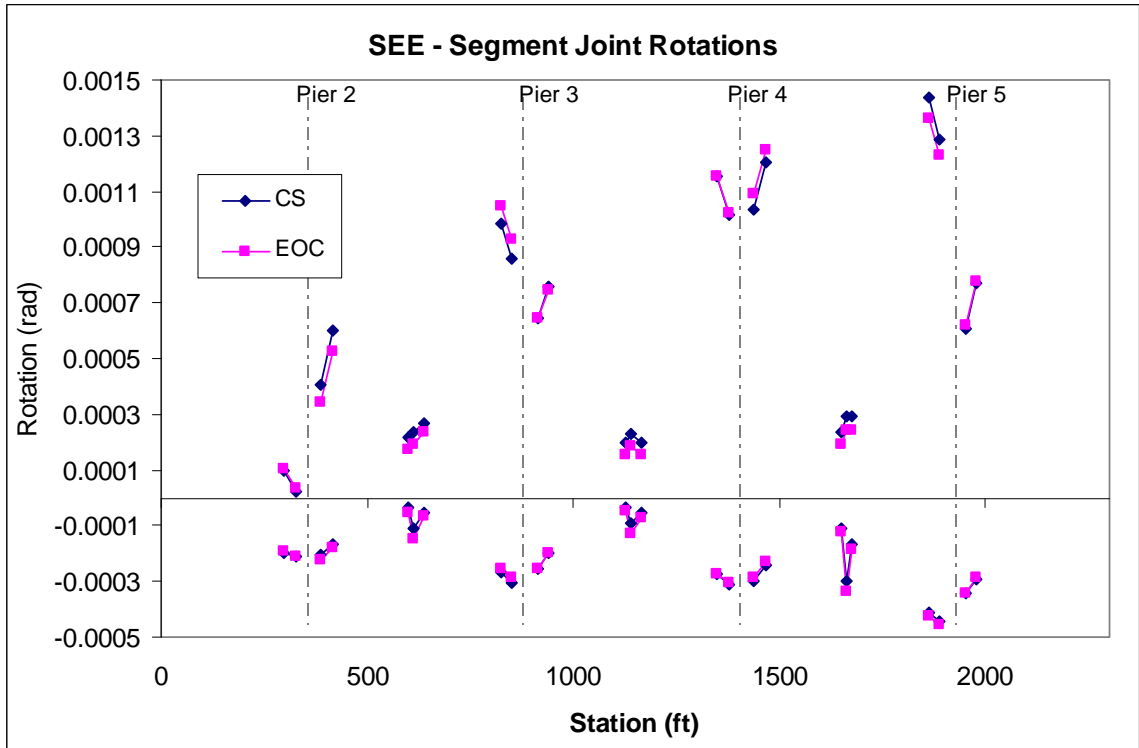
### ***FEE***

The model was subjected to three FEE ground motion sets. Each set contained three spectrum compatible ground motion components. The maximum rotational demands of the nonlinear elastic superstructure segment joints members are shown below.



**SEE**

The model was subjected to three SEE ground motion sets. Each set contained three spectrum compatible ground motion components. The maximum rotational demands of the nonlinear elastic superstructure segment joints members are shown below.

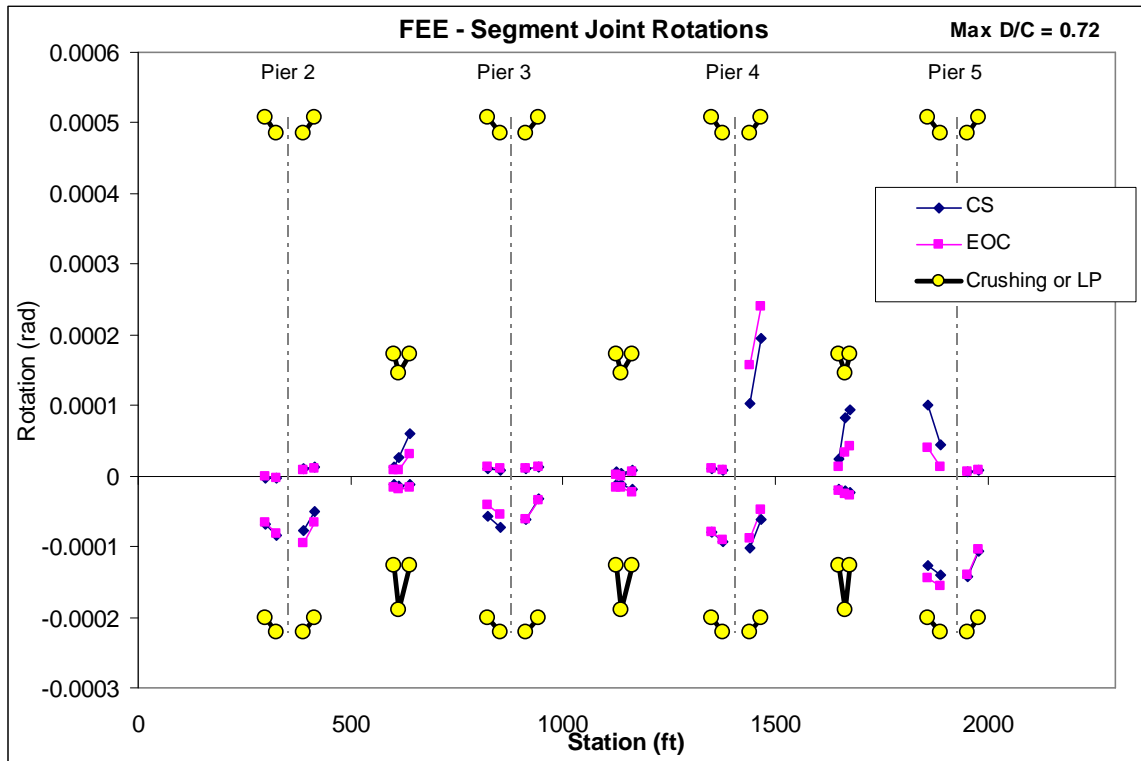


## 7. Demand/Capacity Ratios

### FEE

The superstructure response due to an FEE event, must not exceed an “essentially elastic” response. Thus the segment joint rotations must not exceed the elastic rotation limit and must close fully once the earthquake has subsided. The elastic rotation limit was defined as the rotation based on the lesser of: an extreme compressive strain of 0.003; or a tendons stress of 210 ksi (i.e. the limit of proportionality).

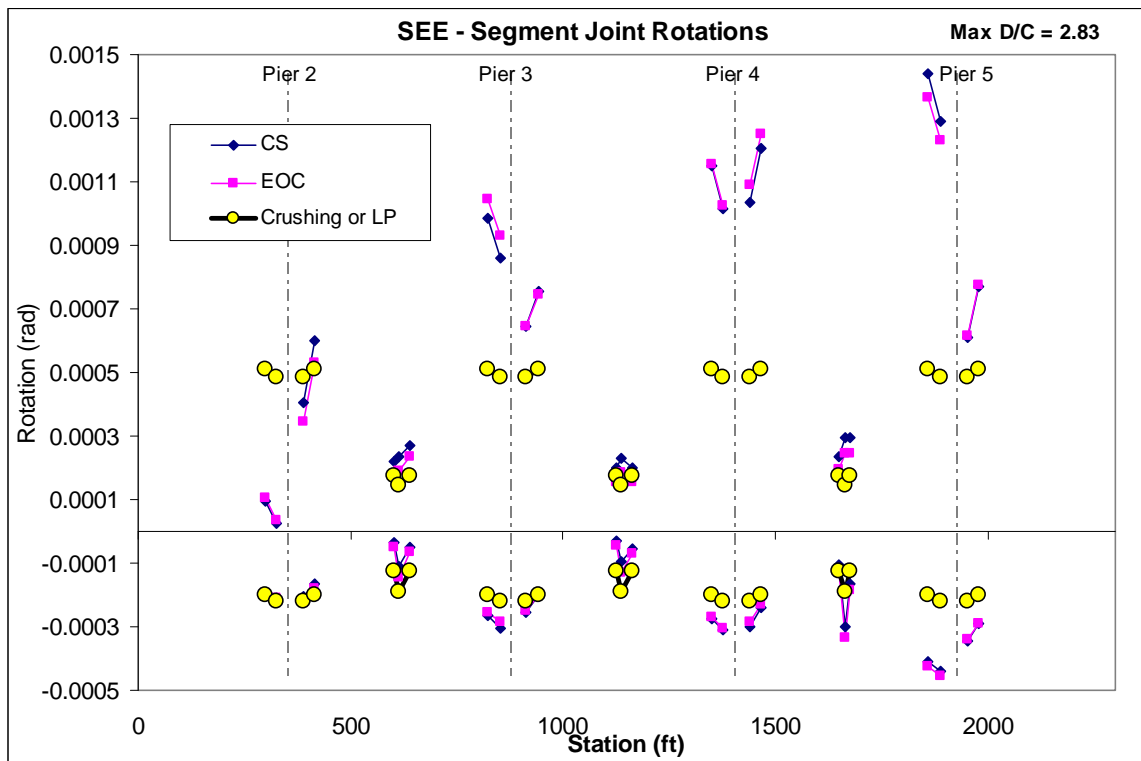
The FEE superstructure bending moment demands based on EOC and CS stress state are compared with the elastic rotation capacities (see figure below). All segment joints remained within the elastic rotation limit for the FEE event.



### SEE

The superstructure must not exceed a rotation that will prevent the joint from closing fully. Thus, as with the FEE design level, the segment joint rotations must not exceed the elastic rotation limit,

The SEE superstructure bending moment demands based on EOC and CS stress state are compared with the elastic rotation capacities (see figure below). Nearly all segment joints exceed the elastic rotation limit. The maximum D/C was 2.83 due to positive bending rotations near Pier 5. The largest D/C for the span joints was 2.04 and occurred due to positive bending in the span 4 midspan segment joint.



### Conclusions

The superstructure segment joints will exceed the elastic limit during an SEE design level event. This conclusion is consistent with results from the longitudinal push-over analysis.

Options to consider are: increase the PT across the segment joints to increase the clamping force across the joint thereby reducing the segment joint demands; increase the debond length of the PT tendons by increasing the size of each tendons.